ATMOSPHERIC ELECTRICITY AND
TETHERED AEROSTATS. VOLUME I

AIR FORCE EASTERN TEST RANGE
PATRICK AIR FORCE BASE, FLORIDA

11 MAY 1976

028098

AFETR-TR-76-07

ATMOSPHERIC ELECTRICITY AND
TETHERED AEROSTATS, VOLUME I

Range Measurements Laboratory
Air Force Eastern Test Range (AFSC)
Patrick AFB, Florida

11 May 1976

Approved for Public Release;
distribution unlimited

Prepared for

DEFENSE ADVANCED RESEARCH PROJECTS AGENCY
1400 WILSON BLVD
ARLINGTON, VIRGINIA

LEGAL NOTICE

OTHER NOTICES

This technical report has been reviewed and is approved for publication.

TOXEY A. HALL, Project Engineer
Metric Engineering
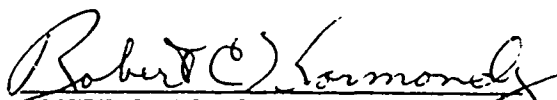Pan American World Airways, Inc.

ELMER E. SHEPPARD, Program Manager
Sensor Platforms Branch
Range Measurements Laboratory
Directorate of Range Engineering

WALTER H. MANNING, JR., Chief
Range Measurements Laboratory
Directorate of Range Engineering

FOR THE COMMANDER

ROBERT C. KORMONDY, Colonel, USAF
Director of Range Engineering

REPORT DOCUMENTATION PAGE	READ INSTRUCTIONS BEFORE COMPLETING FORM

1. REPORT NUMBER	2. GOVT ACCESSION NO.	3. RECIPIENT'S CATALOG NUMBER
AFETR-TR-76-07		

4. TITLE (and Subtitle)	5. TYPE OF REPORT & PERIOD COVERED
ATMOSPHERIC ELECTRICITY AND TETHERED AEROSTATS, VOLUME I	FINAL, 1 APR 73 THRU 30 JUN 74
	6. PERFORMING ORG. REPORT NUMBER
	N/A

7. AUTHOR(s)	8. CONTRACT OR GRANT NUMBER(s)
TOXEY A. HALL	ARPA ORDER 2176

9. PERFORMING ORGANIZATION NAME AND ADDRESS	10. PROGRAM ELEMENT, PROJECT, TASK AREA & WORK UNIT NUMBERS
RANGE MEASUREMENTS LABORATORY (ENL) AIR FORCE EASTERN TEST RANGE PATRICK AIR FORCE BASE, FLORIDA 32925	N/A

11. CONTROLLING OFFICE NAME AND ADDRESS	12. REPORT DATE
DEFENSE ADVANCED RESEARCH PROJECTS AGENCY 1400 WILSON BLVD. ARLINGTON, VIRGINIA 22209	11 MAY 1976
	13. NUMBER OF PAGES
	254

14. MONITORING AGENCY NAME & ADDRESS(If different from Controlling Office)	15. SECURITY CLASS. (of this report)
RANGE MEASUREMENTS LABORATORY (ENL) AIR FORCE EASTERN TEST RANGE PATRICK AIR FORCE BASE, FLORIDA 32925	UNCLASSIFIED
	15a. DECLASSIFICATION/DOWNGRADING SCHEDULE N/A

16. DISTRIBUTION STATEMENT (of this Report)

A

DISTRIBUTION STATEMENT A
Approved for public release;
Distribution Unlimited

17. DISTRIBUTION STATEMENT (of the abstract entered in Block 20, if different from Report)

A

18. SUPPLEMENTARY NOTES

Volume I is a summary of in-house research and sponsored research. Volume II presents final reports from 4 studies by outside contractor.

19. KEY WORDS (Continue on reverse side if necessary and identify by block number)

Atmospheric Electricity
Balloons
Conducting and Non-Conducting Tethers
Corona Discharge
Electric Field Perturbations
Faraday Cages
Lightning Effects, Protection, Warning Systems
Potential Gradient Anomalies
Space Charge Plumes
Tethered Balloons, Tether Currents

20. ABSTRACT (Continue on reverse side if necessary and identify by block number)

This report presents findings of a two year program conducted by the Range Measurements Laboratory (RML) of the Air Force Eastern Test Range for the purpose of determining interaction of tethered balloon systems with atmospheric electricity (particularly lightning) and identifying feasible protective systems. After a brief introductory section math models of effects of tethered balloons on surrounding electrical field are presented. These models are then compared with measurements taken during extensive flight testing. Effects of both well-conducting and poorly-conducting tethers are shown.

Section 3 presents a statistical approach to the prediction of lightning strikes to tethered balloons.

DD FORM 1473 1 JAN 73 EDITION OF 1 NOV 65 IS OBSOLETE

20.

Section 4 describes results of an extensive series of tests wherein balloon tethered samples, both wire rope and synthetic fiber, are exposed to simulated lightning currents. Properties of metals which contribute to lightning damage are also modeled.

Section 5 defines systems and techniques for hardening balloon and support equipment and protection of operating personnel, including description of lightning warning systems available or developable with minimum technical risk.

Sections 6 and 7 present conclusions and recommendations oriented toward tether materials, grounding and shielding systems, warning devices, and operational concepts.
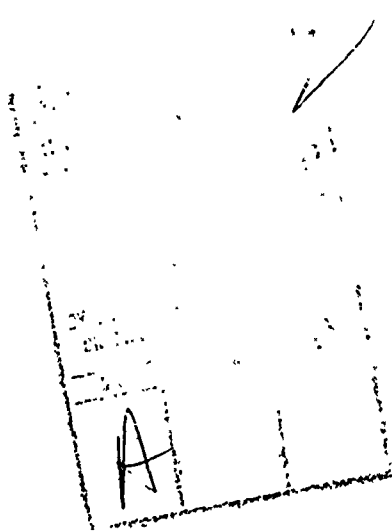
ERRATA PAGE

VOLUME I

Page 2-20   Equation 2-20, change to read

$$P_c = L\left[\ln\left(\frac{2L}{b}\right)-1\right]^{-\frac{1}{2}}$$

Page 2-22   Figure 2-9, change formula

$$V = 100(1-e^{-kb}) \quad \text{to} \quad V = 10^4(1-e^{-kh})$$

Page 3-18

    Line 9   Change "experienced"

          to "experienced"

    Line 22   Delete comma after "cloud"

    Line 25   Change "envelope"

          to "enveloping"

Page C-1

    Formula C-1

        Change superscript d^1 to α'

        Change superscript β^1 to β'

ABSTRACT

This report presents findings of a two year program conducted by the Range Measurements Laboratory (RML) of the Air Force Eastern Test Range for the purpose of determining interaction of tethered balloon systems with atmospheric electricity (particularly lightning) and identifying feasible protective systems. After a brief introductory section math models of effects of tethered balloons on surrounding electrical field are presented. These models are then compared with measurements taken during extensive flight testing. Effects of both well-conducting and poorly-conducting tethers are shown.

Section 3 presents a statistical approach to the prediction of lightning strikes to tethered balloons.

Section 4 describes results of an extensive series of tests wherein balloon tethered samples, both wire rope and synthetic fiber, are exposed to simulated lightning currents. Properties of metals which contribute to lightning damage are also modeled.

Section 5 defines systems and techniques for hardening balloon and support equipment and protection of operating personnel, including descriptions of lightning warning systems available or developable with minimum technical risk.

Sections 6 and 7 present conclusions and recommendations oriented toward tether materials, grounding and shielding systems, warning devices, and operational concepts.

i

PREFACE

This report compiles the results of a research program on the
interaction of tethered balloons with atmospheric electricity.
The program was sponsored by the Defense Advanced Research Pro-
jects Agency (DARPA), was directed by the Range Measurements
Laboratory (RML) of the Air Force Eastern Test Range, and was
conducted by RML with the assistance of academic and industrial
researchers.

Volume I is a summary and interpretation of the four research
reports generated by the program plus additional information
derived internally at RML. Section 5.2.2., Hardening of Critical
Balloonborne Systems, was prepared by Mr. Henry B. O. Davis, Jr.
of RML's Sensor Platforms Branch.

The research reports in their original form are presented as
Volume II. It is believed that the research summarized in
Volume II has scientific value beyond the scope of this program.
Therefore, Volume I does not purport to supplant the information
in Volume II. Information from Volume II, where used, is refer-
enced by applicable sections. References to other works are
indicated by numbers in brackets as listed in the bibliography
in Appendix E.

This program benefited greatly from extensive use of an instru-
mented aircraft operated by the NASA Kennedy Space Center. The
outstanding contributions of Dr. Don J. Latham, Dr. Edward T.
Pierce, Mr. Gary H. Price, and Mr. James R. Stahmann are acknowl-
edged. Appreciation is also expressed to Professor Charles B.
Moore and Dr. Martin A. Uman for their valuable assistance and
guidance.

CONTENTS

CONTENTS

ILLUSTRATIONS

ILLUSTRATIONS - Continued

ILLUSTRATIONS - Continued

ILLUSTRATIONS - Continued

ILLUSTRATIONS - Continued

ILLUSTRATIONS - Continued

x

TABLES

SECTION 1

INTRODUCTION

1.1 PURPOSE

The Defense Advanced Research Projects Agency/Range Measurements
Laboratory (DARPA/RML) Atmospheric Sciences Program was created
to extend the operational capability of tethered balloon systems
by minimizing operational limits imposed by lightning hazards.

1.2 PROGRAM OBJECTIVES

The program was designed to accomplish the following goals:

1. Identify, test, evaluate, and recommend an
    operator-oriented lightning hazard warning
    system.

2. Develop and qualify protective systems and
    safety procedures for personnel at the op-
    erating site.

3. Provide a lightning-related data base for
    specifying a tether cable containing conduc-
    tors for transmitting electrical power to
    balloons.

4. Develop and qualify protective systems for
    the tether, balloon, and balloonborne systems.

5. Provide a realistic assessment of lightning
    hazards based on sound theory, verified by
    experimentation wherever possible.

1.3   PROGRAM APPROACH

It was determined that two basic issues existed which could be clarified by experimental investigations:

1. How is the probability of a lightning stroke affected by the conductivity of the tether?

2. What are the relative vulnerabilities to damage of well-conducting or poorly-conducting tethers?

The probability of an elevated structure such as a tethered balloon receiving a lightning flash is related to the alterations of the electrical field around the structure, particularly the intensification of the field distribution around the top. In order to examine the effect of the balloon system on its electrical environment, a' research contract was given to the university of Miami (Florida) School of Atmospheric and Oceangraphic Sciences. Under this contract, Dr. Don J. Latham designed a series of experiments and the required equipment to make the necessary measurements. He performed math modeling and data analysis relative to this investigation. Dr. Latham also functioned as principal consultant to the program.

Sixteen flights were conducted using the ground instrumentation from 14 Sep 73 through 7 Dec 73. On eight of these tests, the electric field above the balloon was measured by an instrumented aircraft operated by NASA/KSC.

Based on the experimental data and other information, additional modeling and criteria for estimating the probability of lightning flashes to balloons were prepared by Dr. Edward T. Pierce and Mr. Gary H. Price, under a contract with the Stanford Research Institute.

Concurrent with this effort, materials testing by exposure to artificial lightning was conducted by Mr. James R. Stahmann of the Lightning & Transients Research Institute of Miami, Florida. Mr. Stahmann also prepared most of the recommendations for personnel safety and equipment protection.

Throughout the program, additional assistance was provided by Dr. Martin A. Uman, University of Florida, and by Professor Charles B. Moore, New Mexico Institute of Mining and Technology. The program approaches and results were reviewed by these two scientists.

The results of these investigations are summarized by RML in this volume. Volume II contains the final reports of each of these investigations.

Atmospheric electricity is a complex and many-faceted subject. While a substantial theoretical structure has evolved, many areas remain relatively undefined. In some cases, the theory, based on simplifying assumptions lends insight to, rather than accurately quantifying, the physical reality. These factors occasionally tend to preclude unanimity among atmospheric scientists. This report has been reviewed to varying depths by the scientists involved, but they were, in general, unable to apply the necessary time for a detailed review. Pursuant to their review, many recommended changes have been made; however, for the reasons stated above, it would be unfair to represent this report as a concensus of the program consultants.

SECTION 2

INTERACTION OF THE BALLOON SYSTEM
WITH ATMOSPHERIC ELECTRICITY

2.1 NATURAL ELECTRICAL ENVIRONMENT

Characteristics of the natural electrical environment are summa-
rized by Pierce and Price (Volume II, Part B, page 3) as follows:

> "In fair weather and quiet unpolluted conditions, the
> atmospheric electric field E_z is directed vertically
> and decreases fairly steadily with increasing height,
> perhaps from +100 V/m at z = 0 to 10 V/m at z = 4 km*.
> Atmospheric convection and pollution modify this simple
> picture, especially in the lower atmospheric layers.
> If the atmospheric conductivity at height z is λ_z, then
> we have the relation

$$J_z = E_z \lambda_z \qquad\qquad (2-1)$$

> where J_z is the air-earth current. Measurements show
> that J_z is relatively constant with height as compared
> with E_z and λ_z. Typically, $J_z = J \sim 2 \times 10^{-12}$ A/m^2. At
> ground level λ_z might be 2×10^{-14} mho/m in an unpolluted
> locality with a corresponding value of $E_0 = 100$ V/m.

---

* Using the normal sign convention of atmospheric
electricity by which a positive charge in the
upper atmosphere produces a positive field at
the earth's surface below.

"When clouds are present, the fair weather environment is changed in two respects. The cloud particles modify the profile of λz with height, while charge-generating mechanisms become active within the clouds. The electric fields increase in magnitude over fair weather conditions and — because of the charge generation — may be of either sign.

The greatest electrification is associated with thunderclouds. The field at the ground below a thundercloud rarely exceeds 10 kV/m and does not change greatly between ground level and the cloud base. Within the cloud, the general peak fields are typically 40 to 50 kV/m, but there is some evidence that localized very intense fields approaching 400 kV/m also exist. The electrical structure of a thundercloud is very complicated in detail, but can often be represented macroscopically by a net positive charge in the upper part of the cloud, an excess of negative charge in the main body of the cloud, and a small net positive charge towards the cloud base."

2.2 EFFECT OF A CONDUCTING TETHER

When a balloon tethered by a grounded, well-conducting material is introduced to the environment which has been described, a rapid transfer of charge (time constants to be discussed later) will result in the maintenance of ground potential at the tip of the tether. This in turn results in a rearrangement of the equipotentials such that the ground equipotential will be extended to the full height of the tether. The equipotentials above the balloon will be compressed, with resulting field intensification. This intensification gradually decreases with increasing altitude until a point is reached some thousands of meters above the balloon where the presence of the balloon is not evident.

Conversely, at ground level near the tether, the spacing between equipotentials is increased owing to the ground equipotential being lifted to the height of the balloon, diminishing the electrical field at this point. This effect decreases with horizontal distance away from the balloon until, at a distance equal to the height of the balloon, the presence of the balloon has no apparent effect on the local potential gradient. The field pattern as altered by the balloon is shown in figure 2-1. The equipotential pattern in the vicinity of the balloon can be determined by solving Poisson's equation:

$$\nabla^2 \phi = -\frac{\rho}{\varepsilon_0} \qquad (2\text{-}2)$$

where ϕ is the potential in volts and ρ is the space charge density in coulombs per cubic meter.

In cylindrical coordinates with circular symmetry assumed,

$$\frac{\partial^2 \phi}{\partial r^2} + \frac{1}{r}\frac{\partial \phi}{\partial r} + \frac{\partial^2 \phi}{\partial z^2} = -\frac{\rho(r,z)}{\varepsilon_0} \qquad (2\text{-}3)$$

where r is the radial coordinate and z the vertical coordinate of the cylindrical system. A computer solution of this equation in finite difference form has been prepared by Latham (Volume II, Part A, page D-2).

FIELD INTENSIFICATION ABOVE
BALLOON

EQUIPOTENTIALS

FLUX LINES

REDUCED FIELD NEAR TETHER ON
GROUND
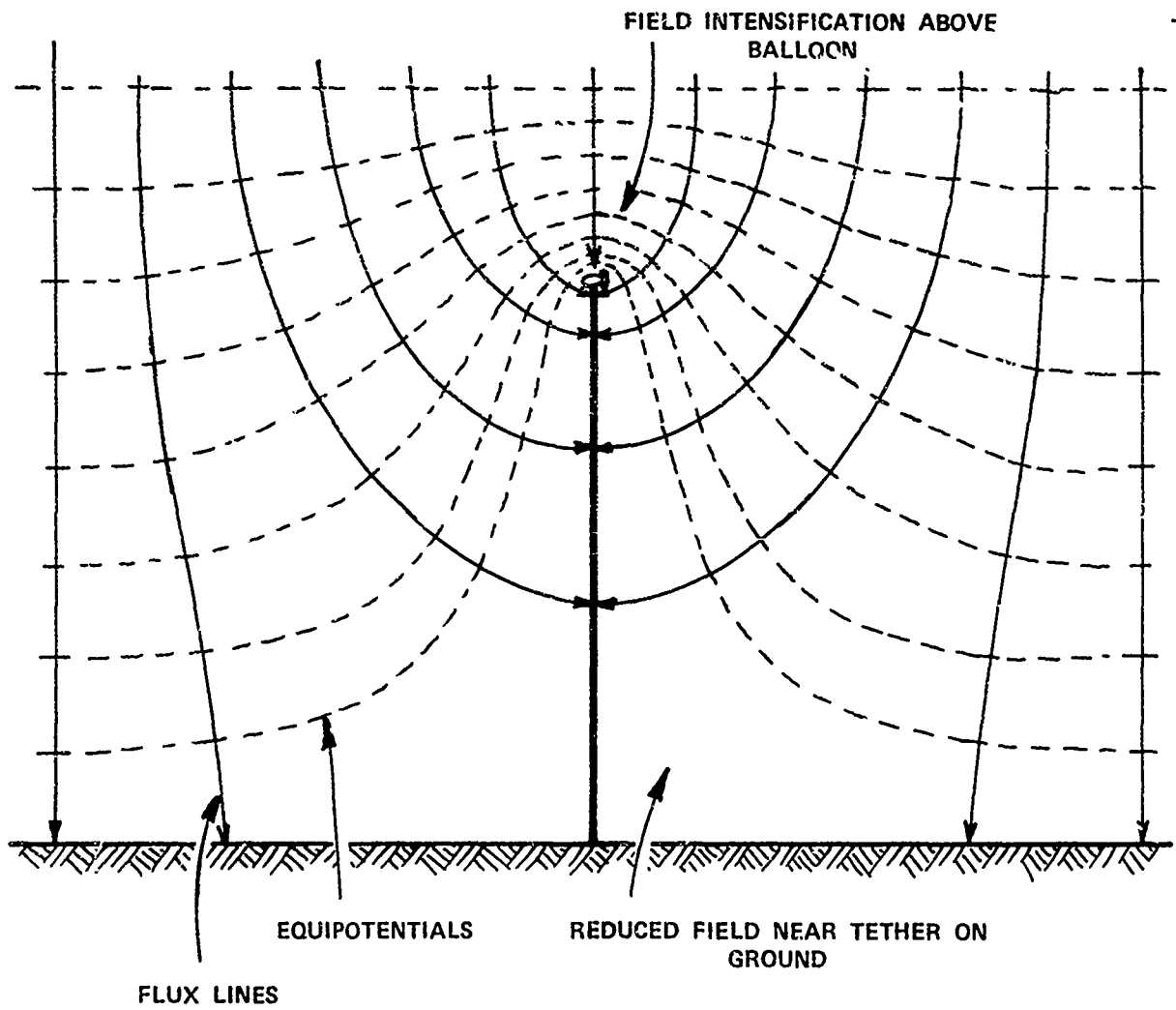
Figure 2-1. Distortion of Electric Field by the Balloon/Tether System

2.3 MATH MODELS FOR FIELD DISTORTION BY THE BALLOON/TETHER SYSTEMS

Three geometric models of the system were compared with measurements. These models provide the following descriptions of the system: (1) grounded vertical prolate ellipsoids, (2) grounded horizontal prolate ellipsoids, and (3) horizontal prolate ellipsoids charged to some arbitrary value.

2.3.1 The Grounded Vertical Prolate Ellipsoid Model

The geometry of this model is shown in figure 2-2. The model presumes that the effect of the balloon is insignificant compared to that of the tether, and therefore ignores the balloon. Potential and potential gradient formulas associated with this model are:

Potential at any point z, outside the prolate ellipsoid is given by:

$$\phi = - E_o z \left(1 - \frac{\dfrac{2}{\sqrt{\xi + a^2}} + \dfrac{1}{c} \ln \dfrac{\sqrt{\xi + a^2} - c}{\sqrt{\xi + a^2} + c}}{\dfrac{2}{a} + \dfrac{1}{c} \ln \dfrac{a - c}{a + c}} \right) \qquad (2-4)$$

a

(z, r)

$c = \sqrt{a^2 - b^2}$

b
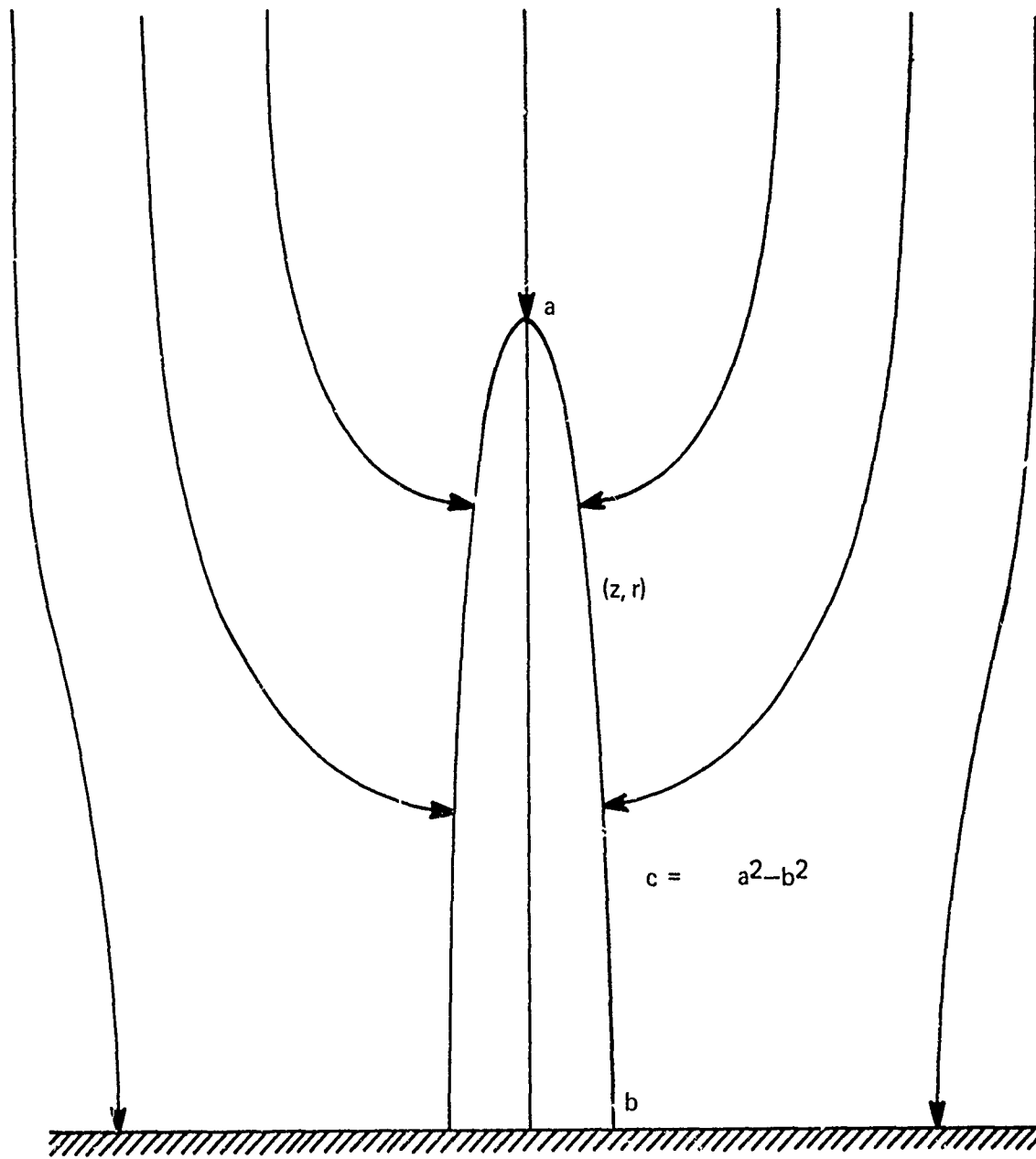
Figure 2-2. Tether Modeled as a Grounded Vertical Prolate Ellipsoid

the vertical component of the field

$$E_z = E_0 \left(1 - \frac{\sqrt{\dfrac{2}{\xi + a^2}} + \dfrac{1}{c} \ln \dfrac{\sqrt{\xi + a^2} - c}{\sqrt{\xi + a^2} + c}}{\dfrac{2}{a} + \dfrac{1}{c} \ln \dfrac{a - c}{a + c}} \right.$$ (2-5)

$$\left. -2E_0 z^2 \left[\frac{1}{\left[\dfrac{2}{ac^2} + \dfrac{1}{c^3} \ln \dfrac{a - c}{a + c} \right] \left[(\xi + a^2)^{3/2} (2\xi + a^2 + b^2 - z^2 - r^2) \right]} \right] \right]$$

and the horizontal component of the field,

$$E_r = - 2E_0 rz \left(\frac{1}{\left[\dfrac{2}{ac^2} + \dfrac{1}{c^3} \ln \dfrac{a - c}{a + c} \right] \left[(\xi + a^2)^{1/2} (\xi + b^2) (2\xi + a^2 + b^2 - z^2 - r^2) \right]} \right)$$ (2-6)

where a is the height of the ellipsoid

     b is the base radius

     $c = \sqrt{a^2 - b^2}$

     ξ is a parameter such that a set of confocal ellipsoids
     is defined by

$$\frac{z^2}{\xi + a^2} + \frac{r^2}{\xi + b^2} = 1$$ (2-7)

From equation 2-5 formulas have been determined for three situations of particular interest:

1. Intensification of the vertical field directly above the tether at an altitude z.

$$E_z(3) = E_0 \left(1 - \frac{\frac{a}{z} + \ln\frac{z-a}{z+a}}{2\left(1 + \ln\frac{b}{2a}\right)} - \frac{a^3}{2\left(1 + \ln\frac{b}{2a}\right)(z)(z^2 - a^2)} \right) \qquad (2\text{-}8)$$

This is relevant to streamer formation and triggering of lightning strikes.

2. Suppression of the vertical field on the ground at a distance r from the tether point:

$$\frac{E_z}{E_0} = 1 - \frac{\frac{2}{x} + \ln\frac{x-1}{x+1}}{2\left(1 + \ln\frac{b}{2a}\right)} \qquad (2\text{-}9)$$

where $x = \sqrt{1 + (r/a)^2}$

This relationship is important in the proper location of lightning warning systems based on monitoring the E-field. See figure 2-3.

Pierce and Price achieved similar results from a slightly different approach (see Volume II, Part B, page 53).

3. The radial field component near the tether at a height z.

$$E_r = \frac{E_0 z}{2\, b\left(1 + \ln\frac{b}{2a}\right)\sqrt{1 - \frac{z^2}{a^2}}} \qquad (2\text{-}10)$$

See figure 2-4. The radial field is the prime cause of corona discharge.
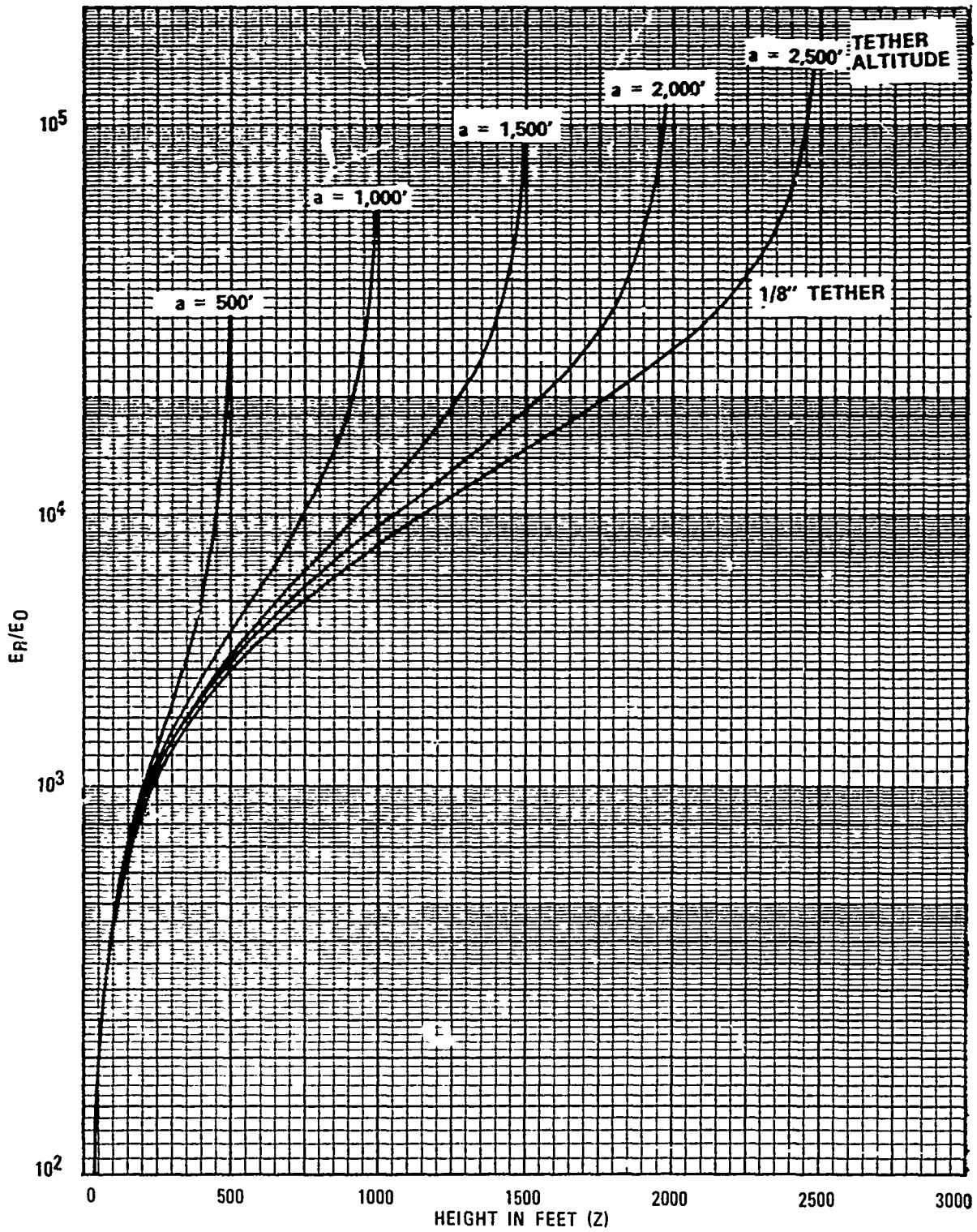
Figure 2-3. Intensification of Radial Component of Electrical Field
(E_R) Near Tether at Altitude (a)
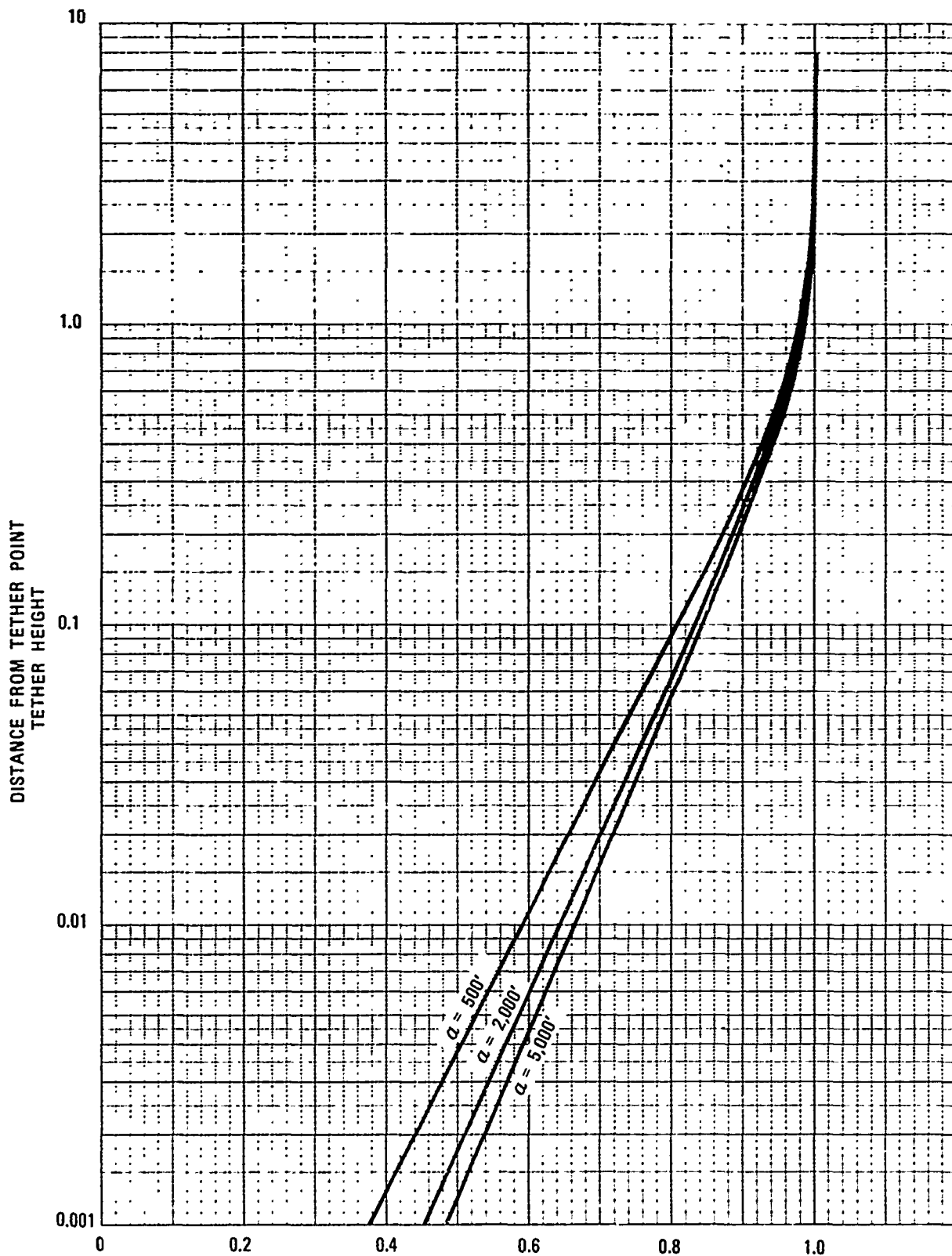
Figure 2-4 — Supression of Vertical Field (E_Z) on the Ground at Some Distance (R) From the Tether Point With a Balloon at Altitude (a)

2.3.2   Grounded Horizontal Prolate Ellipsoid Model

The effect of the balloon (neglecting the effect of the tether) can be estimated by modeling the balloon as a horizontal prolate ellipsoid (see figure 2-5), isolated at some altitude such that the potential outside the influence of the balloon is of value "V." If the tether is conductive, and grounded, the balloon is at zero potential (relative to the earth's surface). The potential near the balloon is then:

$$\phi = - E_0 (z + h) + \frac{E_0 \; (z + h)}{\frac{a}{c^2 b^2} + \frac{1}{2c^3} \ln \frac{a - c}{a + c}}$$

(2-11)

$$\left(\frac{\sqrt{\xi + a^2}}{c^2 \; (\xi + b^2)} + \frac{1}{2c^3} \; \ln \frac{\sqrt{\xi + a^2} - c}{\sqrt{\xi + a^2} + c} \right)$$

and the vertical field intensification directly above the balloon is:

$$\frac{E_z}{E_0} = 1 - \frac{\frac{\sqrt{z^2 - c^2}}{z^2} + \frac{1}{2c} \ln \frac{\sqrt{z^2 + c^2} - c}{\sqrt{z^2 + c^2} + c}}{\frac{a}{b^2} + \frac{1}{2c} \ln \frac{a - c}{a + c}}$$

(2-12)

$$+ \frac{2 (z+h) c^2}{\left(\frac{a}{b^2} + \frac{1}{2c} \ln \frac{a - c}{a + c} \right) z^3 \sqrt{z^2 + c^2}}$$

$$c = \sqrt{a^2 - b^2}$$
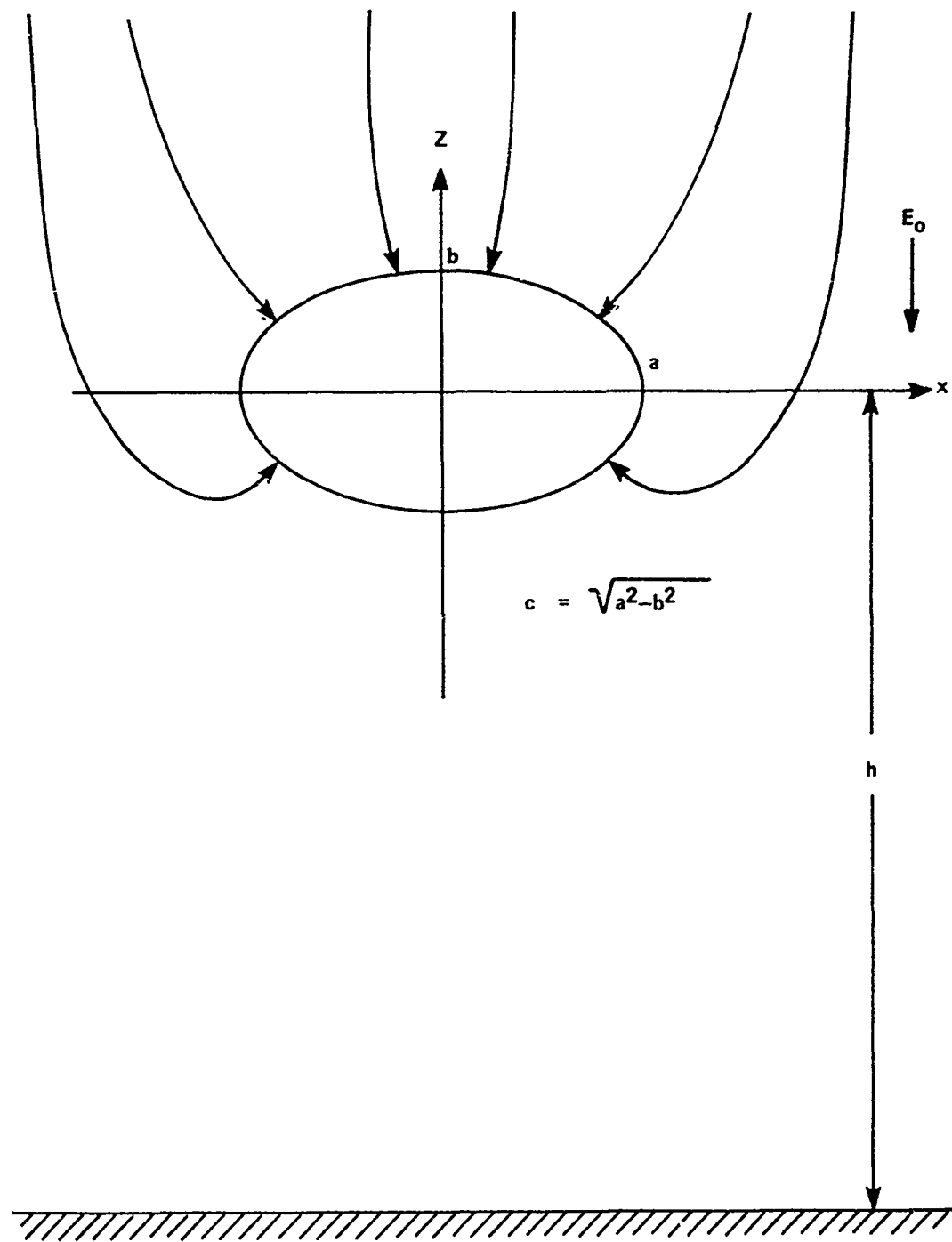
Figure 2-5. The Balloon Modeled as a Horizontal Prolate Ellipsoid

2.3.3 Charged Horizontal Prolate Ellipsoid Model

If the tether is assumed to be a poor conductor, the balloon will be charged to some value, $Q = - C\phi$, where C is the system capacitance

$$\phi = \frac{Q}{8\pi \epsilon_o} \left[\frac{1}{c} \ln \frac{\sqrt{\xi + a^2} + c}{\sqrt{\xi + a^2} - c} \right] \qquad (2-13)$$

and the field above the balloon is

$$E_z = \frac{Q}{4\pi \epsilon_o} \cdot \frac{1}{z(z^2 + c^2)^{1/2}} \qquad (2-14)$$

Calculated theoretical values of C are given in paragraph 2.5.

2.3.4 Space Charge Models

Latham has estimated the effect of corona space charge on potential gradient above the balloon by modeling the space charge as a conical plume extending from a point near the upper end of the tether (see figure 2-6). The following expressions were obtained for the vertical gradient (E_z) and the lateral gradient (E_x):

$$
E_z \doteq \frac{\lambda}{4\pi\varepsilon_0} \left\{ \left[\frac{1}{\sqrt{1+\tan^2\theta}} - \frac{\tan^2\theta}{3(1+\tan^2\theta)^{3/2}} \right] \right.
$$

$$
\left[\frac{z_0}{\left(\sqrt{(1+\tan^2\theta)(x_0^2+z_0^2)} \right) \left[\sqrt{(1+\tan^2\theta)(z_0^2+x_0^2)} \right] - x_0} \right]
$$

$$
+ \frac{x_0 \tan^2\theta}{3(1-\tan^2\theta)} \left[\frac{z_0}{\left[(1+\tan^2\theta)(x_0^2+z_0^2)-x_0 \right]\sqrt{z_0+x_0^2}} \right.
$$

$$
\left. \left. - \frac{2(1+\tan^2\theta)z_0}{\left[(1+\tan^2\theta)(x_0^2+z_0^2)-x_0^2 \right]^2} \right] \right\} \tag{2-15}
$$

$$
E_x = \frac{\lambda}{4\pi\varepsilon_0} \left[\left(\frac{1}{\sqrt{1+\tan^2\theta}} - \frac{\tan^2\theta}{3(1+\tan^2\theta)^{3/2}} \right) \right.
$$

$$
\left(\frac{\partial}{\partial x_0} \ln \left(2\sqrt{(1+\tan^2\theta)(x_0^2+z_0^2)}-2x_0 \right) \right)
$$

$$
\left. + \frac{\partial}{\partial x} \frac{x_0 \tan^2\theta}{3(1+\tan^2\theta)\left[(1+\tan^2_0)(x_0^2+z_0^2)-x_0^2 \right]^2} \right] \tag{2-16}
$$

2-14

FLIGHT PATH

NASA 6

SPACE CHARGE

600 M

V/M

SIDE VIEW

FIELD GRAPH

SPACE CHARGE

PLUME

10°

TOP VIEW
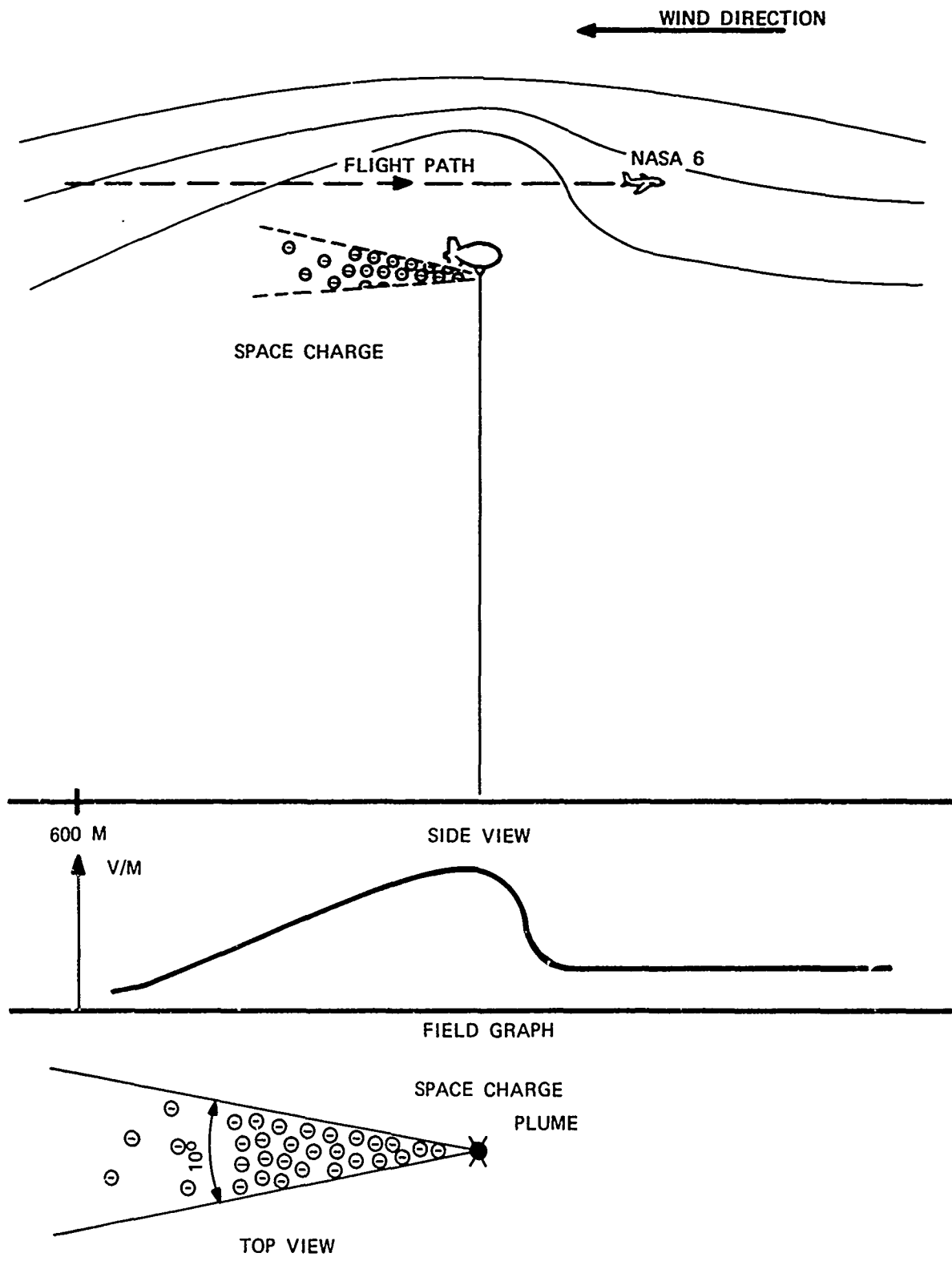
Figure 2-6.   Space Charge Plume As Detected By NASA-6 Instrumented Aircraft

where θ is the cone half-angle and λ is the line charge density
(assuming no spreading). (This model is more fully explained
in Volume II, Part A, Appendix E.)

For computing the effect of space charge on potential gradient
below the balloon, Pierce and Price modeled the vertical incre-
ment of space charge as a semi-infinite line charge (see figure
2-7). They obtained the following expression for the perturba-
tion (ΔE) of potential gradient caused by this space charge:

$$\frac{\Delta E}{\varepsilon_o} = -\frac{C}{2\pi\varepsilon_o} L \left\{ 1 + \frac{r}{L} \ell n \left(\frac{1 + [1 + (r/L)^2]^{1/2}}{r/L} \right) \right\} . \qquad (2\text{-}17)$$

where r is radial distance from the tether point, L is tether
length, C is system capacitance, and ε_o is permittivity of free
space.

2.4 MODELS FOR TETHER CURRENT

2.4.1 Intercepted Air-to-Earth Current

Charles B. Moore has calculated the flux capture cross section
for tethered balloons. Segments of this paper have been pre-
sented [1], but it is not yet available in its entirety. The
following is similar in approach to Moore's work. Also see
derivations by Pierce & Price, vol II, part B Appendix.

The tether distorts the electrical field since field lines must
intersect an equipotential surface at right angles. Since a well-
conducting tether is essentially a zero-volt equipotential, all
field lines within a certain distance of the tether curve over to
the tether and terminate on it as shown in figure 2-8. Thus, it
can be said that field lines which might otherwise have terminated
on the ground have been "captured" by the tether.

$$E_z = \int_o^h \frac{i(l)}{2\pi\epsilon_o Wl} \left(1 + \frac{r}{(r^2+l^2)}\right)dl$$
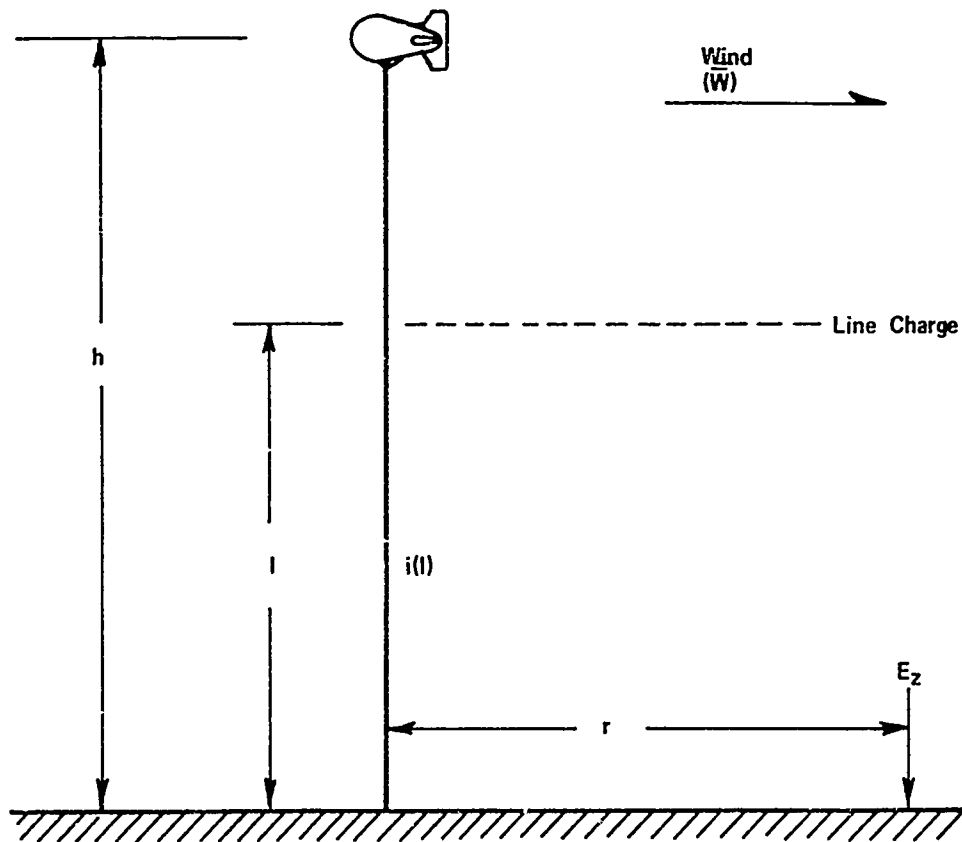
Figure 2-7. Model of Field Resulting From a Corona-Produced Line Charge
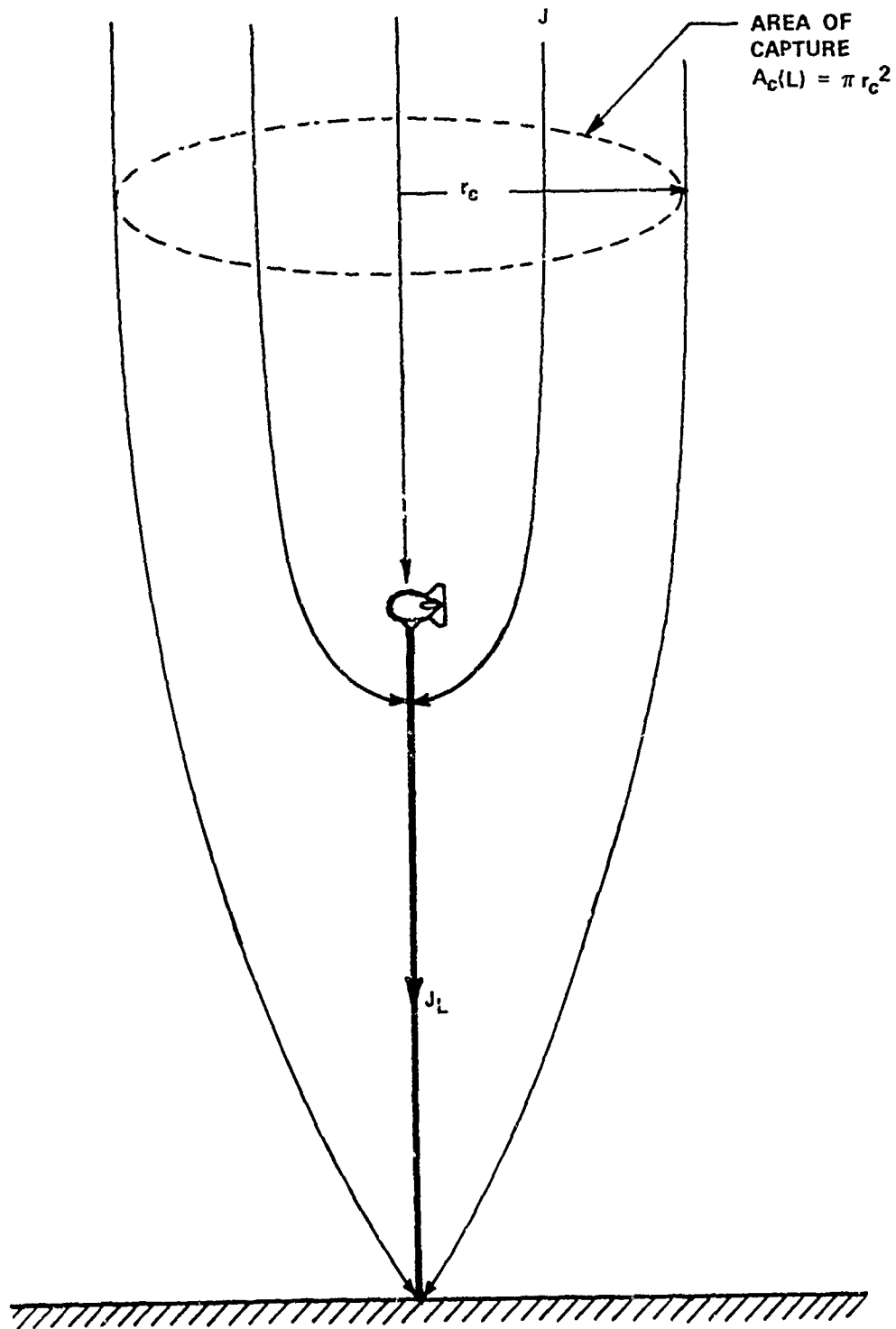
Figure 2-8.   Capture of Air-to-Earth Current by a Well-Conducting Tether

Since the field lines represent paths of charge flow from the
ionosphere to ground, this captured charge must now flow down
the tether. The most remote field line captured (considering
its radial distance from the extended line of the tether) is the
field line which terminates on the tether at ground level.

If that line is followed back along its trajectory until it is
perpendicular to an assumed flat earth, then the distance at
that altitude from the field line to the extended line of the
tether defines a radius of capture. Outside this radius field
lines will not be captured, but will have their trajectory dis-
torted to an extent which decreases as horizontal distance from
the tether increases. Within that radius, all field lines ter-
minate on the tether, and the air-to-earth current associated
with these lines will flow down the tether.

The radius of capture generates an area of capture. There will
be a component of tether current flowing down the tether equal
to:

$$I_{TA} = \pi R_c^2 J_z \tag{2-18}$$

where R_c is the radius of capture (in meters) and J_z is the air-
to-earth current (in amperes per square meter).

Based on the modeling of the tether as a grounded vertical prolate
half ellipsoid of length L and base radius b, Pierce and Price
(Volume II, Part B, page 5) have derived the following formula
for the area of capture, $A_c(L)$

$$A_c(L) = \frac{\pi L^2}{\ln\left(\frac{2L}{b}\right) - 1} \tag{2-19}$$

From which it follows that

$$R_C = L \left[\ln\left(\frac{2L}{b}\right) - 1 \right]^{1/2}$$

(2-20)

Moore (Volume II, Part A, page 19) has suggested a rough rule of thumb that the radius of capture is about half the balloon altitude.

2.4.2 Corona Current

The second component of the current along a conductive tether is due to corona. Corona is the ionization of air by intense fields which have been further intensified by the presence of highly curved or pointed conductors. The charge liberated into the air by the corona process is supplied by current flowing in the tether from ground. The occurrence of corona requires a potential gradient at the surface of the conductor, in excess of a certain "onset" value", typically 30 kV/cm, but variable with air density and source geometry.

In still air the ions drift away from the source at a rate proportional to potential gradient. Since the gradient decreases with distance from the conductor, the charge liberated by the corona process tends to accumulate around the source. The presence of this space charge reduces the local gradient thereby limiting corona production. If the ions are carried away by wind, the rate of corona production increases.

It has been shown that corona current produced by a point is proportional to the excess of potential over onset potential and also to the ion velocity [45] or,

$$i = a(V-V_o) \quad (W^2 + C^2 V^2)^{1/2}$$

(2-21)

In this equation, the square root term is the vector magnitude of ion velocity due the combined effects of wind and potential. V is the potential (referenced to ground) which would exist if the field were not distorted by the source.

V_o is the onset potential and a has a theoretical value of $2 \pi \varepsilon_o$ (5.56×10^{-11} farads/meter) [46], and W is wind velocity. C is an arbitrary constant.

Equation (2-21) applies to a point in corona. Corona current due to an incremental length of tether would have the same form, however, the total corona current would be determined by integrating (2-21) with respect to length from the point where onset occurs, to the upper end of the tether.

The relative values of computed tether current due to corona current and captured air-to-earth current under typical conditions are shown in figure 2-9.

2.4.3 Well and Poorly-Conducting Tethers

According to Pierce and Price, the transition from a poorly-conducting tether to a well-conducting tether is defined by a resistivity:

$$\rho = \frac{\ln\left(\frac{2L}{b}\right) - 1}{\pi \lambda L^2} \qquad (2-22)$$

where ρ is the transitional resistivity (ohms/meter)

  L is the tether length (in meters)

  b is the tether radius (in meters)

  λ is the air conductivity (typically 10^{-14} mhos/meter)

If tether resistivity is less than this value, then the tether can be considered well-conducting. The current flowing down the tether, excluding corona current, represents the air-to-earth current collected within an intercepting area $A_c(L)$ defined in equation 2-19. Conversely, if tether resistivity is much greater than the value given by (2-22), then the current flowing down the tether is E/ρ and the equivalent intercepting area is:

$$A_r(\rho) = \frac{1}{\lambda \rho} \qquad 2-21$$
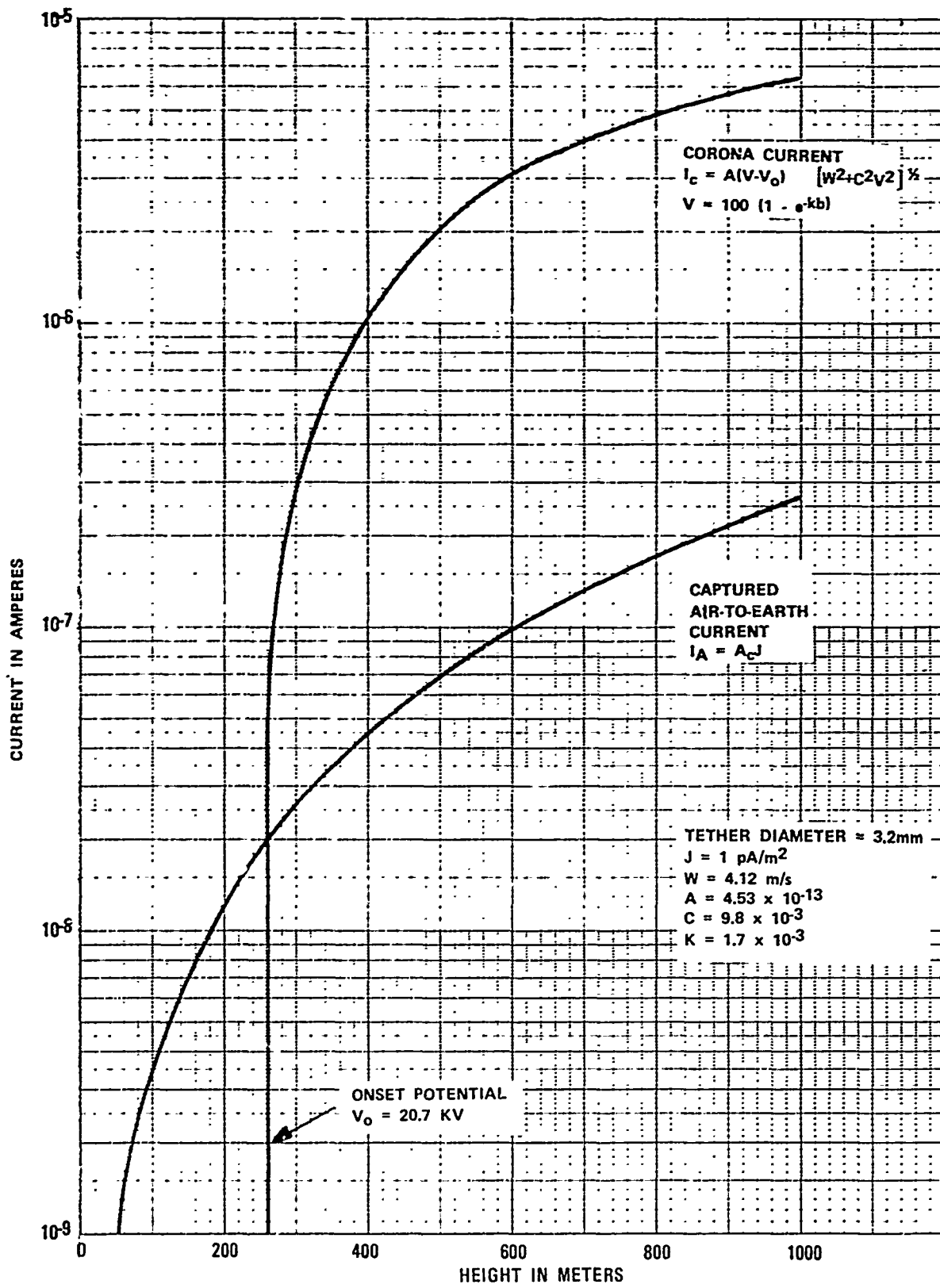
Figure 2-9.   Theoretical Tether Current

The transitional value just stated is that value of resistivity for which A_r (ρ) = A_c(L) for existing tether dimensions and electrical conditions. The transitional value is also that value for which the current flowing in the tether effects surface charge transfer sufficient to reduce the potential gradient along the tether. In figure 2-10, the transitional resistivity is plotted alongside of measured values of tether resistivity for various degrees of environmental exposure. Alignment of these two curves indicates that the synthetic fiber tethers under operational conditions are poorly-conducting when clean and are transitional to well-conducting after a few days of atmospheric contamination. Experimentation conducted to determine the resistance of operational tethers is described in appendix B.

2.5 SYSTEM CAPACITANCES

For several of the models described herein, system capacitances are required. Latham has calculated the following for the three balloons used (Volume II, Part A, Appendix C):

These capacitances are plotted in figure 2-11.

2.5.1 Capacitance of Balloon to Free Space

Schjeldahl (5,300 ft^3) ["Baldy"]	300 pF
BJ+3 (84,000 ft^3)	900 pF
Family II (205,000 ft^3)	1400 pF

2.5.2 Capacitance of Tether Cable to Ground

This capacitance is approximated by C = 1.3 h, where C is capacitance (in picofarads) and h is balloon height (in feet). More precise formulation is given in the referenced section of Volume II.

Pierce and Price obtained similar results by a different approach. (See Volume II, Part B, page 22.)

(A) RESISTIVITIES OF NOLARO SAMPLES
    EXPOSED TO CAPE CANAVERAL ENVIRONMENT

(B) REGIONS OF WELL AND POORLY CONDUCTING
    TETHER BEHAVIOR
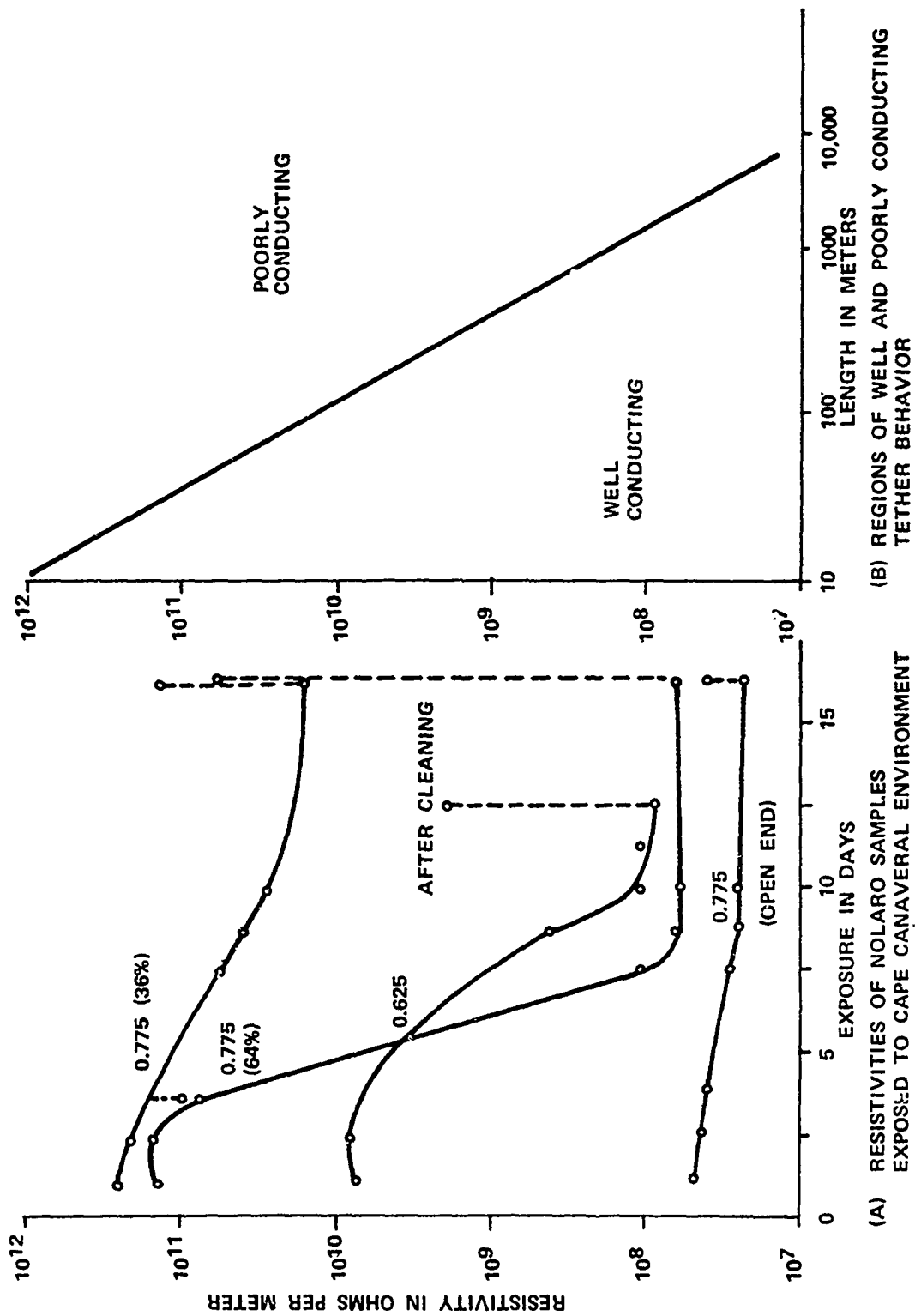
Figure 2-10.   Tether Resistivity
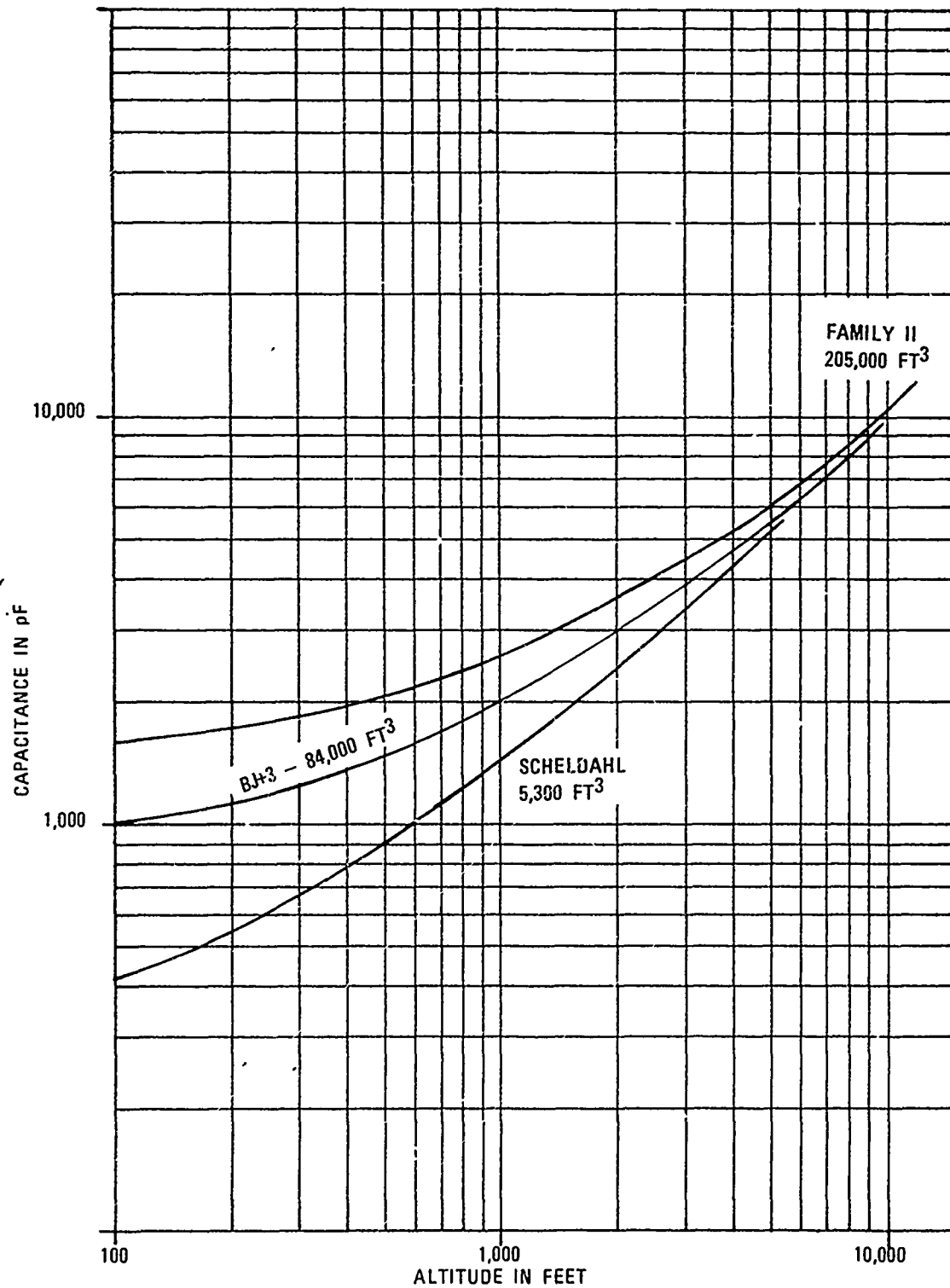
Figure 2-11. Capacitances of Balloon Systems

2.5.3 Capacitances of Ungrounded Winch to Ground

For the experiments which involved isolating the conductive tether from ground, Pierce and Price calculated the capacitance of the horizontal segment from the sheave to the winch (93 pF) and the capacitance of the winch (4.3 nF). These calculations are for a nonoperational system, but the formulation applies to concepts which could be encountered in operational systems (see Volume II, Part B, page 22).

2.6 RESULTS AND INTERPRETATION OF EXPERIMENTS

2.6.1 Data From Instrumented Aircraft Overflights

The aircraft flights were conducted on upwind and crosswind headings, which carried the aircraft directly above the balloon at flight levels nominally 100, 200, 500, and 1,000 ft above the balloon (see figure 2-6). The intent of these tests was to determine the extent of field intensification above the balloon for each type of tether and to determine the applicability of the system models devised. In all, eight such flights were conducted: Three over the 5,300 ft^3 Baldy balloon with steel tether and two with nylon, one over the 84,000 ft^3 BJ+3 with a 0.625 inch Nolaro tether, and two over the 205,000 ft^3 Family II balloon with 0.775 inch Nolaro.

To provide a baseline, the aircraft also flew identical patterns over the 500 ft wind tower at Kennedy Space Center.

2.6.1.1 Processing of Aircraft Data

Measurements of the E-field when the aircraft was directly above the balloon were compared with the theoretical models as follows:

1. Theoretical field intensifications (E_z/E_O) based on the grounded prolate ellipsoid model and also

the grounded conducting horizontal ellipsoid model were computed for each flight level. These theoretical values and the actual measurements, are compared in figure 2-12.

2. Assuming the balloon to be a charged prolate ellipsoid in free space, a mean value of charge on the balloon was computed from equation 2-14.

    The mean charge thus determined was assumed to be the "measured" charge of the balloon. This charge was then reinserted into equation 2-14, and a theoretical potential gradient anomaly was plotted as a function of height above the balloon. These curves, plotted together with the observed anomalies, are given in figure 2-12.

3. Theoretical values of charge for a balloon charged to equilibrium with the ambient field were computed, based on the assumption that a balloon at zero potential in a region where the ambient potential is V, must be charged to a value $Q = CV$ where C is the capacitance from balloon to air. These values are given in table 2-1 along with the "measured values" calculated from equation 2-14.

2.6.2   Processing and Evaluation of Ground Data

2.6.2.1   Field Measurements at Ground Level

For determining the effect of the balloon systems on vertical field at various points on the ground, field mills were placed at intervals of 10, 100, 200, and 500 feet downwind from the tether point; however, wind shifts were frequently encountered during the tests. The value of the E-field at each measuring
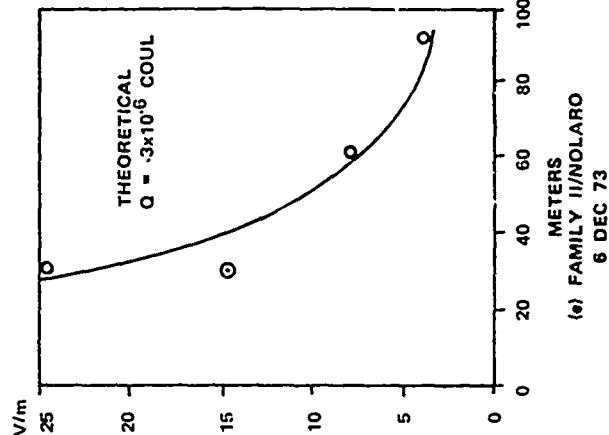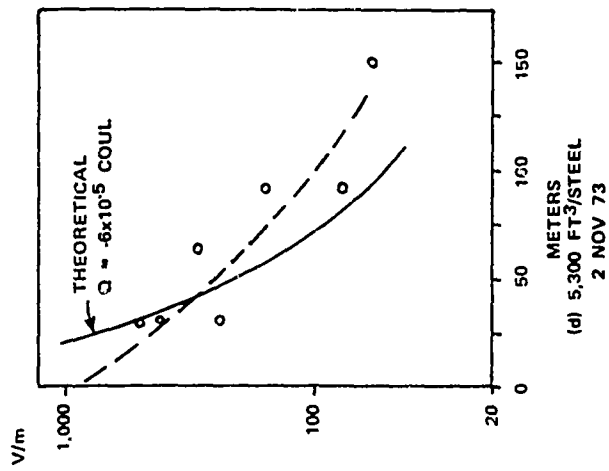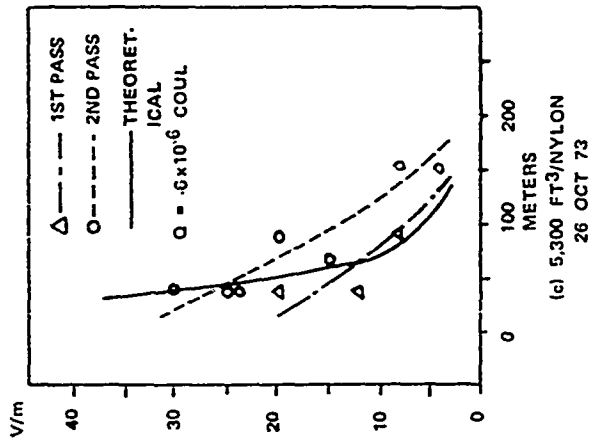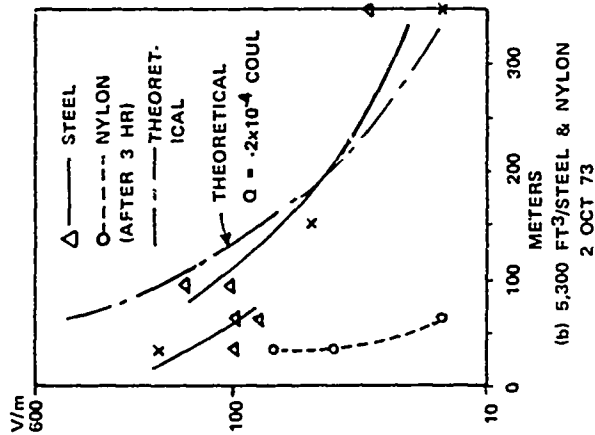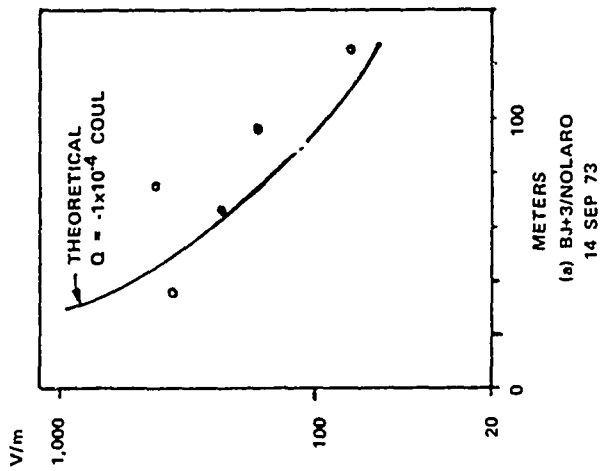
Figure 2-17. Potential Gradient Anomaly as a Function of Height Above the Balloon in Meters

TABLE 2-1

NASA OVERFLIGHT DATA

Date of Flight	Balloon/Tether	Altitude in meters	Inversion Height in meters	Ambient Pot. Grad. V/m	Capacitance of Balloon in picofarads	Charge on Balloon in coulombs*	
						Theoretical	Calculated
14 Sep 73	BJ+3/Nolaro	1,067	NA	80	900	-7.7×10^{-5}	-10^{-4}
2 Oct 73	Baldy/Steel	396	NA	80	300	-9.5×10^{-6}	-2×10^{-4}
26 Oct 73	Baldy/Nylon	1,219	1,500	35	300	-1.3×10^{-5}	-6×10^{-6}
2 Nov 73	Baldy/Steel	762	1,200	150	300	-3.4×10^{-5}	-6×10^{-5}
6 Dec 73	Family II/Nolaro	1,524	1,400	5 (at balloon)	8,000	-1.2×10^{-3}	-3.5×10^{-3}

* Theoretical charge is calculated from Q = CV

Calculated charge is from measured electric field anomalies

location after the winch and balloon had been physically removed from the test area (or in some cases before it arrived) was taken as the unperturbed ambient.

For selected tests, the field suppression ratio E_z/E_O was plotted as a function of the ratio of radial distance to balloon height (r/a). The theoretical field suppression for the grounded vertical ellipsoid model was plotted on the same graphs for comparison.

The data for a flight of the 5,300 ft^3 Schjeldahl balloon with steel tether is given in figure 2-13. As indicated by these graphs, the vertical ellipsoid model agrees reasonably well with the data at the 100 and 200 ft locations. The measurements at the 10 ft location were largely dominated by the winch truck, a massive grounded structure with sufficient vertical development to affect readings at that location.

In a separate analysis of the 2 November data, Pierce and Price compared the actual field suppression with that predicted by two models: (1) a grounded vertical prolate ellipsoid (similar to Latham's) and (2) a horizontal line charge to account for the effect of corona-produced space charge flowing downwind as discussed in paragraph 2.3.4.

As shown in figure 2-14, the line charge model fits the data more closely than the vertical ellipsoid model - an indication that space charge has a pronounced effect at ground level as well as at flight level. A related effect noted during testing was variation in field and in earth current as wind direction changed. Unfortunately, wind direction was not recorded. Professor C. B. Moore has detected space charge blowing downwind from dielectric tethers with sufficient concentration to corrupt measurement of air conductivity by balloonborne instruments (per informal conversations).
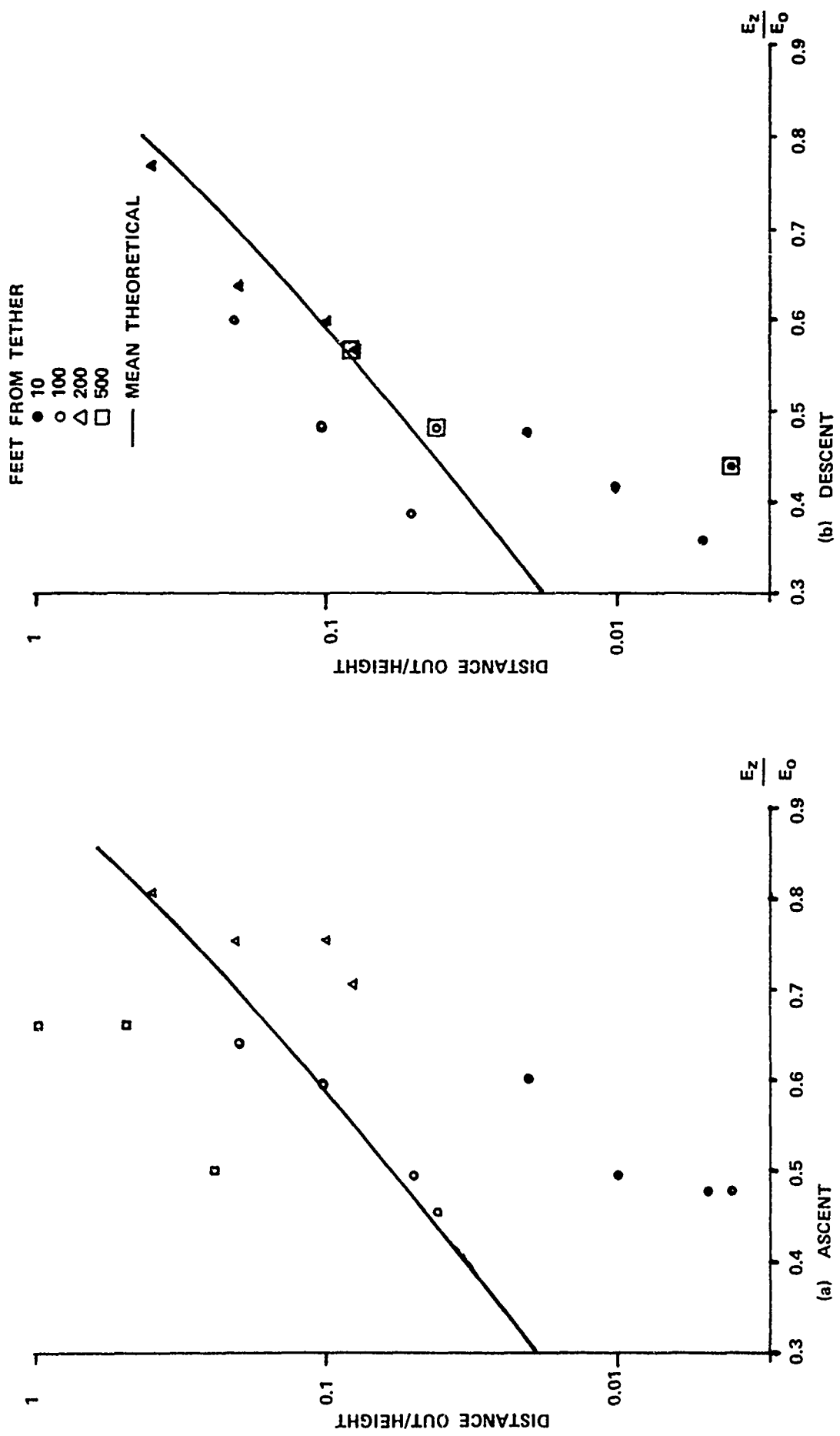
Figure 2-13. Suppression of Potential Gradient at Ground Level
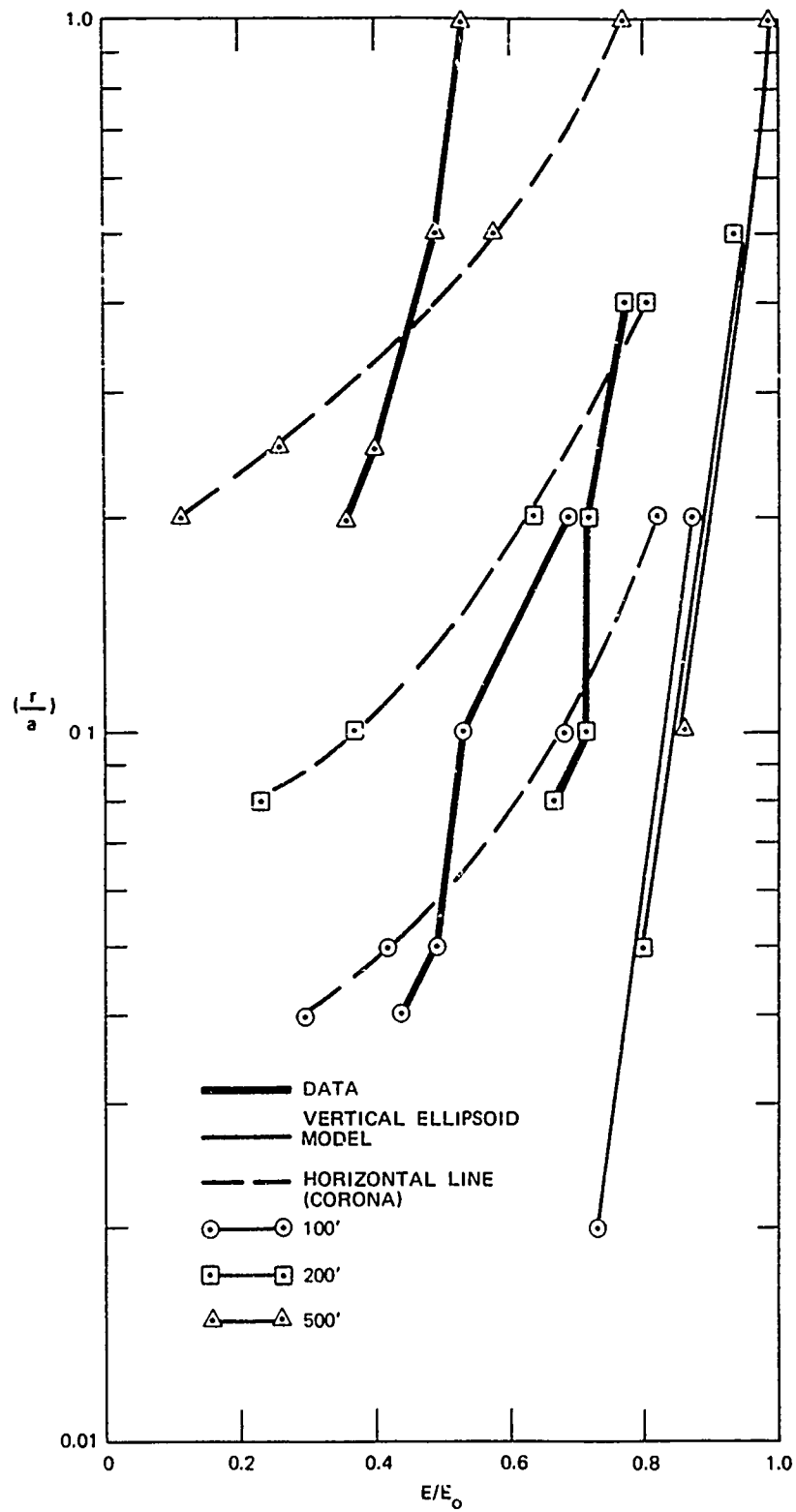
Figure 2-14. Vertical Field Supression on the Ground at Various Distances From Tether Point, Comparison of Data With Vertical Ellipsoid and Horizontal Line Charge Models

Poorly conducting tethers (i.e., nylon and Nolaro) did not appreciably suppress the vertical field at ground level under static conditions. However, during descent, small field perturbations were noted. This was attributed to rapid physical lowering of bound negative charge on the balloon.

2.6.2.2 Tether Current

Well-Conducting Tethers

Tether current vs altitude is plotted in figure 2-15 for several flights when the balloon was flown with a 1/8-inch diameter steel cable tether. The currents observed are considerably in excess of that predicted by the "capture" effect discussed in section 2.4.1. The magnitudes and attitude dependence of the data are more conformed to the theoretical corona current suggested by Chalmers and Mapleson [2].

$$I_C = kW^{1/4} (Fh)^{7/4} \quad \text{see paragraph 2.4.2} \tag{2-21}$$

A plot of this formula for $k = 10^{-8}$ is included in figure 2-15. The data agrees reasonably with the research done by Chalmers and Mapleson, differing primarily in the evaluation of the factor k. This difference is attributable to the difference in the diameter of the tether used. In several of the tests, abrupt increases occurred as the balloon ascended from 1,500 to 2,000 feet (25 Sep, 17 Oct). This change has been interpreted as the initiation of corona current.

A comparison of the RML test data with that obtained by Davis and Standring [3] (Volume II, Part B, page 10) is shown in figure 2-16. The dashed line in curve (A) represents the discontinuity period marking the transition from captured air-to-earth current to corona current.
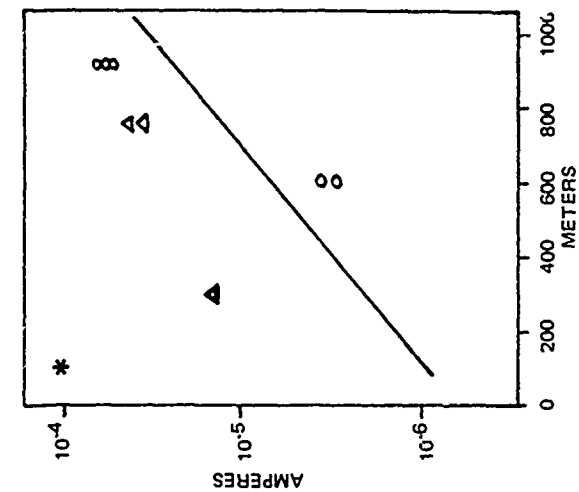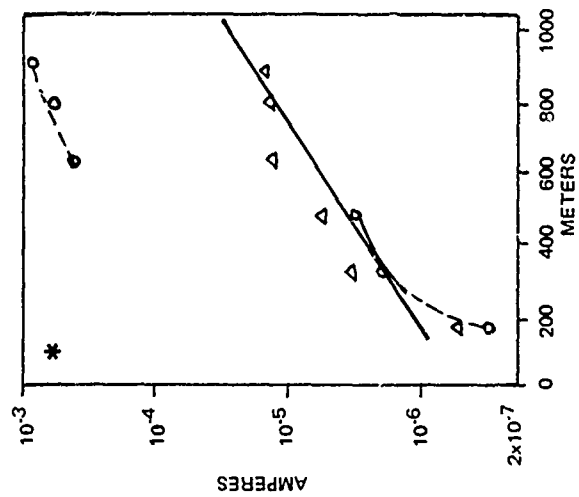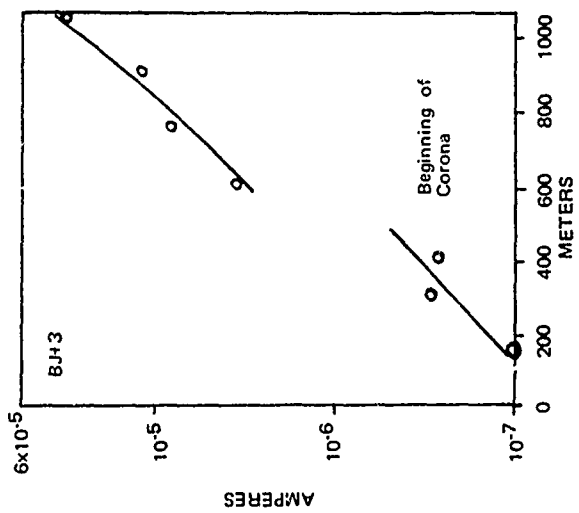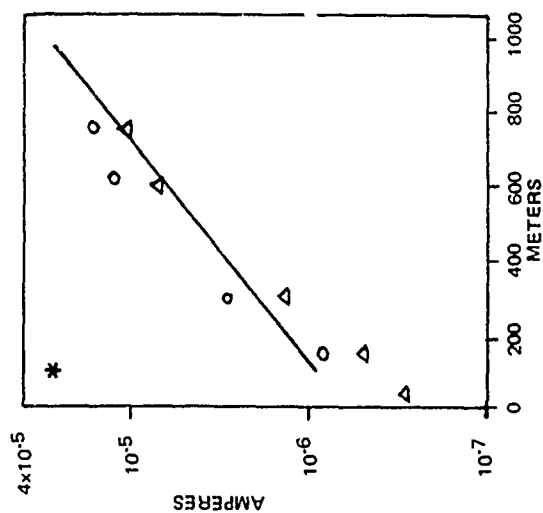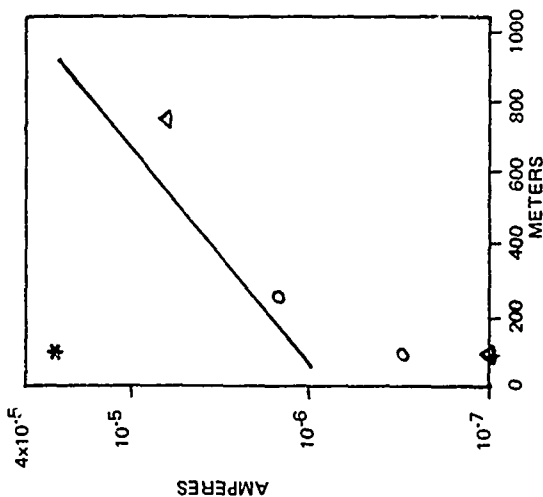
Figure 2-15. Tether Current as a Function of Balloon Altitude in Meters
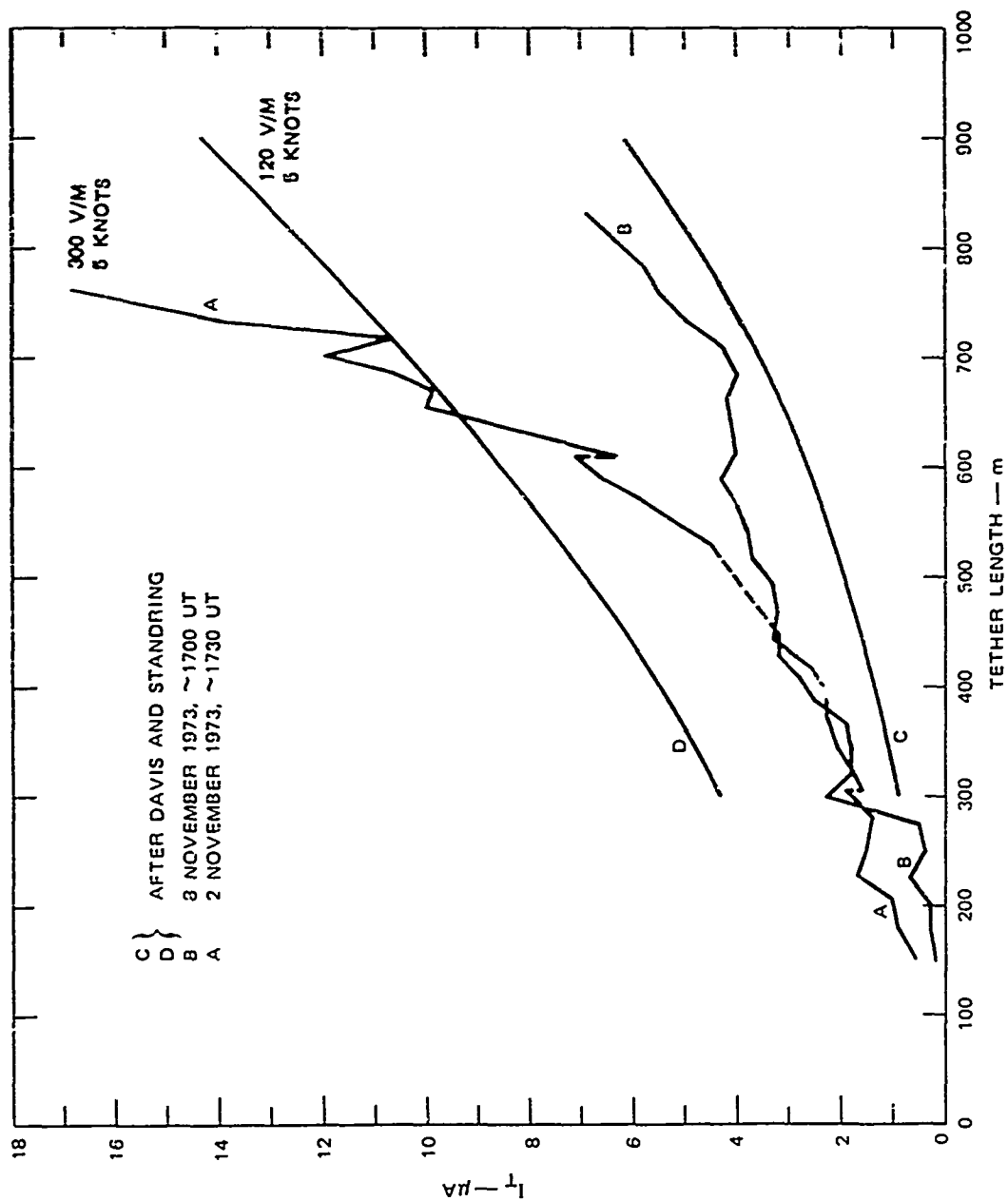
Figure 2-16. Current in Conducting Tether as a Function of Balloon Altitude

2-35

The data from Davis and Standring (curves 1 and 2) is "smoothed" from data which, according to the authors, varied as much as 5 µA from the fitted curve. It is likely that this smoothing masks a discontinuity similar to that observed between 1,500 and 2,000 feet in the RML data. Because the tethers used by Davis and Standring were larger* corona current would be initiated at a higher altitude, possibly beyond the 900 meters shown here.

Dielectric Tethers

Eight of the sixteen flights were flown with dielectric tethers, three with the 5,300 ft³ balloon (commonly referred to as Baldy) and 1/4-inch nylon, one with the 84,000 ft³ BJ+3 balloon and 0.625 inch Nolaro, the remaining four with the 205,600 ft³ Family II balloon and 0.775 inch Nolaro. During these flights, the tether current varied from 10^{-7} to 10^{-9} A. Only slight dependence of current on altitude was noted, but a much stronger dependence on field was evident. This dependence is shown in figure 2-17. This data is from the 5,300 ft³ balloon tethered by a 1/4-inch diameter un-jacketed nylon rope. Here it can be seen that tether current was on the order of a µA and followed variations in gradient until met by a brief rain shower at 1447, at which time a sharp increase was noted, despite a reduction of gradient.

Figure 2-18 shows similar data from the 205,000 ft³ balloon tethered by 0.775 inch jacketed Nolaro. Here it may be seen that the tether component is driven negative by a 30% reduction of gradient. During this period the current appears to be responding to ΔE more than E. This is evident from the comparison of the tether current with the air-to-earth current measurement 500 feet out. The latter is considerably influenced by displacement current. During this flight, the balloon was above the boundary layer.

---

* Davis and Standring's work was based on 5mm (0.2 inch) diameter rope. This project used 3.2mm (0.125 inch) diameter rope.
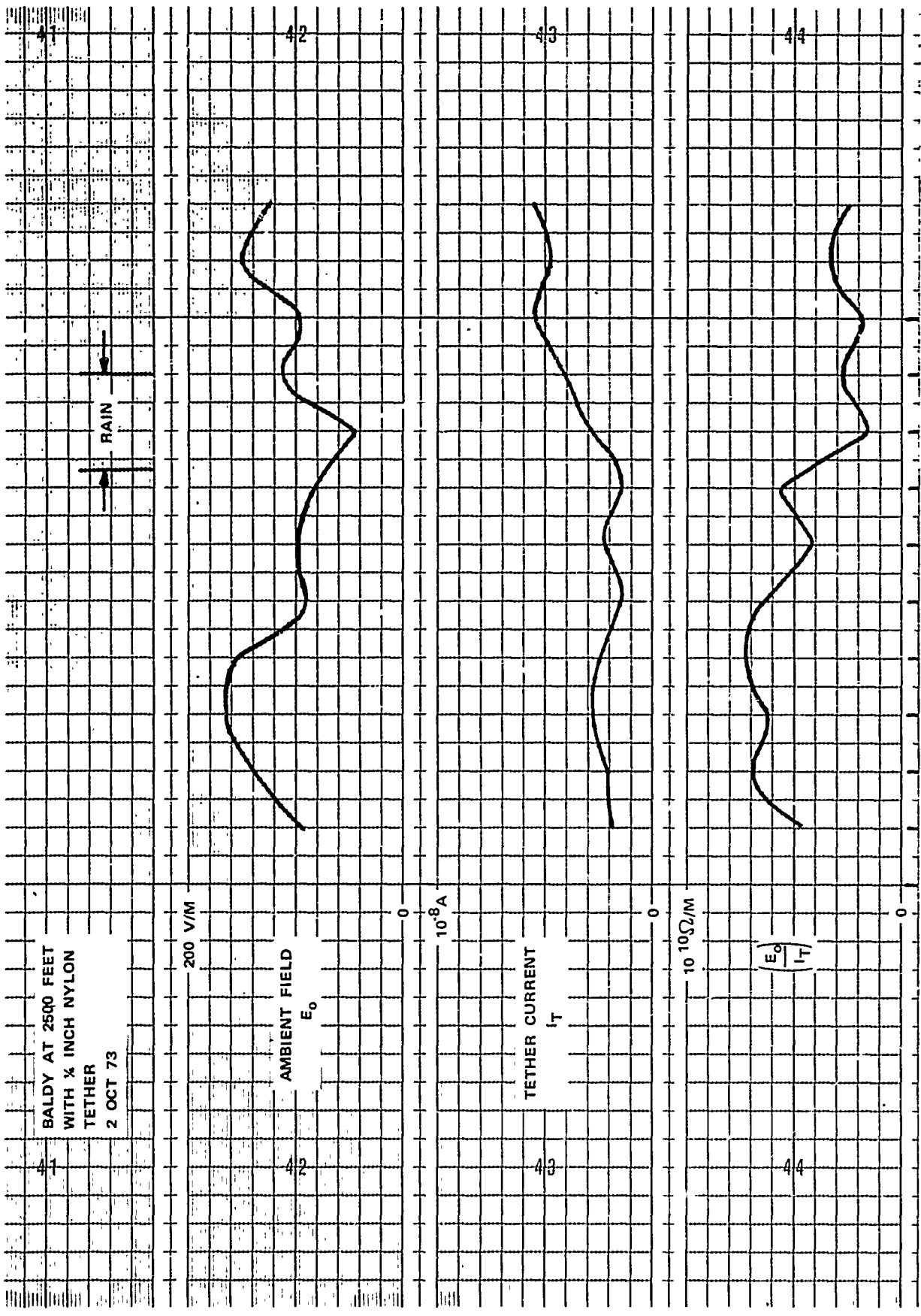
Figure 2-17. Effect of Rain on Tether Current
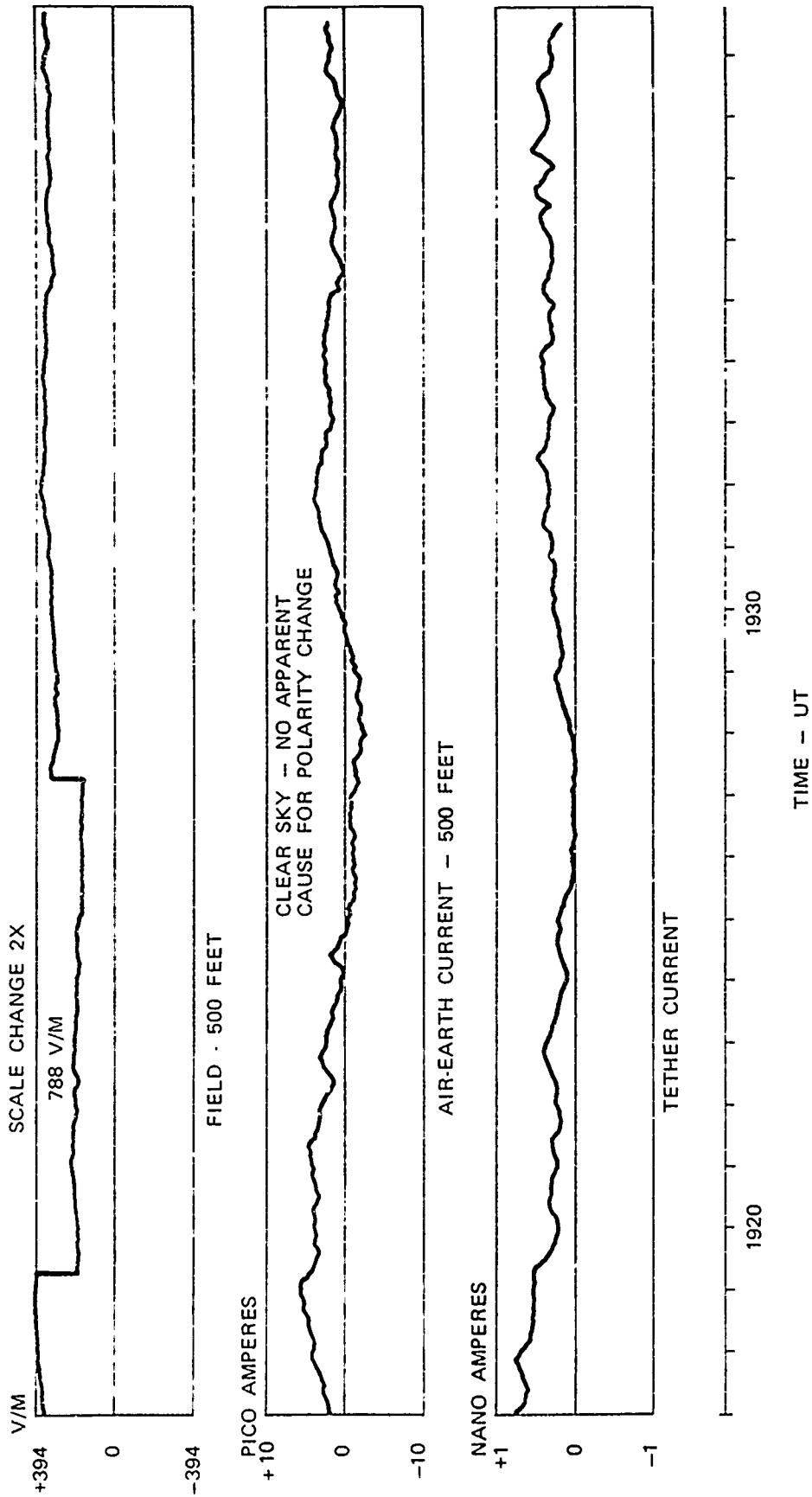
Figure 2-18.   Tether Current on 0.775 Inch Nolaro Tether

Induced Currents

Currents induced in wire rope tethers by distant lightning were
measured using an rf current probe. A pulse measuring 300 A peak-
to-peak was received from a storm which was at least 30 km away
(no weather was in sight at the time). On another occasion, a
25 A peak-to-peak pulse was received from a storm which, accord-
ing to the sferic characteristics was probably over 100 km away.
Figure 2-19 is a photograph of a typical sferic of the type re-
ceived.

VERTICAL SCALE:
60 A/cm

TIME SCALE:
20 μs/cm
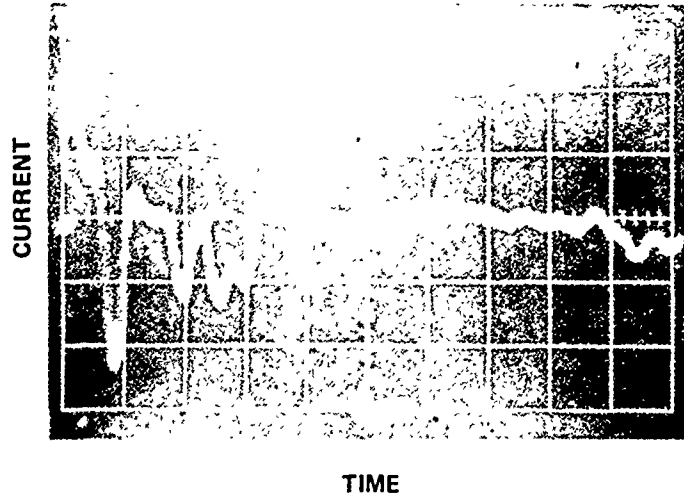
Figure 2-19. Sferic Pulse Received on a 1/8-Inch Steel Tether Cable
With Balloon Height of 2,500 Feet

2.6.3 System Charging Time for a Conducting Tether

During several flights using 1/8-inch steel cable with the 5,300 ft^3 balloon, the winch was isolated from ground. The system was allowed to float to its equilibrium potential, which was measured by means of a specially calibrated field mill mounted under the winch. Theoretically, this equilibrium potential should be the mid-altitude potential for the balloon.

$$V_e = \frac{E_o h}{2} \qquad\qquad (2\text{-}23)$$

During these experiments, an audible crackling from corona was heard in the vicinity of the fairlead sheave, and potentials up to 40 kV were measured. Potential gradient increased from an unperturbed ambient of 120 V/m to values of 4 to 8 kV per meter 10 feet from the sheave and 250 V/m 500 feet away. When the system was discharged by a grounded chain, sparks approximately 1 cm long would leap to the chain and almost instantaneously restore the gradient to normal values. The signal conditioning circuitry for the field mill usually failed during the experiment for causes which were never identified. However, a complete set of data was obtained on 31 October and the system charging time was as indicated in figure 2-20. The equilibrium potential was 40 kV, as compared to a value of 55 kV computed from (2-23) and values of 64 to 73 kV implied by the measurements of Vonnegut, Markson, and Moore'[4].

The charging time constant computed from the 31 October experiment was approximately 6-7 seconds. With the system capacitance as given in figure 2-11, a corona charging resistance of approximately 1.5×10^9 ohms was calculated.

As indicated in figure 2-20, the conducting tether system achieves equilibrium in less than a minute, and is therefore capable of charging at approximately the rate of balloon ascent.
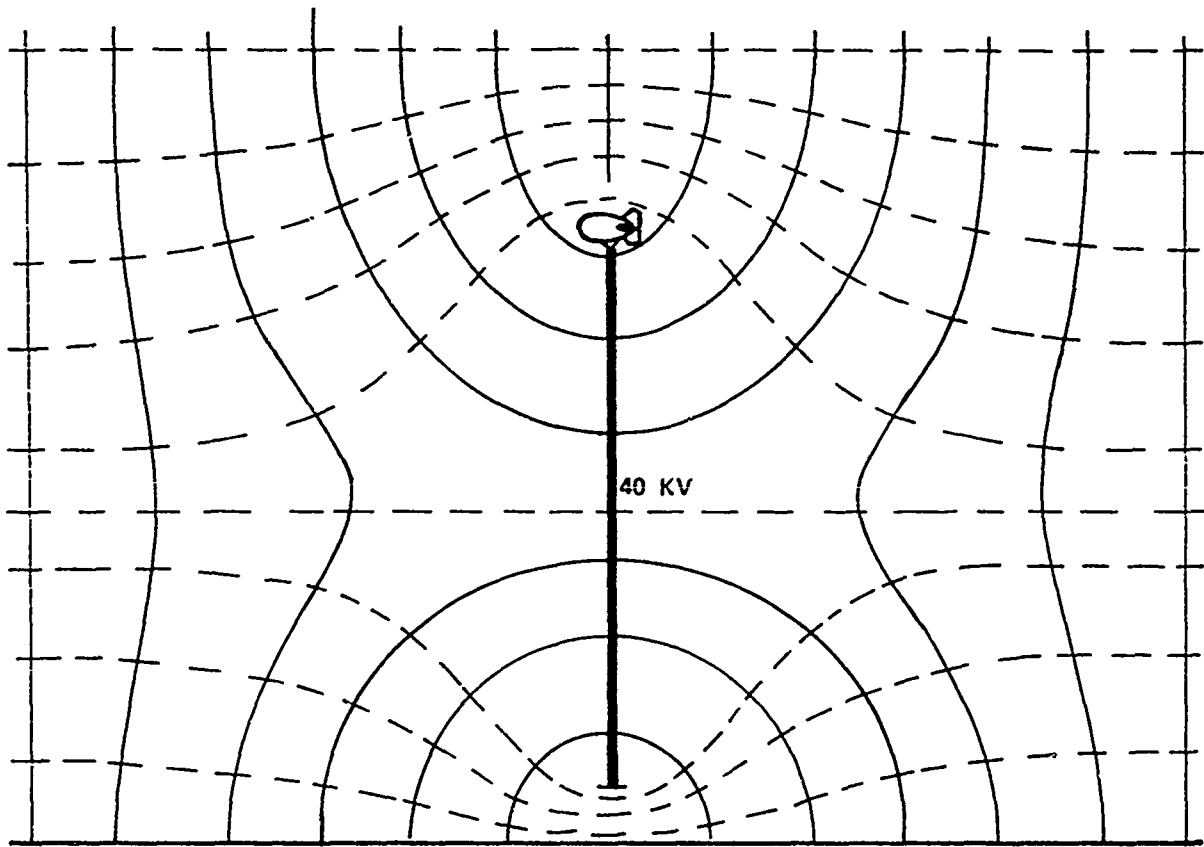
(a) THEORETICAL FIELD PATTERN

40 KV
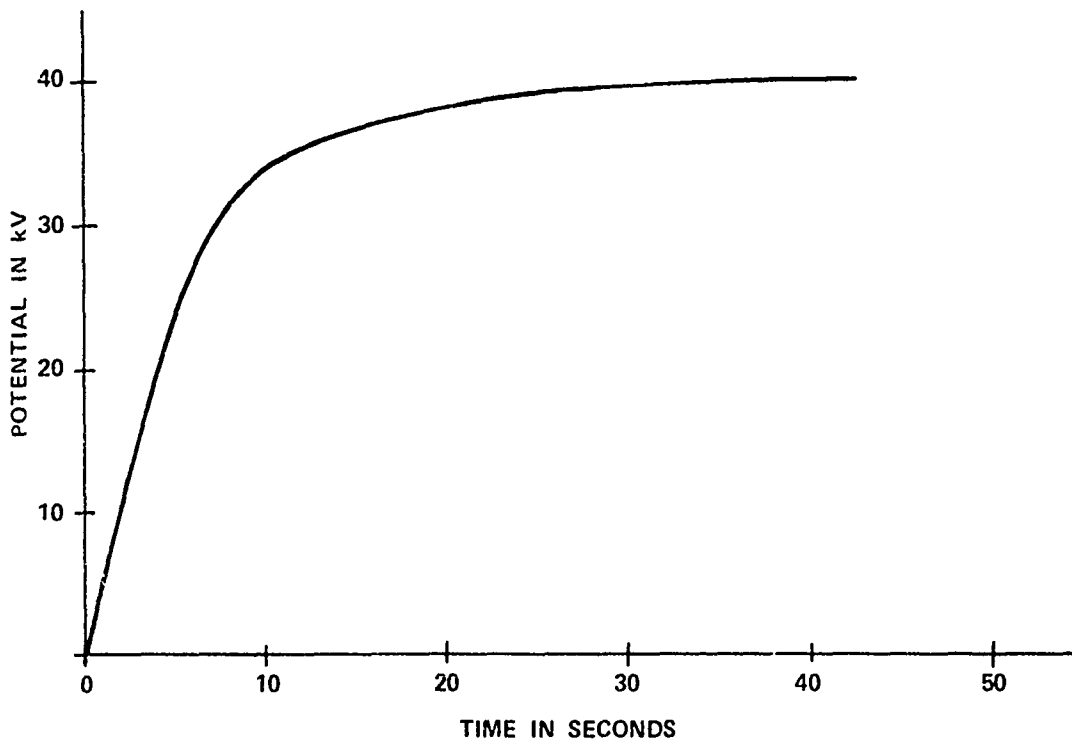
(b) SYSTEM CHARGING TIME

Figure 2-20. The Effect of Isolating a Conductive Tether

2.6.4 Comparison of System Models with Measurements

Measured field intensification above the balloon greatly exceeded values predicted by the two grounded conducting ellipsoid models, as indicated in figure 2-21. Note that the greatest intensification occurred for the BJ+3 balloon with a 0.625 inch Nolaro tether. This balloon appeared to be fully charged within one hour of ascent. The apparent charge acquired by the BJ+3 was consistent with current measured in the tether. Measured tether resistance for the 0.625 Nolaro was found to be fully one order less than that of the other materials, e.g. 0.775 Nolaro (see figure 2-10a). This is a possible consequence of environmental exposure.

Somewhat closer agreement between measurement and theory was achieved for the horizontal charged ellipsoid model. See figure 2-21 and table 2-1 (page 2-29). However, all of these models tend to underestimate field intensification high above the balloon and to overestimate it near the balloon. It has been determined that this failure of the balloon system to model as a simple geometric shape is the result of a cloud of space charge extending downwind from the balloon, and creating a field anomaly which predominates over the physical geometry of the system. The presence of this space charge plume is indicated by the data from the flight of 2 Nov 73 (see Volume II, Part A, page 15). On the upwind pass 33 meters above the balloon, a gradual increase in vertical field was noted while the aircraft was downwind, and a rapid decrease was detected immediately above the balloon. The space charge was modeled as a wedge-shaped distribution. This model with a cone angle of 10° was in reasonable agreement with the field variations on both vertical and lateral axes of the aircraft. This modeling is described in greater detail in Volume II, Part A, page 12, page 13, and appendix E.

2-42
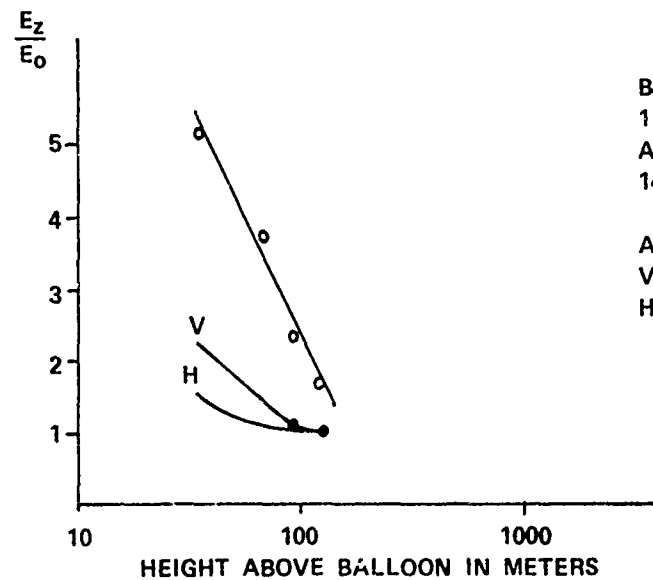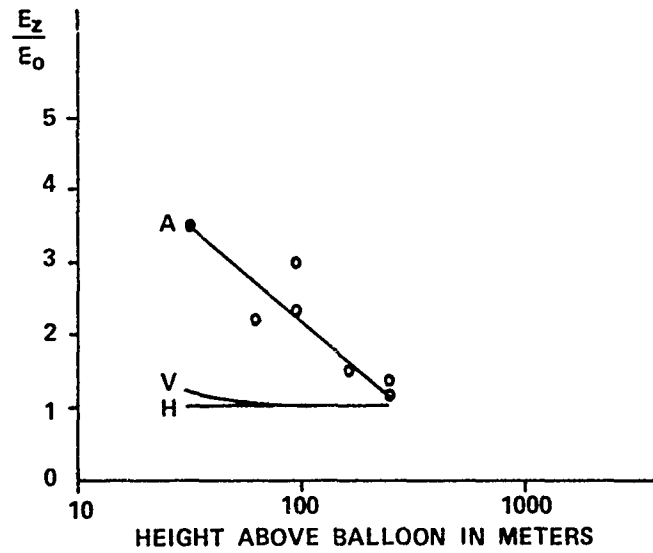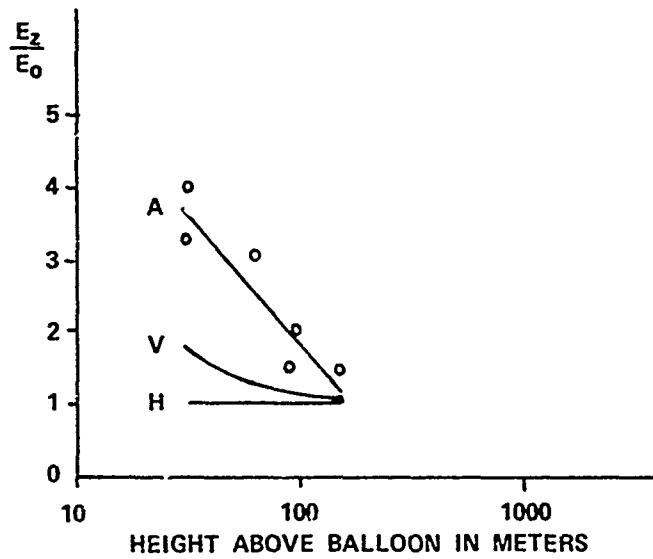
Figure 2-21. Field Intensification Over the Balloon,
Comparison of Measurements With Models

2-43

Additional evidence of this space charge distribution is given by the fact that tether current is apparently dominated by corona current (for the conductive case) rather than by intercepted air-to-earth current (see Volume II, Part A, page 19).

The 5,300 ft^3 Schjeldahl balloon with a 1/4-inch nylon tether produced negligible field intensification immediately after ascent. However, charging as indicated by increased field intensification was apparent a few hours after ascent.

The Family II balloons, flying at altitudes in excess of 7,000 feet, produced negligible field intensification. This is attributed (by Latham) to the fact that these balloons were flying well above the atmospheric boundary layer in an area of relatively high air conductivity. Consequently, more charge was transferred through the air surrounding the tether than through the tether itself. This observation is consistent with the very low tether currents measured (less than 1 nA).

As shown in figure 2-13, ground level potential gradient measurements on a balloon with a well-conducting tether agree reasonably well with those computed for a vertical prolate ellipsoid if we consider two perturbations: (1) The winch truck obviously biased measurements at the 10 ft location. (2) As Pierce and Price determined, space charge flowing downwind from the tether causes a deviation from that computed for the vertical prolate ellipsoid model. (Their line charge model predicts this effect qualitatively, and the agreement of the model with actual data would probably be closer if crosswind diffusion were considered.

The poorly-conducting tether did not appreciably affect potential gradient at ground level— apparently due to the failure of this tether material to produce corona current or intercept flux lines to an appreciable extent.

Current flowing in well-conducting tethers agreed more closely with that predicted for corona current than with intercepted air-to-earth current. Current flowing down poorly-conducting tethers is determined by ambient potential gradient and tether resistance. The charge assumed by the balloon is consistent with the current and charging times involved.

2.7 SUMMARY

A tethered balloon will charge to a value near ground potential. For a wire rope tether, this charging is accomplished in less than a minute. If the tether is a poor conductor, two hours or considerably longer may be required. Once equilibrium has been achieved, the balloon with a poorly-conducting tether produces a field intensification comparable to and possibly equal to that of the balloon with a well-conducting tether. The balloon with

a well-conducting tether produces a corona space charge which diffuses downwind in a roughly conical patterr. This space charge increases the potential gradient at the balloon's altitude to distances downwind which would be outside the influence of balloon/tether geometry.

Conversely, potential gradient at ground level underneath this charge plume is suppressed. The associated corona current flowing in the tether determines the tether current.

In the absence of space charge (as in the use of poorly-conducting tethers), the dominant geometry of the balloon system at and above flight level is that of a charged horizontal prolate ellipsoid.

At ground level and at intermediate altitudes near a well-conducting tether, the dominant geometry is that of a grounded vertical prolate ellipsoid. In a sector of about 20° downwind, potential gradient is more affected by space charge than by direct effects of the tether.

2-46

SECTION 3

PREDICTION OF LIGHTNING STRIKES TO TETHERED BALLOONS

No precise method of determining the probability of lightning striking a balloon has been developed. However, a systematic approach has evolved for predicting the number of lightning flashes a tall structure will receive during a given period. While lacking the desired precision, this method, based on combined theory and observation is probably the best available approach. As presented by Cianos and Pierce, the procedure is described roughly as follows:

The distance from which the structure will attract cloud-to-ground lightning is determined. This radius is converted to an area of attraction. This area is multiplied by the number of flashes to ground per unit area. This figure is then increased by a factor to account for lightning triggered by the structure. Pierce and Price have given guidance for extending this approach to tethered balloons (see Volume II, Part B, pages 24—45).

3.1 FLASH DENSITY

The estimated number of lightning flashes per square kilometer, per unit time is given by [6].

$$\sigma = \sqrt{0.03T + 0.0009T^4} \tag{3-1}$$

where T is the number of thunderstorm days for the time unit considered.

This expression as function of thunderstorm days per month is shown in figure 3-1. The thunderstorm day statistic is an accepted measure of thunderstorm activity and is available for all parts of the world.

$$\sigma_m = aT_m + a^2 T_m^4$$

FLASH DENSITY (σ_m) — FLASHES PER MONTH/KM^2

THUNDERSTORM DAYS PER MONTH
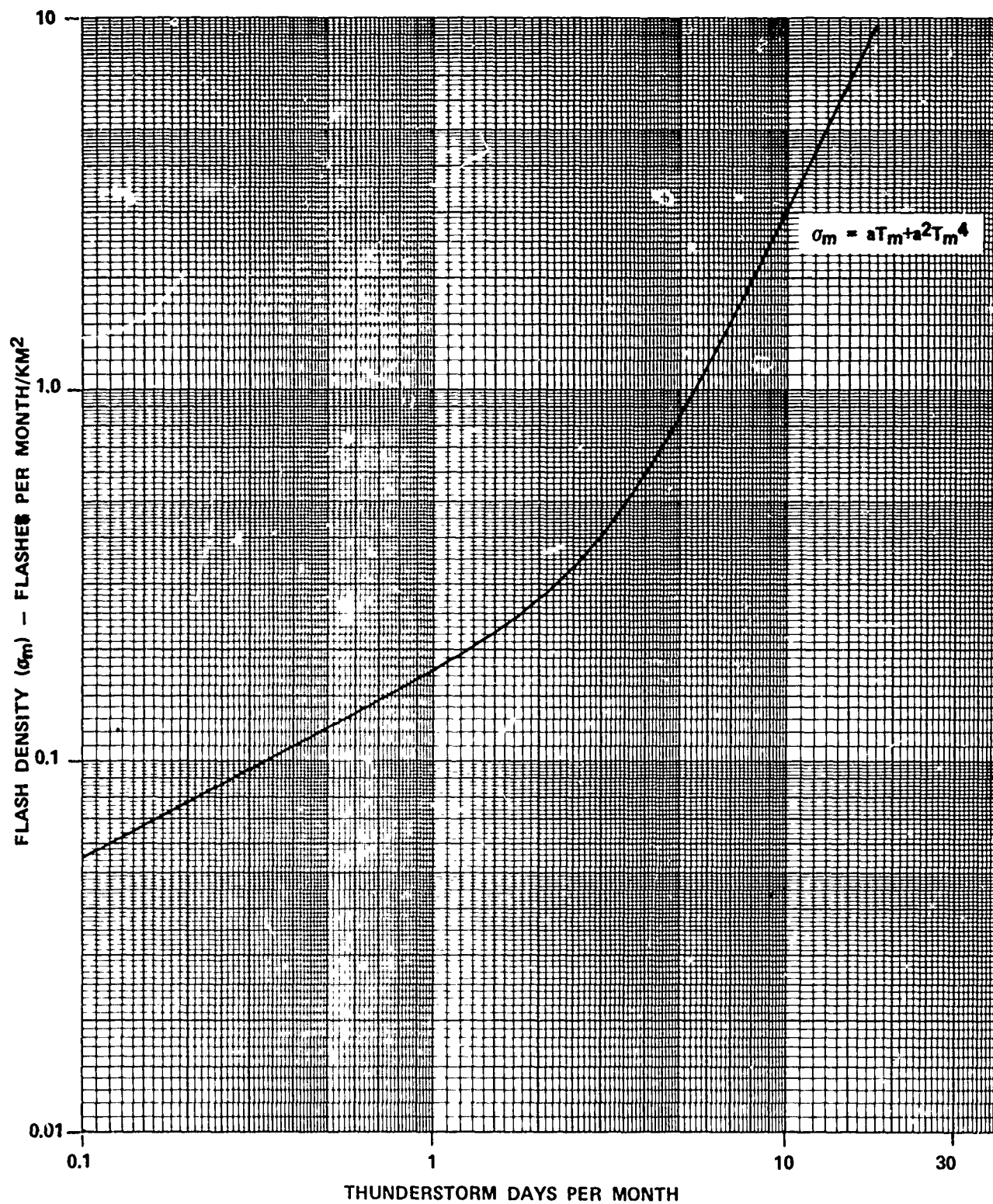
Figure 3-1. Flash Density

3.2 PROPORTION OF FLASHES GOING TO GROUND

The flash density includes intercloud and intracloud flashes, as
well as flashes to ground. The fraction of all flashes which go
to ground is given by Cianos and Pierce [7] as

$$P = 0.1 \left[1 + \left(\frac{L}{30} \right)^2 \right] \qquad (3-2)$$

where L is the latitude (degrees) of the structure.

They also give the following formula, which is attributed to
research performed by Westinghouse

$$P = 0.05 + \frac{\sin L + 0.05}{(T_m + 3)^{1/2}} \qquad (3-3)$$

where T_m is the monthly flash density.

Flash densities for the latitudes of Cape Canaveral and Cudjoe
Key, as computed using equations (3-2) and (3-3), are plotted in fig-
ure 3-2. It may be seen that equation (3-3) represents the worst
case during the months of low thunderstorm activity.

The estimated number of flashes to ground is given by the product
$\sigma_m P$ Monthly predictions for Cape Canaveral and Cudjoe Key,
Florida are given in table 3-1.

3.3 AREA OF ATTRACTION

The area over which the balloon can be expected to attract all
lightning which would otherwise go to ground is known as the area
of attraction, A_a:
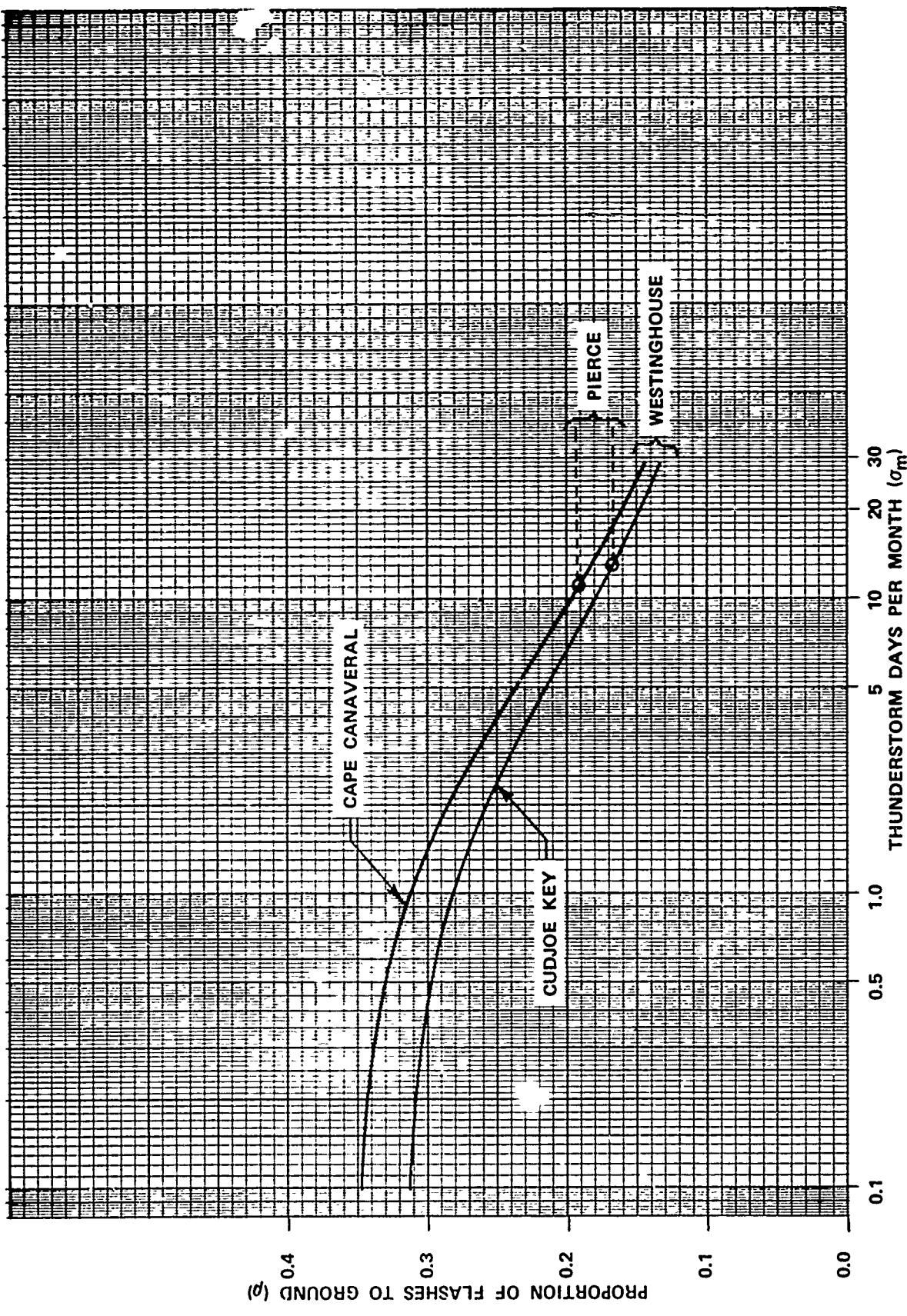
Figure 3-2. Proportion of Flashes to Ground at Telta Operating Sites

TABLE 3-1

ESTIMATED NUMBER OF LIGHTNING FLASHES TO OPEN GROUND AT TELTA OPERATING SITES

Month	Thunderstorm Days (T_m)	Flash Density (σ_m)	Proportion of Flashes to Ground	Flashes to Ground/km²
		Cape Canaveral		
Jan	0.5	0.123	0.331	0.041
Feb	1.5	.223	.298	.066
Mar	3.1	.420	.263	.110
Apr	3.5	.490	.257	.126
May	6.9	1.499	.218	.327
Jun	12.3	4.579	.190	.870
Jul	13.9	5.832	.190	1.108
Aug	15.1	6.873	.190	1.306
Sep	9.2	2.593	.201	.521
Oct	3.1	.420	.263	.110
Nov	1.0	.176	.313	.055
Dec	0.7	.146	.323	.047
Annual	70.5			4.687
		Cudjoe Key		
Jan	0.4	0.110	0.167	0.018
Feb	1.2	.195	.302	.059
Mar	1.6	.232	.267	.062
Apr	1.9	.262	.260	.068
May	4.0	.592	.225	.133
Jun	6.5	1.342	.201	.270
Jul	9.5	2.760	.190	.524
Aug	12.8	4.954	.190	.941
Sep	11.1	3.741	.190	.711
Oct	4.0	.591	.226	.134
Nov	1.0	.176	.283	.050
Dec	.7	.146	.292	.043
Annual	54.7			3.013

$$A_a = \pi r_a^2 \tag{3-4}$$

where r_a is the radius of the area of attraction given by:

$$r_a = 80\sqrt{h}\left[\exp(-Ah)-\exp(-Bh)\right] + 400\left[1-\exp(-Ch^2)\right] \tag{3-5}$$

where h is the balloon height in meters

    ., A = 0.02
       B = 0.05
       C = 0.001

As indicated in figure 3-3, radius of attraction is 400 m for altitudes above 150 m. Thus we may say that the area of attraction is 0.5 km² at practical balloon operating altitudes.

This woul   mply that a balloon flying continuously at Cape Canaveral '   d intercept (4.7)(0.5) ≈ 2 naturally occurring strokes per year, vith one of them occurring during the month of heaviest thunderstorm activity—August. This optimistic figure fails to consider the tendency of tall structures to trigger lightning – which is discussed in 3.4.
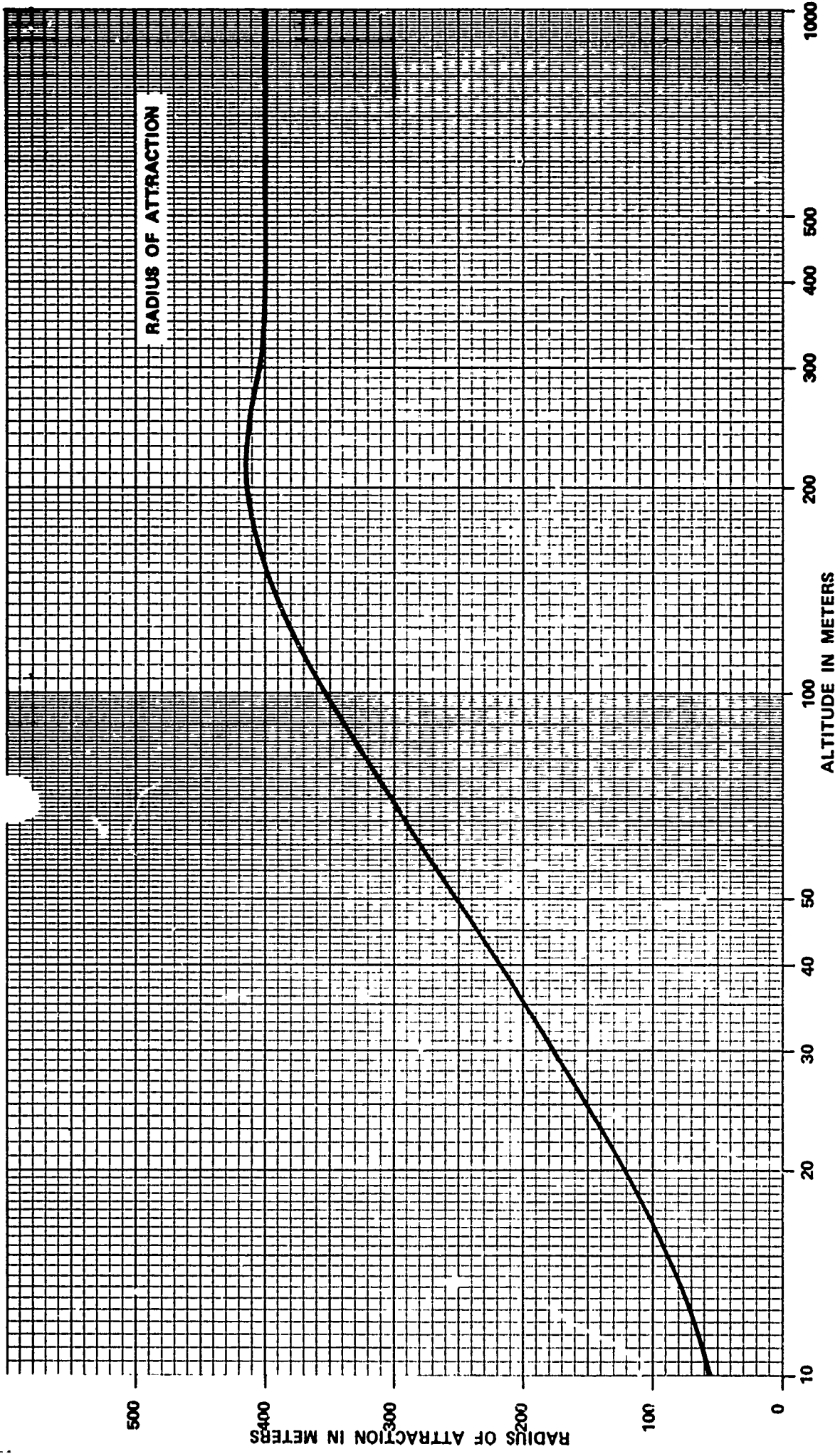
Figure 3-3. Radius of Attraction (r_a) as a Function of Balloon Height

3.4 THE TRIGGERING FACTOR

According to Pierce [9, 10] the triggering of lightning by tall structures, aerospace vehicles, or other mechanisms tends to occur when the ambient potential gradient is between 3 and 30 kV/m and the potential discontinuity between the tip of the structure and the unperturbed environment is 0.3 to 6 MV. Based on observed probability distributions of potential gradient in thunderstorms and assumed critical values, two expressions for a "triggering factor" F_T have been presented:

$$F_T = 1 + (0.01)[2.5^{(12-2000/h)}]$$ (3-6)

and

$$F_T = 1 + 2^{(9-1500/h)}$$ (3-7)

The triggering factor F_T multiplied by the predicted strike incidence as computed in 3.3 (see figure 3-5) would provide an estimate of lightning incidence with triggering included:

$$N = \sigma p A_a F_t$$ (3-8)

These two equations for F_T (3-6 and 3-7) are a theoretical/empirical mix. However, the empirical data base is deficient in the following respects:

1. The data base consists of a relatively small number of observations.

2. Effective heights are all below 400 meters. Cianos and Pierce [11] advise caution in their use outside that range.

3. The data is based on tall buildings and towers, some located on mountain tops. Differences in configuration can be expected to affect results.

For reasons discussed in Volume II, Part B, page 31, Pierce and Price suggest that equations (3-6) and (3-7) will considerably overstate F_T at balloon altitudes, but no quantitative expression is presented there. Nor do Pierce and Price feel that available knowledge provides a basis for confidence in any formula for F_T at some thousands of feet. For the predictions needed here, however, a formula is required, even if it is to be applied cautiously. Accordingly a revised formula for F_T has been prepared by RML based on equations (3-6) and (3-7) and on data given in Volume II, Part B, page 30.

Both equations (3-6) and (3-7) have the form

$$F_T = 1 + a[b^{(c-d/h)}] \qquad (3-9)$$

which by appropriate changes of base may be expressed:

$$F_T = 1 + Ae^{B/h} \qquad (3-10)$$

where

$A = a^{bc}$

$B = d \ln b$

A least-squares fit of actual data (Volume II, Part B, page 30) to equation (3-10) gives A = 70.5 and B = 830.9

$$or \qquad\qquad F_T = 71e^{-(831/h)} \qquad\qquad (3-11)$$

This fit has a correlation of 0.997, but only involves 4 data points. Note that at a height of 1km, (3-11) is in close agreement with the value of 30, predicted by Pierce and Price in Volume II, Part B, p. 30.

Figure 3-4 includes triggering factor vs balloon height as computed using equations 3-6, 3-7, and 3-11 and according to both actual data and theoretical work by Horvath [12].

3.5 WORST CASE PREDICTIONS

The worst case of lightning incidence would occur at Cape Canaveral in August, during which an average of 15 thunderstorm days is experienced. Figure 3-5 is a plot of the predicted number of flashes in August as a function of balloon altitude. Three curves are shown on this graph:

1. The predicted number of strokes with downward leaders (without triggering). This prediction is considered unrealistically optimistic.

2. The predicted number of strokes based on the exponential fit to actual data equation (3-11).

3. The predicted number of strokes based on the triggering factor as formulated by Cianos and Pierce. This estimate is considered pessimistic for normal balloon flight attitudes, and is included as a probable maximum.

3-10
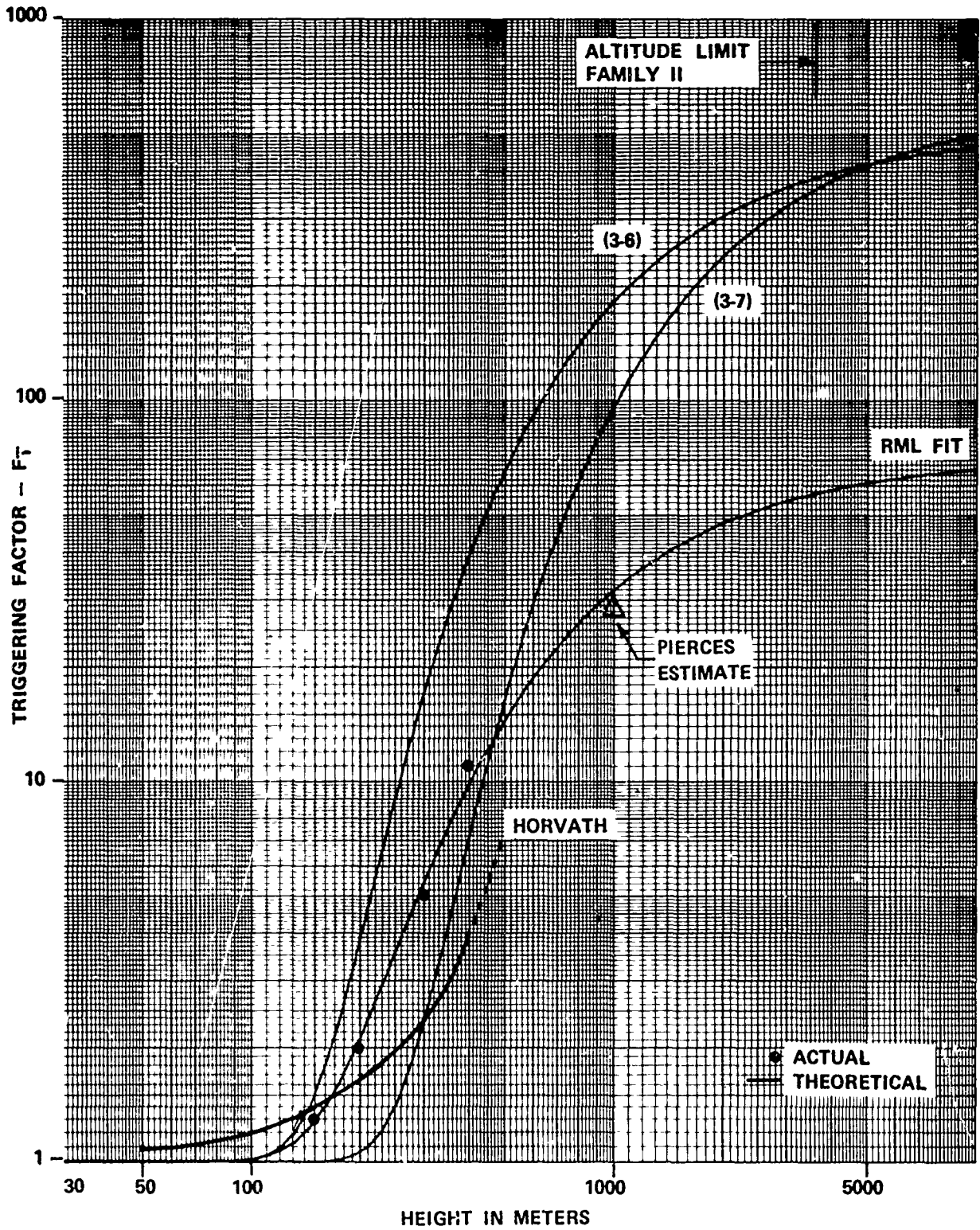
Figure 3-4. Triggering Factor as a Function of Balloon Height

3-11
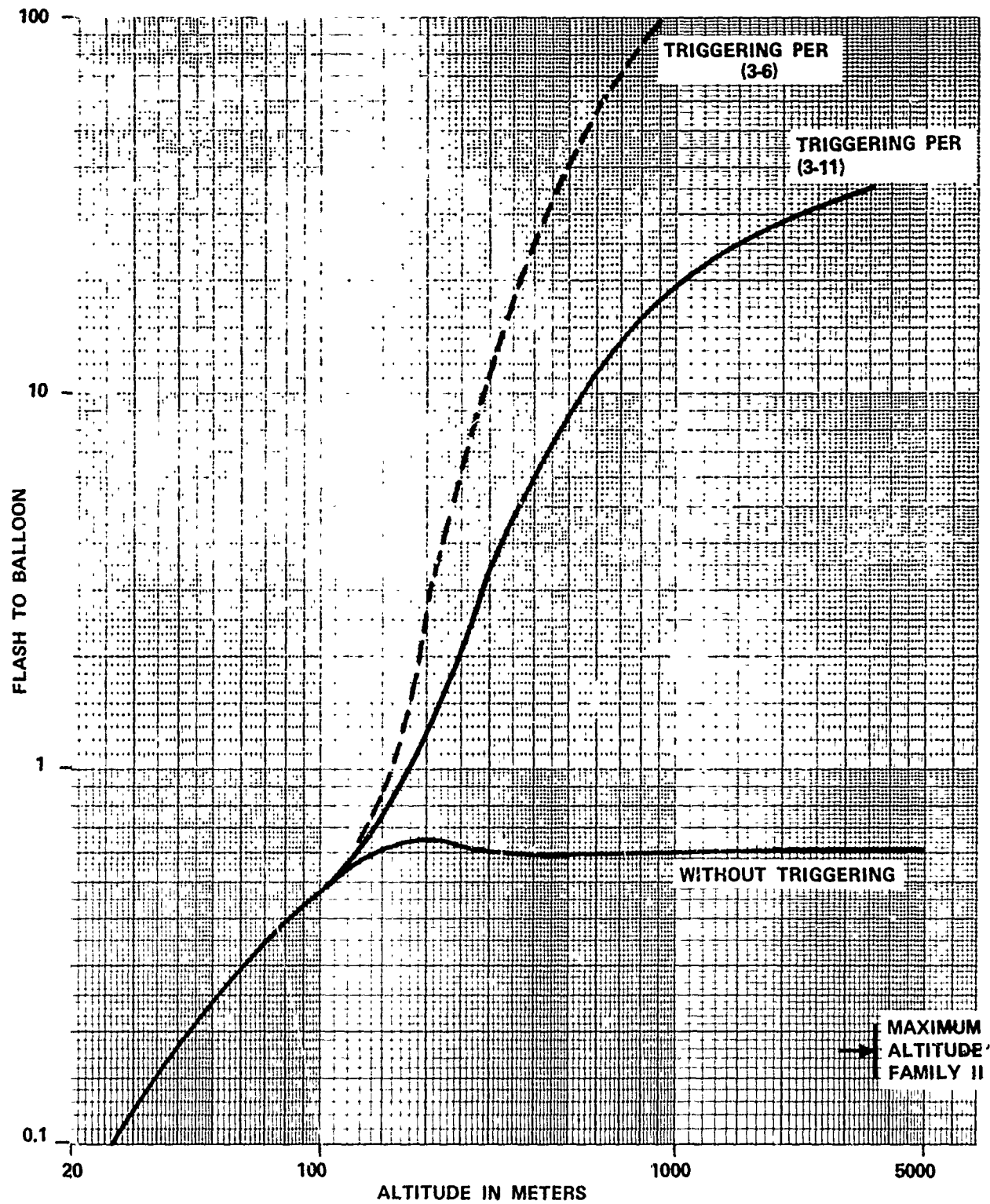
Figure 3-5. Predicted Flashes to Balloon in August

3.6 HAZARDOUS PROXIMITY TO CHARGE CENTERS

A question which frequently arises is "How close to the balloon must lightning occur for a lightning hazard to exist?" Lightning channels have been known to travel tens of kilometers; however, strikes to ground within 10 km of charge center are more commonly encountered. It is useful to define a geometric region around the balloon such that a lightning hazard exists if it contains a charge center capable of producing lightning. Latham (Vol II, Part 1, p 45) has suggested for this region a cylinder of radius equal to the balloon altitude, and of height equal to twice the altitude. Another boundary could be derived, an adjusted radius of attraction based on the assumption that lightning triggered by the balloon is actually "usurped" lightning which would otherwise have discharged to outlying regions. An adjusted radius of attraction (r_a') can be defined:

$$r_a' = r_a F_t$$

Both of these relationships are plotted in Figure 3-6. Interpretation is as follows. The straight line is the radius of the cylinder suggested by Latham. When a lightning-producing cloud is closer than the distance indicated by this line, there is a high probability of lightning to the balloon. The curved line is radius of action adjusted for triggering. If lightning is being produced within the range indicated by this curve, a lightning flash to the balloon is a theoretical certainty. For altitudes below 3 km, the two curves are in apparent conflict. Recollection of the Cudjoe Key incident of 18 August 1972, when a balloon operating at 4,000 feet was struck from approximately five miles away, implies that neither case is sufficiently conservative. Actually there is no clearly defined line which separates safety from danger. Lightning channels have traveled much farther than five miles. The CKOL incident indicates that a balloon is endangered when a charge center capable of producing lightning is within five miles of the balloon.

⊙ CKOL
   18 AUGUST 1972
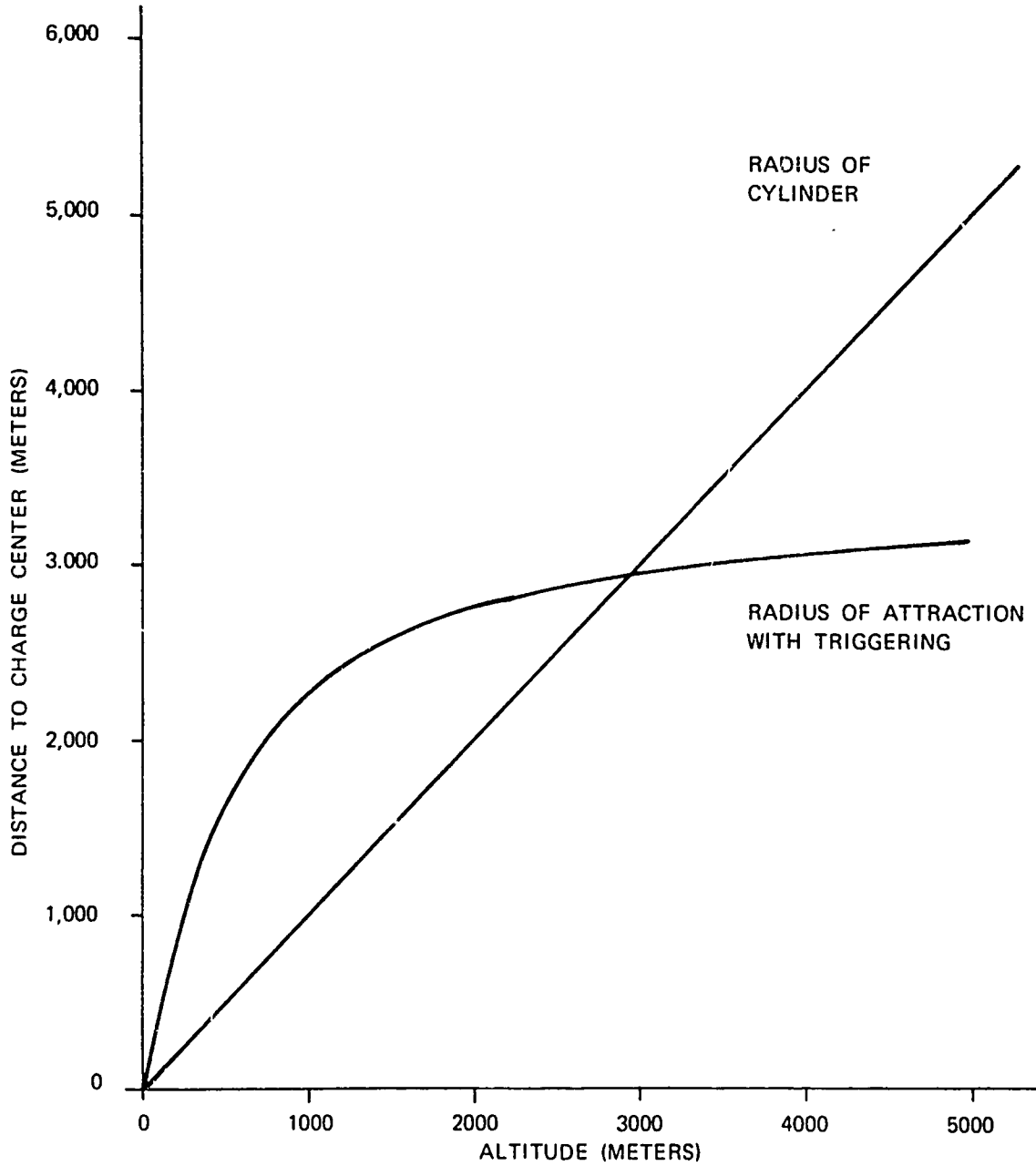
FIGURE 3-6 ESTIMATED STRIKING DISTANCES

Additional insight into hazardous ranges can be derived from observed distances between successive strokes. For example, if two successive strokes from the same charge center strike the ground 6 km apart, this implies that one of them is striking at least 3 km from the originating charge center. Figure 3-7 from Pierce [13] after Hatakeyma [14], shows the pattern of strike points for 11 flashes occurring during a 15 minute period. It is interesting to note that the motion of the charge center is small scale compared to the scattering of the strike points. Note from the histogram that spacings of 3 km are typical, but 10 km spacings were encountered in this small sample. It is to be expected (in accordance with previous sections) that the striking distance to a tethered balloon will greatly exceed those shown here, which presumably are to open ground and low structures. These statistics, taken as minima, imply that a charge center at a distance of 10 km (6 mi) constitutes a hazard, especially when effects of balloon height are considered.

3.7 RELATIVE PROBABILITIES OF LIGHTNING TO BALLOONS TETHERED BY WELL OR POORLY-CONDUCTIVE TETHERS

The findings of our experimentation (Section 2) are that a balloon tethered by a poorly-conducting material creates considerably less distortion of the ambient field immediately after ascent than does a well-conducting tether. However, it has also been shown that the balloon with dielectric tether does transfer charge at a rate determined by the extent of surface (and possibly internal) contamination of the tether, and so intensifies the ambient field at flight altitude increasingly with time. An uncertainty is introduced when we contemplate the dynamics of field near thunderstorms where the ambient potential can build up to tens of kilovolts per meter and collapse and recover at a rate of 2 or 3 times per minute in extreme cases.
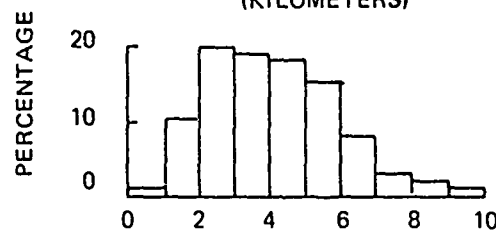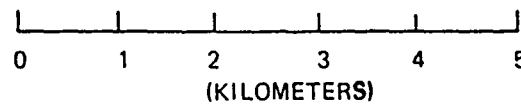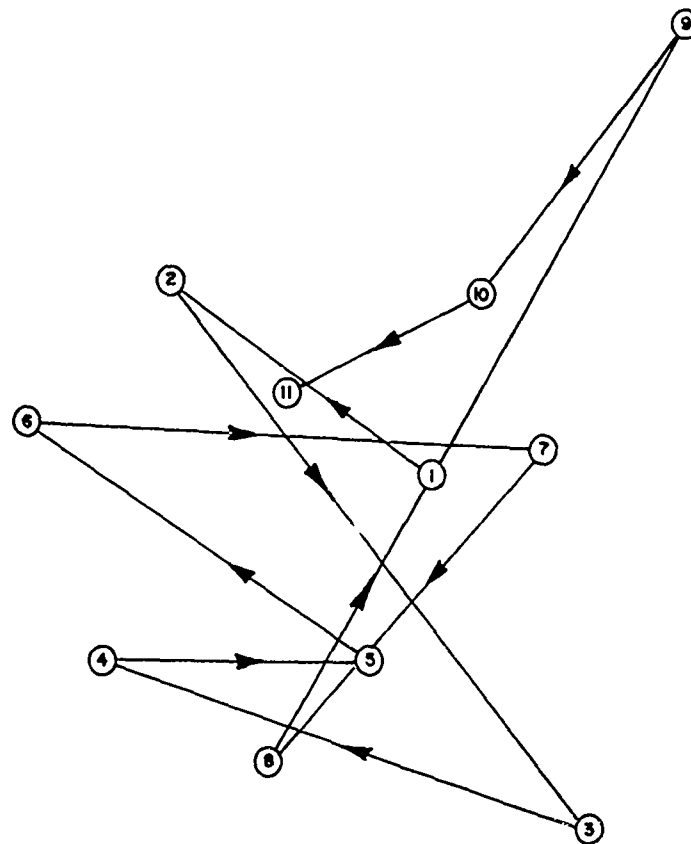
FIGURE 3-7
POSITIONS OF SUCCESSIVE FLASHES FROM A STORM
MOVING AT 30 km/HR

A brief summary of known experiences with lightning strikes to balloons follows:

Davis and Standring [3] cite the loss or damage of 135 "unprotected" balloons. Lightning strokes to 65 balloons with lightning rods were recorded. These losses were sustained during the Second World War when balloons were flown in massive barrages. However, the total number of balloons involved is not given; neither is the extent of damage to the 65 "protected" balloons described. It is implied that at least some of these balloons had wire rope tethers, but the actual proportions of conductive or dielectric tethers are unfortunately missing.

Hodkinson [15] describes a lightning strike to a balloon tethered by a steel wire rope. The balloon was flying at 2,750 feet in a sleet storm when the stroke occurred. There were minor damages to ground based electronics near the tether point but no apparent damage to the balloon or tether.

A BJ balloon operated by AFCRL at Holloman AFB was struck by lightning while flying in a thunderstorm at an altitude of 500 feet [15]. This balloon was tethered by a 3/8 inch diameter 3/9 VHS plow steel rope. The on-board electronics were damaged, but balloon and tether survived intact.

A logging balloon operated by Bohemia Lumber Company, Eugene, Oregon, was struck by lightning while flying at an unknown altitude. The tether (1-1/4 inch carbon steel) was undamaged, but the hull sustained minor damages. An air terminal was added, and no subsequent lightning damage has been noted. This balloon is left inflated under all weather conditions and may have experienced other undetected lightning strikes; however, the operating location is in a region of very low lightning incidence.

3-17

A Nolaro-tethered 2D7 balloon operated by RML received a lightning stroke while flying a Cudjoe Key in light rain at an altitude of 4,000 feet. The originating charge center for this stroke was estimated to be five miles away. An observer described the storm as a cumulonimbus with anvil top to 30-40 k feet. He estimated the distance to the near edge of the storm to be 5 miles. Upon closer questioning as to the certainty of this estimate, he said that it was "not 3 miles nor was it 10." He also observed cloud to ground lightning approximately 5 miles away. The witness is an experienced military and civilian pilot. People of such background have some knowledge of meteorology and also tend to be better than average judges of distance. This is the only occasion on record when there was any knowledge of the distance to the originating charge center. The Nolaro tether was damaged but remained intact. This incident is described more fully in reference [19] and also in 4.3.

In an early attempt to trigger lightning, Moore [1] conducted a series of balloon flights to an altitude of 6,000 feet above Mount Withington in New Mexico. Approximately 15 flights were conducted during thunderstorms, some of which enveloped the balloons. Several balloons were destroyed, but there was never any indication that lightning currents were being conducted down the tether. On at least one occasion lightning was seen to flash within the cloud, envelop the balloon, whereupon a shredded balloon would fall from the sky secured by a bright undamaged tether wire. The balloons so affected were made of thin mylar while neoprene balloons were undamaged. Prof. Moore maintains, with considerable supporting evidence and analysis, that the tether was shielded by a sheath of corona; however, this is a point of scientific controversy.

Professor Moore does not represent this phenomenon as a consistent mode of protection which should be used to support a selection of conductive tethers over dielectric tethers. Indeed the majority of the program consultants express the opinion that a balloon tethered by a conductive rope is generally more likely to attract lightning than one tethered by a dielectric rope. The emerging opinions are, however, that (1) with regard to attracting lightning, the advantage of a dielectric tether over a conductive tether is less than has been assumed, (2) this advantage may not accrue to an overall safety advantage, considering such factors as total system survivability.

SECTION 4
EFFECTS OF LIGHTNING ON BALLOON TETHERS

4.1   CONDUCTION OF LIGHTNING CURRENTS DOWN BALLOON TETHERS

Prior to the transfer of charge, the path of a lightning flash
is determined by the formation of a conductive column of ionized
air known as a "leader." The extent of damage to a material
is closely related to the path of the lightning currents as de-
termined by the leader. Since a good conductor provides a
more convenient electrical path than the surrounding air, a
lightning channel which encounters a conductive tether will
follow it to ground. Most of the lightning current will be
conducted by the tether material. The survival of the tether
will depend on its ability to dissipate the heat of the dis-
charge without softening.

While a poorly or transitionally-conducting tether material of-
fers a less attractive path to ground than the metallic tether,
it generally presents a better path than the surrounding air.
The tether in most cases represents to the searching leader,
a reasonably dielectric cable sheathed in a more conductive sur-
face. The observed tendency is for the leader and resulting
flash to propagate along the air-dielectric interface, but oc-
casionally it breaches the tether sheath and creates mechanical
damage. This breaching occurs on a random basis, and the sur-
vivability of a Nolaro tether is therefore less predictable than
that of the metallic tether.

4.2   SUITABILITY OF ARTIFICIAL LIGHTNING FOR SURVIVABILITY ASSESSMENT

The lightning strike simulations performed for this program by the Lightning Transients Research Institute consisted of 4-megavolt sparks of approximately two meters length, developed by a Marx generator. The resulting peak current and half power pulse width depended on the test medium, but were typically 17 kiloamperes and 50 microseconds respectively. Continuing currents were simulated by discharging 600 Vdc banks of storage batteries with up to 300 amperes available current across an arc initiated by the marx generator.

According to Uman [17,18], there are four characteristics of lightning which are significant in the design of aerospace protective systems:

1. The initial breakdown process.

2. Current and energy transfer from the lightning channel to the vehicle.

3. Electric and magnetic fields generated by a direct or nearly direct strike.

4. The shock wave produced by the expanding lightning channel.

The work referenced above indicates that, in general, the breakdown modes of natural and simulated lightning are similar - at least to the extent that spark simulation of the strike point is physically realistic.

4-2

The charge transfer resulting from a laboratory spark (about 0.85 coulomb in the cited example) is comparable to that of a weak subsequent stroke in a multi-stroke flash. Electric and magnetic fields and shock waves are less realistically simulated by laboratory sparks. However, they are of lesser importance in priorities established for this program where the principal regions of interest were streamer formation and thermal damage.

4.3 DIELECTRIC TETHERS

The lightning incident which occurred at Cudjoe Key on 18 August 1972 is depicted in figure 4-1; the tether was damaged at five places along the tether. This damage is shown in figures 4-2 and 4-3. This flash appears to have been of typical intensity. Based on the damage, J. R. Stahmann of LTRI estimates that the flash contained multiple strokes, with peak currents of about 20 to 40 kiloamperes [14]. The breaking strength of the tether was reduced from its nominal value of 26,000 lb to 8.000 lb. This reduction is ominous considering that pulls of this magnitude have on rare occasions been experienced and are most probable under circumstances where lightning would be encountered.

The Cudjoe Key incident is the only known documented instance of a stroke to a balloon with a dielectric tether. It therefore provides the total data base for investigation of natural lightning strokes to balloons tethered by Nolaro or other dielectric materials.

As shown in figure 4-4, damage to Nolaro produced by the LTRI Marx generator closely resembles that from natural lightning at Cudjoe Key. During the LTRI tests there were over 100 test exposures to simulated lightning of Nolaro and Kevlar 29 samples.
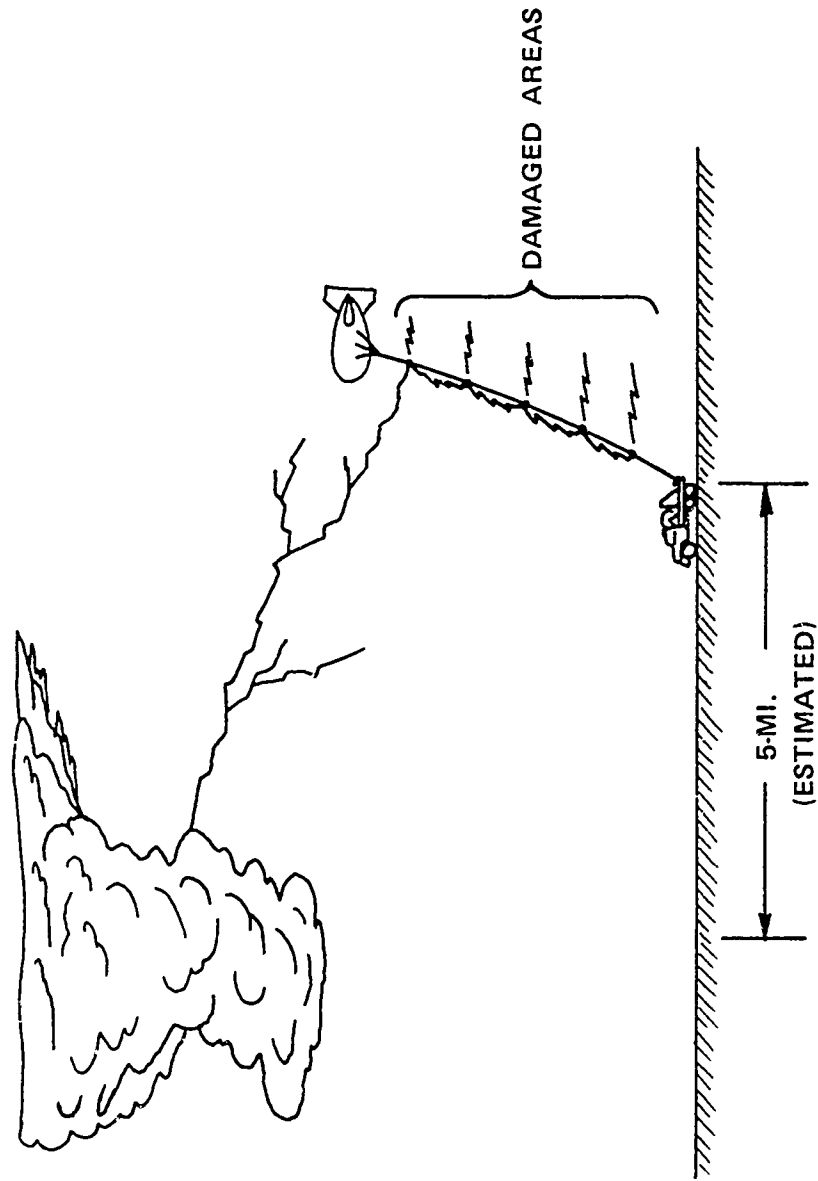
Figure 4-1. Lightning Incident at Cudjoe Key on 18 August 1972
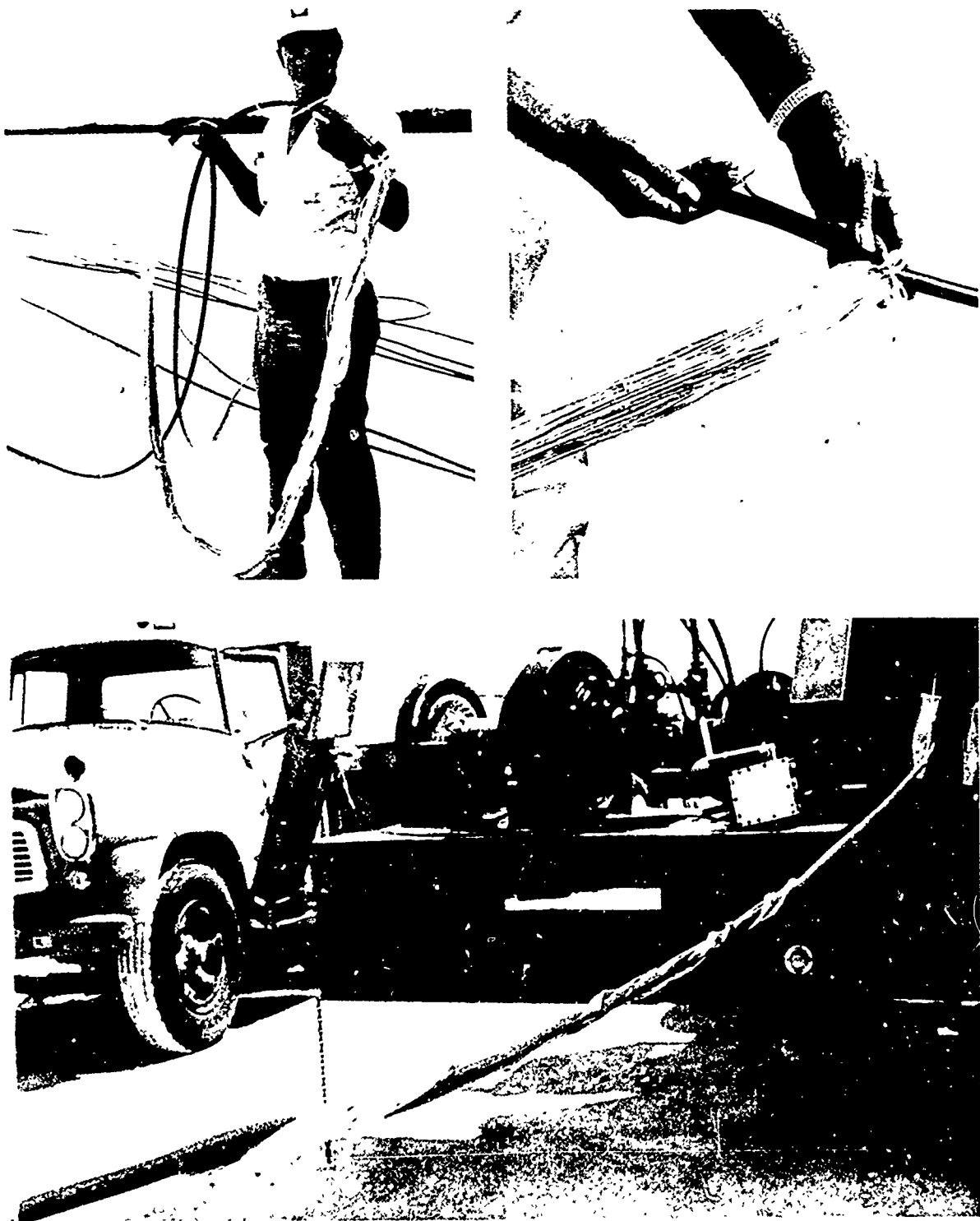
Figure 4-2. Damage Sustained by a 0.775-Inch Nolaro Tether
Struck by Lightning at Cudjoe Key on 18 August 1972

Pitting of Steel Surface
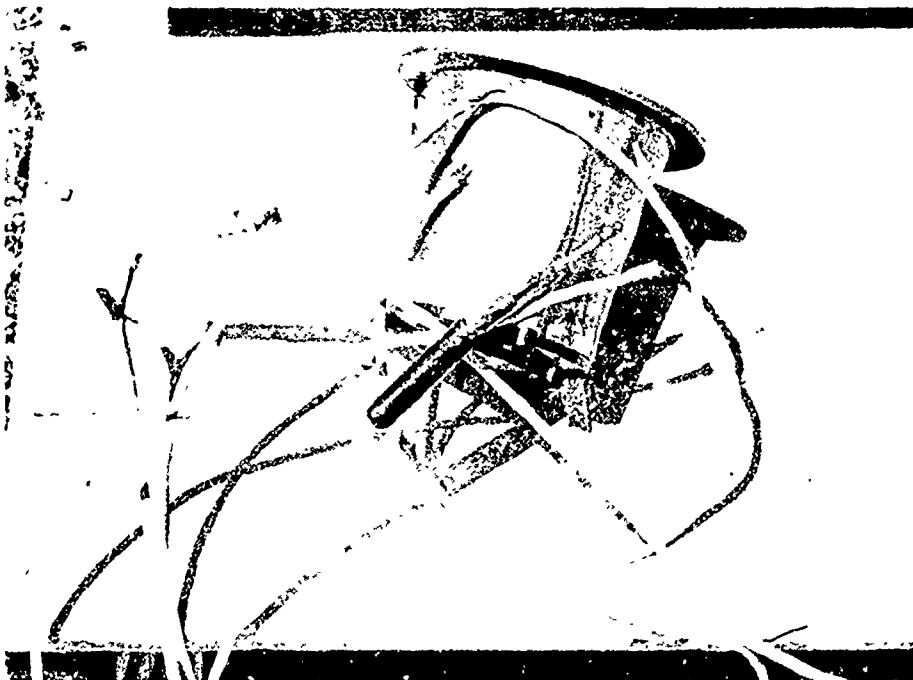
Damaged Interphone Cable

Figure 4-3. Equipment Damage From Lighning Stroke at Cudjoe Key on 18 August 1972
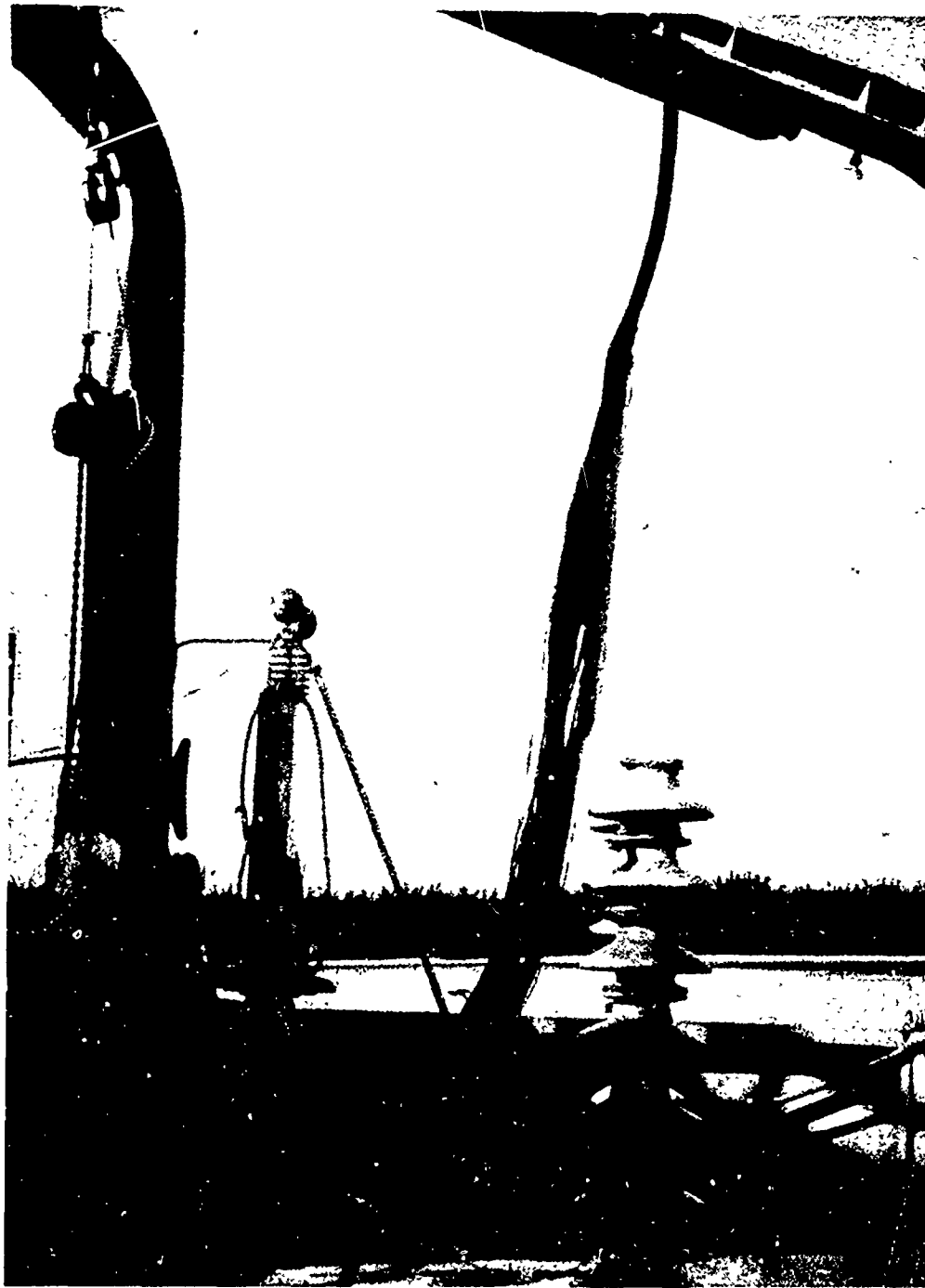
Figure 4-4. 0.625-Inch Nolaro Tether Damaged by Strokes From the LTRI Lightning Simulator

It may be generalized from these tests (which are documented in Volume II, Part D) that the sparks tended to flash down the outside of the jacket, except in those cases where the jacket was breached by the streamer or where streamer entry was artificially assisted by insertion of wires through the jacket. In general, the energy guided down the exterior of the jacket did not cause damage - but sometimes resulted in polishing the jacket.

"Prepuncturing" the jacket did not appear to greatly increase the vulnerability of the material, nor did wetting the surface of the jacket. For example, 10 samples of dry tether were subjected to an aggregate of 36 high-voltage and 8 high-current flashes without discernible damage. * Two superficially wet pieces were subjected to three high-voltage discharges, each without damage. On the other hand, the exposure of eight pieces of Nolaro which had been saturated with water to 68 high voltage strokes resulted in 14 punctures of the jacket and two areas of major damage involving the loss of 2-inch and 4-1/2 inch lengths of jacket. These tests are listed in tables 4-1 and 4-2.

A damage effect noted in the Cudjoe Key incident was a striation or deep grooving of the jacket. This effect was also noted in one instance where saturated Nolaro was subjected to high-voltage discharge. The effect was duplicated by exploding a section of jacket with air pressure. This indicates that the striations probably resulted from rapid expansion of gas within the tether rather than from surface erosion by the spark.

* In another test program, LTRI exposed smaller diameter Nolaro ropes to pulses varying from 15 kA and 25 microseconds to 85 kA and 250 microseconds. Ropes with polyurethane jackets were weakened, in some uses to 25% of normal breaking strength, while ropes with polyethylene jackets only sustained surface damage [23].

4-8

TABLE 4-1

TESTING OF WET AND DRY NOLARO SAMPLES

Material	Sample	Condition	Discharge Applied	Results
0.775 Nolaro	1	Dry	3 High Voltage	No visible damage
0.775 Nolaro	2	Dry	1 High Current (150 kA)	No visible damage
0.490 Nolaro	2	Dry	1 High Voltage	No visible damage
			1 Multiple High Voltage & 150-kA current	No visible damage
0.625 Nolaro	2	Dry	5 High Voltage & 1 200-kA Current	No visible damage
0.625 Nolaro	3	Dry	1 High Current (200 kA)	No visible damage
0.625 Nolaro	5	Dry	15 High Voltage	No visible damage
0.460 Kevlar	1	Dry	3 High Voltage	No visible damage
0.460 Kevlar	2	Dry	1 High Voltage & 1 Multiple High Voltage (150 kA) Current	Surface polished
0.460 Kevlar	3	Dry	5 High Voltage & 1 High Current (200 kA)	No visible damage
0.460 Kevlar	4	Dry	1 High Current (200 kA)	No visible damage
Totals	25	Dry	34 High Voltage 7 High Current	10 No visible damage 1 surface polished
0.775 Nolaro	1	Wet	3 High Voltage	No visible damage
0.460 Kevlar	1	Wet	3 High Voltage	No visible damage
Totals	2	Wet	6 High Voltage	2 No visible damage

TABLE 4-2

TESTING OF SATURATED NOLARO SAMPLES

Material	Sample	Condition	Discharge Applied	Results
0.775 Nolaro	1	Saturated	2 High Voltage	5 Punctures on 2d discharge
0.775 Nolaro	4	Saturated	15 High Voltage (11-15 prepunctured)	3 punctures on 13th discharge
0.775 Nolaro	4	Saturated	8 High Voltage	3 punctures in first 6; 2-inch section dejacketed on 8th discharge
0.490 Nolaro	1	Saturated	6 High Voltage	4.5-inch length damaged on 6th discharge
0.490 Nolaro	2	Saturated	3 High Voltage & 1 combined High Voltage 2 (140-kA)	No visible damage
0.625 Nolaro		Saturated	10 High Voltage	No visible damage
0.625 Nolaro		Saturated	14 High Voltage	Striations, 3-inch section damaged
0.625 Nolaro		Saturated	4 High Voltage	35-inch section dejacketed on 4th discharge
0.625 Aluminized Nolaro		Saturated	25 High Voltage	Slight scorching of paint only
0.460 Kevlar		Saturated	3 High Voltage	No visible damage
Totals	12	Saturated	90 High Voltage, 1 Multiple High Voltage	11 punctures, 37 inches dejacketed, 3 no visible damage, slight paint scorching.

4.3.1 Enhancement of Surface Flashover

In response to severe damage to aircraft radomes by lightning, a Lightning Diverter Strip has been developed by McDonnell Douglas Corporation [5]. This strip consists of a row of small copper disks bonded to a resistive substrate as shown in figure 4-5. These diverter strips are used to convey lightning current from the radome to the skin of the aircraft where it can be more safely distributed. The strip promotes the formation of an ionized channel along its surface such that no appreciable energy is dissipated in the material.

J. R. Stahmann of LTRI [23] has suggested that a similar function might be served by the application of aluminum paint to the surface of a dielectric tether. The principal features of the approach are:

1. The tether resistance would not be appreciably reduced, since the paint is actually a conductive powder suspended in a dielectric.

2. In high fields, the paint would encourage streamer formation along the surface of the tether in a manner similar to that of the lightning diverter strips.

The concept was tested using an aluminum spray paint consisting of 4% aluminum powder having grain diameter less than 10 microns, suspended in a polystyrene vehicle. This paint was applied to clean 0.625-inch Nolaro. A 10 cm length of the coated tether was found to have resistance in excess of 10^{12} ohms before and after application of the paint.

1/2 INCH

RESISTIVE SUBSTRATE

COPPER DISKS
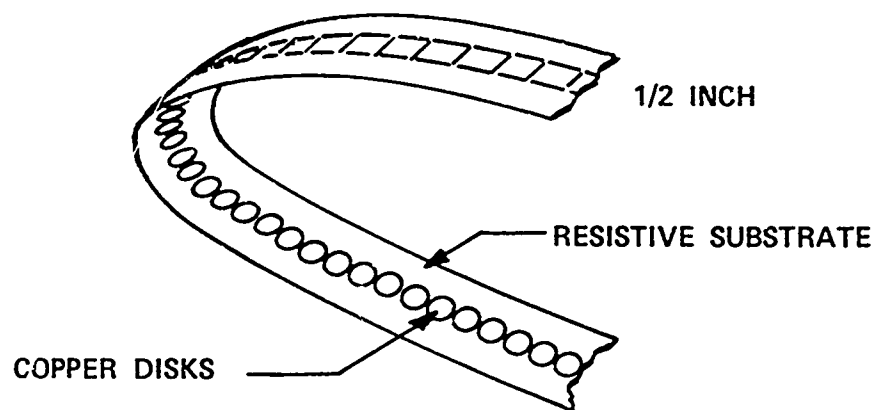
Figure 4-5. Segmented Lightning Diverter Strip

Comparative testing of coated and uncoated Nolaro was conducted
to investigate:

a)   Tendency to attract discharges
b)   Streamer formation
c)   Survivability

Tendency to Attract Discharges

The tendency of the material to provide a preferential path to
ground, relative to the surrounding air, was evaluated by adjust-
ing two gap spacings — one from the Marx generator high-
voltage bus to the test specimen and the other directly to ground.
Increasing the spacing of either gap enhances the probability of
the other gap firing. The test configuration for this experiment
is shown in figure 4-6.

If we borrow from circuit theory the transformation shown in fig-
ure 4-7, it would appear that the ratio $\frac{b}{C-a}$ is a crude indication
of the relative attractiveness of the sample material to lightning
strokes.

The results of this testing are presented in table 4-3 and are
summarized as follows:

An electrode was suspended 10 inches above a painted sample
which was grounded at a distance of 86 inches. The control
air gap was set for 54 inches. Both gaps flashed, indicat-
ing approximate equivalence of 54 inches (C) of air to 86
inches of painted sample material plus 10 inches of air. If
we subtract the 10-inch air gap (a) from both quantities,
we find that 86 inches (b) of painted tether has an attrac-
tiveness to lightning equal to that of 44 inches of air.

TABLE 4-3

DETERMINATION OF RELATIVE ATTRACTIVENESS TO LIGHTNING OF ALUMINIZED AND NONALUMINIZED NOLARO TETHERS

Sample Type	Sample Air Gap a	Effective Sample Length b	Chopping Gap C	Preference Ratio $\frac{b}{C-a}$	Results
1) Aluminized	10	86	54	1.95	Gaps a and C fired
2) Nonaluminized	10	83	55	N/A	Gap C fired, gap a did not
3) Nonaluminized	10	83	75	1.28	Gap C fired, gap a did nct
4) Nonaluminized	10	67	79	0.97	Gap a fired, gap C did not.

$$\frac{1.95 \quad \text{(Aluminized)}}{1.28 \quad \text{(Nonaluminized)}} = 1.53; \frac{1.95}{0.97} = 2.01$$
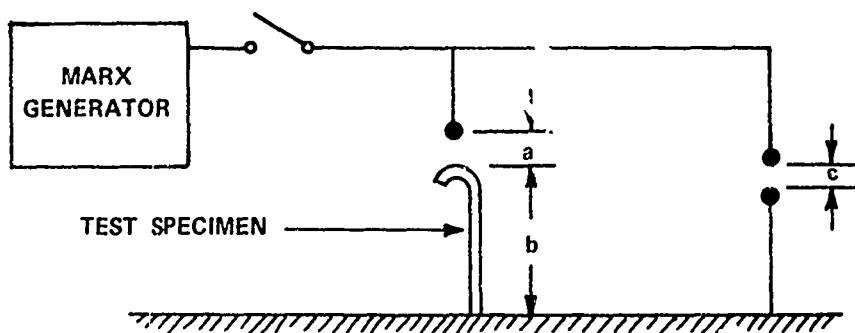
Figure 4-6. Setup for Streamer Photography
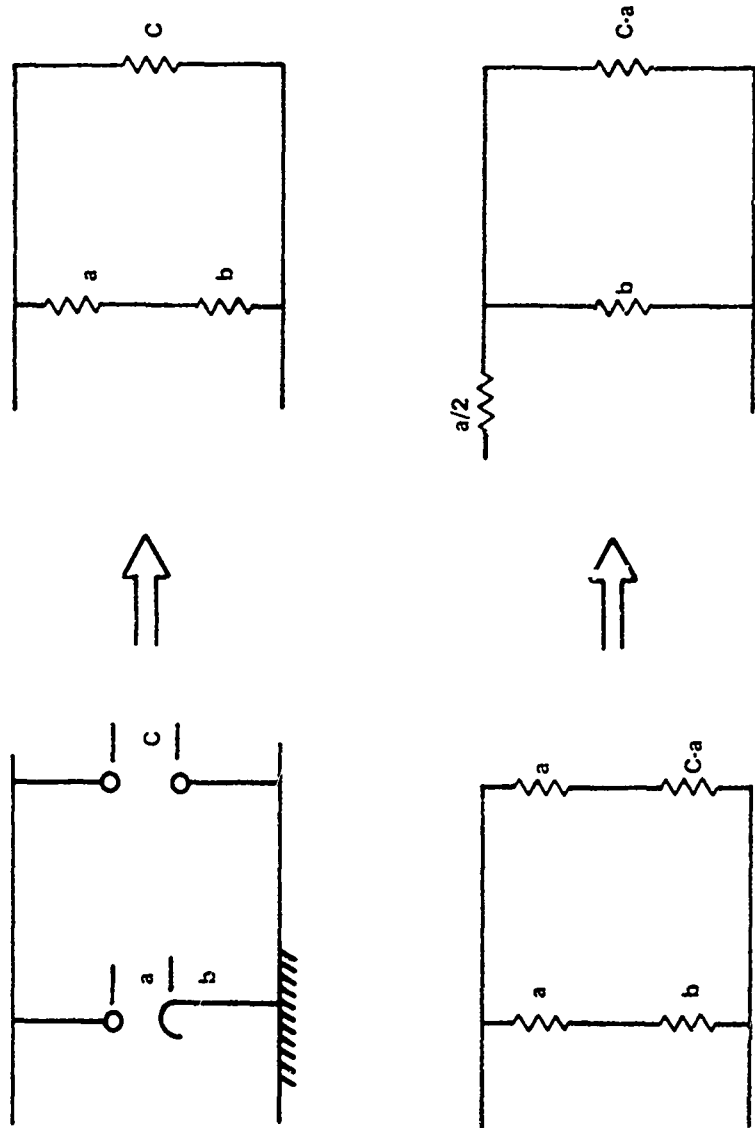
Figure 4-7. Equivalent Circuits for Test Sample and Air Gaps

To quantize this relationship, we define and compute a material-to-air "preference ratio" of 1.95:1.

A sample of uncoated but otherwise identical material of approximately the same length (83 in.) was then substituted, but the 10-inch air gap would no longer fire. When the air gap was increased from 55 inches to 67 inches, the "hot" electrode for the 10-inch air gap then flashed to a grounded electrode 75 inches away in preference to the sample. In this case the 75-inch gap functioned as a control gap, implying a preference ratio less than 1.27. The sample length was then reduced to 67 inches, and it was determined that a 79-inch control gap could initiate a spark across the 10-inch air gap. This indicates a material-to-air preference ratio of 0.97. It may therefore be concluded that the attractiveness of the aluminized Nolaro tether material exceeds that of the uncoated Nolaro by a ratio in the range of 1.53 to 2:1. These relationships are given in table 4-3, and typical discharge · are shown in figure 4-8 (b) and (d).

Streamer Formation

By adjusting the gaps so that the discharge occurred across the "C" gap (located away from the camera), it was possible to photograph streamers forming across the "a" gap (between the electrode and the test sample).

Photographs of streamer formation on bare and aluminized tether samples are presented in figure 4-8 through 4-1υ. Formation of streamers on unpainted Dacron Nolaro is shown in figures 4-8(b) through (d) and 4-9(a) and (b). As shown in 4-8(b) and (c), the streamers formed from the electrode down to the sample. Figures 4-8(d) and 4-9(a) and (b) show a peculiar "sausage-like" configuration in the fully developed streamers.

4-16

(a) Control (No Discharges)
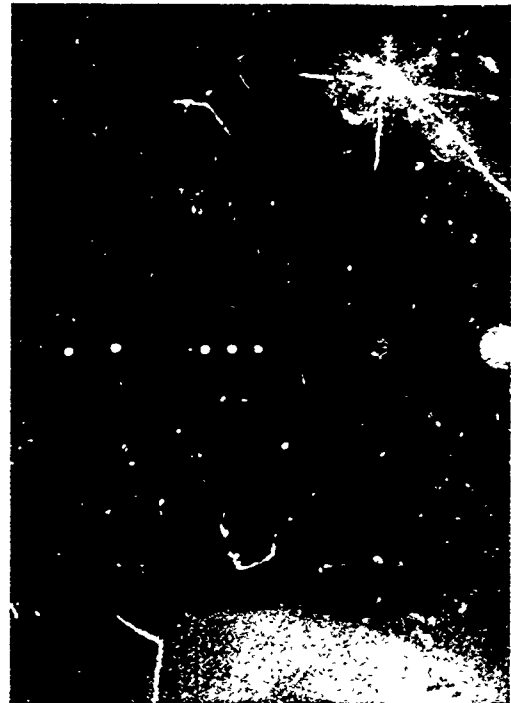
(b) Short Downward Streamer
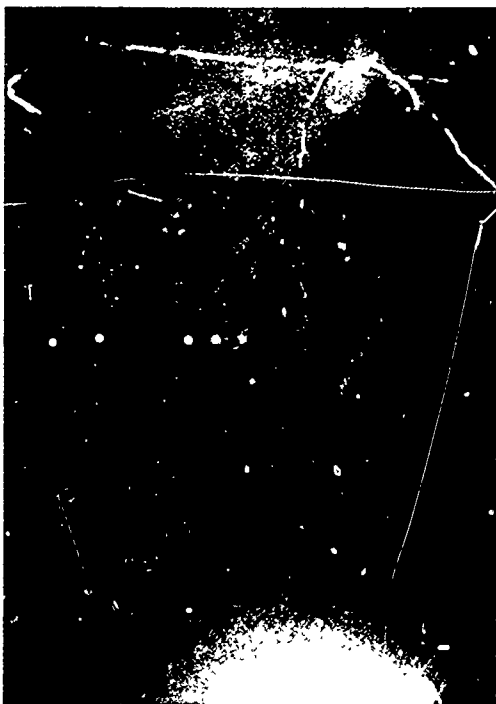
(c) Downward Streamer, Control Gap 55 inches

(d) Downward Streamer, Control Gap 67 inches

Figure 4-8.   Streamer Formation on Unpainted Nolaro Tether

(a) Unpainted Cable, Control Gap 55 inches

(b) Unpainted Cable, Control Gap 67 inches

(c) Painted Cable, Upward Streamer, Control Gap 43 inches
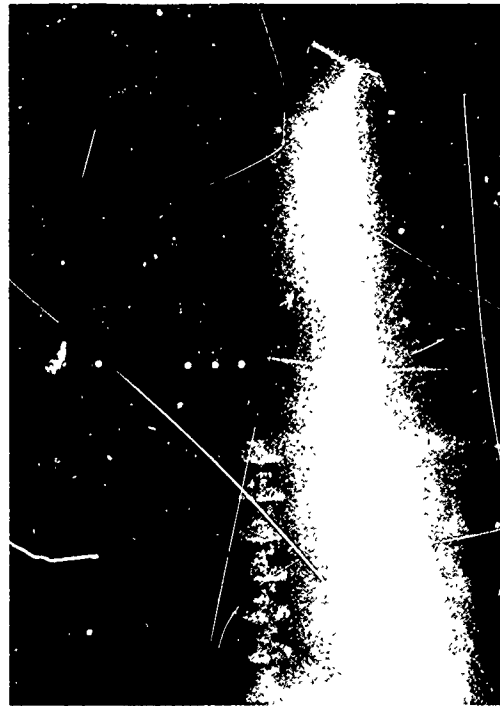
(d) Painted Cable, 86-inch Total Gap, 35-inch Air Gap, Control Gap 43 inches

Figure 4-9. Streamer Formation on Unpainted and Painted Nolaro Tethers

(a) Painted Cable, 15 kA Discharge (Camera Aperture Decreased 14 Stops)

(b) Unpainted Cable, 75-inch Gap to Capacitor, 77-inch Total Gap, Control Gap 79-inches

Figure 4-10. Streamer Formation on Painted and Unpainted Nolaro Tethers

The cause of the intensity nodes in these streamers is not understood. A possible explanation could be intermittent areas of increased conductivity along the length of the sample. If so, then localized heating at such node points would be likely and could account for the intermittent damage noted in testing and experienced during the actual strike at Cudjoe Key in August 1972.

Figures 4-9(c) and (d) show streamer formation on aluminized Nolaro. In (c), the downward development of streamers from the electrode is evident as in 4-8(b). However, a segment of streamer is also visible on the tether. Careful inspection of the original photos indicates (though not conclusively) that this streamer originated on the sample rather than at the electrode.

Figures 4-10(a) and (b) show 15 kA discharges on the surface of aluminized and uncoated samples respectively. Although both channels have approximately the same appearance, the camera was set for a much smaller opening for 4-10(a) than for (b), indicating that the air surrounding the aluminized sample was more heavily ionized than that surrounding the uncoated sample. (On the sample in figure 4-10(b), the discharge arced to a capacitor 75 inches away instead of the 79-inch air gap.)

4.3.2 Effect of Aluminum Paint on Survivability

The relative survivabilities of aluminized and uncoated samples were investigated as follows:

1. A saturated, uncoated sample of 0.625-inch Nolaro was subjected to four high-voltage discharges. On the fourth discharge, this sample was dejacketed along a 3.5-foot length. The resulting damage is shown in figure 4-4.

2. A saturated sample of aluminized (but otherwise identical) Nolaro was subjected to 25 high-voltage discharges without experiencing any perceptible damage other than a slight scorching of the paint. As indicated by table 4-2, this is the best survival rate attained with saturated samples.

The experimentation described above includes the first known photography of streamer formation on poorly-conducting ropes. The total activity involved less than one day of testing, which is not enough to be considered conclusive.

The heavier ionization of air around the aluminized tether than around the uncoated sample may be interpreted as an indication that the aluminum paint enhances streamer formation outside rather than inside the jacket. The observed survivabilities of the two materials tend to support this premise. On the other hand, the tendency of the aluminized sample to form its own streamer as well as the indicated measures of attractiveness imply that an aluminized tether is more likely to receive a lightning stroke than the nonaluminized tether.

This apparent survivability enhancement considered along with the greater "attractiveness" to lightning presented by the painted tether presents a dilemma regarding the actual value of protection which could increase the probability of a lightning strike. This same dilemma exists with respect to lightning rods. It must be assumed that the probability of a strike is high as indicated in section 3 before such approaches are appealing.

A proper assessment of the effectiveness of a protective system must be based on the product of stroke probability and survival probability. These estimates cannot be made reliably from the present data base.

4-21

4.3.3 Dielectric Tethers With Integral Conductors

Since Nolaro rope is considerably lighter than steel wire rope of
equivalent breaking strength, Nolaro tethers with "built-in"
transmission lines have been considered. Such ropes have been
used for oceanography and for glider tow cables. The simplest
rope to construct and the most resistant to normal wear and han-
dling would have the electrical conductors near the center [21,
22]. This construction was simulated by inserting AWG 14 wire
down the center of a length of 0.775-inch Nolaro. When subjected
to a high current impulse (175 kA), the sample was totally de-
stroyed by the ensuing explosion. Selected frames from high-speed
movies of this test are shown in figure 4-11. This is the prob-
able result of any lightning stroke to a fiber tether containing
small electrical wire, since the construction encourages the pen-
etration of the dielectric strength member by the lightning cur-
rent.

The effect of electrical wires on the outside of the fiber
strength member was investigated by subjecting 0.625-inch Nolaro
with wire helically wrapped around the outside of the jacket to
pulses ranging from 70 kA to 175 kA peak. It was possible to
vaporize the wire without damaging the strength member. This,
together with the results of the conductive paint experiment
described on page 4-20, would indicate that the survivability of
the tether is enhanced by any measure which greatly increases
the conductivity of the outside of the tether relative to the
inside. In a test program performed for the Air Force Cambridge
Research Laboratory [23], it was determined that a conductor of
sufficient mass to survive the energy dissipation may retain enough
heat to burn the strength member. In this manner it is possible
that a metallic fitting such as a thimbl could burn through a
Nolaro tether which might otherwise survive a lightning flash.
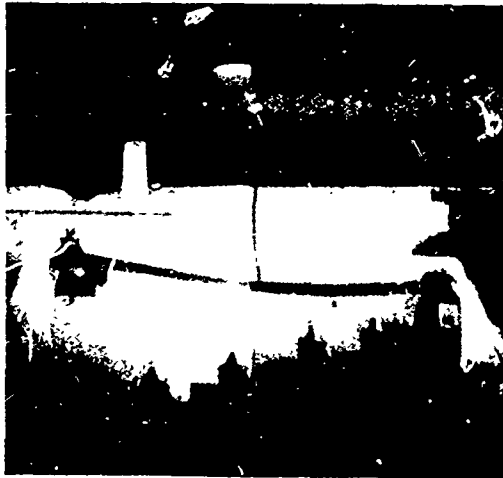
1

2

3

4

Figure 4-11. Explosion of Nolaro Tether With AWG 14 Wire Inside

4.3.4 Tubular Tethers With Gaseous Fuel

To assess added hazards resulting from the flow of inflammable gas through a tubular tether, a sample was constructed by removing a portion of the fiber from several feet of 0.775-inch Nolaro and inserting 1/2-inch OD nylon tubing. As shown in figure 4-12, a wire was inserted through the jacket of the tether to assure streamer entry, and the sample was exposed to a 200 kA pulse. The sample exploded as shown in figure 4-11, except that the nylon tubing was undamaged and no propane was ignited. The gas flow was allowed to continue while the exposed tubing was subjected to ten high-voltage pulses. The tubing was then pressure checked at 150 lb_f/in^2 (psi), and no leaks were detected.

4.3.5 Summary

For low to moderate-intensity strokes that can be simulated, the survivability of jacketed Nolaro rope is fairly high. Conditions which increase the superficial conductivity of the jacket do not appear to increase the vulnerability of the tether. In fact, there is evidence that any increase of surface conductivity relative to internal conductivity ppears to enhance the survivability of the tether.

Conversely, any introduction of conductors to the interior of the jacket increases the likelihood of the jacket being punctured by the streamer and physical destruction of the rope.
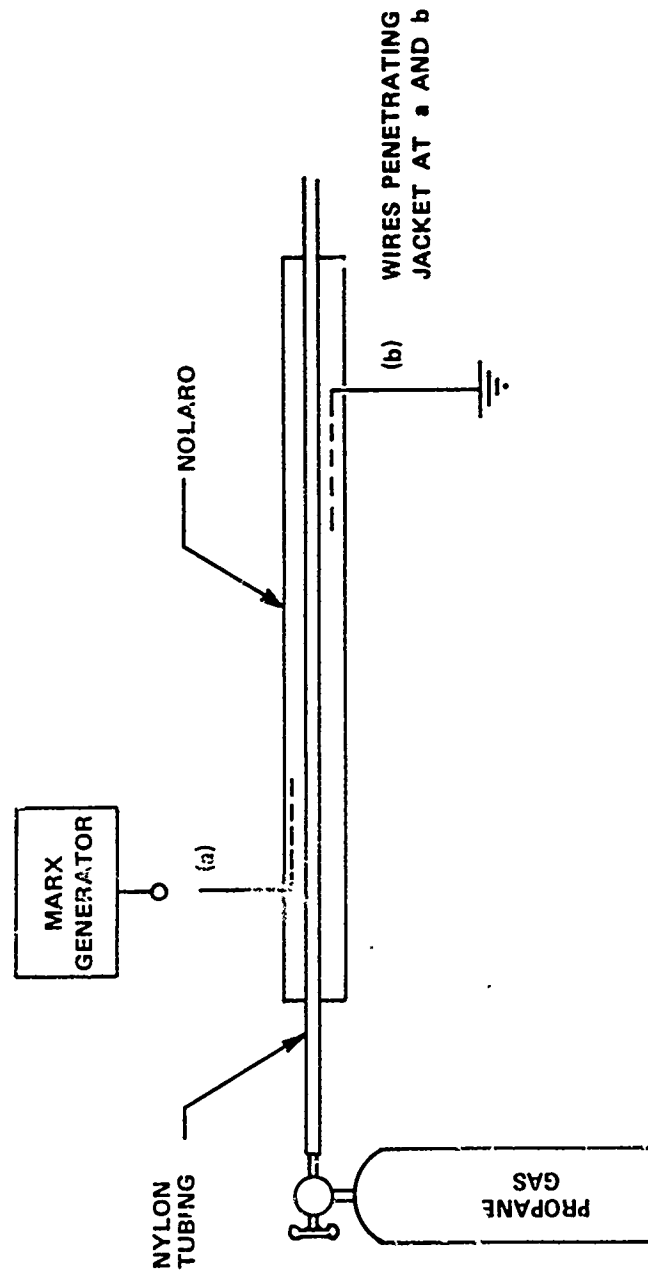
Figure 4-12. Test Setup for Tubular Tether With Propane Gas

4.4 CONDUCTIVE TETHERS

Theoretical aspects of lightning survivability:

As indicated earlier the effects cf lightning are more predictable on a conductive tether than on a dielectric tether. Once the leader contacts the tether, the grounded conductor provides a highly preferential path for conduction of the lightning current to ground. The tether material undergoes a temperature rise described in the next several paragraphs.

Lightning Waveform Models

According to Cianos and Pierce, [24] a typical lightning stroke would rise to a peak value of 20 kA in 1 micro-second and fall to half of the peak value in 50 micro-seconds. A pulse of this description can be represented by:

$$i(t) = I_o (e^{-\alpha t} - e^{-\beta t}) + I_i (e^{-\gamma t} - e^{-\delta t}) + 200$$

$$\text{for } 0 < t < 0.5 \text{ sec} \tag{4-1}$$

where: I_o = 2.1×10^4 A

I_i = 2×10^3 A

α = 1.7×10^4 s^{-1}

β = 3.5×10^6 s^{-1}

γ = 10^3 s^{-1}

δ = 10^4 s^{-1}

The I_o term represents the high current phase, the I_i term represents an intermediate current, and the 200 A dc term, a continuing current. This would be a "typical" stroke of

moderate severity. The high current phase could be fol-
lowed by succeeding strokes of slightly lower peak value
and the continuing current is frequently absent. Further,
values of I_o as high as 200 kA have been presented by
Cianos and Pierce [25] and also by Uman [26,27]. A well-
conducting tether receiving a lightning current will be
heated by two mechanisms: (1) burning and fusion at the
point of arc contact and (2) resistive (I^2R) heating along
the length of the tether. Another factor influencing light-
ning damage to conductors is skin effect - the tendency of
high frequency currents to flow predominantly near the
surface of a conductor. If initially we treat the light-
ning current as a step function, then at the instant of
application, the current will flow entirely on the surface
of the conductor. With time, the current will diffuse
into the material and will eventually be distributed evenly
throughout the cross section.

At a given instant, the current density throughout the
conductor can be expressed in terms of the skin depth δ.
The skin depth is that depth into a conductor for which the
current density is equal to the current density at the surface
divided by ε (the Napierian base: 2.718).

Therefore, referring to figure 4-13

$$J_z(r) = J_o \exp\left[-\frac{(r-a)}{\delta}\right]$$ (4-2)

where

$J_z(r)$ is the current density at some arbitrary radial
distance r from the center

J_o is the surface current density

a is the radius of the conductor

δ is the skin depth

Skin Effect in the Frequency Domain

A survey of skin effect as developed in several standard texts
on field theory has failed to reveal a solution for δ in the
transient case. However, a steady-state solution is commonly
encountered, and is useful for crude estimation of transient
effects when used in conjunction with the power spectrum of a
pulse.

For a frequency f, the skin depth is $\delta = \dfrac{1}{\sqrt{2\pi F \mu \, \sigma}}$ (4-3)

where μ is the permeability of the material and σ is the conduc-
tivity of the material. Equation (4-3) is an approximation appli-
cable to the steady state case with a sinusoidal wave of frequency
f that is considerably smaller than the radius (a).

From the Fourier transform of the high current term in (4-1) we
can determine the power spectrum

$$S(f) = I_o^2 \left\{ \left[\frac{\alpha}{\alpha^2 + (2\pi f)^2} - \frac{\beta}{\beta^2 + (2\pi f)^2} - \frac{\omega}{\alpha^2 + (2\pi f)^2} - \frac{\omega}{\beta^2 + (2\pi f)^2} \right]^2 \right\}$$

4-28

(4-4)
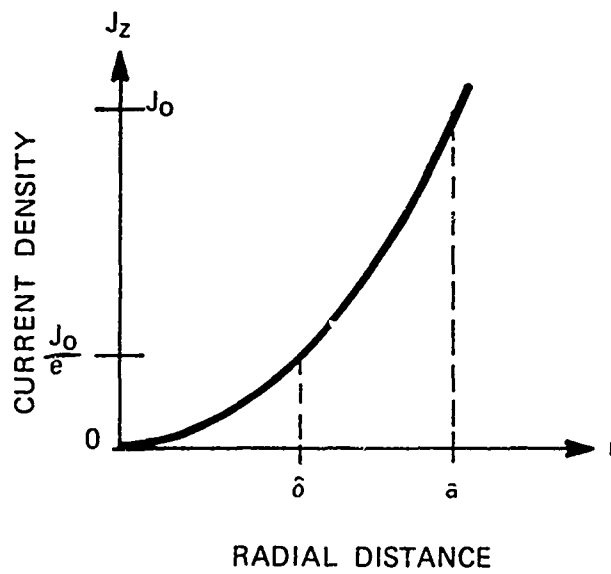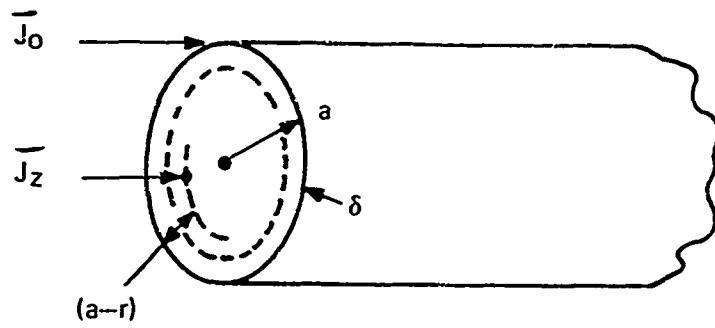
Figure 4-13. Steady–State AC current distribution in a cylindrical conductor.

which for the specified values of I_o α and β can be approximated by:

$$S(f) = \frac{1.535}{1 + (\frac{f}{2705})^2} \quad (amps)^2/Hz \tag{4-5}$$

The power spectrum and skin depth for this hypothetical high current pulse are plotted in figure 4-14. From this figure it is apparent that half of the power in this pulse is below 2705 Hz. For 2705 Hz the skin depth of a stainless steel conductor is about 6 mm, while that of extra improved plow steel (a high carbon steel) is about 0.15 to 0.3 mm at the same frequency.
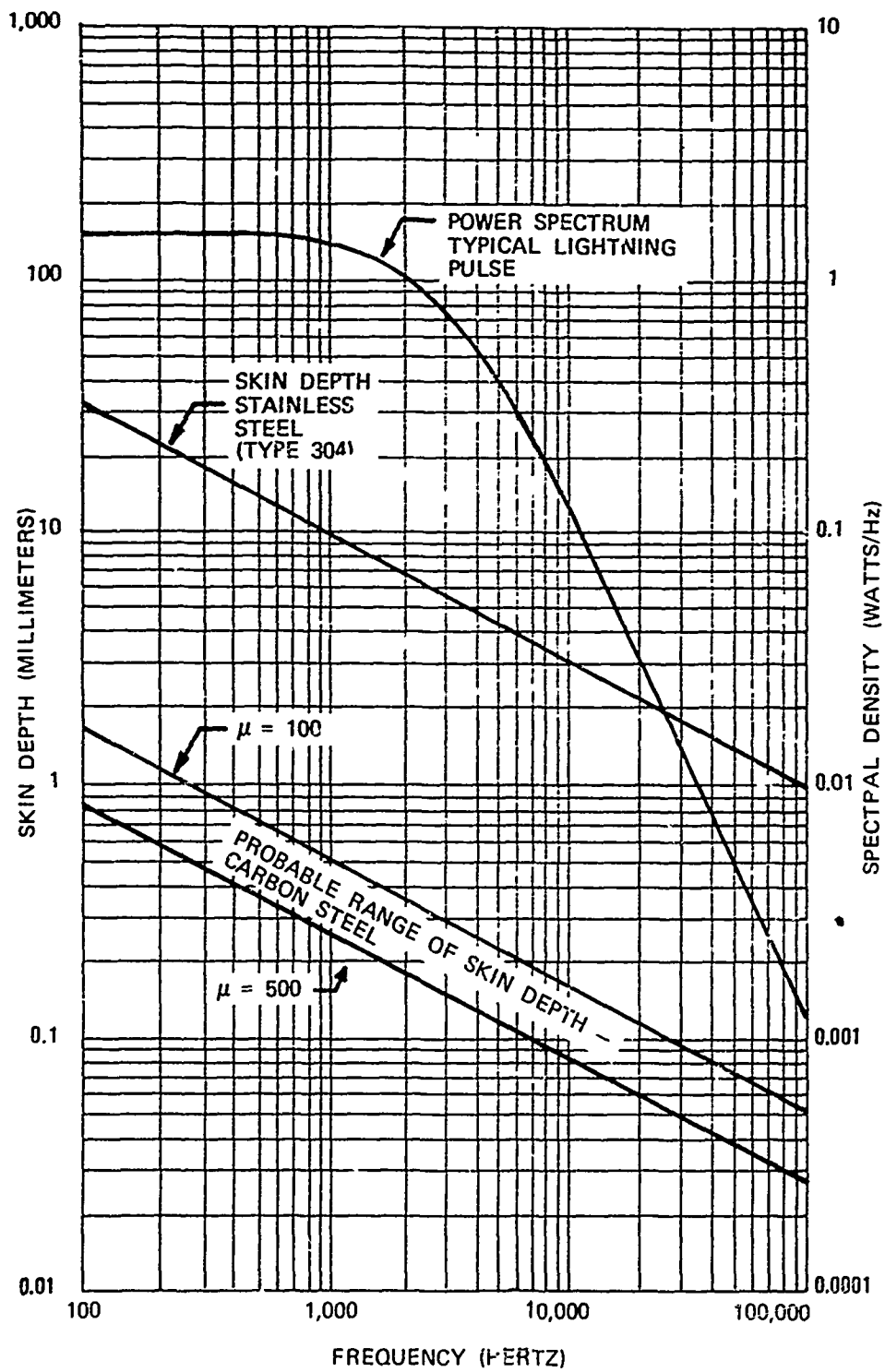
Figure 4-14
Skin Depth — Typical Steel Cable Alloys

4-31

TABLE 4-4

Physical and Electrical Characteristics of Two Steel Alloys

	Stainless Steel Type 304	Carbon Steel Monitor AA
Tensile strength klb/in^2	260	300
Density (lb/in^3)	0.290	0.283
Specific heat (Btu/lb/F°)	0.120	0.110
Melting point (F°)	2650	2642
Thermal conductivity (Btu·in/Hr/ft^2/F°)	113	349
Thermal coefficient of expansion (in/in/F°)	9.6x10^{-6}	6.53x10^{-6}
Resistivity Ω -cmil/ft	432	125
(micro ohm·cm)	72	26.3
Thermal coefficient of resistance	0.00275	0.00778
Relative permeability	1	100-500

Transient Skin Effect

Analytical solutions for transient current density in a conductor are less commonly encountered than steady state solutions. However, Haines [28] has developed a solution for transient skin effect due to exponential pulses of the type used to represent the high current portion of a lightning pulse. The theoretical current density in a 3/8-inch diameter stainless steel cable is shown in figure 4-15a, while comparable curves for carbon steel of the same diameter are given in figure 4-15b. In both cases the forcing function is:

$$i(t)=2.1 \times 10^4 [\exp(1.7 \times 10^4 t)t - \exp(3.5 \times 10^6 t)]$$

$$(4-6)$$

In figure 4-15b, current densities at the center, mid-radius, and outside of the cable are given, along with the mean current density, which has the same form as (4-6). Note that initially, all of the current (1000 A/mm^2) is flowing on the surface but that current equalizes throughout the cross section in about 9 microseconds. Thereafter, current density at the center is greater than that on the surface. This phenomenon is known as "inverse skin effect".

In the case of carbon steel (monitor AA), the diffusion time is much longer than the pulse duration and the pulse subsides before substantial diffusion of current into the center of the cable occurs. Restriction of most current to the outside of the cable results in a peak surface current density exceeding that of stainless steel by an order of magnitude. Current in the inner half of the cable remains too insignificant to plot on the same scale as surface current. Note that the polarity of the surface current changes from positive to negative after about 55 microseconds. Since the current density at the center remains near zero, this constitutes an inverse skin effect.

These two examples indicate that the effect of a high current
pulse on a carbon steel cable is very different from the effect
of an equivalent pulse on a stainless steel cable. Specifically,
the current diffuses into the stainless steel cable rapidly,
while the slower diffusion into the carbon steel cable inten-
sifies current density near the surface. It is likely that this
could result in surface burning and unequal expansion with re-
sulting exfoliation of the carbon steel. These factors indicate
that skin effect will intensify damage to a material for which
diffusion time is long compared to the pulse duration. Theory
and computer programs relevant to figure 4-15 are given in
appendix C.
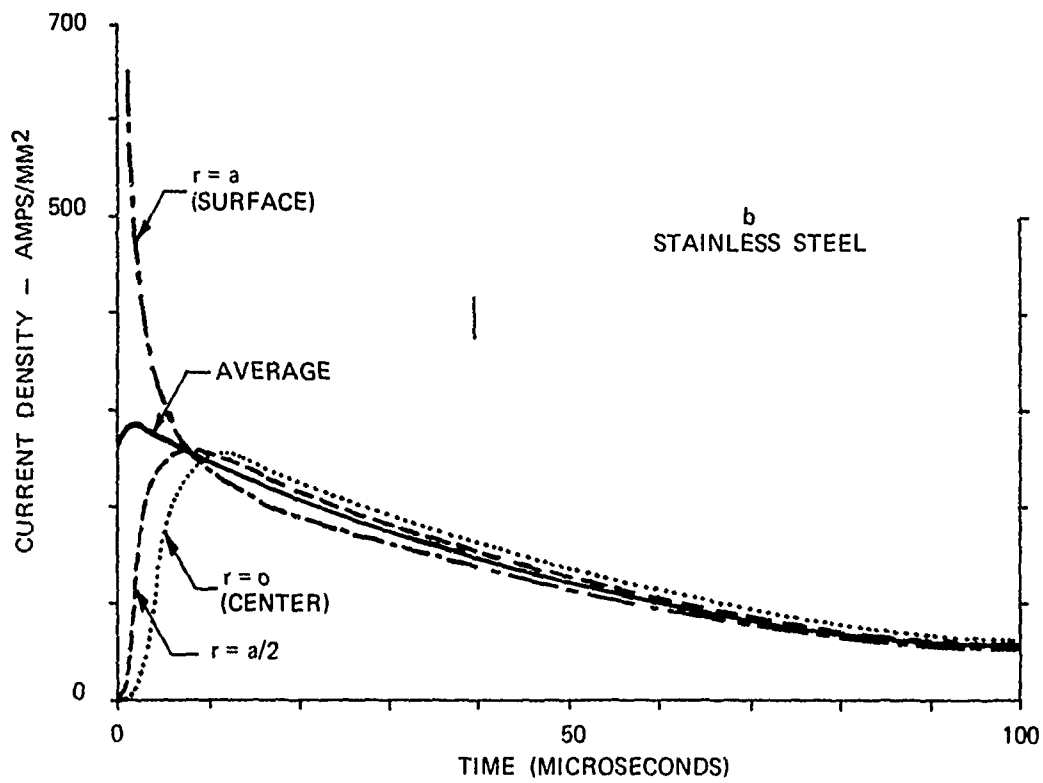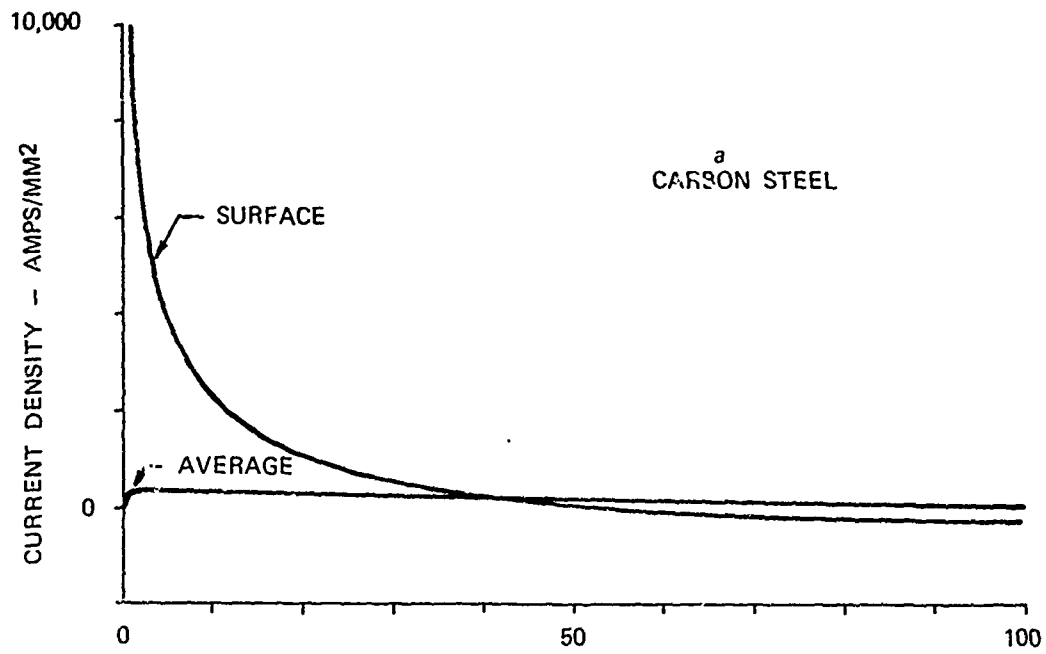
Figure 4-15.
Current Density in Wire Rope during High Current Pulse

The work by Haines indicates that a substantial diffusion of current occurs in a time on the order of

$$\tau = \frac{\mu \sigma a^2}{\gamma_1^2}$$

$$\text{(4-7)}$$

where $\gamma_1 = 3.832$

This parameter is plotted for the applicable alloys and diameters in figure 4-16. For reference the current waveform described by equation (4-1) is included. From this graph it is apparent that for a 0.375-inch diameter stainless steel cable, diffusion occurs in about 2.5 microseconds, and at the end of this period the lightning pulse is still near its peak value. In the case of the plow steel, diffusion requires at least 3.5 milliseconds, during which time the lightning pulse decays to about 1% of peak value.
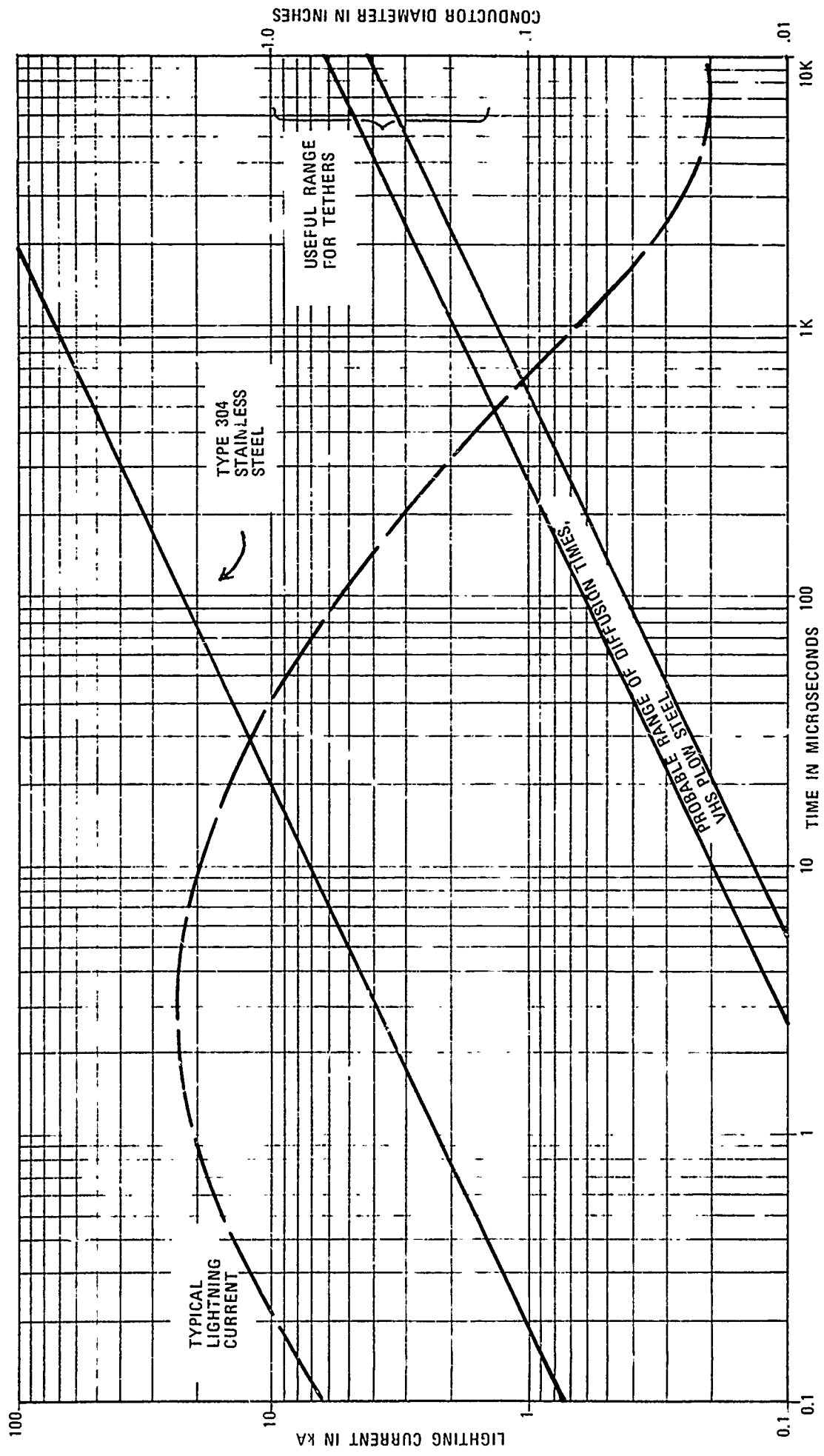
Figure 4-16. Diffusion Times for Typical Steel Cable Alloys and Diameters

4-37

The time required for a current transient to diffuse into a conducting cylinder has been computed as a means of estimating the value and rise time of current induced in wires in conduits and shielded cables by high current pulses applied to the surface. A diffusion time constant is defined.

$$\tau_d = \mu\sigma d^2 \tag{4-8}$$

Where d is the thickness of the shield or conduit. Vance [29] computed the following relationship between induced pulse rise time τ_r, the driving pulse decay time $\tau_\alpha = \frac{1}{\alpha}$ and diffusion time constant τ_d

$$\alpha\tau_d \gg 1 \qquad\qquad t_r = 0.38\tau_d$$

$$\alpha\tau_d = 1 \qquad\qquad t_r = 0.15\tau_d$$

$$\alpha\tau_d \ll 1 \qquad\qquad t_r = 0.236\tau_d$$

4-38

It is apparent that the diffusion times and skin depth of the
alloys considered here are considerably affected by their perme-
abilities. Because stainless steel permeability is low relative
to plow steel, the skin depth is greater and diffusion time is
less. This means that lightning current would tend to equalize
more rapidly through the cross section of a stainless steel cable,
and the material would be more evenly heated. Since the plow
steel has a higher permeability, relatively little of the high
current transient would diffuse into the interior of such a cable;
but on the other hand much of the current would be concentrated
near the surface, where heating would be more intense. It has
been observed, however, that thermal damage is caused primarily
by the continuing current rather than the high current pulse.

Heat Transfer

The intent of this section is (1) to show that thermal time con-
stants for the steels discussed are long enough to preclude appre-
ciable heat transfer during the high current phase of a typical
lightning stroke and (2) to produce a coarse estimate of the
spatial extent of heating around an arc contact.

A cylinder being heated by an arc is depicted in figure 4-17.

The actual size of the arc as it contacts the cable is probably
quite small, on the order of millimeters. Some motion of the arc
can be expected, but it could also remain essentially stationary.
A small area around the channel is heated by radiation. The
total heated area which could be called the "surface contact area"
is probably about 1-1.5 cm in diameter. The potential across
this arc is approximately 10 volts irrespective of material con-
ductivity. [31]. The energy dissipated in the arc can be esti-
mated by:

$$\int_0^\tau Vi(t)dt - 10 \int_0^\tau i(t)dt \qquad Joules \qquad (4-9)$$
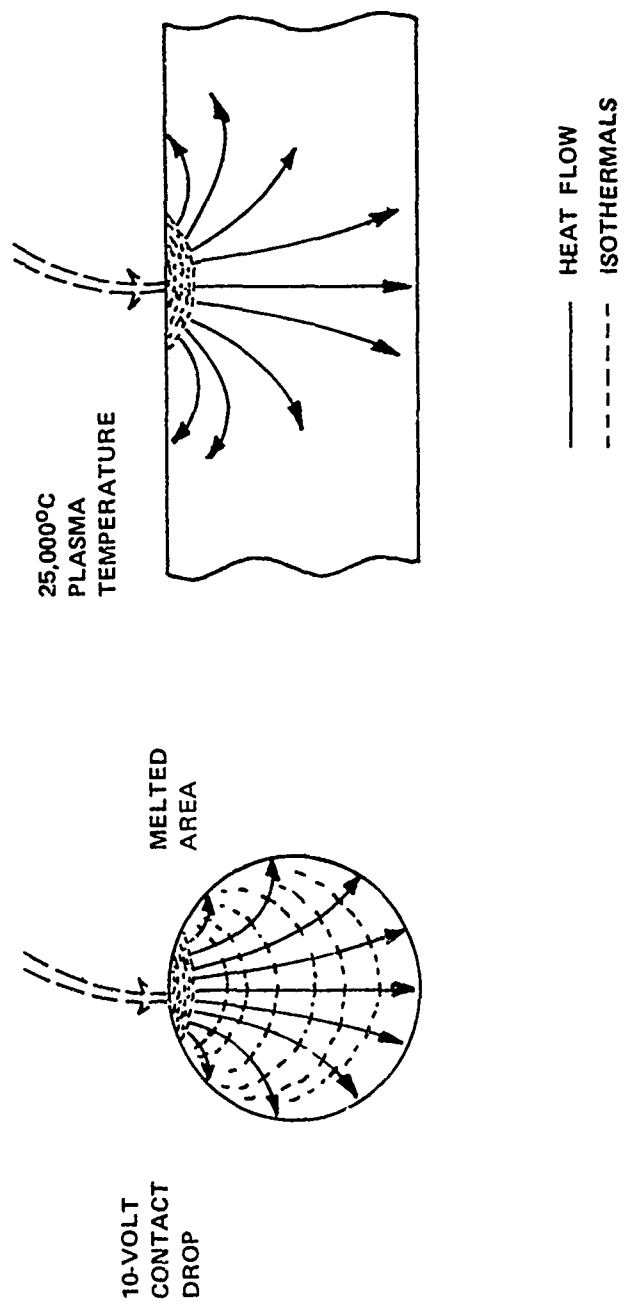
Figure 4-17. Heat Flow Into a Conducting Cylinder From an Arc Contact

The lightning channel at the point of contact can have a temperature of 25,000°F which results in melting at the point of contact; the spatial extent of the instantaneous temperature rise is not apparent from any of the sources consulted for this study: If, however, we assume that the surface is raised to a very high temperature during the high current phase, and that heat transfers inward at a rate determined by tether geometry and physical characteristics, then the spatial extent of heating can be estimated. Figure 4-18, based on theory given by Jacob [32] , indicates the temperature of the center of a 3/8 inch metal cylinder relative to a temperature suddenly applied to the outside. This graph indicates that a solid 3/8-inch cylinder of carbon steel would have a thermal rise time of about 0.8 second, while a similarly configured stainless steel rod would required about 3 seconds. A wire rope, owing to air space between wires, would require longer to equalize, but the approach is admittedly imprecise.

The portion of the wire rope affected by the arc will experience a temperature rise given by

$$\Delta T = \frac{E}{\rho_v \, V \, C_p} \tag{4-10}$$

where ΔT is the temperature rise (Centigrade or Kelvin)

E is the energy dissipated in the material (joules)

ρ_v is density of material. $(kg \cdot m^{-3})$

V is volume in which the energy is dissipated (m^3)

Cp is the specific heat of the material (Joule/kg K°)

For an arc contact the energy is given by

$$E = \int_0^\tau v \, i(t) \, dt = 10 \int_0^\tau i(t) \, dt \tag{4-11}$$

where τ is the duration of the strike

v is the voltage of the arc (10V)

i(t) is the current waveform.

4-41
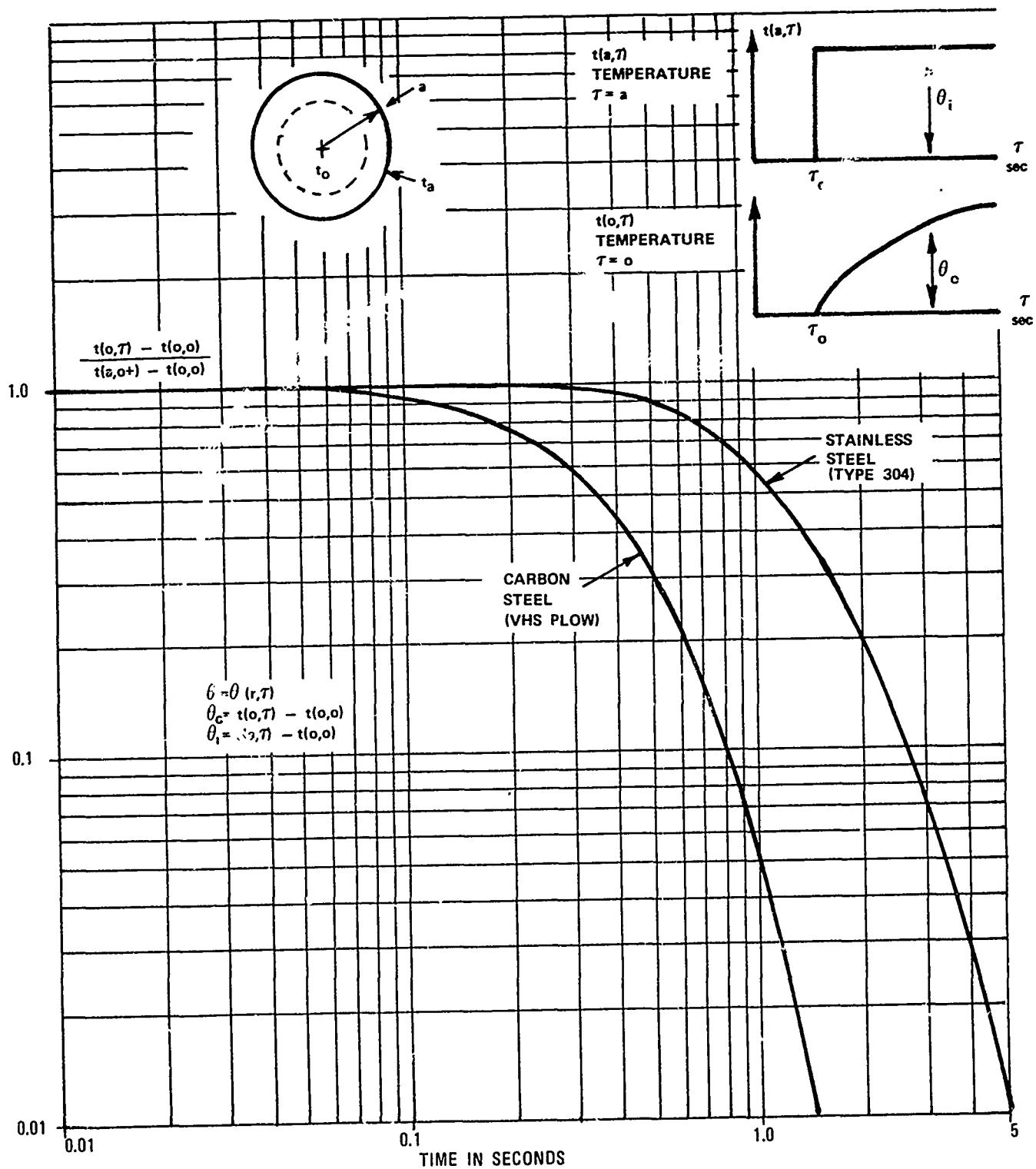
Figure 4-18.   Transient Heat Flow Into a 3/8-Inch Steel Cylinder

The depth of penetration (δ_ρ) is not known, but if we assume
that it can be based on heat transfer, then an estimate of δ_ρ is *

$$\delta_\rho = 1.6 \sqrt{\alpha\tau} \quad \text{meters} \tag{4-12}$$

where α is the thermal diffusivity of the tether alloy.

Then for a surface contact area of 1-cm radius, the affected volume is:

$$V = (1.257 \times 10^{-7}) \sqrt{\alpha\tau} \ m^3$$

$$= (2.53 \times 10^{-7}) \sqrt{\alpha\tau} \ m^3 \text{ for stainless steel}$$

$$= (4.69 \times 10^{-7}) \sqrt{\alpha\tau} \ m^3 \text{ for carbon steel}$$

To assess the heating due to a typical high current phase, consider
a 21-kA, 50-microsecond, high current pulse accompanied by a 2-kA,
1-millisecond intermediate pulse, both integrated over 10 milli-
seconds.

$$E = 10 \int_0^{10^{-2}} (2.1 \times 10^4) \exp[(-1.7 \times 10^4)t] dt \tag{4-13}$$

$$+ 10 \int_0^{10^{-2}} (2 \times 10^3) \exp[-10^3 t] dt$$

$$E = 32 \text{ joules}$$

For stainless steel the depth of penetration is 0.32 mm in 10
milliseconds (from 4-12). The 32 joules of energy will be dissi-
pated in a volume of 2.53×10^{-8} m^3 and the predicted temperature
rise would be

$$\Delta T = \frac{32 \text{ Joules}}{(8027.2 \text{ kgm}^{-3}) (2.53 \times 10^{-8} m^3)(502 \text{ J} \cdot \text{kg}^{-1})}$$

$$= 314^\circ C \text{ or } 565^\circ F$$

* Derivation in appendix D.

This is a tolerable temperature since the damage point for stainless steel is 1000°F. It must be realized, however, that heating at the surface will be much more intense.

Similarly for carbon steel, the depth of penetration in 10 milliseconds is 0.597 mm and the same 32 joules would be dissipated in a volume of 4.68×10^{-8} m^3. For this case the temperature would be elevated by an amount:

$$\Delta T = \frac{32}{(7833.4)(4.68 \times 10^{-8})(460.24)}$$

$$= \quad 190°C \text{ or } 341°F$$

Carbon steel is damaged when the temperature is elevated beyond 600°F. Assuming initial temperatures of 72°F, these peak temperatures may be expressed as percentages of maximum allowable temperature:

Stainless steel;

$$\frac{72° + 565°}{1000°} \quad = 64\%$$

Carbon steel:

$$\frac{72° + 341°}{600°} \quad = 69\%$$

Experiments indicated that the advantage of stainless steel was substantially greater than these calculations show.

Figure 4-19 gives predicted temperature rise for stainless steel (type 304) and carbon steel (VHS plow steel).
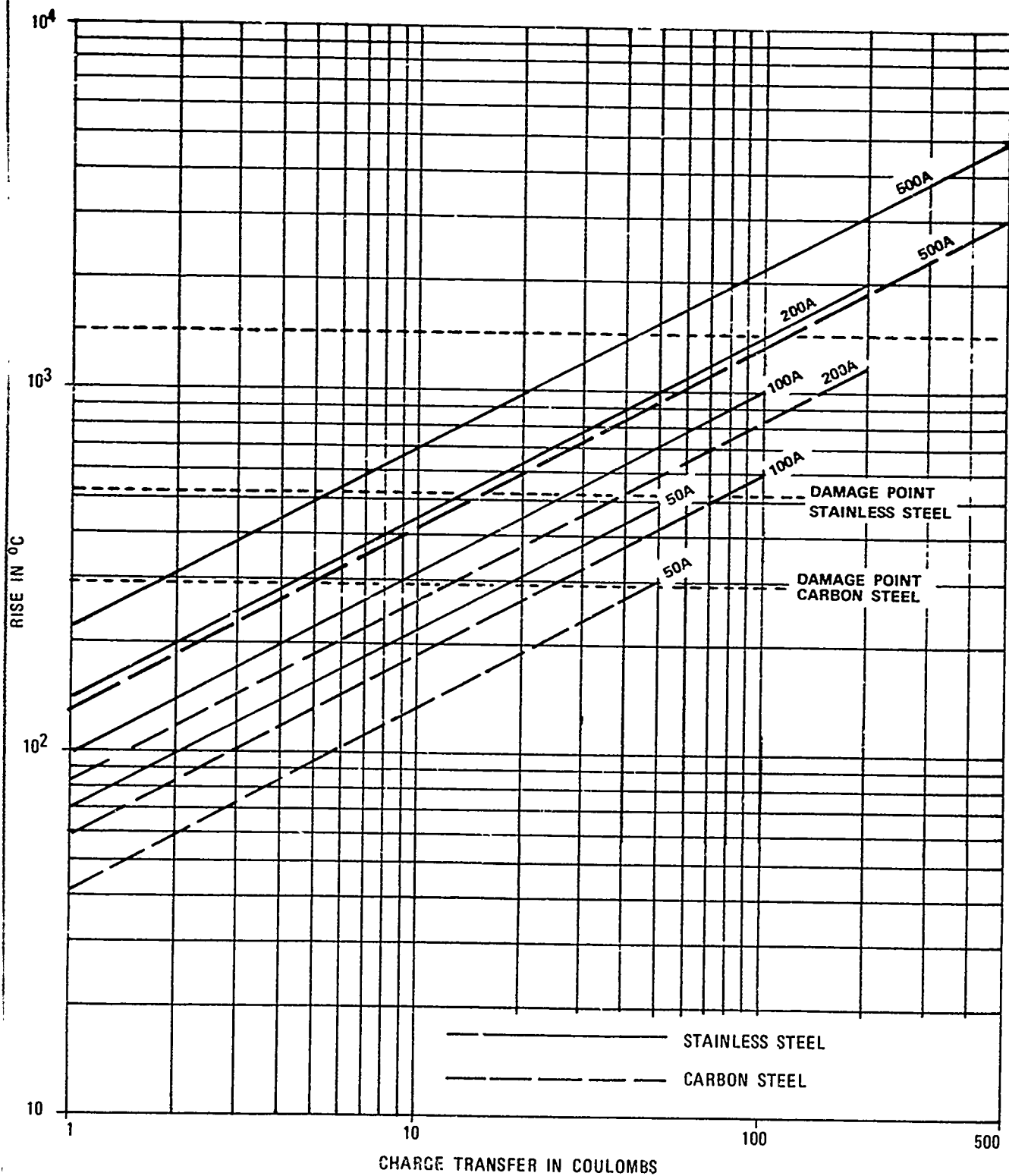
Figure 4-19. Predicted Temperature Rise Near Point of Arc Contact

Resistance Heating

Away from the point of arc contact, the cable is heated resistively. In this case the energy balance equation is:

$$R \int_0^\tau i^2(t)\, dt = MC\rho\Delta T \qquad (4\text{-}14)$$

The term $\int i(t)\, dt$ which we shall represent by $\mathfrak{z}$, is known as the action integral. Statistics on the action integral are available [33]. The resistance of a tether section, of length $\Delta\ell$ is:

$$R = \frac{4\Delta\ell\rho_0\,(1+\alpha\Delta T)}{\Pi D^2} \qquad (4\text{-}15)$$

Where ρ_0 is the resistivity of the tether material at $293°\,K$, α is the thermal coefficient of resistance, and D is the tether diameter. The mass of this section is:

$$M = \frac{\Pi\delta D^2\Delta\ell}{4} \qquad (4\text{-}16)$$

Where δ is the density of the tether material. Neglecting resistance changes due to expansion, we encounter a temperature rise

$$\Delta T = \frac{1}{\alpha}\ \frac{\mathfrak{z}}{A-\mathfrak{z}} \qquad (4\text{-}17a)$$

where
$$A = \frac{\Pi^2\delta C\rho D^4}{16\ \alpha\ \rho_0} \qquad (4\text{-}17b)$$

Note that unlike the arc contact situation the action integral, not simply the charge transfer, is the factor determining temperature rise.

As we compare the tendencies of stainless steel and carbon steel to heat under the influence of equal action integrals it is apparent that the only characteristic (other than tensile
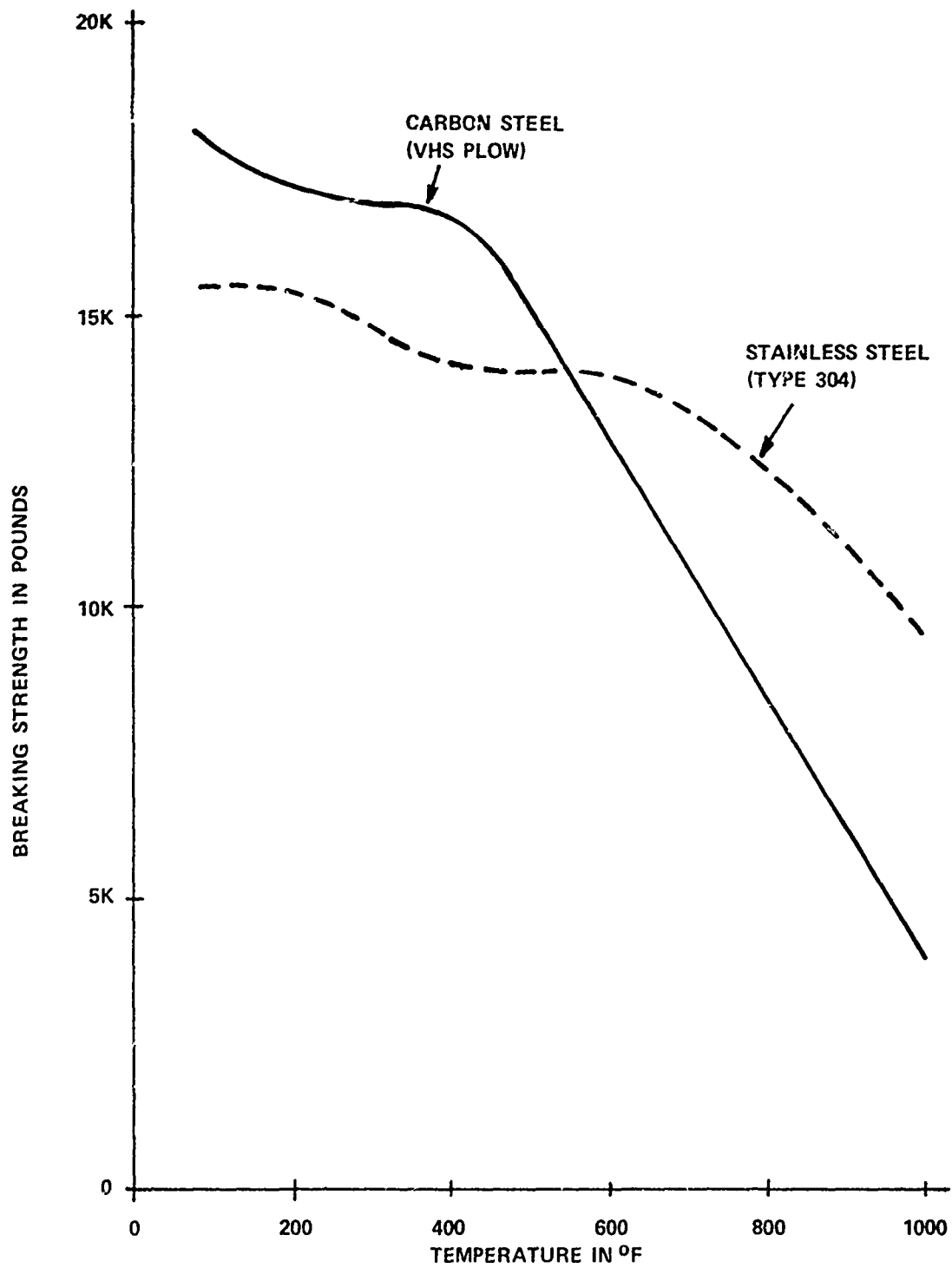
Figure 4-20. Effect of Elevated Temperature on Strength of 0.404-Inch Diameter Wire Rope

strength), that differs greatly between the two is electrical resistivity. The substantially higher resistivity of stainless steel indicates that the temperature of a given cross-section of stainless steel subjected to a certain lightning current would be increased more than would an equal cross-section of carbon steel under the same circumstances. Whether or not stainless steel would reach its damage point of 1000°F more rapidly than carbon steel would reach the 600°F required for permanent damage is of critical importance. Figure 4-20, based on information obtained from U.S. Steel [34], shows the breaking strength of two wire rope tethers of equal diameter, one made of stainless steel, the other of extra-improved plow steel (Monitor AA) a very high strength carbon steel. Notice that while the carbon steel has higher breaking strength at room temperature, both ropes have the same strength at 550°F, and beyond that stainless steel has superior strength. Table 4-5 gives calculated action integrals necessary to effect various temperature rises in the two cables and their probabilities of occurrence. Note that a greater action integral is required to damage the carbon steel than stainless steel. Note also that in either case a stroke of such intensity is relatively improbable. However, as we consider rope diameters which could be used on smaller balloons the probability of damage increases.

An effect not considered here and difficult to assess is the additional heating resulting from minute arcs across the interstices of the individual wires of the rope. An additional uncertainty is introduced by the fact that metals behave somewhat differently under rapid heating conditions than gradual heating conditions. The high temperature strength data used here was only available for gradual heating rates.

Table 4-5

EFFECT OF LIGHTNING CURRENT ON BREAKING STRENGTH OF WIRE ROPE TETHERS

Carbon Steel - Monitor AA

Temp. (°F)	Breaking Strength (lb)	Action Integral Coulomb Amps	Probability of Occurrence (%)
75°	18,126		
200	17,122	1.8×10^6	0.85
400	16,820	3.3×10^6	0.43
600	12,881	4.1×10^6	0.33
800	8,487	4.6×10^6	0.29
1000	4,033	5.0×10^6	0.27

Stainless Steel, Type 304

Temperature(°F)	Breaking Strength(lb)	Action Integral Coulomb Amps	Probability of Occurrence(%)
75	15,515		
200	15,421	0.6×10^6	2.7
400	14,210	1.1×10^6	1.4
600	14,110	1.3×10^6	1.2
800	12,314	1.4×10^6	1.1
1000	9,556	1.6×10^6	1.0

Notes: Both tethers have 0.069 in^2 cross section. Temperature performance is based on information obtained from U.S. Steel. Probability estimates are from reference [34].

Results of Exposure of Wire Rope to Simulated Lightning

Samples of various wire rope sizes and materials were exposed to
simulated lightning by the Lightning and Transients Research
Institute, Miami, Florida. The two types of waveforms used are
depicted in figure 4-21.

High Current Pulses

The high current pulses used to simulate the transient portion
of a lightning stroke are of damped oscillatory form which may
be represented by:

$$i(t) = I_o e^{-at} \sin\omega t \qquad (4\text{-}18)$$

where I_o and a may be determined by fitting an exponential curve
to peak values on the oscilloscope photographs and ω can be based
on the first line crossing. For these waveforms, charge transfer
was computed from:

$$Q = {}_o\!\int^{T/2} I_\rho \sin\omega t \, dt = \frac{2I_\rho T}{\pi}$$

where I_p is the peak value of the sinewave, T/2 is the time to
the first line crossing, and $\omega = 2\,\pi/T$.

The action integral is determined by:

$$\mathfrak{J} = {}_o\!\int^{\infty} (I_o e^{-at}\sin\omega t)^2 dt \qquad (4\text{-}19)$$

$$\mathfrak{J} = \frac{I_o{}^2}{4a} - \frac{aI_o{}^2}{4(a^2 + \omega^2)} \qquad (4\text{-}20)$$

4-50

230,000 A

a)   High Current Transient

4 MV TRIGGER

300 A

0   1S
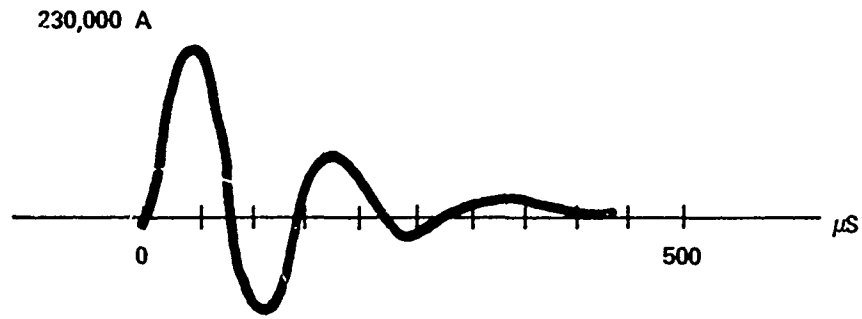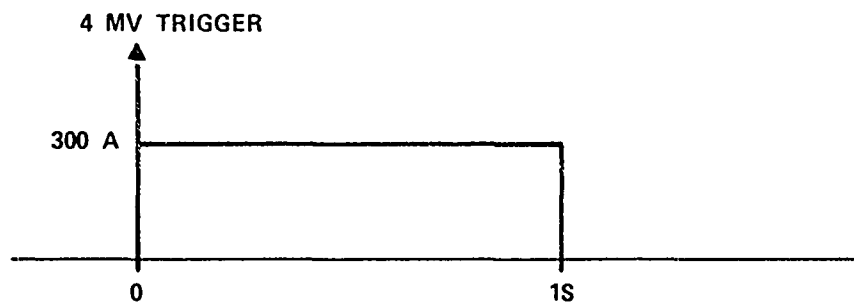
b)   High Coulomb Transfer

Figure 4-21.   Typical Waveforms — Simulated Lightning
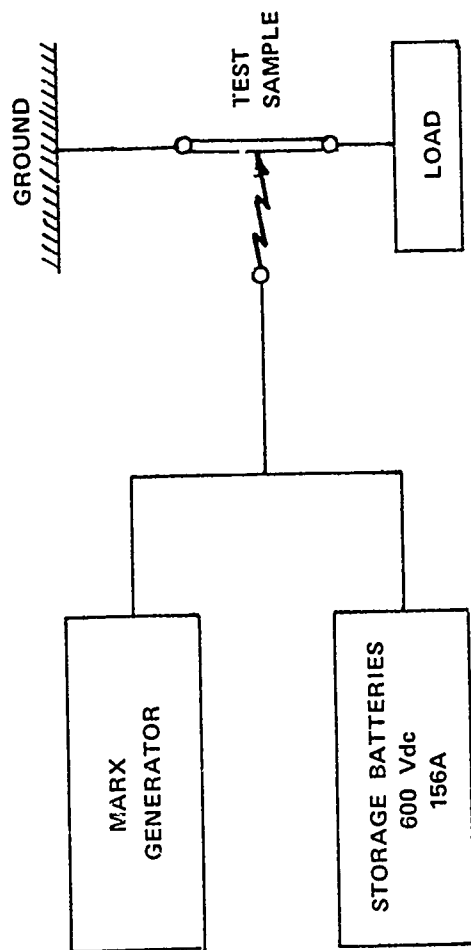
Figure 4-22. Test Configuration for High Coulomb Transfer to Loaded Wire Rope Sample

GROUND

TEST SAMPLE

LOAD

MARX GENERATOR

STORAGE BATTERIES
600 Vdc
156A

High Coulomb Transfers

Continuing currents were simulated by delivering 156 amperes dc
from a bank of storage batteries tc the test sample across an arc
which was initiated by a high voltage pulse from the Marx gen-
erator. (See figure 4-22.) This is an approximate average value
for continuing currents and charge transfers typical of severe
strokes that can be duplicated by controlling the exposure time.
This current waveform is analytically much simpler than the high
current pulse. Charge transfer is simply the time current pro-
duct and action integral is the current-charge transfer product,
i.e.,

$$Q = IT$$
$$\Theta = I^2T = QT$$

Load Testing

After the test exposure, those samples which had not failed under
test were pulled to destruction and the breaking strength noted.
Sufficient time for the specimen to cool (generally days) elapsed
before the load testing. Therefore, only the permanent damage
resulting from the test exposure was apparent. Failure at less
than the nominal breaking strength indicated that a portion of
the specimen cross section had been heated beyond the allowable
temperature for the materials: 600°F for plow steel and 1000°F
for stainless steel. Temporary reduction of breaking strength
could not be determined.

To assess short-term effects, several tests were performed with
the 1/4-inch rope loaded to slightly over 20% of room temperature
break strength. These specimens failed for exposures of 80 cou-
lombs or greater. Several interesting effects were noted. It
appeared that momentum of the load resulting from the elonga-
tion of the rope accelerated the breaking of the rope. This
effect would probably be less pronounced with a constant pull
type of test machine. It may also be surmised that reduction of
cross section due to "necking" of the material causes more rapid
heating once the failure process has begun.

Test Specimens

Wire rope specimens of carbon and stainless steel having approx-
imately the same cross section were selected for comparative
testing. The 6x19 ropes were closest matches available from
existing inventories of the TELTA project and the AFETR Range
Contractor and are not considered suitable for use as balloon
tether since they are not torque-balanced. However, they are
suitable for comparing the relative survivabilities of carbon
and stainless steel ropes of equal cross section.

The 3/8-inch diameter 3 x 18 specimen is a torque-balanced rope
developed for oceanography with an electrical conductor in each
strand. This rope is suitable for use as a tether-transmission
line, although a slightly larger diameter would be advisable for
the 205,000 ft^3 2D7 balloons.

Test Results

The effects of high coulomb and high current pulses on 3/8-inch
diameter 6 x 19 wire rope are shown in table 4-6 and figure 4-23.
When breaking strength is plotted as a function of action inte-
gral, the effect of the high current pulse (shown as a circle)
is not consistent with that of the high coulomb transfer (shown
as a triangle). This is because the same value of action inte-
gral was computed for a 220 kA pulse which only delivered 7.2
coulombs and the 156 ampere 300-coulomb pulse which produced
much greater damage. An additional inconsistency is the apparent
"improvement" of carbon steel by a 220 kA pulse. It has been
suggested that an inadvertent "tempering" of the specimen was
produced (Vol II, Part D, Page 16).

In figure 4-23b, the residual strength is plotted as a function
of charge transfer and is seen to be approximately logarithmic.
In either case the stainless steel retains greater strength than
the carbon steel. The dependence of damage on coulomb transfer
rather than action integral implies the pre-eminence of arc con-
tact damage over resistive heating. Visual inspection revealed
melt spots, discoloration, and other evidence of burning.

4-54

Since the testing of the 3/8-inch 6 x 19 rope did not indicate temporary loss of strength, it was decided to perform high coulomb testing of a cable suspending a realistic operating load of 20% break strength. A maximum weight of 1500 lb was available at LTRI so 1/4-inch diameter 6 x 19 rope having nominal room tempertature breaking strength of 6,500 to 7,500 lb was selected for this test. The grade of carbon steel desirable for tether use was more closely duplicated in this rope than in the 3/8-inch 6 x 19 rope. The results of these tests are shown in table 4-7 and figure 4-24. Stainless steel failed under test for 100 coulombs or more, while the carbon steel failed at 80 coulombs. As indicated in figure 4-24, the residual strength tends to vary with charge transfer except for "improvement" of stainless steel at 32 coulombs. The arcs produced during this test sequence were quite variable in area spread and length intensity and some inconsistency of results can be attributed to these effects. Again superior performance of stainless steel is apparent.

The effect of high current pulses on a single strand from the 3 x 19 oceanographic rope is given in table 4-8 and figure 4-25. Here it can be seen that residual strength is approximately linear with charge transfer.
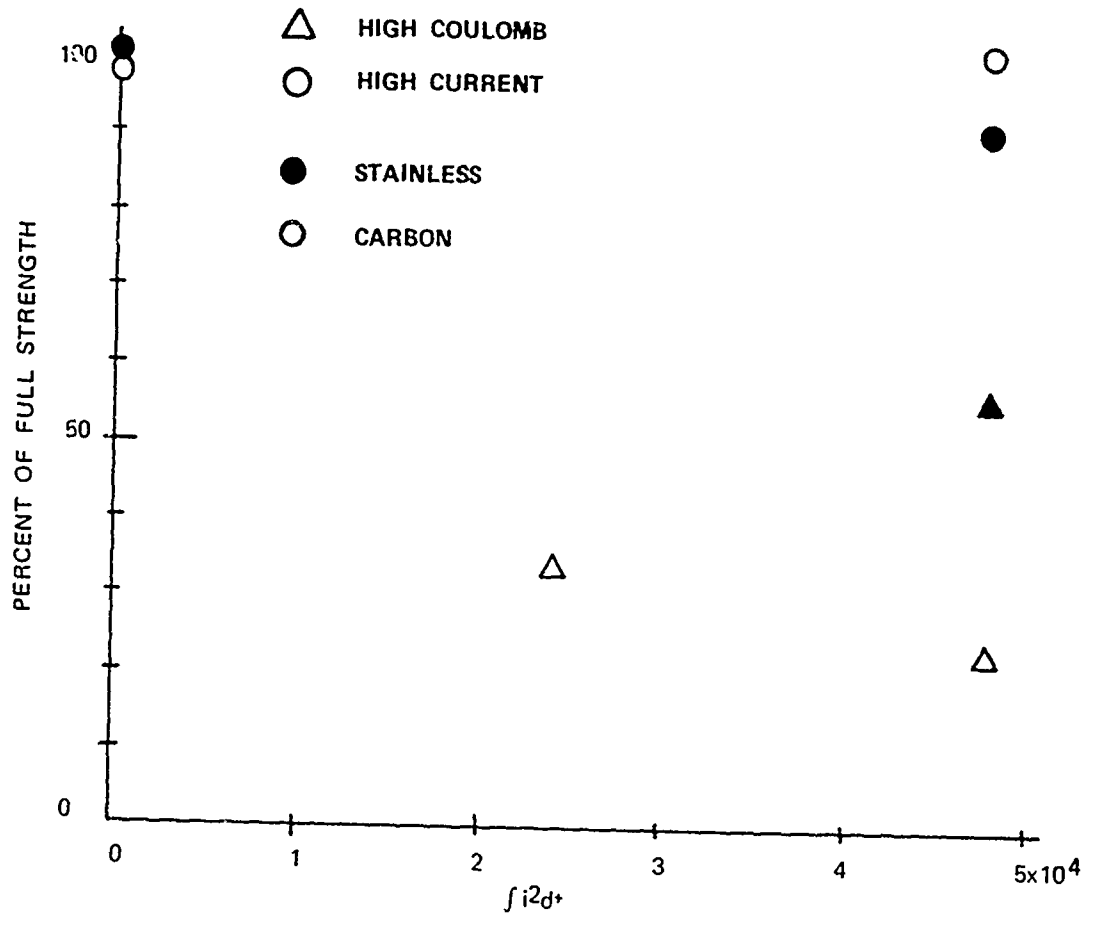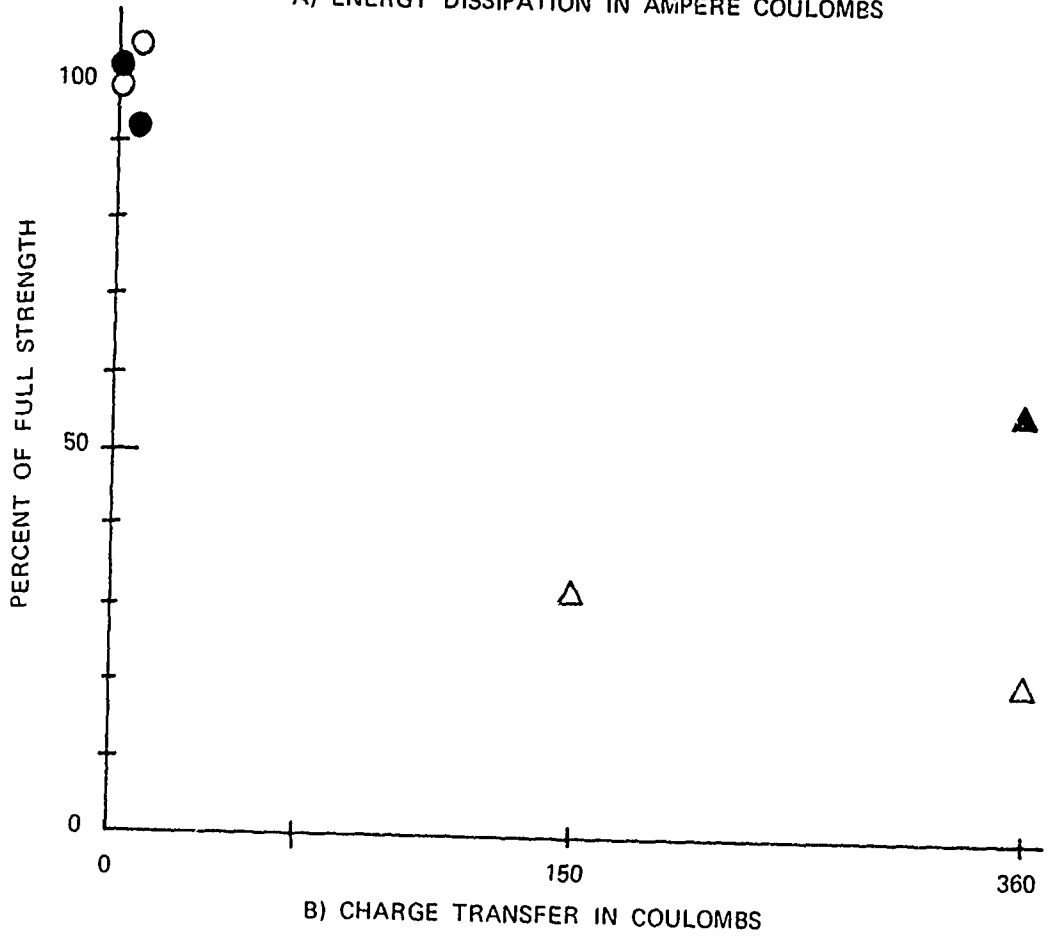
Figure 4-23. Effect of Exposing 3/8-Inch (6x19) Wire Rope to Simulated Lightning

Table 4-6

EFFECTS OF SIMULATED LIGHTNING ON 3/8-INCH DIAMETER, 6x19 IWRC

Material	Peak Current Amps	Charge Transfer Cculombs	Action Integral Cculomb-amps	Probability Level	Breaking Strength (lb)	Remarks
Stainless Steel					14,200	Three unexposed samples
	1.1×10^5	3.6	1.2×10^4	85	13,000	No visible damage
	2.2×10^5	7.2	4.8×10^4	70		
	160	300	4.8×10^4	1.8	8,000	Melting and burning
Carbon Steel	—	—	—	—	13,930	Control run-average of three unexposed samples
	2.2×10^5	7.2	4.8×10^4	70	14,600	Apparent strength increase
	160	150	2.4×10^4	3	4,600	Three discharges with cooling between. Melting and burning.
	160	300	4.8×10^4	1.8	3,200	Burning and melting

Table 4-7

EFFECTS OF SIMULATED LIGHTNING ON 1/4-INCH DIAMETER WIRE ROPE 6 x 19 IWRC with 1500 LB LOAD

Material	Peak Current Amps	Charge Transfer Coulombs	Action Integral Coulomb-amps	Probability Level	Breaking Strength (lb)	Remarks
Stainless Steel (Type 304)					7000	Control run average of three unexposed samples
	156	312	4.87×10^4	1.6	Unknown	Failed during exposure
	156	156	2.43×10^4	3.0	Unknown	Failed during exposure
	156	100	1.56×10^4	6.0	Unknown	Failed during exposure
	156	80	1.25×10^4	9.0	2700	
	156	54	8.2×10^3	16	2900	Several repetitions spread arc
	156	32	5.0×10^3	42	7200	Spreading Arc
	156	16	2.5×10^3	80	2800	More intense arc than above
Carbon Steel (Monitor AA)	-	-	-	-	6500	Control run same for three unexposed samples
	156	80	1.25×10^3	9.0	Unknown	Failed during exposure
	156	80	1.25×10^3	9.0	800	
	15	32	5.0×10^3	42	2500	
	156	16	2.5×10^3	80	2800	
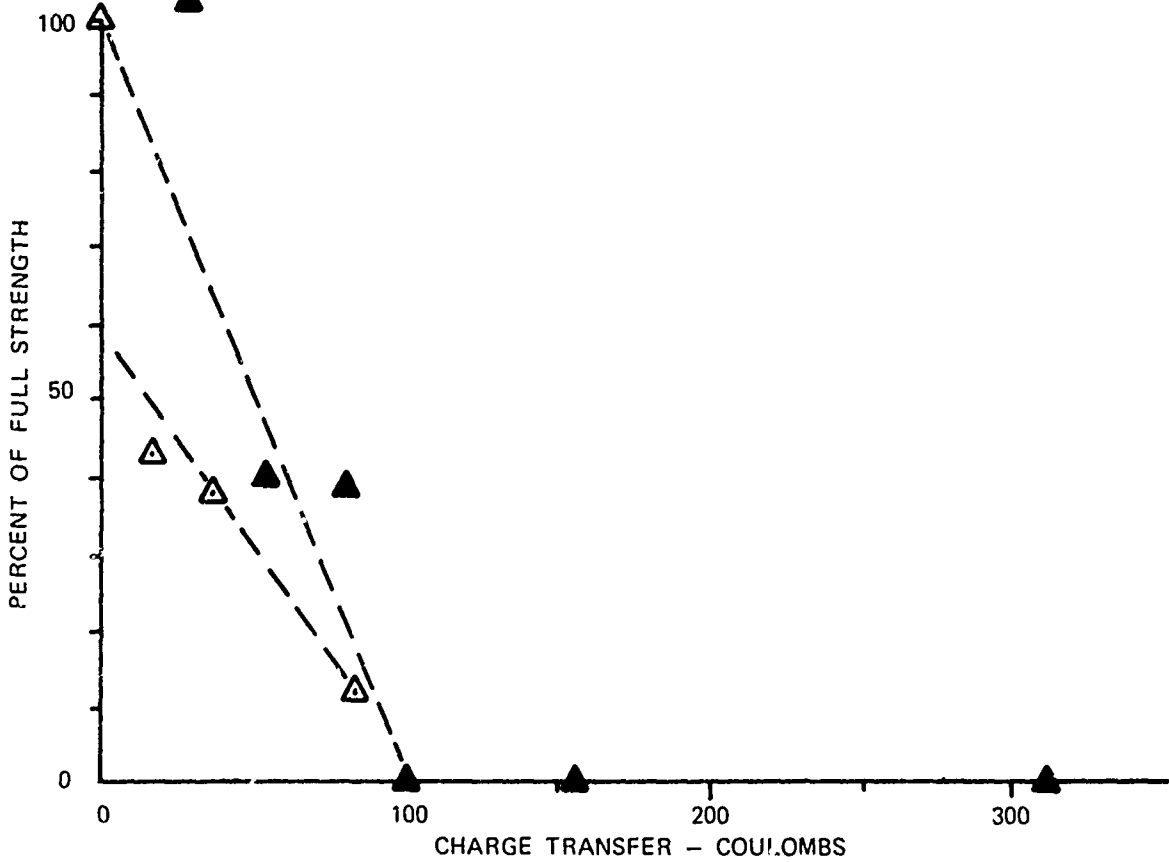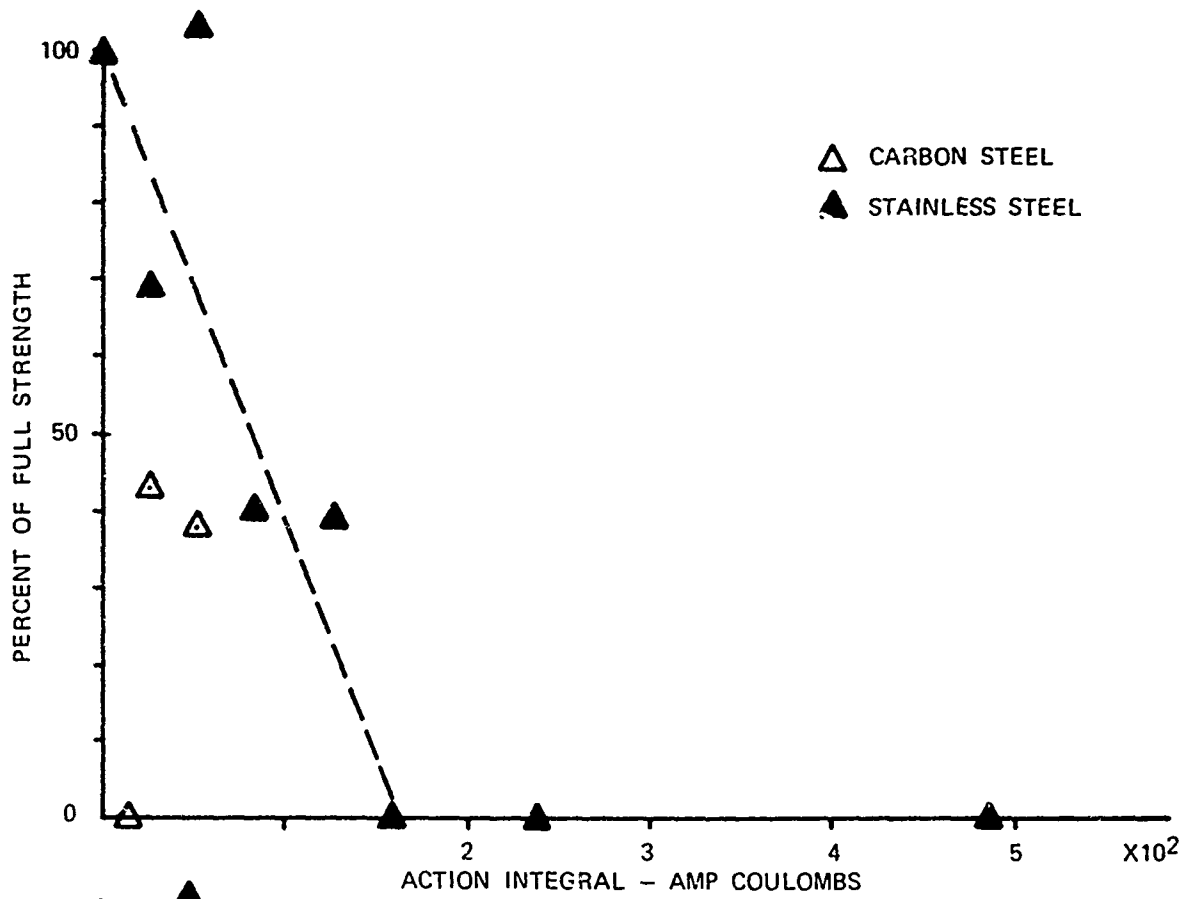
Figure 4-24

Effect of Exposure to Simulated Lightning on 1/4 Inch Wire Rope

Table 4-8

EFFECTS OF SIMULATED LIGHTNING ON ONE STRAND FROM 3/8 INCH DIAMETER WIRE ROPE 3 x 18 WITH INTERNAL AWG 24 COPPER CONDUCTORS

Material	Peak Current Amps (Monitor AA)	Charge Transfer Coulombs	Action Integral Coulomb-amps	Probability Level	Breaking Strength (lb)	Remarks
Carbon Steel					4200	Control run average of three unexposed samples
	5×10^4	1.3	1.2×10^4	0.97	3600	
	$7 \times 5 \times 10^4$	2.1	3.2×10^5	0.93	3400	
	1.25×10^5	2.8	1.1×10^6	0.90	2400	
	1.6×10^5	3.6	1.7×10^6	0.87	3200	
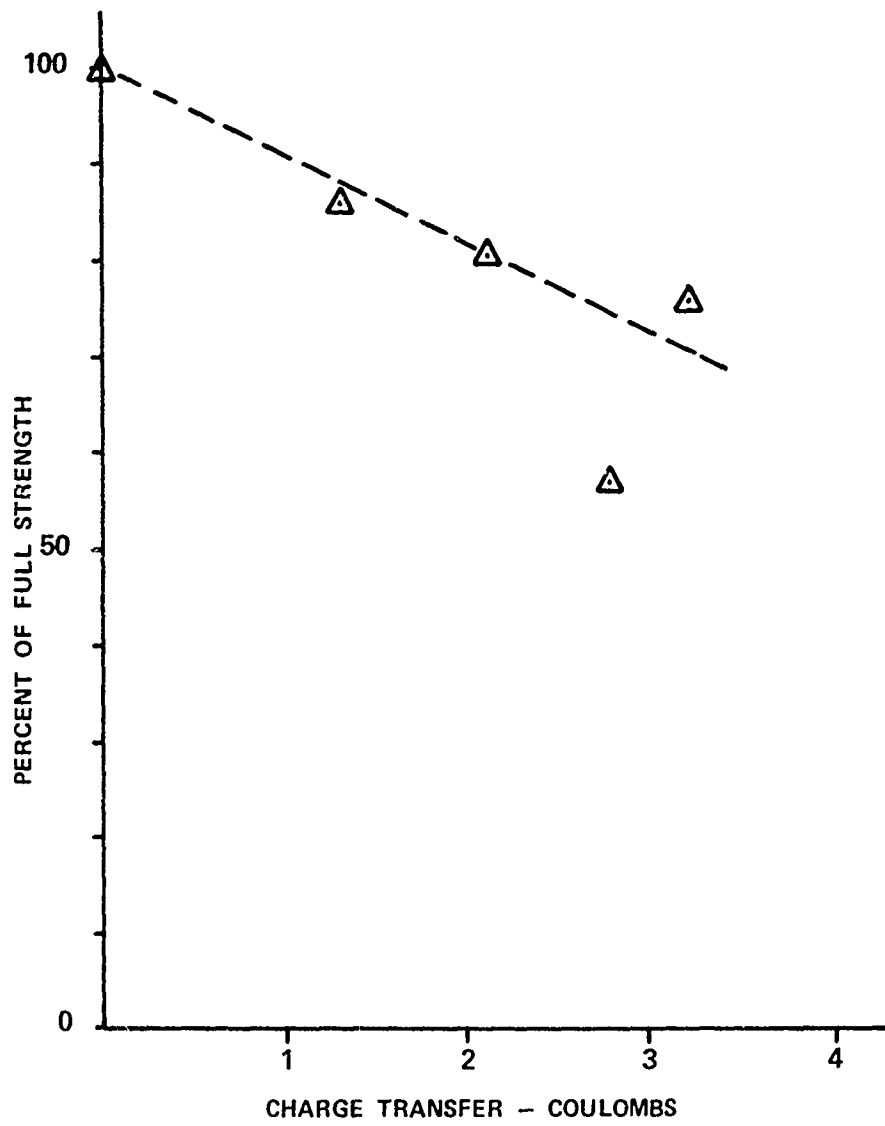
Figure 4-25. The Effect of Simulated Lightning on 1/8 Inch Diameter Rope of High-Strength Carbon Steel.

4.5   COMPARISON OF SURVIVABILITIES OF NOLARO AND WIRE ROPE TETHER

The ratio of weight to breaking strength for steel wire rope is
approximately twice that of Dacron rope and four times that of
Kevlar 29. A strong justification is therefore required for
specification of wire rope as a balloon tether. The apparent
justifications are:

1.   Lightning survivability
2.   Suitability for electric power transmission.

4.5.1   Survivability

First let us consider lightning survivability. The comparison
of wire rope with synthetic fiber rope in this respect is made
difficult by the difference in failure mechanisms of the two and
also by the difficulty of testing the two with uniform simula-
tions.

We have observed in the operational situation that a lightning
flash propagates down the surface of a Nolaro tether without
damaging the tether except at intermittent intervals when the
energy penetrates the jacket and creates severe mechanical dam-
age. The fraction of tether length damaged is small, but when
a tether has been severed the percent of length damaged thereby
is operationally unimportant. The August 1972 incident would
probably have resulted in loss of the balloon if stronger (but
realistic) pulls had been experienced.

A wire rope tether transmits the energy of a lightning flash to
ground in the familiar fashion of an electrical wire. The tether
is likely to sustain its most severe damage at the point where
the arc contacts the material. During the time of exposure the
rope loses strength which may be recovered after cooling if it
does not fail while in a weakened condition. We have been able
to simulate the effects of lightning on wire ropes closely enough
to form the conclusion that wire ropes of practical size for
tethering a 205,000 ft^3 balloon are marginally survivable for

4-62

severe lightning and of course more survivable for lightning of
typical severity. NASA/Kennedy Space Center has performed test-
ing on a 1-1/4-inch stainless steel cable which indicates that
a lightning stroke which could result in its breakage is highly
improbable. Further this rope has survived at least one actual
lightning stroke. Likewise a balloon tether of comparible size
and inferior survivability used for balloon logging has survived
lightning with no perceptible damage. Ropes of this diameter are
too heavy for the Family II balloons. As we decrease diameter to
a size which provides a breaking strength comparable to 0.775
Dacron Nolaro (26,000 lb) the resulting tether (VHS plow, 1/2 Dia)
is reasonably survivable, but of sufficient weight to severely
limit balloon altitude. Any action to decrease weight by using
stronger materials reduces survivability, which is closely re-
lated to mass. The same situation applies to arguments that a
wire rope tether does not require as much ultimate breaking
strength as a fiber rope for equal operational safety.

We do not know whether the tendency for Nolaro to be damaged at
some point and not at others is a result of peculiarities of the
tether in some places or simply a caprice of the lightning chan-
nel. It is apparent that the forming leader occasionally enters
the jacket and at such points, the jacket is blown away and the
dacron burned and weakened. Test results indicate that minor
damage, the only type we were able to evaluate, resembled that
caused by internal pressure. This indicates possible moisture
inside the tether. It will be recalled that, of the Nolaro sam-
ples which were tested only those which had been saturated with
water were damaged.

The realism of our Nolaro testing can be questioned to the extent
that natural lightning is a single spark applied to a sample
several thousand feet long, whereas our simulations were many
sparks applied to samples several feet long. The question then

is whether many short sparks applied to short samples can be considered equivalent to only one long spark traveling down a long sample and any answer which can be offered is conjectural. A second failure of realism in the testing of Nolaro is the inability to produce a low current spark of sufficient duration to simulate continuing current. In this respect the wire rope tethers were more thoroughly and realistically tested.

4.5.2 Electrical Power Conductors

The survivability of a wire rope tether is not diminished by the addition of electrical wires to the rope construction, although strength to weight ratio is slightly decreased. The survivability of the electrical wires, however, is doubtful.

Generally the steel strength members are wound around the electrical conductor, forming a heavy shield. A lightning current flowing down the outside of such a cable would produce a voltage drop, both inductive and resistive greatly exceeding the dielectric strength of any practical insulation. The insulation would fail and a portion of the lightning current would then flow down the electrical conductor which would heat sufficiently to melt the insulation and possibly fuse or vaporize the wires.

It is also possible to build Nolaro or twist lay ropes with electrical conductors, however, unless the wires are outside the jacket, destruction of the tether is a virtual certainty. Construction of a transmission line tether with external wires is possible but difficult.

4.5.3 Methane Supply Tube

Incorporation of a methane supply tube to the tether provides a means of extended operation more adaptable to synthetic fiber rope construction. We have shown that such a system, properly constructed, does not increase the probability of tether damage or add an appreciable fire hazard. Any damage capable of igniting the methane in the tube would be sufficient to destroy this tether, so the remaining concern would be fire prevention on the ground.

4-64

4.5.4 Summary

Wire ropes of suitable size for tethering large balloons have
acceptable lightning immunity. However, electrical transmission
lines would be much more vulnerable to lightning damage. Wire
rope tethers of 1/4-inch diameter or less are relatively vulner-
able. Any wire rope tether will impose a severe operating
limitation on the balloon due to its extreme weight. The sur-
vivability of jacketed Nolaro is less certain, but can possibly
be enhanced by protective coatings. The addition of electrical
wires to fiber rope tethers greatly increases their vulnerabil-
ity to lightning. Addition of a tube with gaseous fuel does
not reduce the survivability of the rope but does provide a
weight-conservative means of extending operating duration.

SECTION 5
PROTECTIVE MEASURES

5.1 PERSONNEL AND GROUND SUPPORT SYSTEM

While relative priorities for the protection of personnel and
equipment can be established, those measures which create a safe
operating environment for personnel generally involve protection
for equipment. Conversely, situations which permit a high risk
of equipment damage usually involve personnel hazards as well.
It is therefore difficult to separate personnel safety and
equipment protection into mutually exclusive categories.

In general, lightning protection is based on shielding, ground-
ing, and surge suppression. A degree of lightning protection is
inherent in good power system design, and much of the existing
body of lightning safety standards for the aerospace industry
apply to the tethered-balloon operation. Further, most of the
inapplicable features of standard protection are obviously in-
applicable due to salient balloon system peculiarities. Here
we shall consider in broad context some of the principles of
protection for tethered-balloon systems and their operating
personnel.

5.1.1 Basic Premises

It is realistic to assume that the site of a full-scale balloon
operation will experience more lightning than the same site
would without a balloon operation. Protection is therefore
more important than it would be in other types of activity.

Personnel and Equipment in the Path of a Direct Strike

When the balloon is aloft, the probable stroke path is down the
tether to earth via a grounding system (or otherwise by a flash-
over at the winch vehicle's tires). With a Nolaro tether, secon-
dary branching to nearby conductive bodies such as the winch
structure, personnel, or other equipment may be expected. If
a wire rope tether is used, the discharge path will probably
be better controlled and more predictable.

Initially, upon contact with ground the lightning current will
disperse from the grounding point as a sheet of current. Many
lightning casualties result from this skin current being di-
verted through the body of an individual standing in the path
of this current flow. The extent of the effect varies, but it
probably presents a hazard up to 50 feet from the stroke contact
point. Within this category, the winch operator and others
standing near the winch are the most endangered individuals.
The winch operator's position can be made safe, but there is
little that can be done for the exposed bystander.

When the balloon is not aloft, the most probable lightning path
is down the mooring tower. Again exposed personnel are en-
dangered.

Personnel and Equipment in Nearby Support Facilities

This category includes shop and instrumentation vans near but
outside of the direct path of the stroke. Within this area,
the principal problem will probably be surges due to currents
induced on electrical cables by the nearby stroke. These
surges could cause equipment damage to an extent determined by

the distance from the tether point. It is assumed that no direct wires to the tether point exist. Within the current operating concept for RML programs the instrumentation, administrative, and mechanical support facilities fall into this category.

5.1.2 Protective Enclosures

The winch operator position is probably the only position within the first category just discussed that can be protected. This position should be "hardened" against lightning. This can be done by a type of enclosure known as a Faraday cage. [Vol II, Part C, P.1]

A Faraday cage (shown in figure 5-1) provides an electrically continuous conductive surface totally surrounding the protected area. Such an enclosure can assume a potential in the hundreds of kilovolts or even megavolts, but these potential drops do not affect the occupants.

There is generally an operational necessity for wiring to and from the outside, so the continuity of the practical Faraday cage must be interrupted for wiring access. If this wiring is improperly installed, there is a possibility of high potential differences being introduced to the interior of the enclosure (figure 5-1b) which could result in discharges to personnel or to equipment. This possibility can be reduced to a low level by bringing wires in through conduits bonded to the exterior surface of the enclosure.

All wiring which can be eliminated should be. However, if communications cables are replaced by radio communications,

A) INTERFACE WIRING IN BONDED CONDUIT

B) UNSHIELDED INTERFACE WIRING
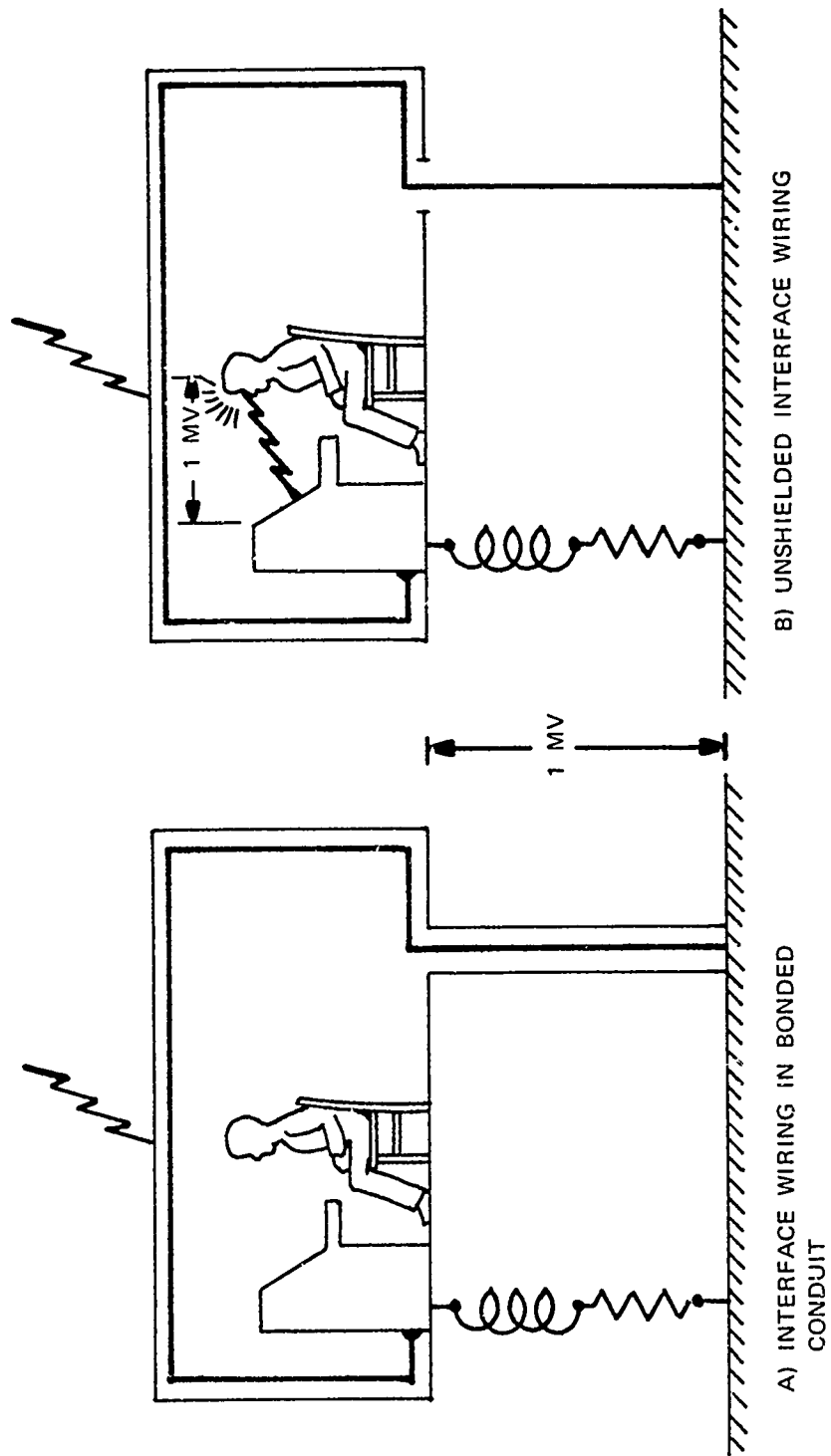
Figure 5-1. Protective Enclosure Based on the Faraday Cage Principle

special care must be taken in the suppression of possible discharges to the antenna. Flush-mounted antennas are to be preferred over whip antennas (which are more likely to produce streamers) even if use of the flush-mounted antenna requires using more than one antenna for the desired coverage. Any un-essential intrusion of conductors into the Faraday cage should be avoided. For example, some gauges could be mounted outside the cage at a location visible from the cage.

5.1.3 Shielding and Bonding

Continuity of the Faraday cage is achieved by assuring that all exterior surfaces are conductive and are electrically connected by a low-resistance path. An acceptable bonding resistance is 2.5 milliohms or less.

Doors with strap hinges may require bonding jumpers to achieve an acceptable bonding resistance. Piano hinges may inherently provide acceptable bonding.

Conduits should be bonded to the exterior of the enclosure around a 360-degree periphery as shown in figure 5-2. Plumbing and fuel or hydraulic lines should be similarly bonded. Some hydraulic lines have internal metallic reinforcement. Such lines should be brought into the enclosure through a peripher-ally bonded feed-through similar to that used for conduits.

A suitable material for this type of enclosure is 0.08-inch thick sheet aluminum. This material is used by the aircraft industry in areas where direct lightning contact is expected.

b. Shielded Cables
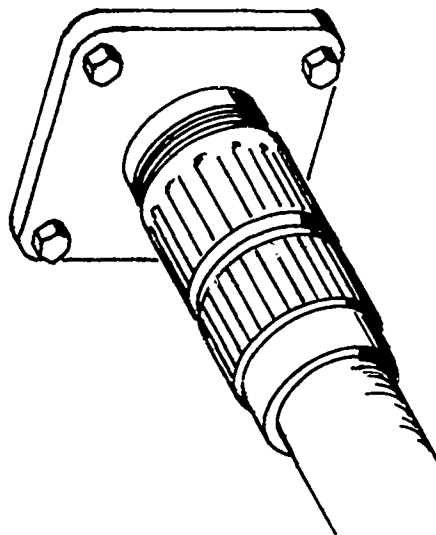
a. Conduits
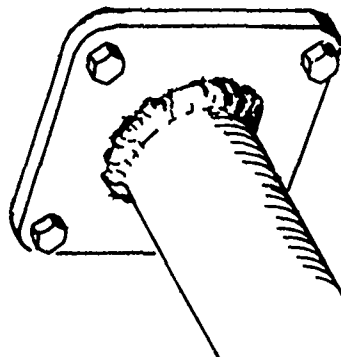
Figure 5-2
Bonding of Electrical Conductors at Entry Points

5.1.4 Grounding

Grounding is less critical to the occupants of a properly designed protective enclosure than is shielding and bonding. Consider for example the situation depicted in figure 5-3. This enclosure is grounded by a cable connected to a high-quality earth ground. Large gauge wire has inductance on the order of 1 microhenry per meter, and earth grounds have contact resistance of from 1 to 100 ohms.

If a lightning current is conveyed to ground through this connection, the enclosure will rise to a voltage:

$$V_g(t) = L \frac{di(t)}{dt} + RI(t) \qquad (5-1)$$

Using the high current portion of (5-1) and assuming a ground resistance of 50 ohms, and 1 microhenry inductance:

$$V_g(t) = 1.06e^{-\alpha t} - 0.99e^{-\beta t} \text{ megavolts} \qquad (5-2)$$

From this calculation it is apparent that a grounding system, however effective, will not prevent the operating enclosure from rising to a very high potential during the transient portion of the lightning flash. The value of a properly designed enclosure derives from the fact that the entire enclosure, rises in potential. This being true, the occupants are equally safe if the enclosure is grounded or floating as in the case of an aircraft struck in flight. The function of the ground in this case is to limit potential rise due to induced surges and more important to provide a controlled path to earth in the case of a

NO. 2 AWG
COPPER WIRE

GROUND ROD

TOWER BASE
MOUNTING PAD

GUY
ANCHOR

18 IN
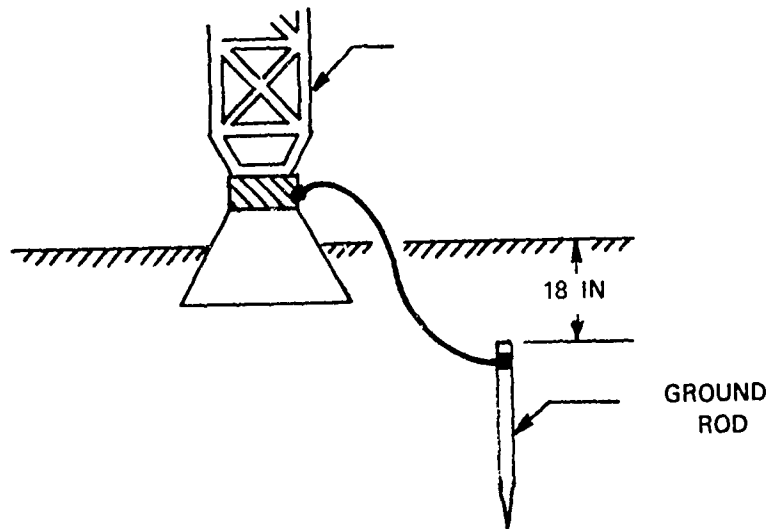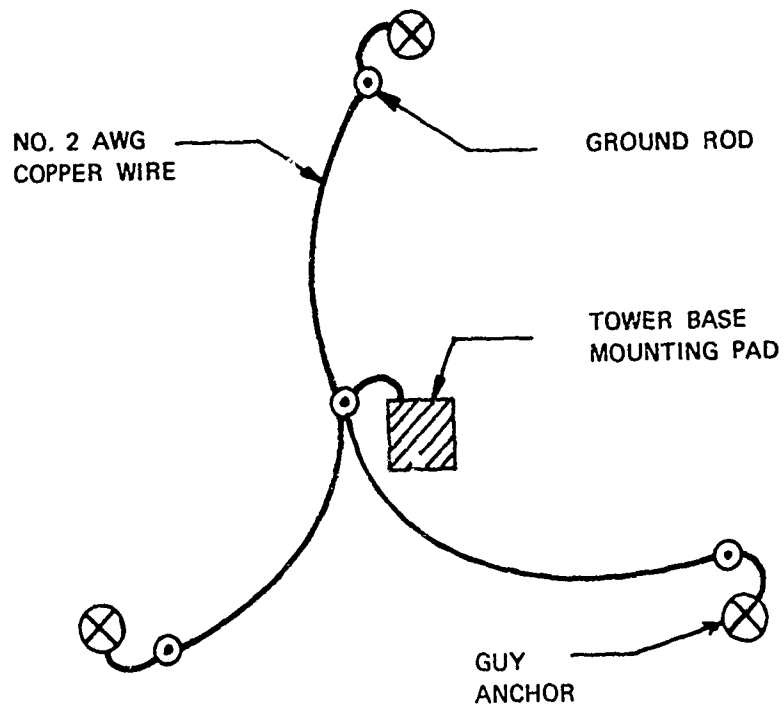
GROUND
ROD

Figure 5-3. Grounding System for Mooring Mast or Other Guyed Towers

direct strike to the enclosure. This reduces (but does not eliminate) the tendency of the flash to arc to grounded objects nearby. Determination of the depth to which ground rods are driven must be based on local soil characteristics.

Ground Planes

The grounding system for areas in the probable path of a lightning stroke should provide a conductive ground plane to reduce personnel hazards due to surface currents. The ground plane should extend a minimum of 50 feet in all directions from the central point. Heavy steel wire mesh or pierced steel planking should be used and continuous bonding assured.

A system of this type, partially implemented for the BJ+3 system at Cape Canaveral, became an operational nuisance and was eventually removed. This indicates the necessity of careful design of such systems, since a safety system must also be designed for utility.

Winch and Ground Sheaves

The winch trucks used for RML programs are designed with emphasis on mobility. This priority plus operational convenience has resulted in the flying sheave on the winch truck, a system which permits the winch to move with the balloon in flight and to approach the mooring tower from downwind. However, this arrangement also tends to guide a lightning stroke to the winch.

The ground sheave on the BJ+3 was safer from a lightning viewpoint, since it permitted the sheave to be located at some distance from the winch and the rest of the operation. The AFCRL system at Holloman AFB, which routes the tether from the sheave to the winch via an underground cable trough, exemplifies a good approach to safely disposing of a lightning flash.

Grounding Systems for Specific Balloon Applications

For winch parking areas, a fixed location should be prepared for
parking the winch truck during flight operations. This area
should be of sufficient size to assure that all associated per-
sonnel activity can be restricted to the ground plane. A con-
venient ground attachment point should be provided for grounding
the flying sheave with a short grounding cable.

Mooring masts should be grounded at the tower baseplate and
also at each guy wire tie point. Each of these points should
be cadwelded (or welded by some equivalent process) to its asso-
ciated ground wire, which in turn can be attached to the ground
stake by a clamp. The central ground should be connected to the
guy wire grounds by AWG #2 bare copper wire. The interconnect-
ing ground wire should be buried at least 18 inches below the
surface of the earth. The ground stakes should be driven to a
distance that will assure the attachment points are also 18
inches below the surface. This system is shown in figure 5-3.

In addition to the above, a ground plane should extend at least
50 feet from the mast. If the winch is to be parked near the
mooring mast, an interconnecting walkway between the two ground
planes should be provided. A monorail system with these fea-
tures is depicted in figure 5-4.

Fixed Enclosures

Fixed enclosures such as support buildings and vans should have
peripheral grounding systems as shown in figure 5-5. Such a
grounding system consists of a continuous encirclement of the
structure by a loop of #2 AWG bare copper wire which shall be
attached to ground stakes at the corners and at any other point

5-10
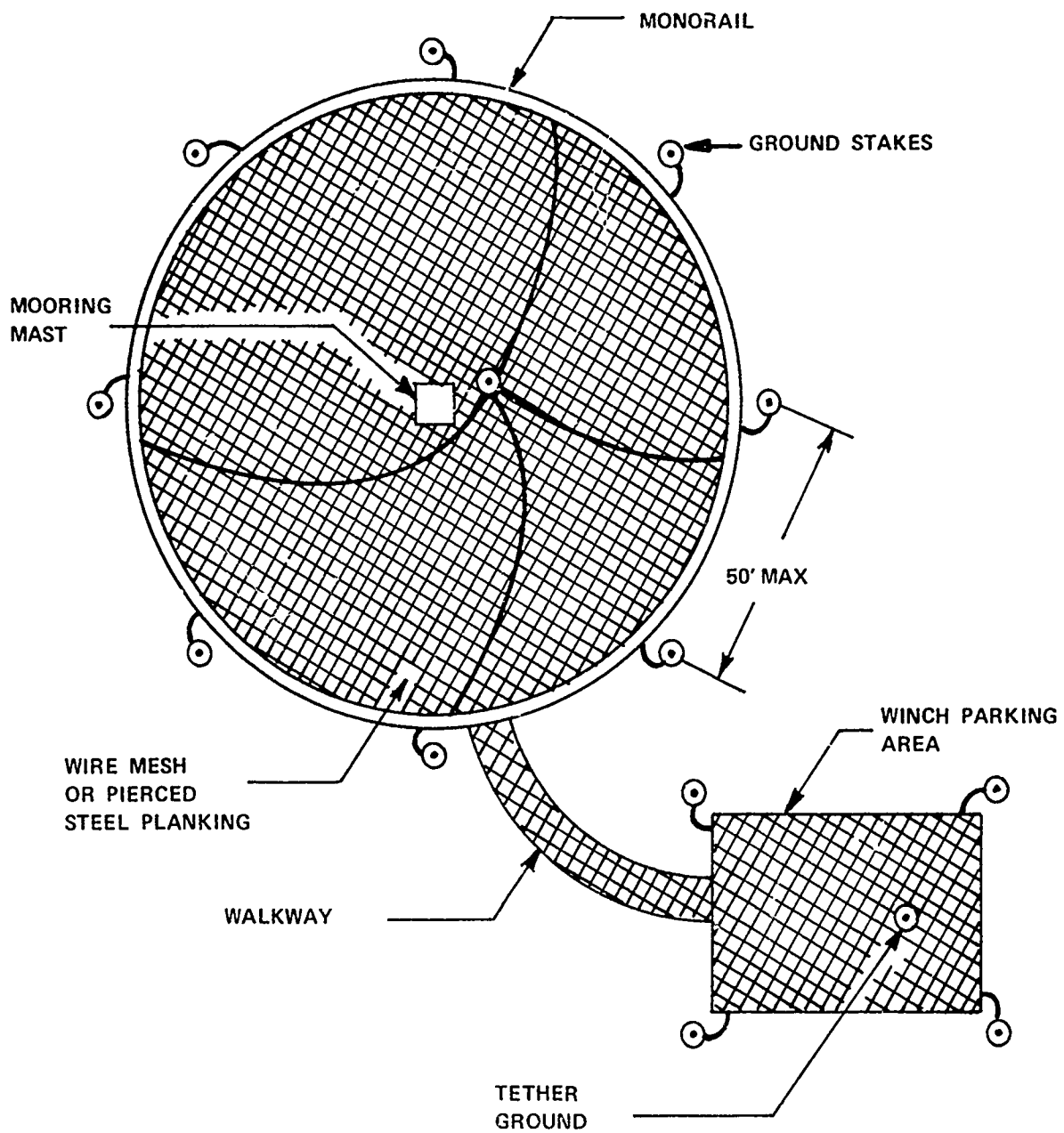
Figure 5-4. Grounding System for a Monorail Mooring System With Adjacent Winch Parking Area

NO 2 AWG BARE COPPER WIRE BURIED TO A
DEPTH OF 18 INCHES

COPPER GROUNDING RODS.
SEPARATION NOT TO EXCEED 50 FT.
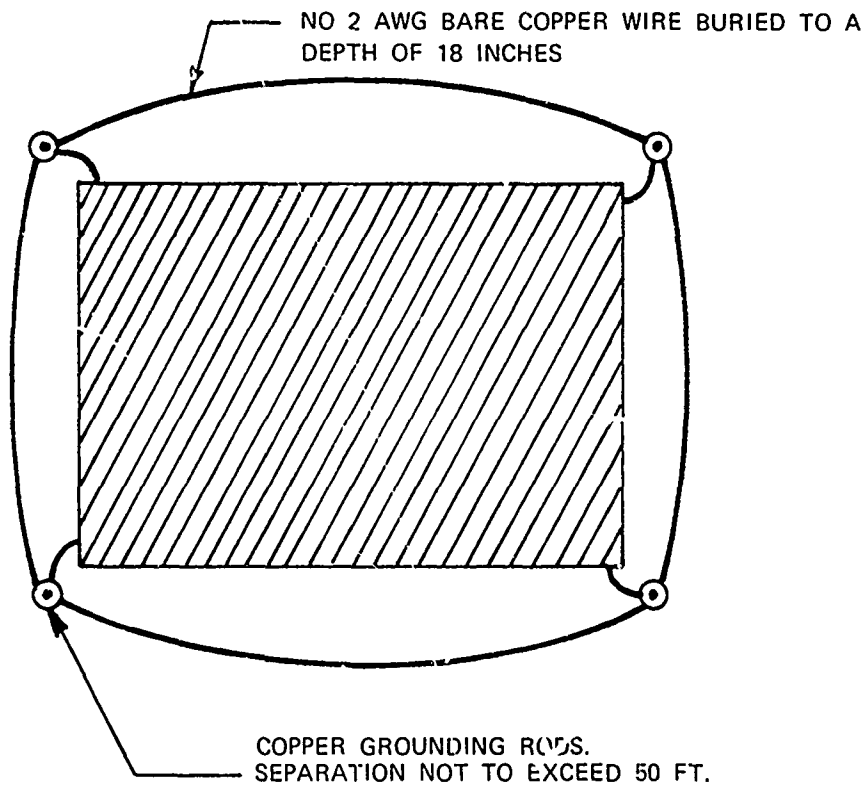
Figure 5-5.   Peripheral Grounding System for Fixed Enclosures

5-12

necessary to prevent a distance exceeding 50 feet between grounding points. Each of the corner stakes should be attached to the middle structure of the building or van.

An ideal power ground would consist of a 1/8-inch thick aluminum base plate slightly larger than the base of the instrumentation racks, upon which the racks rest and to which they are bolted. The aluminum baseplates should be bare if environment permits. Otherwise a conductive anticorrosion process such as irridite or allodyne is permissible. Under no circumstances should the ground plane be anodized or painted. The racks should be depainted at the mounting points and tightly bolted in place. In addition to bonding the power ground to this baseplate, all intrarack wiring should be run under the racks and allowed to rest on the baseplate. The base plate should be connected to the nearest external ground stake.

5.1.5 Protection of Antennas

An antenna in or near the expected direct lightning path should be a slot antenna if available space and operating frequencies exist. There are two justifications for this configuration: 1) The slot antenna, being a flush-mounted antenna is less likely to develop streamers than a whip or multielement antenna, and 2) a slot is inherently self-protecting since the slot constitutes a low-frequency short between the feed lines (see figure 5-6a).

Similar protection is afforded by folded dipole antennas and also by waveguides. The principal disadvantage of a slot antenna is the fact that full 360° coverage would require more than one antenna.
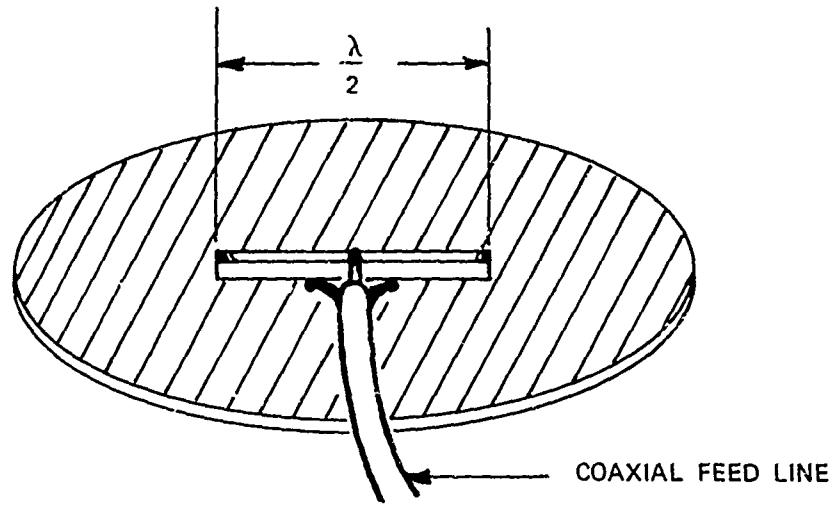
A)   SLOT ANTENNA IN WALL OF ENCLOSURE
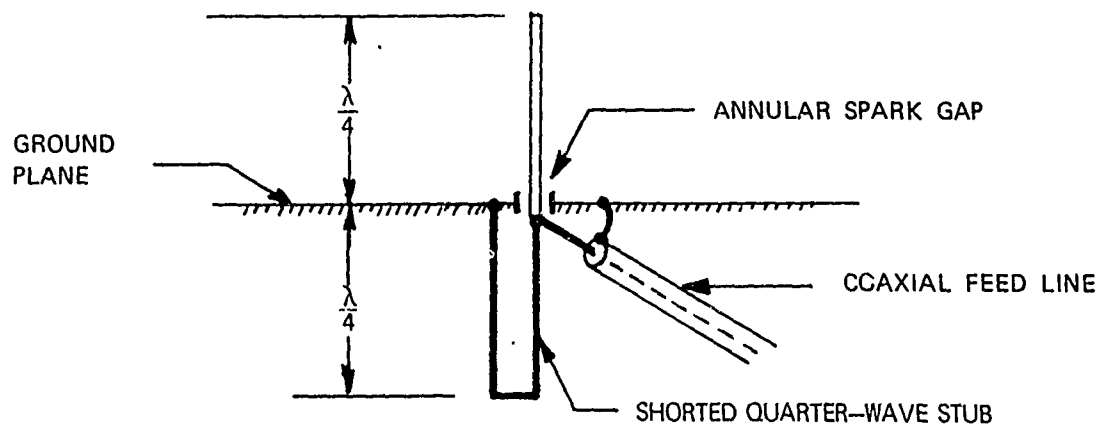
B)   MONOPOLE WITH SHORTED QUARTER-WAVE STUB

Figure 5-6.   Surge Protection for Antennas

Lightning arrestors for airborne monopoles [35] are commercially
available. One such configuration features a spark gap in the
form of an annular ring around the antenna element (figure 5-6b).
Effective lightning protection is also afforded by ι shorted
quarter-wave stub.

Regardless of the antenna type, a second stage of protection
should be provided by a coaxial spark gap at the receiver or
transmitter.

5.1.6 Protection for Winch Operator

The best possible protection for the winch operator is provided
by an enclosure having the features shown in figure 5-7, most
of which have been discussed. The winch operator's position is
fully enclosed and is thoroughly bonded. Windows are protected
by lightning diverter strips. All electrical wiring enters a
compartment below the floor via conduit. Lightning arrestors
are contained in this compartment. Communications with the
operations facility is accomplished by radio link. Headsets
are replaced by a speaker and directional microphone. Special
care is taken to assure that all operational controls are bonded
to the skin of the panel they are mounted on, and that those
parts to be handled by the operator have insulated surfaces.
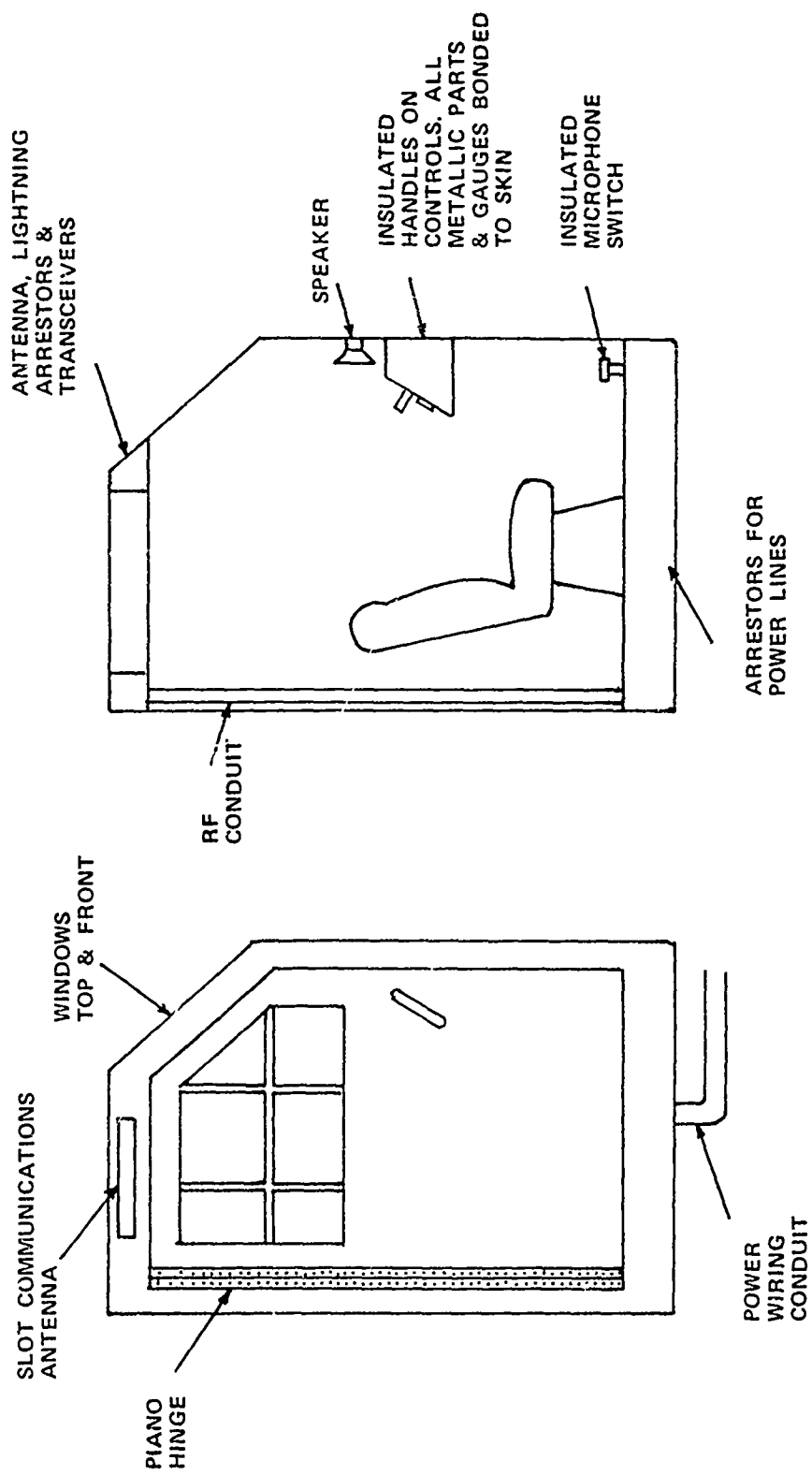
Figure 5-7. Lightning-Hardened Winch Operator's Position

5.2   BALLOON AND BALLOONBORNE SYSTEMS

The balloon-tether system and the balloonborne electronics can
be protected from a direct stroke in two ways: 1) controlling
the tether attachment point and 2) hardening the critical sys-
tems.

5.2.1   Control of Attachment Point

The point of tether attachment can be protected to some extent
by providing air terminals (lightning rods) on the balloon.
With these air terminals any lightning flash attracted by the
system can be conducted to the tether and hence to the ground
without the tether sustaining arc damage.

According to Davis and Standring [3], a protective system con-
sisting of a 3-meter-high air terminal was mounted on the nose
of certain WWII barrage balloons. Other sources [36] indicate
that the system included catenary wires extending from the air
terminal to the two upper tail fins. It is assumed here, but
not explicitly stated in the references, that this system was
grounded to the tether. The destruction by lightning of the
balloons so protected, was reduced by a factor of 3 or 4. The
highest peak current survived by a protected balloon was 30 kA.

Eggers, Brown and Ollila [37], suggest an extension of the
approach as shown in Figure 5-9. The purpose of the high-con-
ductance sleeve is to effect an arc-free transfer of energy
from the lightning terminal to the tether or at least to dis-
tribute the transfer over a length of tether. This effect
could be enhanced by a section of dielectric tether between
the sleeve and the confluence point.

The cruciform tail design of the 2D7 balloons is well suited
to the construction of a Faraday cage as shown in figure 5-8.

HEAT SHIELD
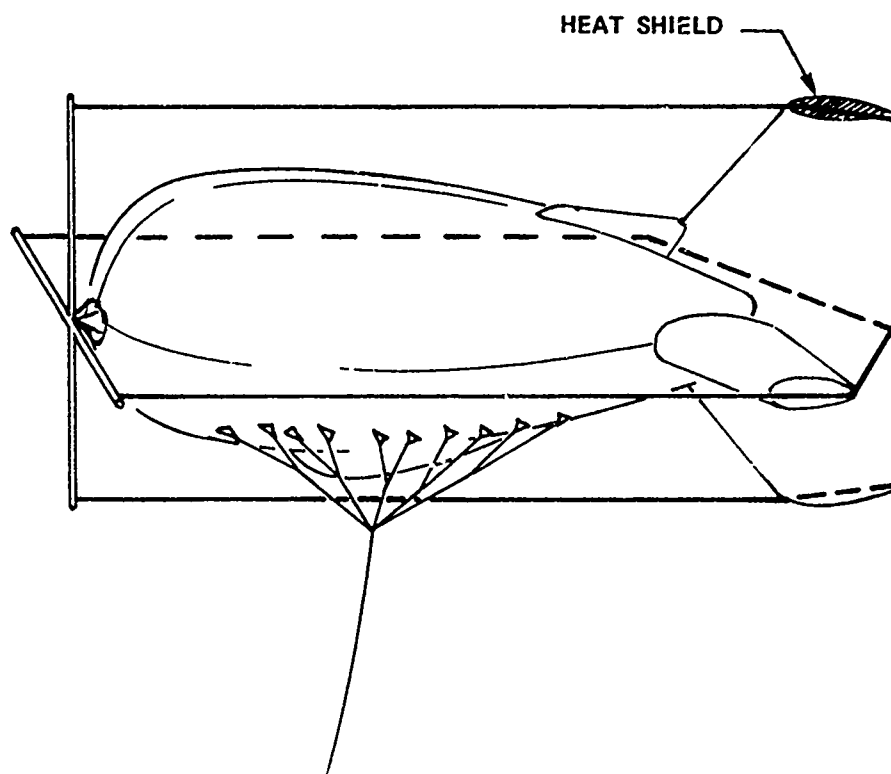
Figure 5-8. Faraday Cage for a Tethered Balloon
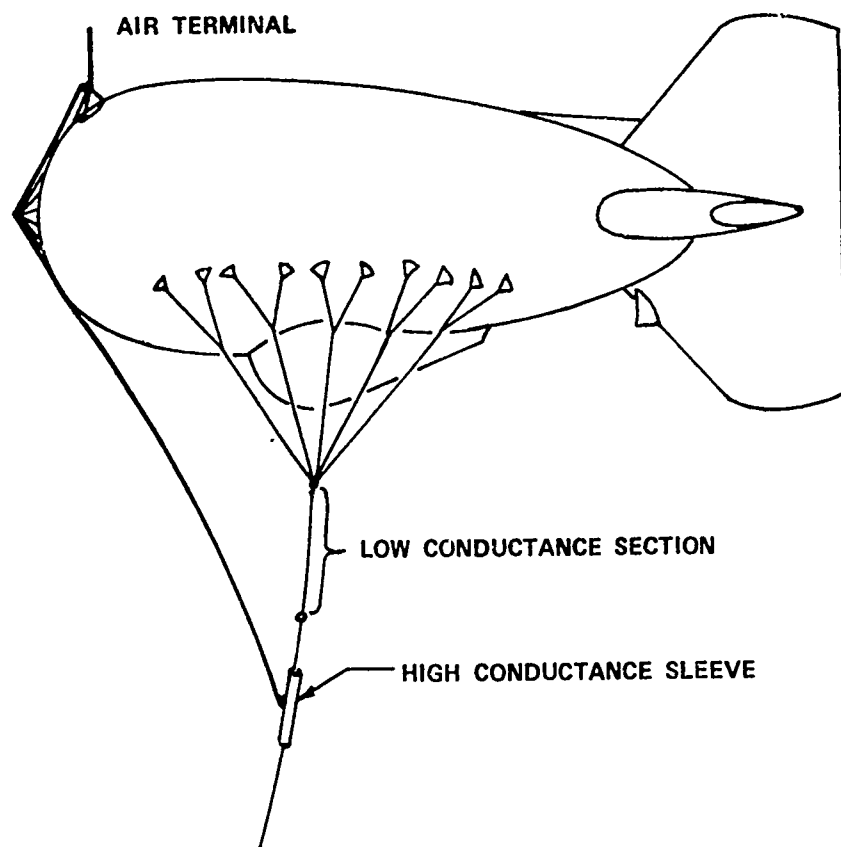
Figure 5-9. Arrangement for Energy Transfer To Tether

Stahman (Volume II, Part D, p 20) suggests the use of conductive confluence lines to provide additional shielding for the payload.

Since a steel cable can sustain a temperature considerably higher than the synthetic materials used for balloon fabric, any part of the balloon hull in contact with wire rope should be protected by a heat shield.

The above measures all apply to a balloon with a well-conducting tether. With a poorly-conducting tether, the means of transferring the lightning current to the tether remains a problem. A high-conductance sleeve of the type discussed above may offer the best solution, particularly if combined with a conductive paint on the tether jacket. However, there is insufficient data for recommending either approach at this time. The severity of the problem and the absence of an obvious solution both suggest further evaluation of these two modes of protection for poorly-conducting tethers.

5.2.2 Hardening of Critical Balloonborne Systems

Although much information on lightning protection has appeared in the literature, very little of this has been applied to the protection of balloonborne equipment. As a result, much of the electronic equipment on the balloon has no more and possibly less protection than the average piece of shielded electronic equipment on land.

Until more data can be collected, the best protection for balloon equipment is the application of aircraft and spacecraft lightning protection techniques. Here again, the situations

are not identical because of the generally low conductivity characteristics of the balloon material and the tether.

At present it is believed that the best protection to electrical and electronic equipment on a tethered balloon can be achieved by techniques designed to limit the potential differences between critical points of the circuits, whether or not the potential difference arises from a fast-rising impulse of a lightning discharge or the accumulation of electrical charges on the balloon surface faster than leakage will permit its diffusion over the surface.

Thus far, lightning has caused no damage to electrical or electronic equipment on RML balloons. However, other balloon users report lightning damage to such critical components as helium valve actuators.

In general, RML has avoided flying when thunderstorms are in the vicinity. For continuous airborne operations, additional precautions will be required to protect equipment and increase operational reliability.

A typical balloonborne system is shown in figure 5-10. System elements that warrant protection are:

     (1)   Gasoline-powered electrical generators

     (2)   Central dc power supply

     (3)   Power-distribution cables

     (4)   Hull and tail fin blowers

(5) Helium valves and associated actuators and control circuits

(6) Telemetry and command system

(7) Payload

(8) Pyrotechnics (if used)

Protective Devices

Considerable progress has been made in recent years in the protection of electrical and electronic equipment from the effects of electrical surges, whether conductively or inductively generated. Among the devices now available for surge protection are a large variety of spark gaps (both air- and gas-filled types) and numerous semiconductor devices such as zener diodes, thyrites, and varactors. These devices are finding increased usage for protecting electrical and electronic devices from damaging electrical and electromagnetic surges. The units are made in many forms and sizes to include almost any voltage or current requirement.

In general these devices have been characterized into four classes as follows:

Class I. Current-sensitive devices such as fuses and circuit breakers.

Class II. Transient suppressors — voltage-limiting devices acting by change of internal resistance.
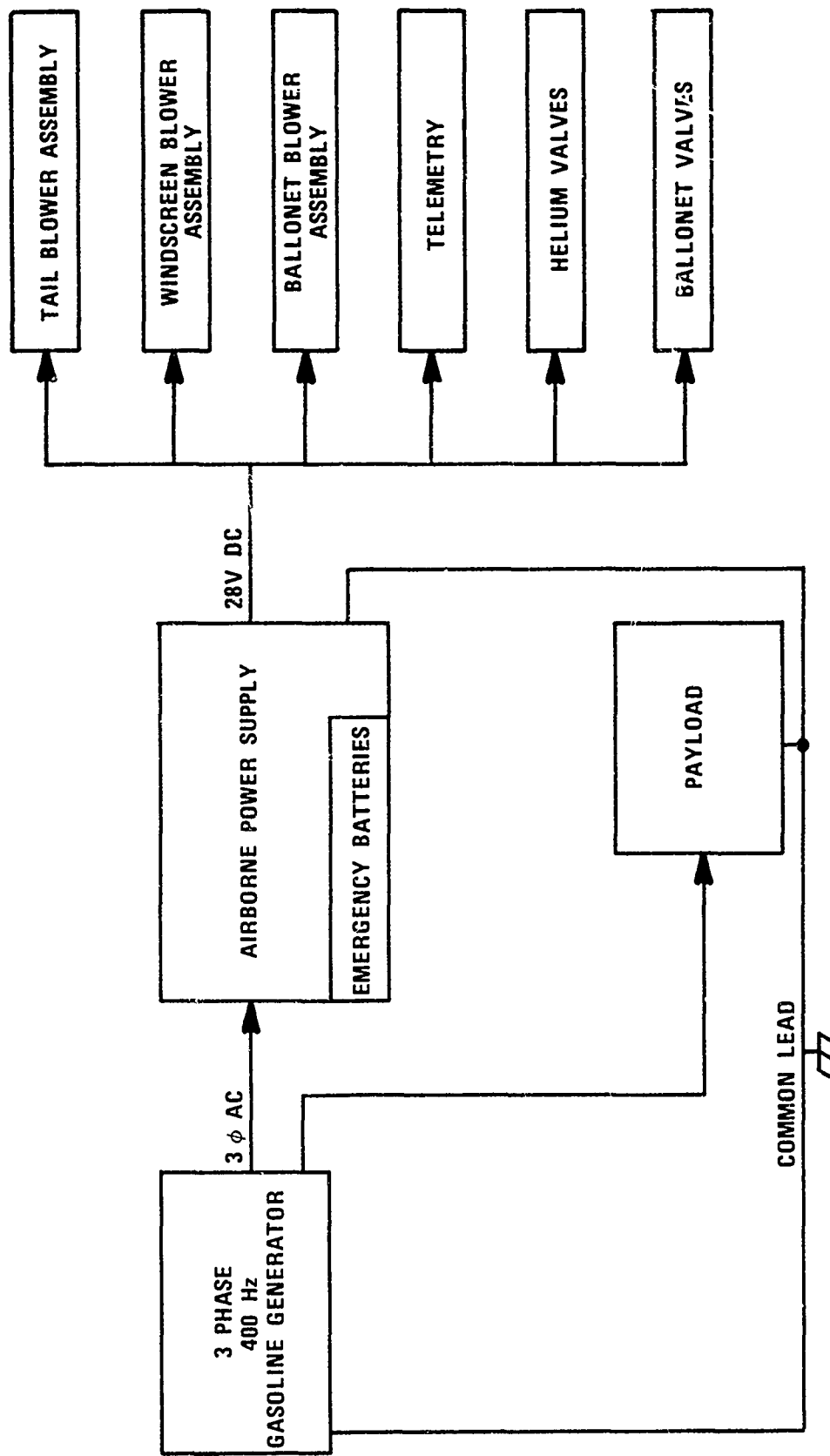
Figure 5-10. Family II Balloon Electronics System

Class III. Voltage-sensitive shorting devices (spark gaps and crowbars).

Class IV.   Combination of those above.

Table 5-1 is a comparison of several of these devices, illustrating clearly their properties and limitations [35].

5.2.3 Corrective Action

The hardening of an existing balloon system may require trade-offs between the balloon lifting capabilities and the additional weight of the shielding, protective devices, and common bus and grounding. It may not be practicable or economically feasible to carry out all of the desirable suggestions. However, each system should be given as much protection as possible commensurate with cost, weight, and operational constraints.

Specifically, the following actions will provide protection for existing balloon systems.

1. As a first effort, replacing all unshielded power cables with cables having a continuous conductive covering grounded by the connector to the bulkhead or equipment box or frame where it is terminated. The overall shield should have no breaks or splices except at the connectors or at branch points on cables with multiple breakouts. Intermediate grounding of the shield to the ground bus may be done.

2. Providing the power distribution system with a single point to the common line. This may not be feasible on a system now in use.

TABLE 5-1 — COMPARISONS AMONG VARIOUS TYPES OF TRANSIENT PROTECTIVE DEVICES

Device type	Advantages	Disadvantage	Remarks
Spark gap	Simple and reliable. Easily fabricated. Very low voltage drop during conducting state. Bilateral operation – same characteristics on either polarity.	Relatively high spark overvoltage. Arc must be extinguished by removing voltage. Seldom available in conveniently packaged assemblies; must be designed for each specific use.	Generally consists of two metal electrodes separated by air with a minimum spark over voltage of 1500 to 3000 V.
Gas diode	Low cost. Small size. Low spark overvoltage (usually 60 to 100 V). Can pass high current for short times. Self-healing.	Poor volt/time characteristics. Will continue to conduct if driving voltage is above 60 to 100 V.	Neon bulb is typical example.
Zener diodes	Small size. Easily mounted. Low firing voltage. Low dynamic impedance when conducting. Self-extinguishing when applied voltage drops below Zener level, conduction ceases.	Expensive. Not bilateral. Voltage across diode does not switch to low value when conducting, but remains at Zener voltage. Not available for voltages below about 5 V. Normally not available for voltages above a few hundred volts.	Can be used to clip a surge voltage and limit the surge to the Zener voltage. Well adapted to semiconductor protection.
Forward-conducting diodes	Small size. Low cost. Provides protection at very low voltage levels. Good surge-current ratings.	Not bilateral. Conduction may occur at normal signal levels with possibility of clipping and frequency multiplication effects. Relatively high capacitance.	Includes standard germanium and silicon diodes.
Silicon-controlled rectifiers	Excellent surge-current rating. Low voltage drop when conducting. Suitable for low voltage circuits.	Must be triggered by an auxiliary circuit. Does not reset automatically. Not bilateral. Expensive.	Can be used as a one-polarity spark gap to prevent surges.
Varistors	Low cost. Small size. Pass higher current than Zener diodes. Self extinguishing. May be bilateral devices. Operate at either polarity.	May have high capacitance. Cannot be clamped at lower voltages. Not available with ratings as low as Zener diodes.	More adaptable to terminal boards, distribution panels, and printed circuits. Zinc oxide types have best overall performance.

3. Running a low-resistance static ground lead between all enclosures and equipment mounts using a solid copper conductor, at least AWG #4. Do not count on cable shields for this purpose. This same conductor should go to the mounts or frames of lights, blowers, and valves.

4. Installing a GE Transzorb surge suppressor or equivalent on all dc blowers, valves, and equipment requiring the 28 V dc power. Use a lightning arrestor such as the Josyln 704-15K36 on input to the equipment.

5. In addition to the suppressors on the dc lines at the input to the telemetry equipment, additional suppressors should be applied to the IC or transistor circuits in the equipment.

On 5 V logic use 1N5907 - 1CT-5

On 10 V logic use 1N5636A

On 15 V logic use 1N5639

6. On ac lines two units should be connected back-to-back to block the normal ac voltage of either polarity. For 117-V lines use two type 1N5558 Transzorbs (transient suppression diodes) in series across the line as below:
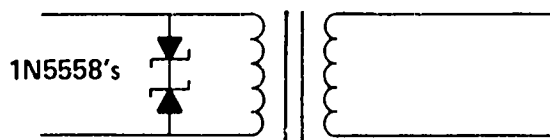
On three-phase sources, such a pair should be used on each phase to neutral.

5.3 LIGHTNING HAZARD WARNING SYSTEMS*

A lightning warning system should have the following attributes:

Reliability - The system should provide information which can be confidently accepted by the user.

Simplicity - Hazard indications should be provided in a nonambiguous form which can be readily understood by operators without specialized training.

Timeliness - The hazard indications should be presented in time for appropriate action to be taken.

Existing lightning hazard warning systems are based on detection of lightning which is actually occurring, conditions which accompany lightning, or some combination of the two.

Lightning detection and warning has been the subject of considerable federally funded research. Many systems under development are costly and require a spatially extensive network of sensors. For most tethered balloon applications, compact, economical and easily interpreted systems are required. The systems described here are believed to be of demonstrated or potential effectiveness and are compatible with the modest funding and relatively small areas available for tethered balloon operations.

5.3.1 Radar

Radar is of great value in tracking approaching storm systems which involve lightning. Radars presently operational do not actually track lightning channels, only rain cells which may or may not be associated with lightning. A useful and highly interpretable radar accessory is isoecho contouring, a signal processing technique which presents a storm system as contours of equal rain cell density. A principal value of radar is its utility as an "Early Warning System." Other enhancements to weather radar will be discussed in 5.3.4.

* Since the beginning of this writing, Ciano and Pierce have prepared an extensive report on lightning warning and avoidance [44].

5.3.2 Sferics

Sferics, a contraction of "atmospherics," refers to low-fre-
quency noise bursts which propogate worldwide from lightning
flashes. Direction-finding systems for these signals have been
used for many years. Such systems are generally based on the
principle of determining azimuth from the ratio of currents in-
duced in two orthogonal loops. Two loops are required because
the duration of a sferics pulse does not allow time to "swing"
a single loop as is commonly done with continuous signals. By
this method, the azimuth to a lightning channel can be measured
within a few degrees. However, because this is a low-
frequency technique, azimuth measurements become unreliable at
ranges of 50 km or less. At the longer ranges for which the
system is functional, inherent azimuth errors produce corres-
pondingly large locational errors.

5.3.3 Time-of-Arrival Difference

Cianos, Oetzel, and Pierce [39] have developed a system, called
the COP system, based on determination of azimuth (actually
hyperbolas of position) from the difference of arrival time of
the vhf portion of a lightning noise burst at two receivers
separated by a distance on the order of hundreds of meters.
This system, being a line-of-sight approach, provides accurate
angular information at ranges practical for tethered balloon
operations.

5.3.4 VHF Azimuth Measurement

An approach suggested by Latham and also by Krider and
Uman [41], [42], is based on crossed-loop reception of vhf energy.

The outstanding feature of this concept is that only the first microsecond of the pulse is measured. Consequently, the resulting azimuth indicates the location where the flash contacted the ground.

For intracloud flashes, azimuth indication is likely to be ambiguous. Such flashes are important because they tend to precede flashes to ground. It is likely that intracloud flashes can be identified by their distinctive frequency spectra. With multiple sensors, time of arrival techniques may provide better azimuth indications than crossed loops.

The system suggested by Latham features digital processing of the data, while the Krider-Uman system uses analog computations. This system is suitable for presentation on a radar scope along with radar cloud data. An artist's conception of such a display is given in figure 5-11, where an azimuth marker developed from the crossed-loop direction finder is pointing at a thunderstorm outlined by isoecho contours. This type of display has been developed by Krider and Uman, and typical accuracies of 2° are obtained.

The digital system proposed by Latham is potentially more accurate, but is thus far undeveloped. The latter system also lends itself to precise location of a lightning strike by real-time triangulation of azimuth from three stations. To implement this approach would require communication of data from two or more antennas, separated by at least 30 miles and a minicomputer or special-purpose logic to perform realtime triangulation and coordinate computations.

The techniques discussed are of greatest value for monitoring the approach of storms from a distance, as in the case of
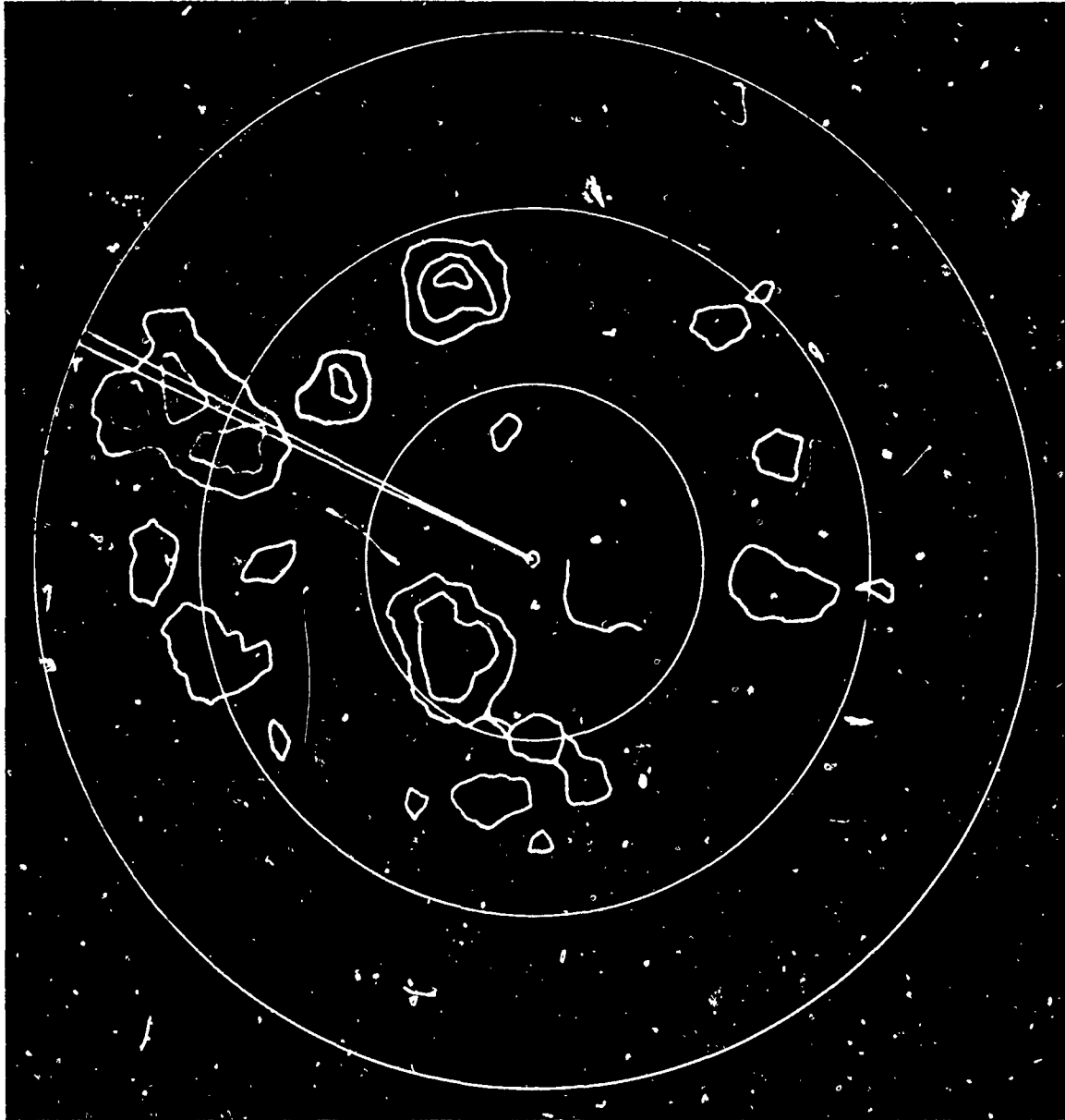
Figure 5-11
Weather Radar with Iso-Echo Contours
and Lightning Azimuth Indication (Artists Conception)

frontal storms, However, most of the lightning experienced in coastal Florida is produced by air-mass storms. These are storm systems which develop and dissipate within a relatively small area, rather than advecting from a distance as do frontal storms.

In general, the development of an air-mass storm is rapid, frequently occurring in less time than is required to recover the balloon. For such storms, the type of warning system most suitable is one which indicates the probability of lightning occurrence within a specific region.

5.3.5   Lightning Warning Based on Electric Field

5.3.5.1   Typical Storm Profile

The ambient electrical field at a given location is modified by the approach of a charged cloud as shown in figure 5-12. Note the cloud dipole is arranged with positive charges at the top and negative charges near the base. At a distance of several miles, the effect of the positive charge in the top is dominant, and the vertical field gradually increases as the cloud approaches. When the cloud is close enough for the effect of the negative base, which is closer, to predominate over the effect of the positively charged top, then the E-field decreases and assumes a large negative value when the cloud is overhead. As the cloud moves away the positive polarity of the E-field is restored and subsequently decreases to a normal fair-weather value as the cloud becomes too distant to have any effect. The type of field profile shown in figure 5-12a occurs with the passage of a charged cloud which is not producing discharges. On the other hand if lightning discharges result, then these discharges result in collapses of the measured local field.

E_2

$100v/M$ 2000

10,000

E_3

a) WITHOUT DISCHARGES
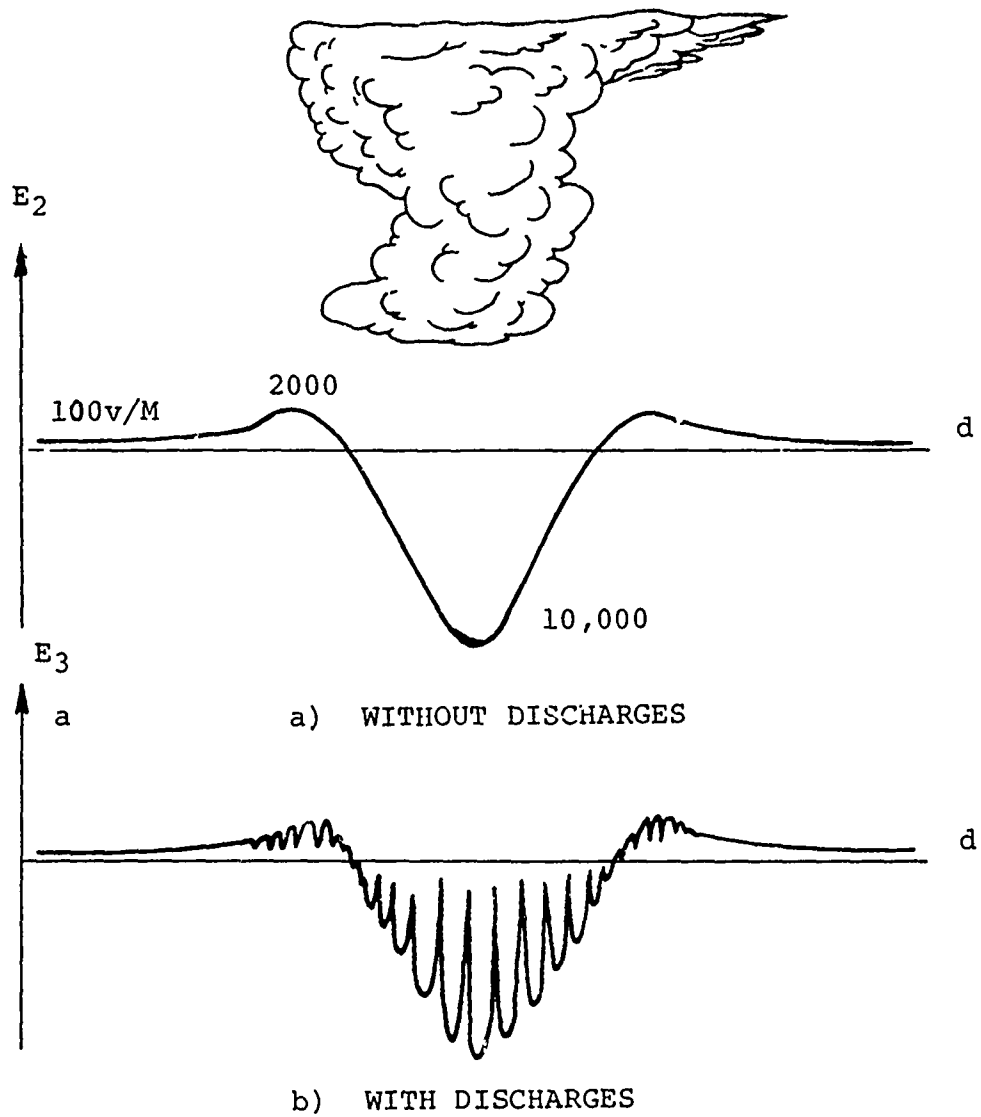
b) WITH DISCHARGES

FIGURE 5-12

EFFECT OF CHARGED CLOUD ON VERTICAL E FIELD

A well-developed storm can replenish this lost charge in 20 seconds. The field profile of a storm with discharges is shown in figure 5-12b. The significant events in a thunderstorm passage as described above are:

a. A gradual positive increase to thousands of volts/meter as the storm approaches closely enough to affect local field.

b. A polarity reversal as the charge of the cloud base becomes dominant.

c. A large negative field, (thousands of volts per meter) as the cloud passes over.

d. The field collapses, with the magnitude and frequency of occurrence indicating the intensity and maturity of the storm.

A number of systems have been built or proposed to interpret these events as an indication of lightning probability. It has also been proposed that estimates of distance to the storm be based on the depth of field collapse. This requires an assumption of the charge released by the discharge. Charge transfer is a variable which can only be presented statistically. This uncertainty is reflected in any estimate of range based on field variation. More qualitatively, there is no way to distinguish between a strong distant strike or a weak nearby strike by observations of field changes.

5.3.5.2 Locating Charge Centers

It has also been suggested that a charge center can be located in realtime by computer processing the data from several field mills. This is theoretically possible, and such computations have been performed with reasonable results on a post-test basis. However, a large array of parameters is involved, and a large computational capability would be required to perform these computations in near-realtime. Further, the evaluation of all such systems is very difficult since the only reliable way to locate a lightning channel, other than by observed damage, is by photography. Reduction of this photographic data to specific locations represents a large analytical effort per calibration point.

Despite these disadvantages, the conservative interpretation of data from field mills is more effective for predicting lightning hazards than other approaches based on instrumentation. The chief difficulty in applying field mills to lightning warning is the scientific background required for interpreting the field mill outputs. Several approaches to automating this interpretation have been contrived, and at least two of these are in limited production. Those which have reached our attention are:

The Nobel Lightning-Warning System

This system was developed by the University of Uppsala, Sweden, for the Nobel Explosives Company to satisfy a legal requirement for a lightning warning system for use at the site of electrically fused blasting. The system consists of an inverted field mill and an indicator box, both of which are portable and are pedestal-mounted (see figure 5-13). A sferics antenna is
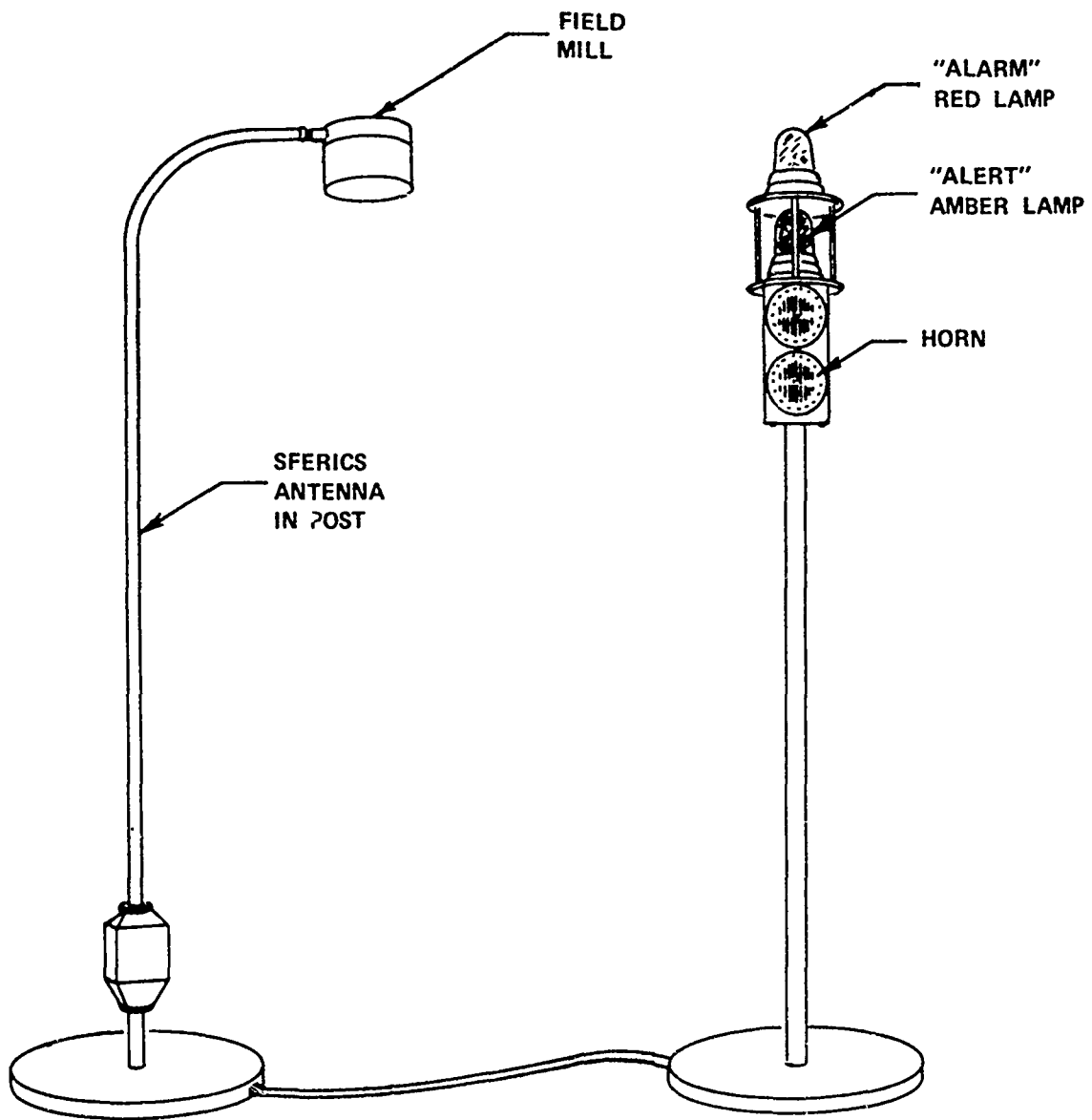
Figure 5-13. Nobel Lightning Warning System

incorporated on the field mill mounting pole. The indicator contains two status lights and a siren. The hazard levels indicated by the device are:

1. **Warning**: 1000 V/m or 1 sferic

2. **Alarm**: Three possible conditions

   a. 2000 V/m

   b. Two sferics within 100 seconds

   c. 1000 V/m and 1 discharge

The designer has expressed the opinion that such devices are only useful for conservative warning and should be kept simple [43].

This system is commercially available in Sweden at a cost of $2,000 - 3,000.

The Electrofields System

A commercially produced lightning warning system is marketed under the trade name "Thor Guard" by Electrofields Inc. of Miami, Florida. In its basic configuration this system consists of a field mill mounted on an aluminum pole, a control and display panel, and a 50-foot data cable. Accessories include a remote capability with standby power and an rf data link. The Thor Guard system is proprietary, and the manufacturer will not release a full description of the system theory; however, the general operation can be described as follows (see figure 5-14).
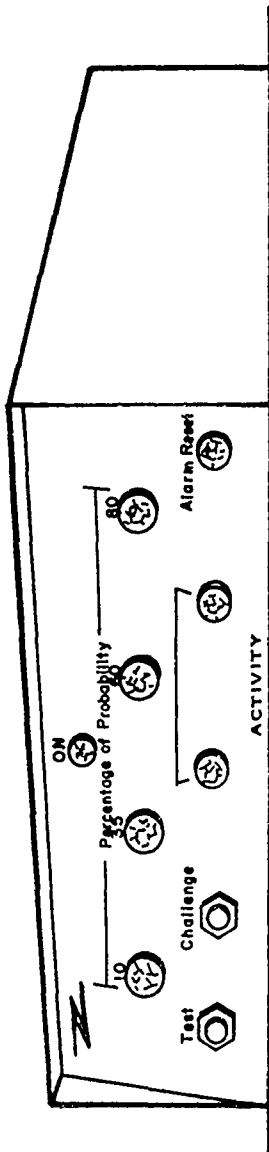
LIGHTNING HAZARD LEVEL INDICATOR

FIGURE 5-14

ELECTRO-FIELDS LIGHTNING HAZARD LEVEL INDICATOR

The Thor Guard display consists of lamps indicating 4 hazard levels. These hazard levels are: 10%, 35%, 60%, and 80% probability of a strike within the range of the instrument — nominally 5 miles, but adjustable for greater ranges. Two auxiliary lamps indicate "activity." An activity light indicates that an electric-field collapse has occurred during the past 5 minutes. Each field collapse resets a 5-minute timer. If 5 minutes elapse with no additional activity, the activity light is extinguished, and a hazard level of 10% or none is indicated. Each of the four hazard levels is conditioned on a combination of activity and field intensity corresponding to some phase of the thunderstorm profile depicted in figure 5-12. These combinations are as in table 5-2 below.

TABLE 5-2

HAZARD LEVELS AND INDICATIONS FOR THE ELECTROFIELDS' LIGHTNING
HAZARD LEVEL INDICATOR

Lamp Color	Probability	Activity	Field Intensity
Yellow	10%	No	Low Positive or Negative
Orange	35%	Yes	High Positive or Negative
Blue	60%	Yes	High Negative
Red	80%	Yes	Very High Negative

A challenge button permits the unit to be reset in the event that an indication is believed to be spurious, and verification is desired.

A Thor Guard was procured by RML in 1973 for evaluation. The system has been installed at various operations facilities for 15 months. It has withstood exposure to the coastal environment and also held calibration well compared to most field mills.

5-38

During the summer storm season of 1974, the system was operated
at the Cudjoe Key tethered-balloon site with chart recorders on
the outputs. For comparison with the instrument indications,
the distances to lightning channels were estimated as closely as
possible by radar and by timing the delay between visual sight-
ing of lightning and thunder. While several sensitivity adjust-
ments were made, it was relatively unusual for lightning to oc-
cur within 5 miles of the site without prior warning from the
Thor Guard. The most recent setting gives an effective range of
approximately 8 miles. Figure 5-15 is a strip chart record of
the Thor Guard's output during a storm passage. Note that during
the period 1730 through 1930 hours, the storm passes within 7
miles (by radar) and that the 80 percent indicator was illuminated
Note also a passage around 2100 of a charge center which created
a positive field, but that no lamps came on and no lightning was
detected.

5.3.5.3   Importance of Location

The ground measurements described in 2.6.2 indicated that a bal-
loon with conducting tether suppressed the vertical field near
the tether point. This effect is negligible at a distance of
one tether height from the tether point. Field mills to be used
as ground-level warning systems should be located outside this
range if a conductive tether is used. Ground-level field sup-
pression by a dielectric tether is negligible and should not
affect the placement of a warning system. More important is the
placement of the field mill relative to nearby obstructions. As
was the case with the balloon, a tall obstruction nearby sup-
presses the field and causes the mill to read low. Conversely,
if the instrument is mounted on top of a pole or other elevated
position, the field is intensified and the instrument will read
high. In either case the instrument must be calibrated relative
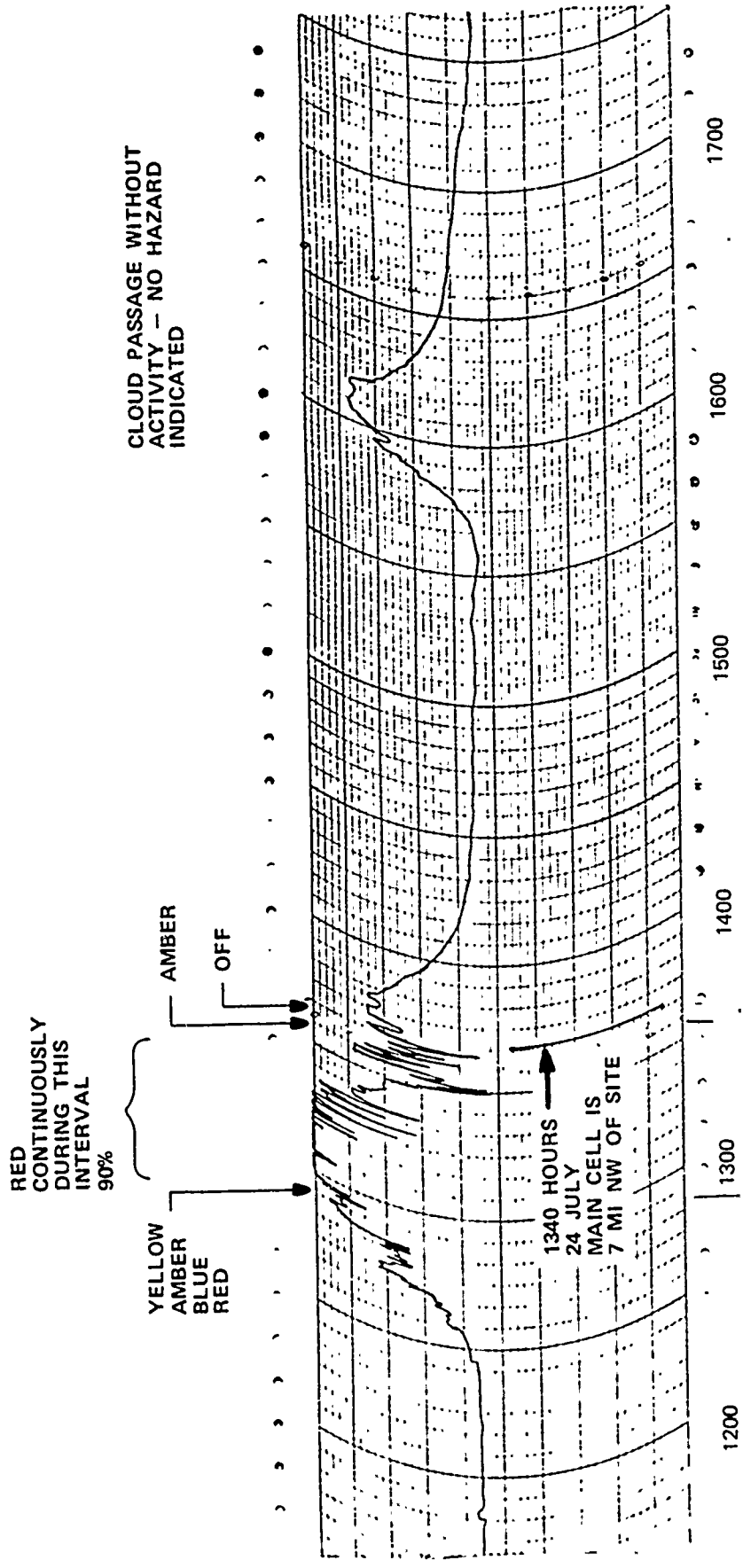
Figure 5-15 Record of Thor Guard Output and Hazard Indications

to a properly calibrated instrument outside the influence of the
site form factor but otherwise subject to the same ambient field.

5.3.5.4 Balloonborne Field Meters

Since an important aspect of the balloon lightning hazard is
field intensification at the top of the balloon, this location
is therefore a logical place to locate a field measuring device.

5.3.6 Tether Current

Tether current is an indirect measure of E-field and is there-
fore a useful indication of lightning hazard. Figure 5-16, from
Davis and Standring [31], shows tether current trends for several
balloons prior to their receiving a lightning flash. These graphs
indicate that a tether current change by a factor of 5 within a
period of five minutes can be regarded as a lightning warning,
especially if the current is driven negative. A logarithmic
current amplifier would permit a single-tether ammeter to accom-
modate the wide range of currents to be expected from either
conductive or dielectric tethers. A mechanical concept suitable
for a tether ammeter is shown in figure 5-17.

5.4. SAFETY PROCEDURES

An interim safety procedure has been prepared. The following
philosophy is presented as a basis for extending the preliminary
procedure into a sounder and more inclusive safety program.

5.4.1 Managerial Action

Most accidents occur because something was valued above safety.
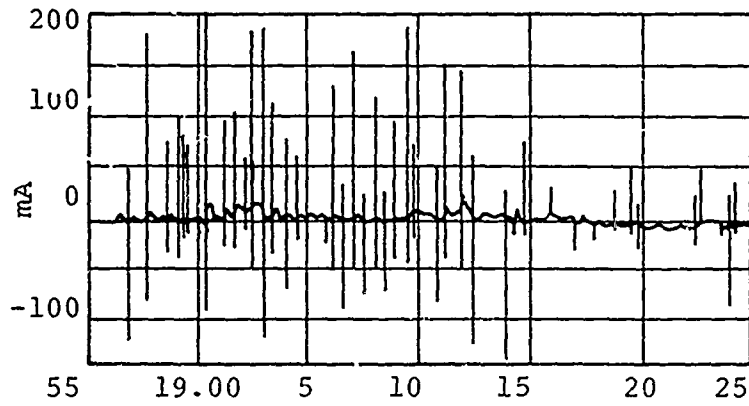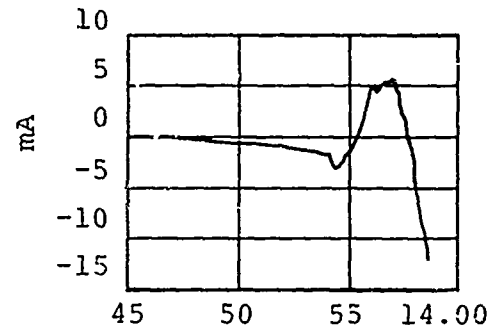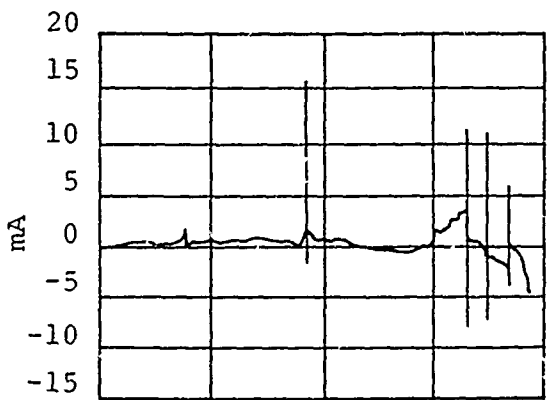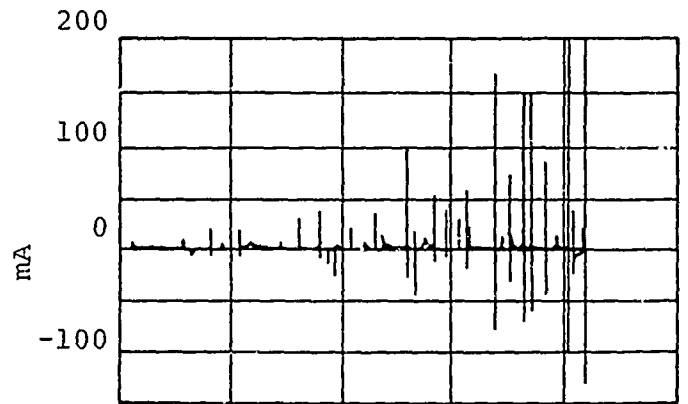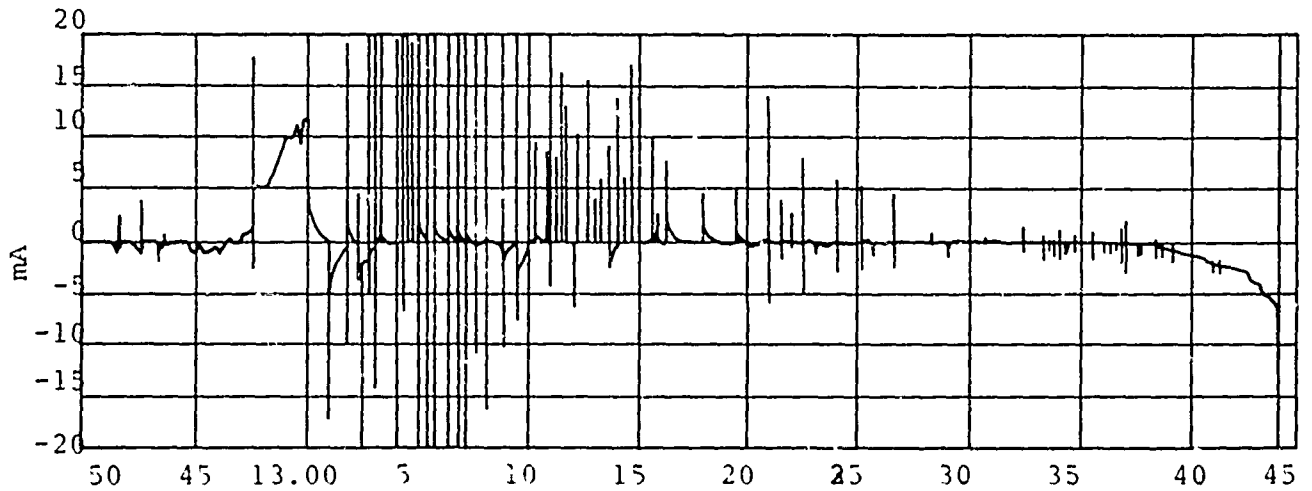
Figure 5-16
Tether Current Prior To Lightning Strikes To Balloon
(From Davis & Standring)
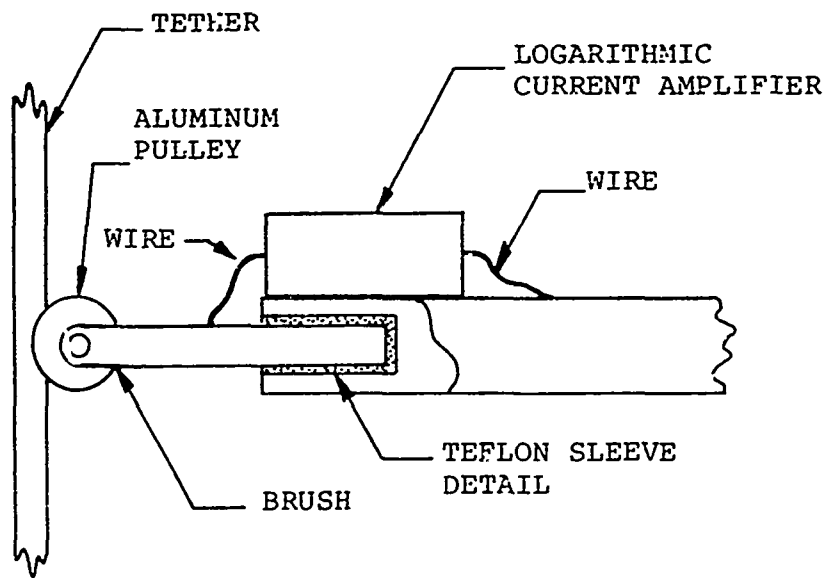
FIGURE 5-17 MECHANICAL CONCEPT - TETHER AMMETER

When an expensive system is exposed to a hazard, personal risks are sometimes taken on a voluntary or even a coercive basis. The probability of accidents occurring under such circumstances is reduced and possibly eliminated by establishing priorities at the management level, and communicating these priorities throughout the organizational structure, so all personnel know exactly what response is expected in an emergency situation.

A particular priority question is whether to recover the balloon or leave it aloft. The type of thunderstorms common in the Florida Keys can develop in considerably less time than is required to recover the balloon. The task of mooring the balloon during a thunderstorm is probably the most hazardous of balloon operations. Accordingly, carefully considered guidelines should be provided as to when the balloon is to be recovered. Indecisiveness in pursuit of this guidance could be extremely dangerous.

5.4.2 Controlled Access

The Cudjoe Key incident in August 1972 indicated that the winch operator's position initially provided some degree of lightning protection. The extent of this protection has subsequently been increased. With implementation of the corrective action in 5.2.3, an even higher degree of safety would be provided.

On the other hand, people afoot are in a much more vulnerable position. If a lightning hazard exists or is imminent, then the pad area should be cleared of all people not actually required there for performing essential duty. If the balloon is not being retrieved, then no one should be required in the winch area other than the winch operator and possibly a driver.

5.4.3 Operational Insight

A procedure written independently of the operations group involved is very likely to be unrealistic. Operations personnel should be heavily involved, if not responsible for preparing the operations safety procedure.

5.4.4 Training

In a potentially hazardous activity, knowledge of safety practices is as much an element of professionalism as is competence in the more routine aspects of the job. It should be a managerial responsibility to assure that all personnel are familiar with, and maintain a proper attitude toward, the safety procedures.

SECTION 6

CONCLUSIONS

6.1 INTERACTION OF TETHERED BALLOON SYSTEMS WITH ATMOSPHERIC ELECTRICITY

The tethered balloon system modifies the ambient electrical field pattern by intercepting field lines which would otherwise extend to earth in an essentially perpendicular pattern. If the tether is a good conductor, more field lines will terminate on the tether than on the balloon. Conversely, if the tether is a poor conductor, the balloon itself is the dominant geometry and more field lines will terminate on the balloon than on the tether.

The charge associated with the intercepted field lines will result in a conventional current flow down the tether. If the tether is a poor conductor, the tether current is the ratio of potential gradient to tether resistivity. In a fair weather field, tether current will generally be on the order of a nano-ampere.

If the tether is a good conductor, the tether current due to intercepted field lines will be greatly exceeded by a current component due to corona discharge. The net current in this case can achieve a fair weather value of milliamperes. This corona current produces a negative space charge plume blowing downwind. The field above this charge plume is intensified, while that below it is suppressed.

The charge transfer effected by tether current allows the balloon to charge toward ground potential. If the tether is a

good conductor, the charging time constant is small compared to the balloon's ascent time. If the tether is a poor conductor, the time constant is on the order of hours but nevertheless charging does occur.

By raising ground potential to the balloon altitude, balloon charging intensifies the field above the balloon and consequently could promote streamering (which in turn could trigger lightning).

Elevation of the ground potential also results in suppression (in essence a shorting) of the electric field at ground level near a well-conducting tether. This effect is not detectable if the tether is a poor conductor.

Distant lightning can induce sufficient current transient on a well-conducting tether cable to damage sensitive electronics. This effect would be more pronounced for nearby lightning. No induced transients were detected on poorly-conducting tethers.

Experiments indicated that two weeks exposure to a coastal atmosphere degraded tether resistivity from that of a poor conductor (10^{11} ohms/meter) to a transitional conductor (10^7 ohms/meter). The latter resistance would decrease even further in high humidity.

6.2 PREDICTION OF LIGHTNING STRIKES TO BALLOONS

The extension of a method of prediction designed for tall structures indicates that a tethered balloon with wire-rope tether flying continuously at an altitude of 12,000 feet would receive approximately 30 lightning flashes during the month of August.

This work cannot be directly applied to a balloon with a poorly-conducting tether. Based on the observed tendency of a balloon to accumulate charge, even when tethered by a poor conductor, and the operational difficulty of maintaining low conductivity, we concluded that a balloon with a well-conducting tether will be experiencing more lightning discharges than would be the same balloon with a poorly-conducting tether, but probably not much more. Being subjective, this conclusion must be weakly stated.

We can state more strongly that assuming the advantage of Nolaro over wire rope can be stated as a ratio as high as ten-to-one, the balloon tethered by Nolaro would still be struck several times during a storm season.

Regardless of tether type, the predicted rate of lightning exposure is sufficient for lightning protection to receive high priority.

6.3   EFFECTS OF LIGHTNING ON TETHER MATERIALS

Lightning currents tend to propagate down the surface of a jacketed Nolaro cable, with occasional localized damage possibly resulting from surface inhomogeneities. This damage is sporadic and difficult to predict.

The effects of the high current phase of a lightning pulse on Nolaro can be realistically simulated, but not the continuing current phase.

Upon striking a wire-rope tether or other conductors, a lightning flash enters at an arc contact point, where localized burning occurs. It is then conducted to ground, with resistance heating occurring along the full length of the rope.

The effects of both the high current transient and the continuing current on a wire-rope tether can be realistically simulated. The survivability of a wire-rope tether is therefore more predictable.

Burning at the arc contact point results in greater reduction of tether strength than does resistance heating. Therefore, samples exposed to simulated lightning generally fail at the arc contact point.

Having greater strength at high temperature, stainless steel experiences less reduction of breaking strength due to arc burning than does carbon steel.

Having lower resistivity than stainless steel, carbon steel experiences less reduction of strength due to resistance heating.

The survivability of a jacketed Nolaro tether is apparently independent of tether diameter.

Wire rope of 0.375-inch diameter is marginally survivable for typical lightning flashes. Rope of 0.25-inch diameter is "fragile," and wire-rope tethers of this size should be made of stainless steel. Rope of 0.5-inch diameter could probably be considered "durable" and carbon steel would be acceptable.

Nolaro tethers with internal electrical conductors are extremely vulnerable to lightning.

Any measure which increases the conductivity of the outside of a Nolaro tether, relative to the inside, appears to increase survivability.

6-4

A coating of aluminum paint on the jacket of a Nolaro tether appears to enhance surface flashover, thereby increasing survivability.

Incorporation of tubing to the tether to supply gaseous fuels to the balloon power plant, does not appear to affect tether survivability.

6.4 PROTECTIVE MEASURES

6.4.1 Personnel and Ground Equipment

Personnel protection is based primarily on protective enclosures and safety procedures.

The effectiveness of a protective enclosure is dependent upon the preservation of shielding integrity by bonding all structural parts and by assuring that all incoming conductors are properly shielded and bonded.

Grounding is of secondary importance to shielding in the effectiveness of protection enclosures; however, proper grounding of the balloon tether and other obstructions in the direct path of lightning is essential for protecting unsheltered personnel.

The safety of unsheltered personnel near a potential strike point (such as the winch or mooring mast) is enhanced by a conducting ground plane which provides more effective distribution of ground currents.

A ground sheave some distance away from the winch would provide greater safety than the presently used flying sheave.

Communications with the winch operator using radio rather than hard wire is inherently much safer.

Slot antennas on the winch provide the best inherent lightning protection.

Speakers and directional microphones are much safer than headsets.

6.4.2 Balloon, Tether, and Balloonborne Systems

The tether can best be protected by minimizing the probability of a direct strike to the tether through the use of a lightning rod (air terminal) on the balloon.

Transfer of lightning current from the lightning rod to the tether is straightforward in the case of a wire-rope tether but more problematical for a Nolaro tether.

Shield wires extending from air terminals on the nose to each of the tail fins will provide a degree of protection to the hull (figure 5-8).

A layer of lightweight heat shield placed between large-gauge wires and the hull provides protection to the hull.

Wire-rope confluence wires will tend to divert lightning away from the payload.

Interconnecting all electrical system grounds by a heavy ground wire provides significant protection.

6-6

Continuous shields on all power and instrumentation cables grounded to the cases of the systems on which they terminate provide further protection.

Semiconductor surge suppressors installed at the inputs and outputs of all critical equipment provide additional protection.

6.4.3 Lightning Hazard-Warning System

Radar augmented by a vhf azimuth-measuring system would be useful for tracking lightning associated with frontal storms.

For air mass storms, an electric field-derived system is more likely to provide adequate warning than radar. The Thor Guard lightning-hazard-level indicator approaches this requirement as well as any other existing system that we are aware of, and is relatively inexpensive.

Lightning strikes to tethered balloons are frequently preceded by abrupt and rapid increases in tether current. If monitored, this effect could possibly provide a final warning.

The extent of balloon charging can be best measured by a field mill at the highest point on the balloon. Owing to high fields anticipated, the field mill need not be very sensitive.

6.4.4 Safety Procedures

The effectiveness of lightning warning systems and protective enclosures is dependent upon their employment in a sound lightning-safety procedure. The indispensable principles of operational-safety procedures are:

Establishing clearly defined criteria for retrieving the
balloon or leaving it aloft. Decisions based on these
criteria must be made quickly, and will frequently be
irreversible

Defining the minimum operating crew during hazardous peri-
ods. Access to the pad area should be carefully restricted.

Assuring operational soundness and practicability of safety
procedures by the participation of operations management in
their preparation

Ensuring that operating personnel are completely familiar
with all appropriate safety procedures

SECTION 7

RECOMMENDATIONS

7.1 PROTECTIVE HARDWARE - GROUND

7.1.1 Winch Modifications

The winch operator's positions should be brought as closely as possible to the action configuration described in 5.1.6. This should be done as soon as practicable. It is assumed that the present configuration will limit the extent to which these safety provisions can be incorporated; however, they should be used as guidance in the procurement of new winch trucks.

7.1.2 Mooring Mast

The mooring mast should be grounded as shown in figure 5-3. All grounds should be periodically checked and replaced or refurbished as required.

7.1.3 Ground Planes

Ground planes should be provided at the mooring mast and in the winch parking area. If necessary funds are available, an installation as shown in figure 5-4 should be built.

7.2 WARNING SYSTEMS

7.2.1 Ground-Level Field Mill

Provisions for temporary installation of a ground-level field mill should be made. This mill will be used for calibration of the Thor Guard. The mill should be located at a distance from the nearest obstruction equal to 10 times the height of the obstruction. Otherwise it should be as close as possible to the Thor Guard.

7.2.2 Weather Radar

A weather radar should be installed on the roof of the operations building at CKOL. If the cost of procuring a standard weather radar cannot be funded, modification of surplus aircraft search radar for a weather application should be considered.

7.2.3 Tether Ammeter

A tether-current ammeter should be installed on the winch to measure rapid, large-scale current increases which are indicative of a lightning hazard. The output of the tether ammeter should also be telemetered to the operations control van.

7.2.4 Balloonborne Field Mill

A field mill should be located at the top of the balloon empennage. A small mill similar to the one used in the Thor Guard is available at moderate cost, and would be adequate for this application. The mill should be modified to provide a logarithmic output from 1 kV/m to 1 MV/m.

7.3 PROTECTIVE HARDWARE - AIR

7.3.1 Hardening of Critical Balloonborne Systems

TELTA project personnel should determine the extent to which the provisions of section 5.2.2 can be implemented, consistent with technical and operational constraints, and should prepare a plan for these modifications.

7.3.2 Control of Attachment Point

1. Wire-Rope Tethers - If a wire-rope tether system is adapted, a protective system should be implemented using lightning rods, shield conductors, and steel

confluence cables as described in section 5.2.1 and
pictured in figure 5-8.

2.   Nolaro Tethers - Owing to the absence of a known re-
liable means of transferring energy from a lightning
rod to a poorly-conducting tether, a protection sys-
tem based on lightning rods is not recommended with
the currently used Nolaro tether system. Research
directed toward determining an appropriate system
will be recommended.

7.4 SAFETY PROCEDURES

It is recommended that a joint meeting of RML, TELTA, and desig-
nated support organizations be convened to address the follow-
ing issues:

1.   What hardware implementations are to be made and in
what priority

2.   Determining the criteria for the decision as to
whether the balloon should be recovered

3.   Establishing the circumstances under which the pad
area is to be cleared

A joint task team should then be formed to prepare an opera-
tional safety procedure commensurate with the results of this
meeting and consistent with operational requirements and equip-
ment limitations.

The procedures developed by the joint task team, upon approval
by the Platform System Branch (ENLP) should then become an
integral part of TELTA operational doctrine.

7.5 TETHER MATERIALS

7.5.1 Wire Rope

Wire rope is not recommended as a primary tether material for the following reasons:

1. Altitude limitations due to weight of tether.
2. Poor survivability of internal electrical conductors.

The substantial weight advantage offered by a Kevlar 29 tether with integral methane supply tube indicates that this would be a more advantageous approach. However, to maintain an optional approach to extended duration flight, procurement is recommended of a 5,000 ft length of 0.438-inch diameter 3 X 18 steel cable, Monitor AAA grade with integral AWG #20 copper wire in the center of each strand. Use of this cable will also require slip rings on the winch and in a swivel at the confluence point.

7.5.2 Preferred Alloys

Wire-rope tethers of 0.110 inch cross section area (nominal 0.375-inch diameter 6 X 14), or greater can be made with reasonable safety from a high-strength carbon steel such as Monitor AAA. Smaller cables should be made of stainless steel if lightning survivability is important.

7.6 ADDITIONAL RESEARCH AND DEVELOPMENT

7.6.1 Interactions of Balloon System With Atmospheric Electricity

Additional measurements of the resistivity of operational Nolaro tethers should be made. These measurements should be directed toward determining:

1. Variations along the length of a tether
2. Variations of a given section with time

7-4

Other tests should include:

1. Measurement of induced currents in a wire tether resulting from storms at known distance. This work could be performed at Patrick AFB using small balloons or kites.

2. Controlled exposure of expendable balloons to lightning.

Exposure of small inexpensive balloons to thunderstorms would provide experimental verification to the theory presented here. Balloons would be tethered with music wire and small diameter Kevlar. If possible, balloons with both tether types would be flown simultaneously during periods of high thunderstorm activity. This investigation would center on relative attractiveness of the two tether types and the effectiveness of simple protection systems. The induced current measurements suggested above could be incorporated with this program.

7.6.2 Tether Materials

Protective Coatings - Further testing to verify the effectiveness of metallic (or other) coatings for protection of dielectric tether materials should be undertaken. Proper adhesion of metallic paints to the neoprene jacket is also a potential problem. Therefore, the existence of suitable materials and processes for applying protective coatings to the tether should be verified.

Energy Transfer - Research should be conducted to identify a means of transferring lightning current from a balloon-protection system to the tether with minimum likelihood of tether damage. This is a weak link in the protection of balloon systems with Nolaro tethers.

INSTRUMENTATION FOR MEASUREMENT OF EFFECTS

OF

BALLOON SYSTEMS ON THE ATMOSPHERICAL FIELD

1.0 INTRODUCTION

Two categories of experiments were performed to measure the interaction of the balloon and tether with the natural electric field - overhead measurements by an instrumented aircraft and ground level measurements using instruments developed for the project. With primary emphasis on the ground measuring systems, the instrumentation system may be described as follows:

2.0 AIRBORNE MEASUREMENTS

Airborne measurements were performed using an instrumented aircraft operated by NASA-Kennedy Space Center. This airplane has two cylindrical field mills, each capable of measuring electric field along two axes.

One mill, mounted on the nose, measured electric field components in the transverse and vertical directions. A second mill on top of the aircraft measured field along the longitudinal and transverse axes. These measurements along with a scale reference, time code, and flight information such as altitude, heading, and airspeed, were recorded by pen recorders. Electric field profiles were recorded by flying the aircraft on courses which carried the aircraft directly over the balloon on upwind and crosswind headings. These patterns were flown at altitude separations of 100, 200, 300, 500, and 1000 feet above balloon altitude. These flights were coordinated with the ground experimenters by radio. A typical 100 ft overflight is shown in figure A-1.

3.0 GROUND MEASUREMENTS

Ground measurements included the measurement of electric field, air-to-earth current, tether current, and tether potential. Except as noted otherwise the instrumentation was designed by Dr. D. J. Latham, University of Miami, and fabricated on the Air Force Eastern Test Range.

3.1 DEPLOYABLE MEASURING SYSTEM

The deployable measuring system consisted of five instrumentation units, a central junction box and associated cabling. Each instrumentation unit consisted of a sensor box and a control box (figure A-2). The sensor box provided conveniently transportable packaging for a field mill and an air-to-earth current antenna with associated electronics. The control box contained a line driver for the field mill, a range switch for the air-to-earth current system, meters for the two measurements, and a calibrator to provide reference levels for calibration of strip recorders. Schematics are included at the end of this appendix.

3.1.1 Field Mills

A field mill is an electromechanical instrument used for measurement of electric fields. A sensing plate is alternately exposed to and shielded from the electric field by a rotating vane. This amounts to chopping the electric field. The low level alternating potential developed between the sensing plate and ground is amplified by a preamplifier, then by a bipolar amplifier. Polarity is determined with respect to a reference generator on the rotor shaft. The resulting output is

A-2
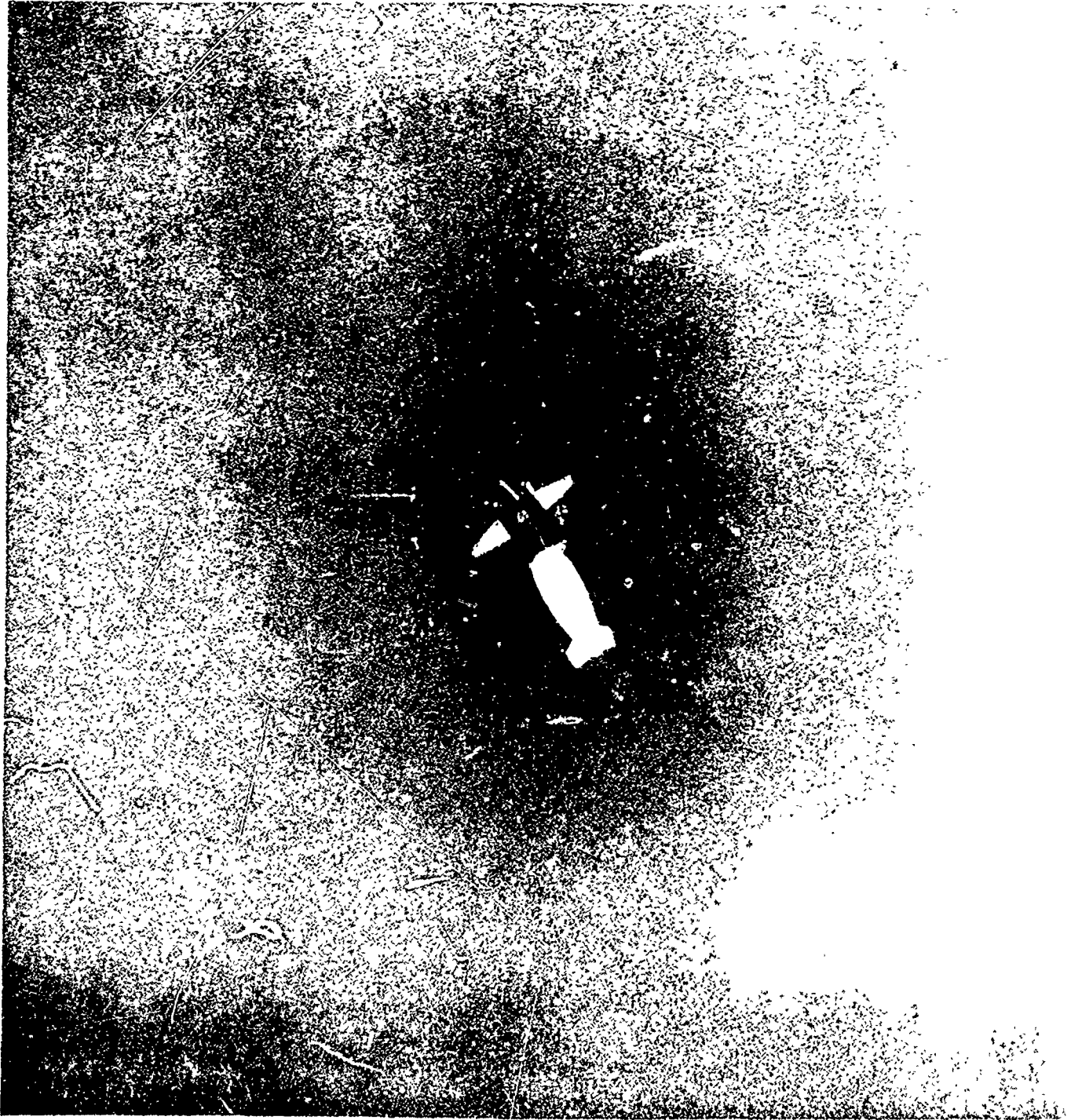
Figure A-1.   Overflight of the 5,300 Cu Ft Balloon By An Instrumented Aircraft

A-3
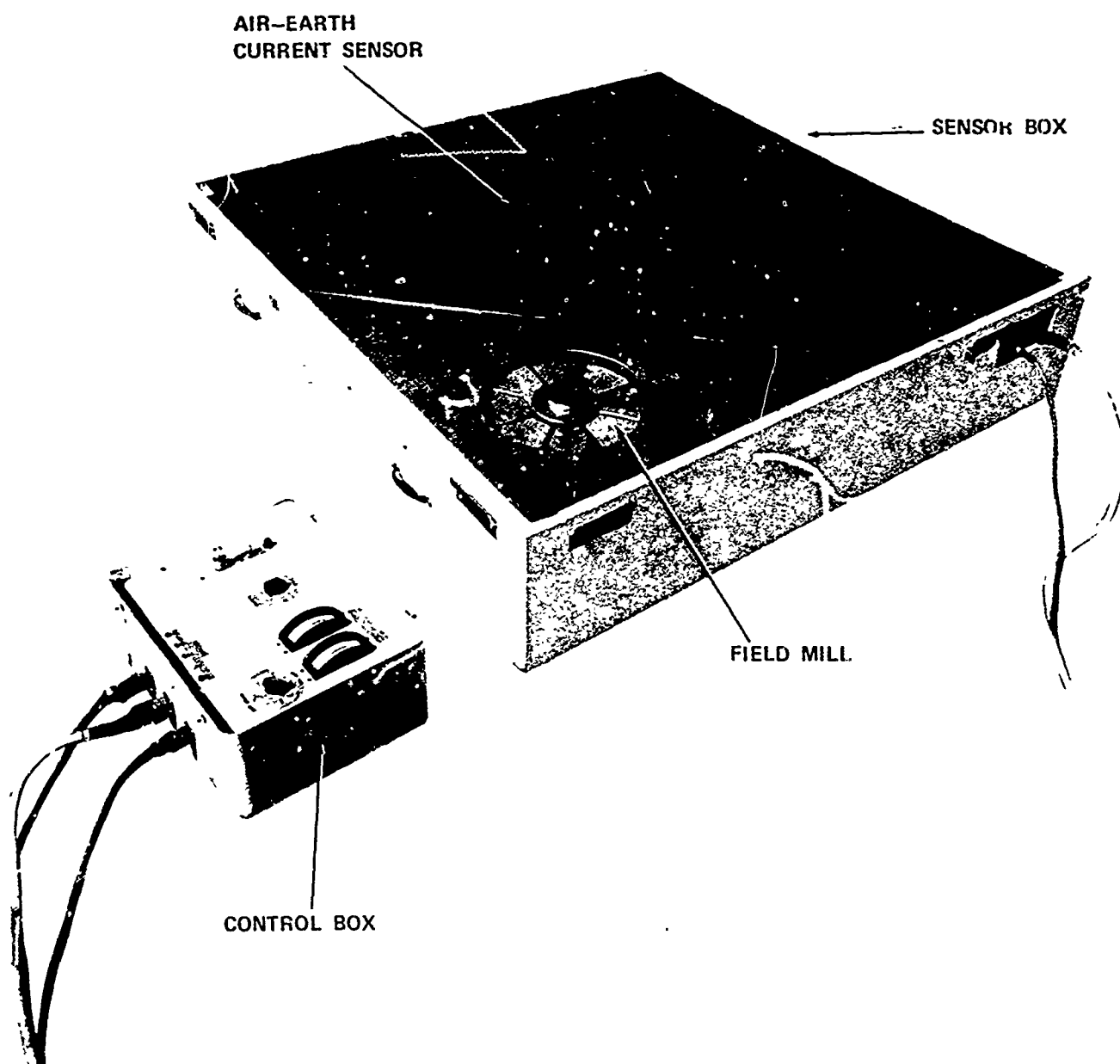
Figure A-2.   Instrumentation Unit of Deployable Measuring System

a full wave rectified signal proportional to E field with polarity determined by that of the field. This signal was filtered in the control box. The field mills were rented from the University of Minnesota at Duluth, where they were developed by Professor D. E. Olson.

3.1.2 Air-to-Earth Current

Air-To-Earth current was collected on an aluminum plate with an area of one square meter. To preserve a high isolation from ground, the "antenna" was mounted on four teflon insulators. The insulators were packaged in two interlocking but noncontacting aluminum cans to retard the accumulation of dust or other contaminants. The sensor was connected to an amplifier by teflon insulated wire. The amplifier was packaged in an aluminum case with access via a terminal with a teflon feedthrough and a noncontacting aluminum shield. The current amplifier was a high input impedance operational amplifier with gain and frequency response determined by a network of resistors and capacitors. The feedback resistors were precision high ohmage, glass encapsulated resistors. In parallel with each was a low leakage capacitor which, together with its associated resistor, provided a time constant of 200 seconds.

The purpose of the long time constant was to diminish the effect of displacement current. Gain was controlled by switching RC networks through the use of specially constructed reed relays. These relays consisted of glass encapsulated reed switches activated by oversized coils which permitted the switches to be mounted on teflon standoffs without contacting the coils. The coils were energized by switch closures from the control box (figure A-3). The design provided current ranges from ±5 picoamps full scale to ±50 microamps full scale in decade steps.
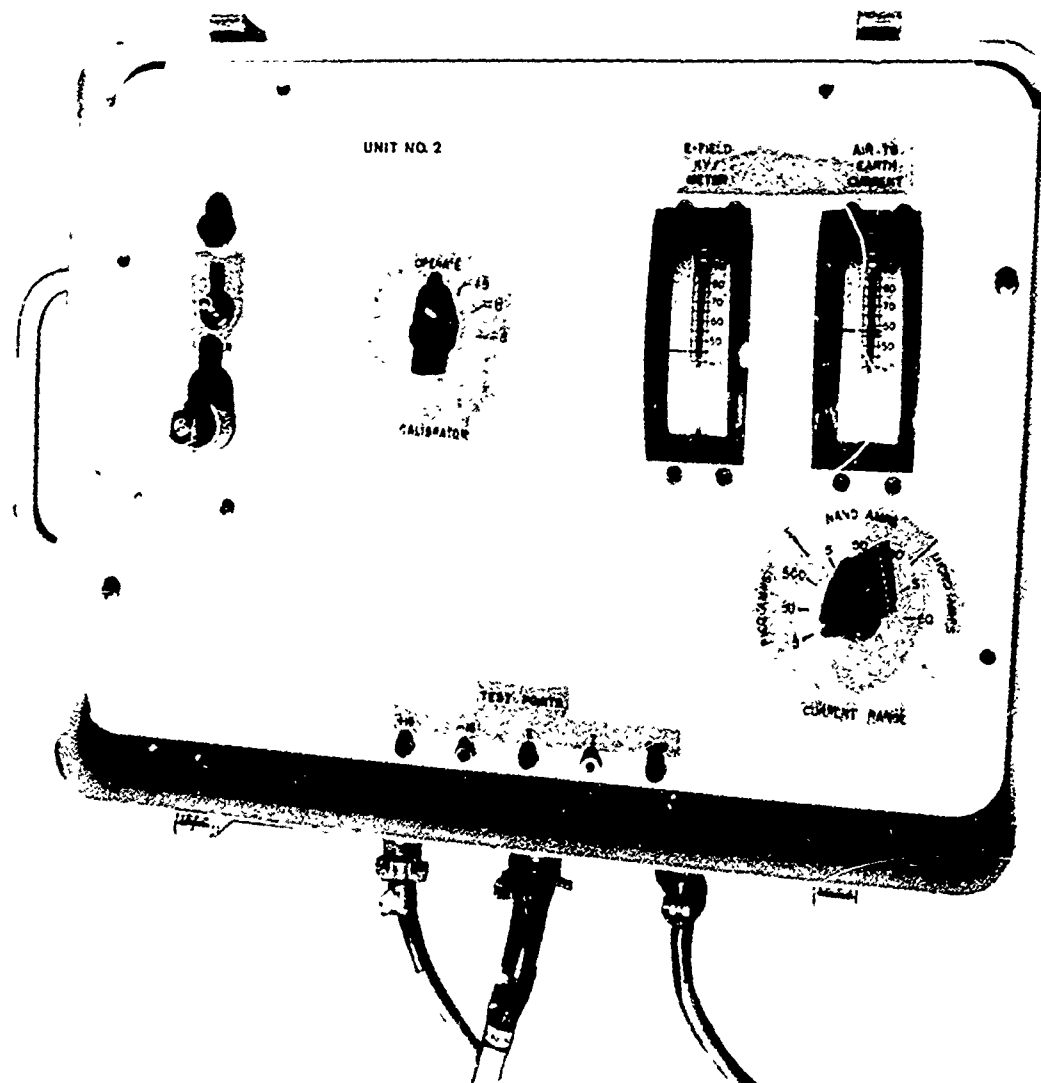
Figure A-3. Control Box — Deployable Measuring System

Only the lower three ranges were used; however, the remaining ranges were deactivated to eliminate leakage problems associated with them when it was determined that they were not essential for the experiments to be performed. Normally four deployable systems were used. They were located in a straight line extending downwind from the tether point at distances of approximately 0, 100, 200, and 500 feet. The downwind orientation was sometimes lost due to wind shift. Each deployable system included a 500-foot cable assembly which routed data to a central junction box (also portable) which was generally located near the winch. Ac power was distributed through this junction box to the five deployable systems via the 500-foot cables. From the junction box a 100-foot data cable routed the measurements to an instrumentation van where the following data was strip recorded:

    Potential Gradient (Inverse of electric field - four locations)
    Air to Earth Current - four locations
    Tether Potential
    Surface Wind Velocity

3.2 WINCH INSTALLATION

To facilitate certain measurements, particularly tether current and tether potential, a special winch installation was mounted on a 30-foot flatbed trailer for use with the 5300-cubic foot Schjeldahl balloon. See figure A-4. Two gasoline powered winches were mounted side by side on an aluminum frame. This assembly was mounted on porcelain insulators which in turn were attached to the trailer. See figure A-5.

The fair lead sheave was mounted on a porcelain insulator at the opposite end of the flatbed. This insulator was held in compression by turnbuckles attached to the platform through porcelain strain insulators (figure A-6).
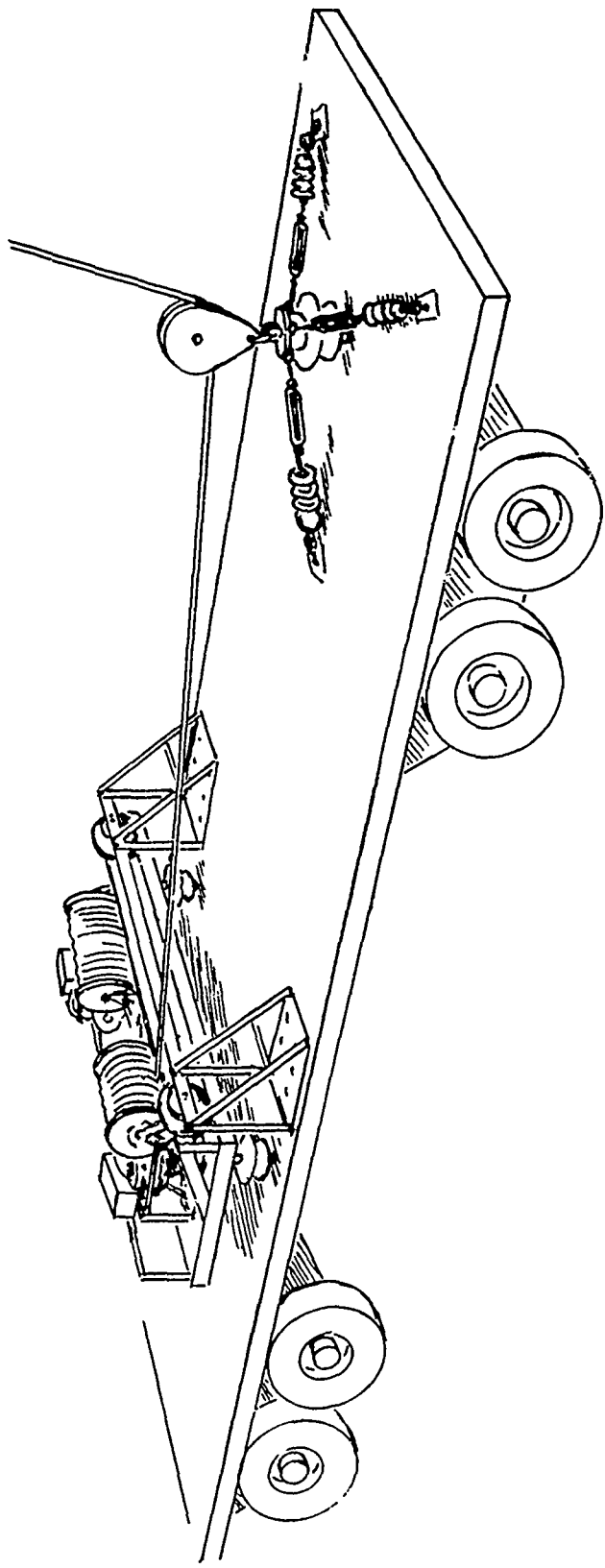
Figure A-4. Winch Assembly

PORCELAIN INSULATOR
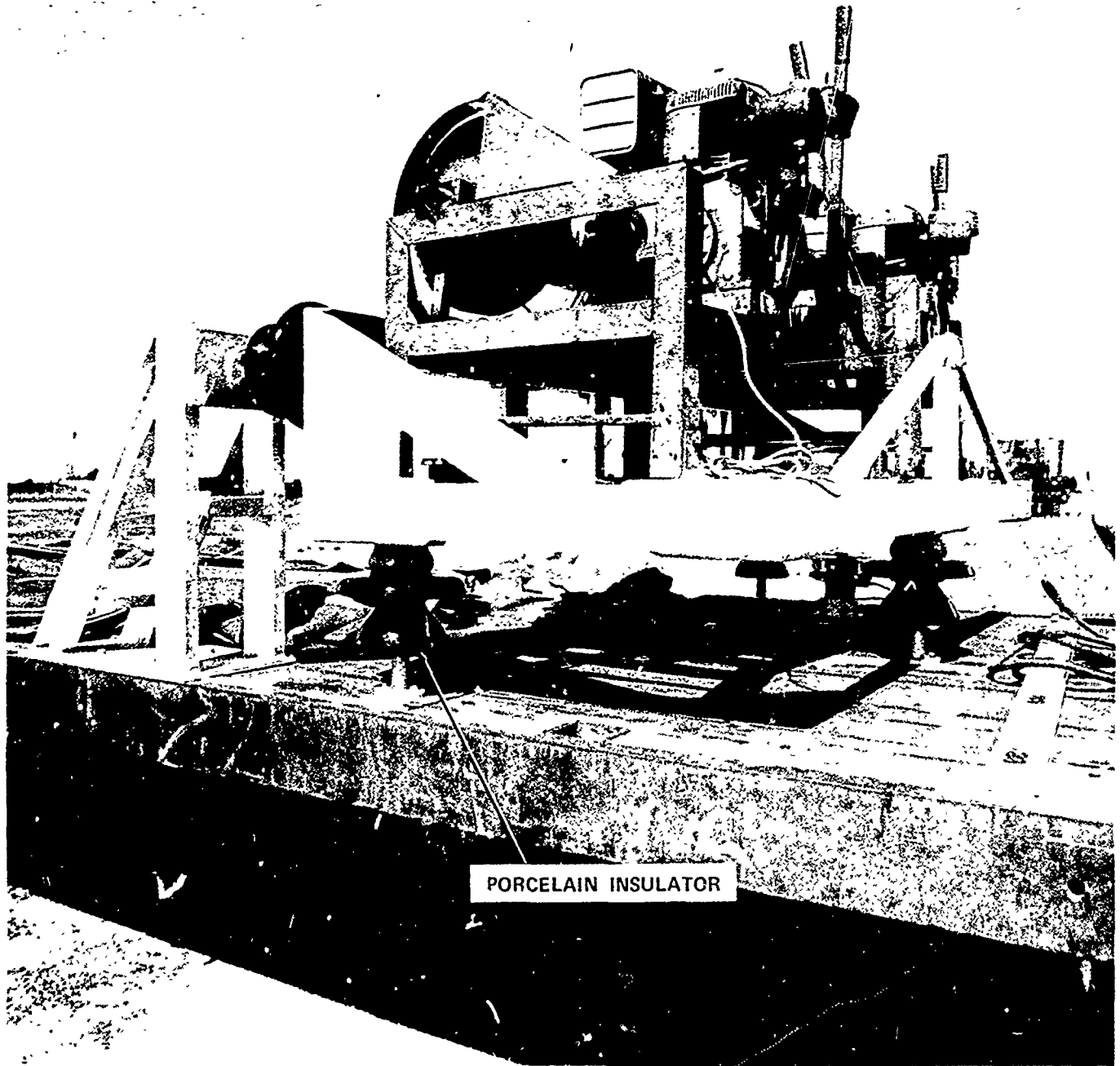
Figure A-5. Installation of Isolated Winches on Flatbed Trailer
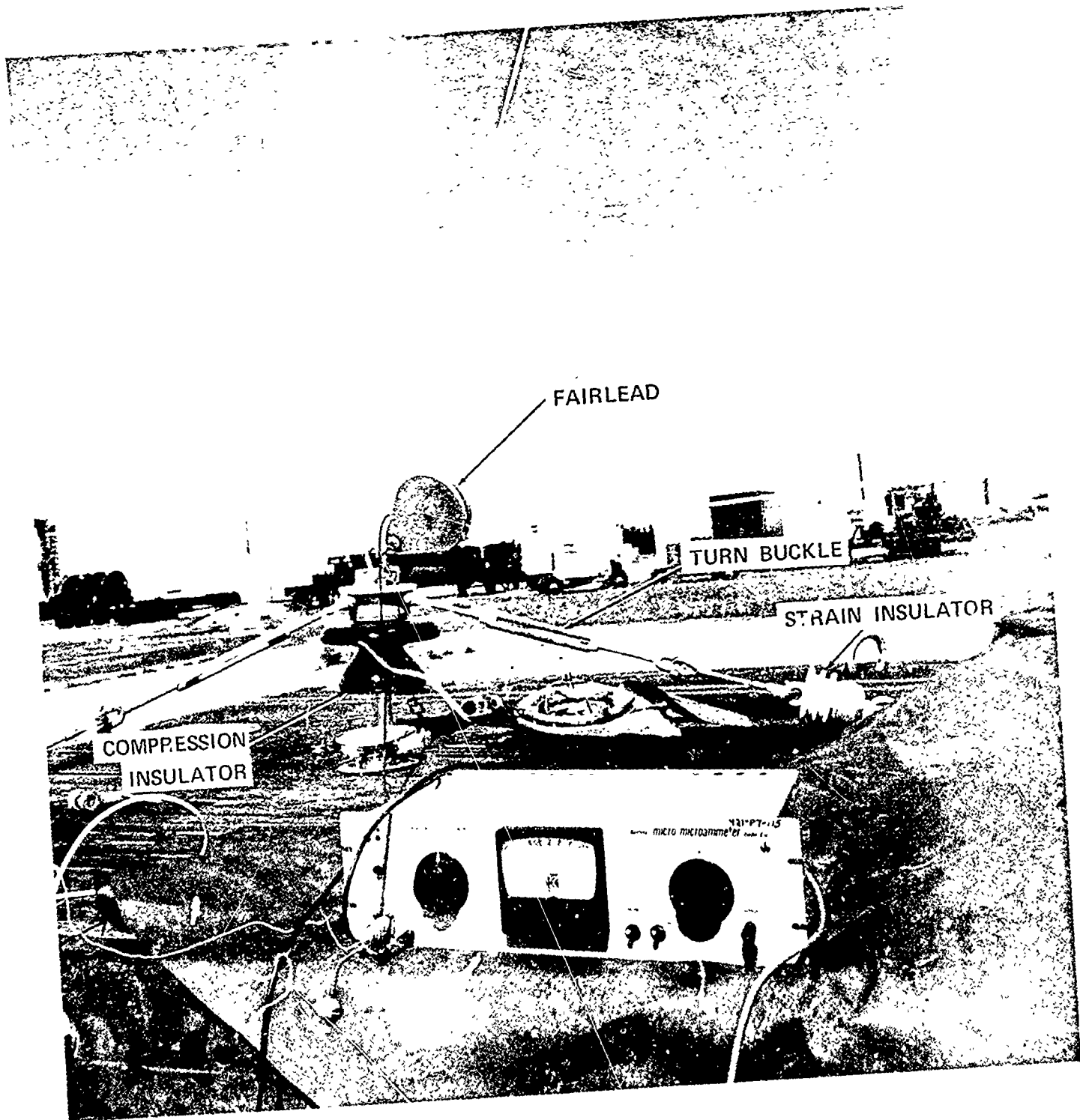
Figure A-6. Porcelain Strain Insulator Arrangement

This packaging permitted the winch to be well insulated from ground or connected to a ground stake as desired. One of the two winches was loaded with 1/8-inch steel wire rope, the other with 1/4-inch nylon rope. This dual winch system facilitated rapid changing of tether.

3.2.1 Tether Current Measurement

Tether current was measured by grounding the system through a picoammeter attached to the fair lead sheave. This arrangement is shown in figure A-6. When wire rope tether was used, the measurements were disturbed by low frequency noise. A passive filter having a response time of several seconds was used to integrate this noise. A picoammeter (Keithley Model 410) was used for these measurements. This type of meter has a recorder output. One of the control boxes was modified to permit connection of the recorder output to a spare wire in the data cable.

3.2.2 Transients From Distant Lightning

Current transients induced on the wire rope tether by distant lightning were detected using a current probe - Singer Model 91197-1. This is an RF current transformer which can be clipped around a conductor. The probe output was displayed on an oscilloscope and photographed, resulting in photographs such as figure 2-19.

3.2.3 Tether Potential

When a wire rope tether was used, it was possible to allow the winch to charge to the mean potential of the balloon - tether system by isolating the system from ground. Two instruments were

used for measuring this potential, 1) an electrostatic volt-
meter, and 2) a field mill.

When the electrostatic voltmeter was used, measurements obtained
were substantially lower than theoretical predictions. It was
assumed that wiring associated with the meter corrupted the
measurement. A more successful approach involving no electrical
connections consisted of a field mill measuring the potential
gradient below a horizontal conducting plane connected to the
underside of the winch (see figure A-7). The gradients created
were so large that the amplifiers associated with the mill were
not used. Instead a signal conditioner consisting of a rectifier
and filter was built. The system was calibrated by applying
known high voltages to the winch structure. At the conclusion of
the measurement, the system was discharged by throwing a grounded
chain across the winch mounting frame. In every case this de-
stroyed the output amplifier of the active filter, but did not
preclude the gathering of data at the cost of one 747 amplifier
per experiment. The cause of this damage was never precisely
determined but it was realized that a large field transient de-
tectable 500 feet away was created.

3.3 MEASUREMENT USING THE FAMILY II SYSTEM

The Family II winch was not designed for use with wire rope
tethers. Since the data gathered using the Baldy System was con-
sidered representative of the effects of larger balloon systems
with well-conducting tethers, it was decided not to subject the
Family II capstan and flying sheave to possible scoring by wire
rope. Two flights were flown however, using the 84,000 cu ft
BJ+3 balloon to lift the 1/8 inch wire rope while tethered with
0.625 Nolaro tether. The Nolaro tether was isolated from ground
by a porcelain strain insulator and current flowing in the wire

A-12

HORIZONTAL CONDUCTING PLANE
AT TETHER POTENTIAL

FIELD MILL

Figure A-7.   Tether Potential Measuring System

rope was measured using the picoammeter. These measurements and overhead measurements by the NASA aircraft indicated that considering differences in altitude, the Baldy system should give data representative of the larger balloons with conductive return. It was also evident from these tests that clean Nolaro was as effective an insulator as porcelain (for the purposes of these tests) and that no elaborate arrangements for system isolation would be necessary for measuring tether current when flying the Family II balloon system. The following technique was devised.

1) The tether jacket was cleaned for a distance of several feet above the flying sheave using methyl ethyl ketone (MEK), thereby creating a high resistance "isolation zone."

2) A connection to the tether was effected by wrapping aluminum foil around the uncleaned tether above the isolation zone. The ammeter lead was wrapped into the foil with the tether and the wrap secured by masking tape.

3) The ammeter was connected to an earth ground.

3.4   EQUIPMENT CALIBRATION

3.4.1   Field Mills

A special structure was assembled for calibration of the field mill installed in the deployable sensor box (figure A-8). This structure permitted the sensor box to be placed between two horizontal conducting planes 20 feet square and separated by 6 feet. A potential difference of 914 volts between the two planes provides a calibration input of 500 volts per meter. The field mill amplifier was then adjusted to provide an instrumen-

A-14

20 FT

6 FT

CONTROL BOX

VOLTMETER

HIGH VOLTAGE POWER SUPPLY
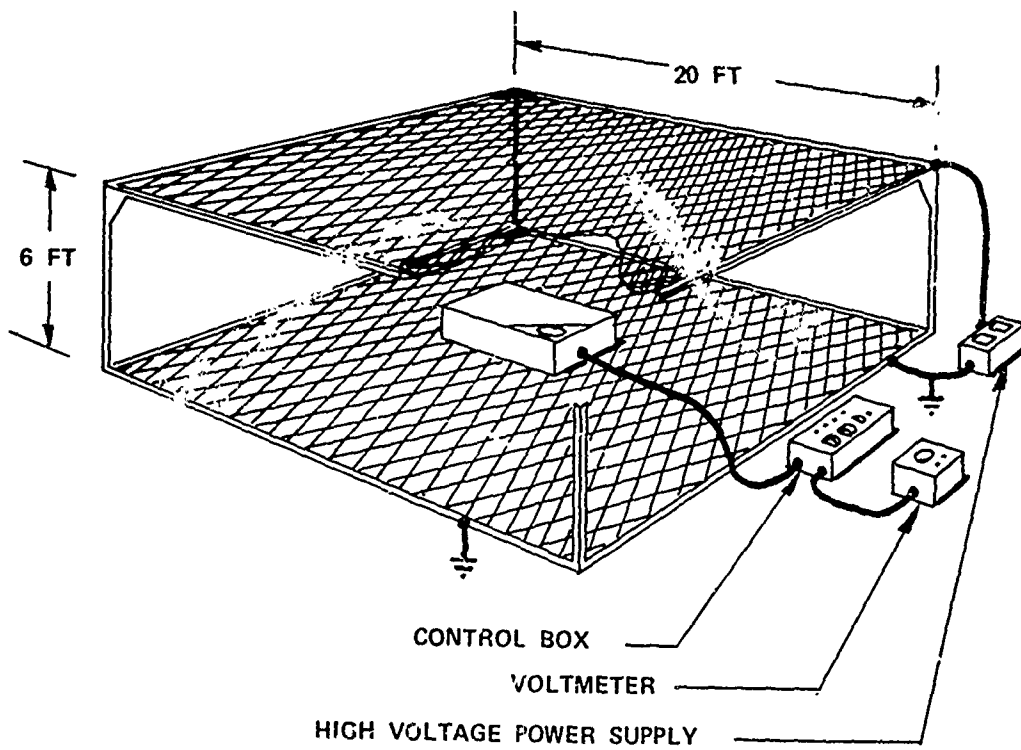
Figure A-8.   Field Mill Calibrator

tation output of -5 V dc and the meters on the control box wire
adjusted for the correct indication. The large dimension of the
structure reduced the effect of fringing. A portable calibrator
for field use consisted of a 20-inch square plate mounted on four
teflon posts, 10 cm high. An associated battery and switch per-
mitted potential gradients of ±365 V/m to be created immediately
above the field mill.

The large calibrator provided calibrations for form factor re-
sulting from the installation in the sensor box. The portable
calibrator was referenced to calibrations in the large calibra-
tor. However, there was no convenient way to determine site form
factor, because the boxes were frequently moved. An attempt was
made to qualitatively assess site differences by comparison of
readings on all systems before balloon ascent.

3.4.2   Air-to-Earth Current

Calibration of the air-to-earth current measuring system was
fixed based on precision of the components used. A one-time
calibration based on known inputs was performed prior to seal-
ing the amplifier units.

3.4.3   Recorder Calibration

Circuitry was included in the control box to place calibration
levels of +5 V dc, 0 and -5 V dc on the data lines for use in
calibrating the strip recorder channels used for E field, air-
to-earth current, and tether potential. After the recorder
channels had been calibrated, 3 point, E field calibrations were
made using the portable calibrator.

3.5   INSTRUMENTATION SCHEMATIC DIAGRAMS

Figures A-9 thru A-13 depict the schematic diagrams of the in-
strumentation discussed in this appendix.
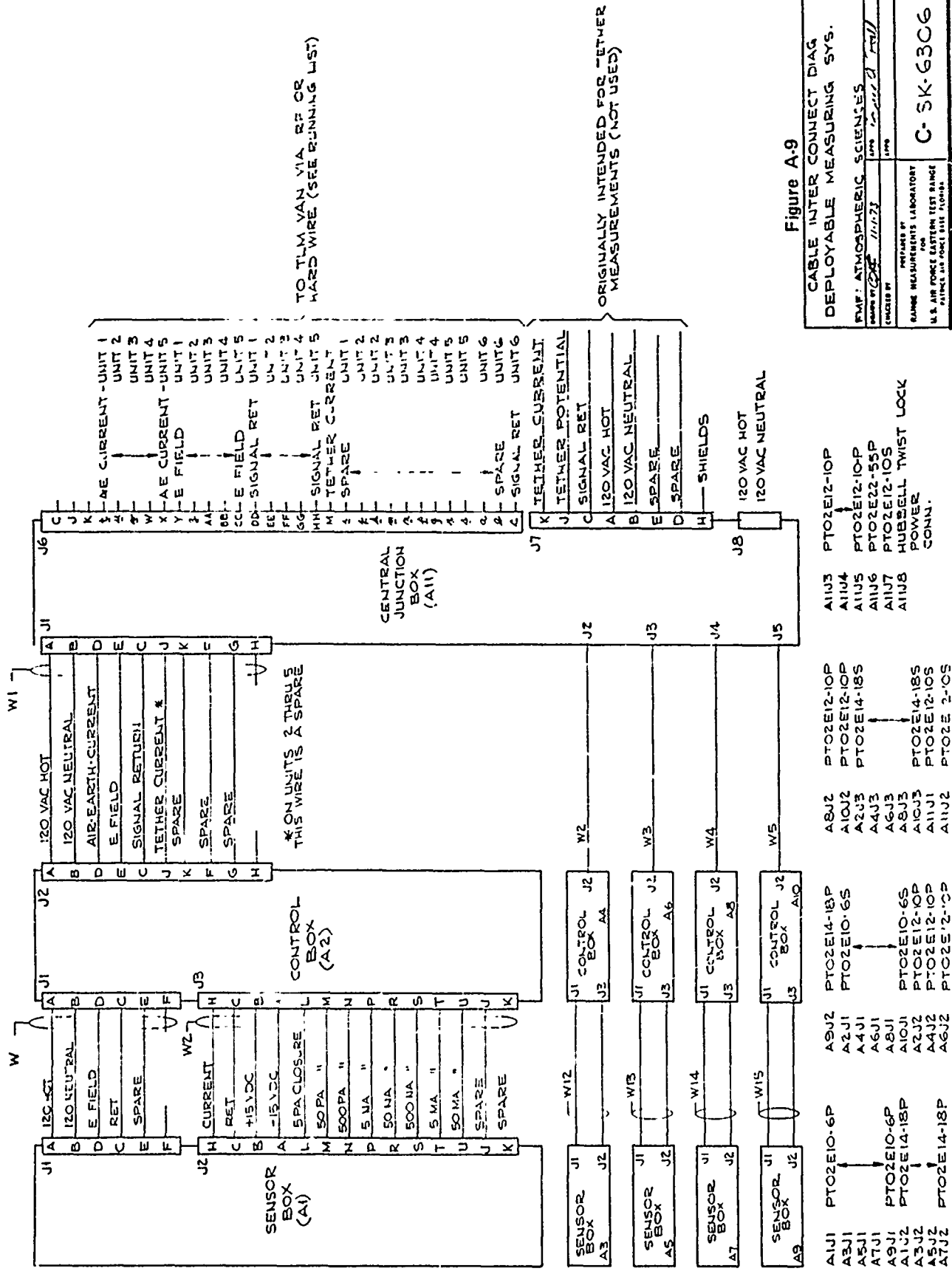
A-16

Figure A.9

CABLE INTER CONNECT DIAG
DEPLOYABLE MEASURING SYS.

C-SK-63C6

A-17

Figure A-10

WIRING DIAG- SENSOR BOX
DEPLOYABLE MEASURING SYS.
FMF: ATMOSPHERIC SCIENCES

A-18

Figure A-11
SCHEMATIC
CURRENT AMPLIFIER, (A1A1)

C-SK-RML-135

NOTES:
1. ALL WIRING INTERCONNECTING RELAYS, RESISTORS R1, R2 & R3, CAPACITORS C1 & C2 AND THE AMP—FET2 INPUT MUST BE TEFLON INSULATED TO INSURE THE PRESERVING OF HIGH INSULATION RESISTANCE.

2. INPUT WIRING FOR 5NA, 50NA, 500NA, 5MA & 50MA —AS BEEN DISCONNECTED BUT COMPONENTS ARE STILL MOUNTED.

* THESE COMPONENTS ARE MOUNTED ON STANDOFFS ON XA1.

A-19
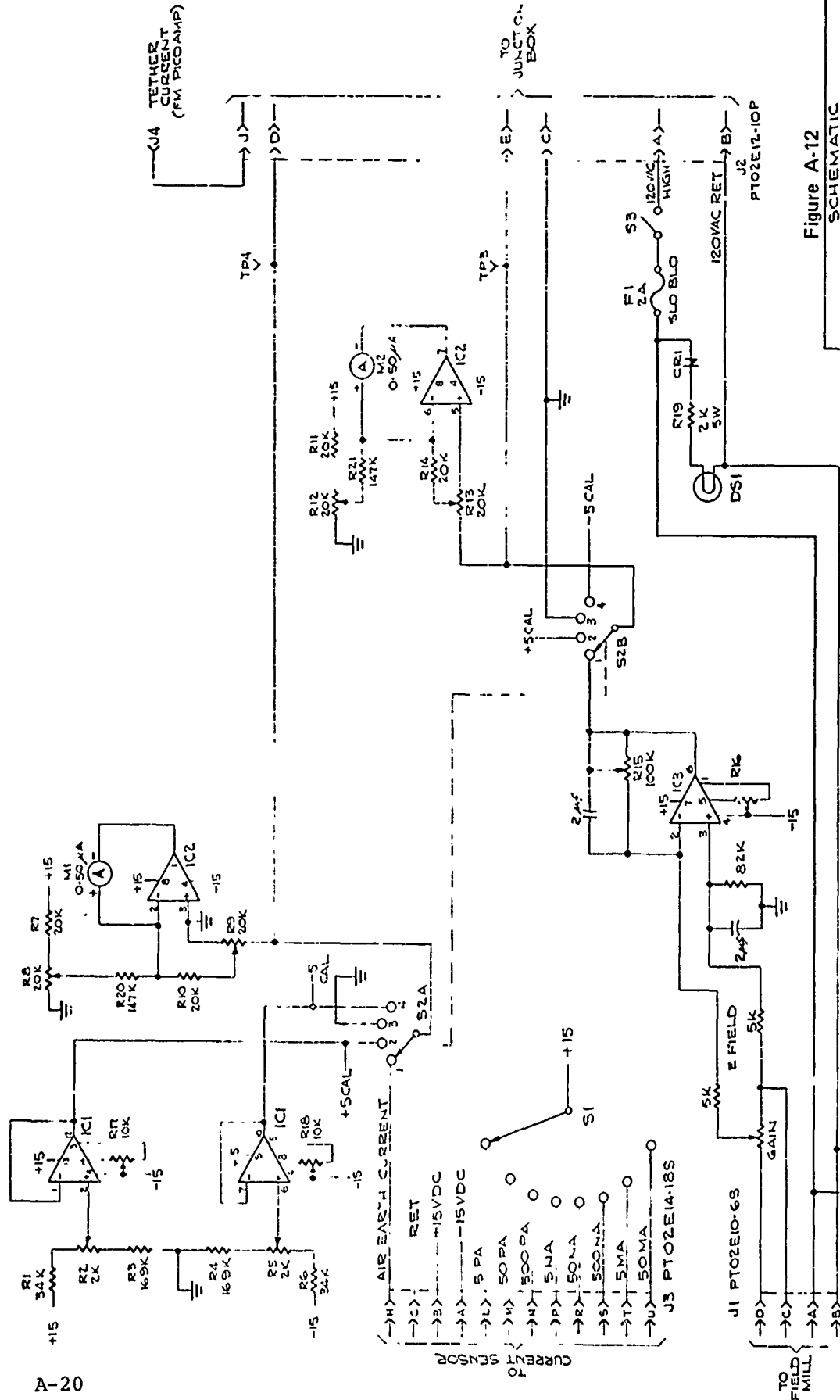
Figure A-12
SCHEMATIC
CONTROL BOX

A-20

CONTROL BOX (UNIT 5)

W15

SIG

SIG RET

-15 VDC

+15VDC

J2 PTO2E12-18P

C1 10µf

R7 100K

MC1485CG IC1

+15VDC

R5 100K

R6 10K

R4 50K

CR1 IN645

R3 500K

R2 500K

MC1485CG IC1

-15VDC

R1 1M

SIGNAL CONDITIONER

FIELD MILL #5

Figure A-13
SCHEMATIC
SIGNAL CONDITIONER FOR TETHER
POTENTIAL MEASUREMENT

FMF: ATMOSPHERIC SCIENCES

DRAWN BY 11-7-73

PREPARED BY
RANGE MEASUREMENTS LABORATORY
FOR
U. S. AIR FORCE EASTERN TEST RANGE
PATRICK AIR FORCE BASE FLORIDA

C-SK-6307

APPENDIX B

THE EFFECT OF A COASTAL ATMOSPHERE ON THE RESISTIVITY OF
JACKETED TETHER

1.0 INTRODUCTION

The tether rope used with TELTA balloons consist of a Dacron-
polyester strength member with a polyurethane jacket which per-
forms the dual functions of weatherproofing and containment of
the Dacron fibers which are arranged in no-lay construction.
Knowledge of tether resistance is of value for prediction of
charge transfer from earth to the balloon and for understanding
the propagation of a lightning flash down the tether. Handbooks
indicate that the tether when clean and dry should have a volume
resistivity comparable to that of air. Materials exposed to
coastal atmosphere acquire a thin film of salt, which can be ex-
pected to decrease resistivity. The experiments described here-
in were performed to determine the rate and degree to which the
resistivity of tether materials is decreased by salt accretion.

2.0 TEST DESCRIPTION

Wire spiral electrodes imbedded in metallic epoxy were moulded
to the end of the sample to effect an electrical connection to
the total cross section of the rope as shown in figure B-1. A
dummy plug approximately 1 inch long was made of epoxy termin-
ated at both ends to check junction resistance. Measured re-
sistance of the plug was 400 ohms.

Thirty samples were made from 0.775 diameter Nolaro. Six sam-
ples were made from 0.625 diameter Nolaro. Capacitance from
jacket to center was not measurable.

Polyurethane Jacket

Metalized Epoxy

Electrode

Dacron Polyester

a   Test Sample

R_j

R_c
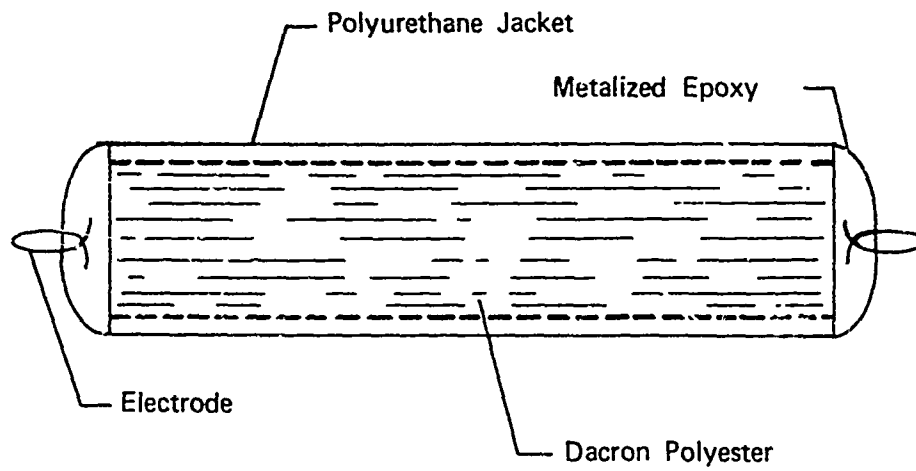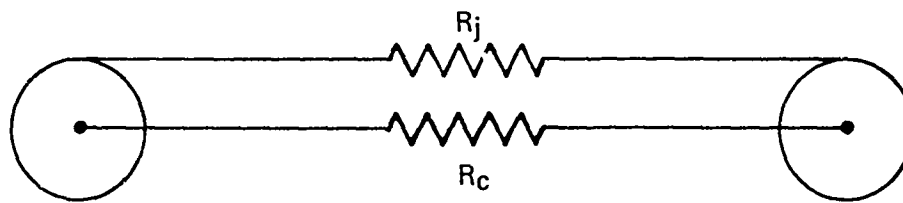
b   Equivalent Circuit

Figure B-1.   Test Sample for Tether Resistivity Measurement

The test samples were washed with Methyl-Ethyl-Ketone (MEK) and suspended at an elevation of approximately 6 feet. The resistance of each specimen was measured daily (except weekends) for two weeks. At the end of this period they were again washed with MEK and remeasured. The resistance behavior of the 36 samples fell into four sets, as shown in figure B-2.

Four samples (group 1) gradually decreased from an initial average resistivity of 2.6×10^{11} ohms/meter to a final value of 2.425×10^9. After washing, they recovered to 1.36×10^{11}, 68% of their original value. This recovery indicates that the resistance drop was a result of superficial contamination, which was removed by washing.

Seven samples (group 2) decreased rapidly from an initial average of 1.5×10^{11} ohms/meter to 6×10^7 in seven days and did not decrease any more. After washing, they recovered to 6.2×10^{10} ohms - about 42% of the initial value.

Eight samples (group 3) had initially low resistance (5×10^7 ohms) and only decreased to about half that value during the test period. The set recovered to approximately 80% after washing. This low resistance was believed to be a result of internal contamination by capillary action through the open end of the tether.

B-3

Figure B-2. NOLARO TETHER RESISTANCE CHANGE WITH EXPOSURE TO ATMOSPHERE CCAFS.
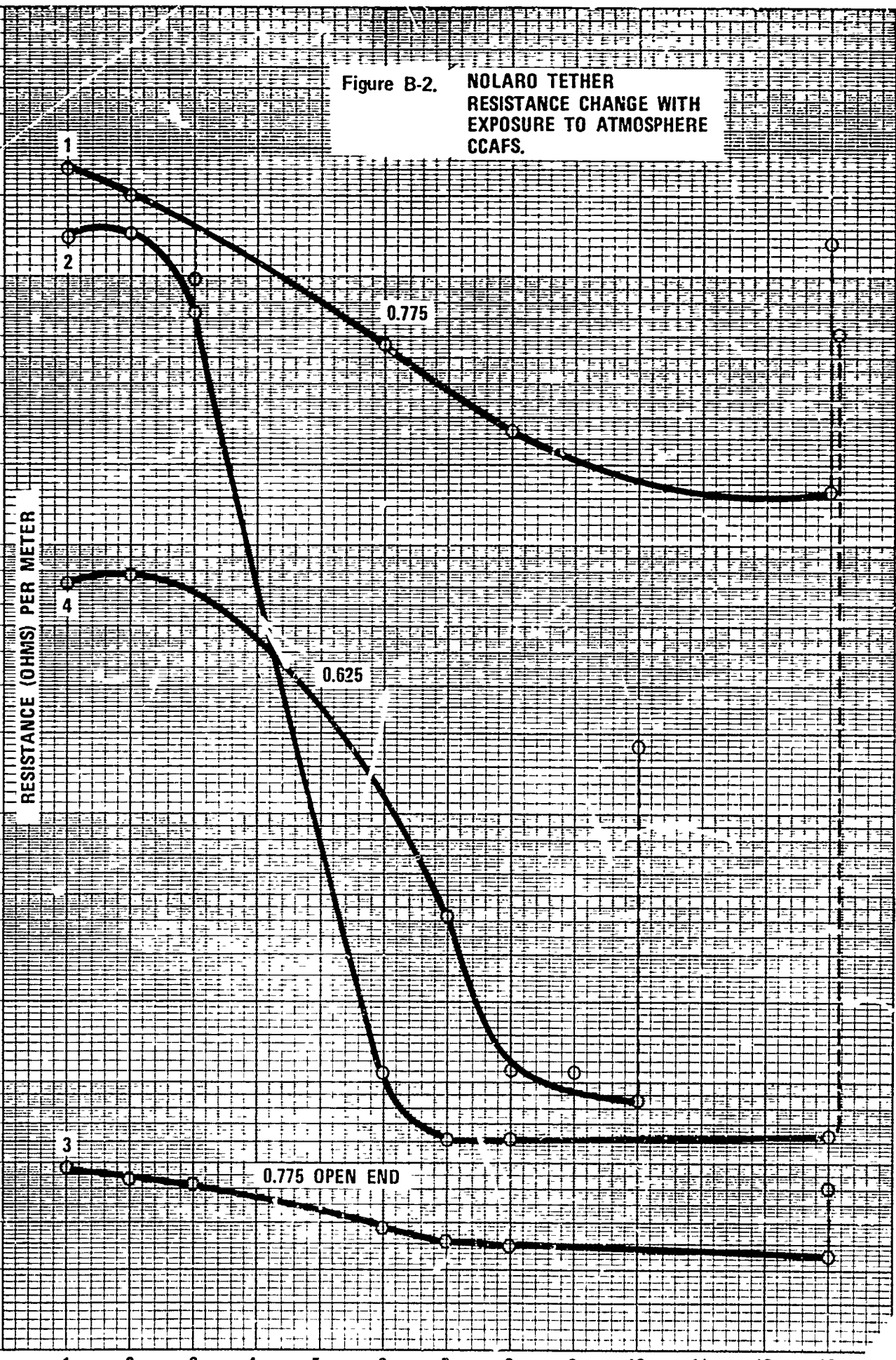
The neoprene jacket was removed from sample #26 on the 13th day, and resistance of the interior fiber portion (R_c) was found to be 5.0 megohms. From this value, and a measured value of 3.8 megohms for the total parallel resistance (R_t), the jacket resistance (R_j) was computed to be 15.8 megohms. Expressed as resistivity these are:

$$R_c = 3.3 \times 10^7 \text{ ohms/meter}$$

$$R_j = 1 \times 10^8 \text{ ohms/meter}$$

$$R_t = 2.5 \times 10^7 \text{ ohms/meter}$$

Note that R_j is near the final value of group 2, which did not experience internal contamination.

The measured values are specified in tables B-1 and B-2.

These measurements indicate that jacketed Nolaro tether exposed to a coastal atmosphere at sea level experiences a dramatic increase in conductivity during a period of several days. The extent to which conductivity at flight altitudes would be affected depends on the rate of diffusion and accretion of atmospheric salt.

3.0 DEPENDENCE OF SALT ACCRETION ON ALTITUDE

As discussed above, the RML experimentation provides a rate of resistance change resulting from salt and dust accretion at a single elevation near ground level and a single location. Other work which has been done indicates that the rate of salt accretion decreases with distance from the beach, not a surprising

result. According to a planning document prepared for NASA –
Marshal Space Flight Center (MSFC), [B-1], suspended particulate
matter in the air is uniformly distributed up to 200 meters and
also in altitude zones which are above 3,000 meters but below
the mixing level. In 1974, MSFC measured the rate of salt accre-
tion at various levels on the 160-meter weather instrumentation
tower at the Kennedy Space Center [B-2]. These measurements in-
dicated considerable variation with wind direction but little
correlatable dependence on altitude, at least up to the 180-
meter height of the tower. Since atmospheric salt originates
at sea level, its transport to higher altitudes is primarily a
result of atmospheric instability. It has therefore been sug-
gested that the distribution of airborne salt is probably uni-
form up to the mixing layer. The vertical distribution of
aphids, up to an altitude of 610 meters has been observed to
correlate with adiabatic lapse rate. The applicability of
aphids to this study is based on the fact that they are weak
fliers and tend to follow air currents [B-3].

As we attempt to predict the accumulation of salt on a balloon
tether, it must be realized the entire length of the tether will
not receive equal exposure time since the balloon may not always
operate at the same altitude. The fact that the upper portions
of the tether are exposed to air more than the lower portions
(which remain wound on the reel for low altitude flights) will
partially compensate for the fact that less salt accretion may
be expected at high altitudes. Rain will limit long term ac-
cumulation of salt on balloon tethers.

These measurements were all made with dry tether. However, a
thin film of salt crystals, having an affinity for water,
would become highly conductive when exposed to high humidity.
Under these circumstances, a Nolaro tether could have all of
the disadvantages and none of the advantages of a steel tether.

TABLE B-1. — TETHER RESISTANCE MEASUREMENTS, 0.625 NOLARO

Sample \ Days	1	2	7	8	9	10	After Cleaning
1*	1.5×10^9	1.8×10^9	1.5×10^8	5×10^7	5×10^7	3×10^7	8×10^8
2*	2.1×10^9	2×10^9	1.75×10^8	5×10^7	5×10^7	4×10^7	5.9×10^8
3*	1.9×10^9	2.2×10^9	1.2×10^8	3.4×10^7	3.2×10^7	3.2×10^7	5×10^8
1	2.3×10^9	2.8×10^9	1.05×10^8	2×10^7	2×10^7	1.6×10^7	6×10^8
2	1.8×10^9	2.2×10^9	1.4×10^8	3×10^7	2.8×10^7	2.6×10^7	4×10^8
3	3.5×10^9	3.5×10^9	9×10^7	2×10^7	1.9×10^7	1.5×10^7	5×10^8
AVG Ω	2.133×10^9	2.417×10^9	1.3×10^8	3.4×10^7	3.32×10^7	2.65×10^7	5.65×10^8
Ω/m	7.162×10^9	7.929×10^9	4.265×10^8	1.115×10^8	1.092×10^8	8.694×10^7	1.854×10^9

NOTE: 1 & 1* WERE CUT FROM OPPOSITE ENDS OF THE PIECE

TABLE B-2. — TETHER RESISTANCE MEASUREMENTS, 0.775 NOLARO

	Sample	Days	1	2	3	6	7	8	13	After Cleaning
HIGH	1	1	$3 \times 10^{10}\,\Omega$	2.8×10^{10}	1×10^{10}	7×10^{9}	3×10^{9}	3×10^{9}	3×10^{8}	2.4×10^{10}
	18		2×10^{10}	2×10^{10}	1.5×10^{10}	2.6×10^{9}	2.1×10^{9}	5×10^{8}	4×10^{8}	1.4×10^{10}
RESISTANCE	24		2.8×10^{10}	3×10^{10}	2×10^{10}	1×10^{10}	8×10^{9}	4×10^{9}	3×10^{9}	1.5×10^{10}
SLOW	27		8.0×10^{10}	5×10^{10}	1.8×10^{10}	1.5×10^{10}	1×10^{10}	9×10^{9}	6×10^{9}	2.075×10^{10}
DECAY	AVG Ω		3.95×10^{10}	3.2×10^{10}	1.575×10^{10}	8.65×10^{9}	5.775×10^{10}	4.125×10^{9}	2.425×10^{9}	2.075×10^{10}
	Sample Length		6"							
	AVG Ω/m		2.592×10^{11}	2.099×10^{11}	1.033×10^{11}	5.676×10^{10}	3.789×10^{10}	2.707×10^{10}	1.591×10^{10}	1.362×10^{11}
1 INTERMEDIATE	28		8.5×10^{9}	5×10^{9}	3.5×10^{9}	1×10^{9}	5×10^{8}	5×10^{5}	5×10^{5}	2×10^{9}
HIGH	2		2×10^{10}	2×10^{10}	1×10^{10}	2.5×10^{6}	5×10^{5}	5×10^{5}	5×10^{5}	1.2×10^{9}
RESISTANCE	3		1.25×10^{10}	1.4×10^{10}	8×10^{9}	2×10^{6}	2×10^{6}	1.8×10^{6}	1.6×10^{6}	8×10^{9}
FAST	8		4×10^{10}	4×10^{10}	1.5×10^{10}	5×10^{7}	5×10^{7}	5×10^{7}	4.5×10^{7}	1.2×10^{10}
DECAY	14		1×10^{10}	1×10^{10}	8×10^{9}	5×10^{7}	2.8×10^{6}	2.4×10^{6}	2.4×10^{6}	4×10^{9}
	16		1.5×10^{10}	1.6×10^{10}	1.3×10^{10}	2×10^{6}	1.7×10^{6}	1.6×10^{6}	Dissected	
	17		3×10^{10}	3×10^{10}	8.5×10^{9}	5×10^{6}	5×10^{6}	5×10^{6}	4.6×10^{6}	1.4×10^{10}
	19		2.5×10^{10}	2.6×10^{10}	1.7×10^{10}	5×10^{6}	5×10^{6}	5×10^{6}	4.9×10^{6}	1.8×10^{10}
	AVG Ω		2.18×10^{10}	2.23×10^{10}	1.135×10^{10}	1.664×10^{7}	9.57×10^{6}	9.471×10^{6}	9.83×10^{6}	9.53×10^{9}
	Ω/m		1.430×10^{11}	1.463×10^{11}	7.448×10^{10}	1.092×10^{8}	6.234×10^{7}	6.215×10^{7}	6.450×10^{7}	6.253×10^{10}

TABLE B-2. — TETHER RESISTANCE MEASUREMENTS, 0.775 NOLARO (CONTD)

Sample \ Days	1	2	3	6	7	8	13	After Cleaning
4	$3 \times 10^6 \Omega$	3.8×10^6	3.8×10^6	3.8×10^6	3.8×10^6	3.8×10^6	3.8×10^6	3.9×10^6
5 (LOW RESISTANCE SET)	1.5×10^7	1×10^7	1×10^7	1×10^6	1×10^6	8×10^6	8×10^5	8×10^6
6	1.1×10^7	1.3×10^7	8.5×10^6	5×10^6	5×10^6	4.8×10^6	4.8×10^6	9×10^6
7	2.5×10^6	2.5×10^6	2.3×10^6	2.3×10^6	2.3×10^6	2.3×10^6	2.3×10^6	2.5×10^6
9	1.4×10^6	1.4×10^6	1.3×10^6	1.3×10^6	1.1×10^6	1.2×10^6	1.2×10^6	1.3×10^6
10	1.8×10^6	1.8×10^7	1.5×10^7	3.5×10^6	3.5×10^6	3.5×10^6	3×10^6	1.3×10^7
11	3×10^6	3.2×10^6	2.9×10^6	2.8×10^6	2×10^6	2×10^6	1.9×10^6	3.5×10^6
12	9×10^6	1×10^7	1×10^7	9×10^6	1×10^7	9×10^6	1×10^7	8×10^6
13	3×10^6	2.9×10^6	3×10^6	3×10^6	3×10^6	3×10^6	3×10^6	2.8×10^6
15	2×10^7	2×10^7	1.9×10^7	2.6×10^6	2×10^6	1.8×10^6	1.8×10^6	1.4×10^7
20	2.8×10^6	2.8×10^6	2.6×10^6	2.6×10^6	2.6×10^6	2.6×10^6	2.2×10^6	3×10^6
21	1.8×10^6	1.8×10^6	1.2×10^6	1×10^6	1×10^6	1×10^6	1×10^5	2×10^6
22	2.4×10^7	1.8×10^7	1.5×10^7	1×10^7	5×10^6	4×10^6	5×10^5	1.2×10^7
23	1.6×10^6	1.6×10^6	8×10^5	7×10^5	8×10^5	8×10^5	7×10^5	1.8×10^6
25	1.5×10^7	1.5×10^7	2×10^7	2×10^7	2×10^7	2×10^7	1.8×10^7	1.7×10^7
26	4×10^6	4×10^6	4×10^6	3.8×10^6	3.8×10^6	3.8×10^6	3.8×10^6	Dissected
29	3×10^6	2.8×10^6	2.5×10^6	2.5×10^6	2.5×10^6	2.5×10^6	1.5×10^6	3.1×10^6
30	3×10^6	3.2×10^6	2.9×10^6	2.4×10^6	2.4×10^6	2.3×10^6	2.3×10^6	4×10^6
AVG Ω	7.83×10^6	7.44×10^6	6.93×10^6	4.37×10^6	3.99×10^6	3.86×10^6	3.43×10^6	6.41×10^6
Ω/m	4.849×10^7	4.304×10^7	4.193×10^7	2.867×10^7	2.618×10^7	2.533×10^7	2.25×10^7	4.206×10^7

References:

[B-1]   Daniels, Glen E. "Terrestrial Environment (Climatic)
        Criteria Guidelines for use in Space Vehicle Development,"
        1964 Revision NASA, TM53872. NASA/MSFC

[B-2]   Williamson, E. L. "Local Atmosphere Salt Profile," Shuttle
        Study Task No 31, 8 July 1974, NASA/KSC

[B-3]   Johnson, C. G. "The Vertical Distribution of Aphids in
        the Air and the Temperature Lapse Rate."

APPENDIX C

TRANSIENT SKIN EFFECT

The concept of skin depth as normally encountered applies to
conductors excited by steady state alternating current. Solu-
tions for the transient case are rarely encountered. However,
M. G. Haines has solved the diffusion equations for several
forcing functions including the overdamped exponential pulse
by which we model the high current lightning transient [28].
This model is formulated as follows:

Given a high current transient:

$$i(t) = I_o(e^{-d^1 t} - e^{-\beta^1 t}) \tag{C-1}$$

The current density at a radial distance r from the center of
the conductor, at some time t is given by:

$$i_z(X,Y) = \frac{e^{-\alpha y} \sqrt{\alpha} \, J_o(\sqrt{\alpha}\, x)}{2\pi a^2 J_1(\sqrt{\alpha})} - \frac{e^{-\beta y} \sqrt{\beta} \, J_o(\sqrt{\beta}\, x)}{2\pi a^2 J_1(\sqrt{\beta})}$$

$$- \sum_{n=1}^{\infty} \frac{\exp(-\gamma_n^2 y)\gamma_n^2 J_o(\gamma_n x)}{\pi a^2 J_o(\gamma_n)} \left[\frac{1}{\alpha - \gamma_n^2} - \frac{1}{\beta - \gamma_n^2} \right] \tag{C-2}$$

where:

i_z (X, Y) is the instantaneous current density, directed along
the longitudinal axis of the conductor, normalized to I_o

a is the radius of the conductor

μ is the permeability of the material

ρ is the resistivity of the material

J_o and J_1 denote Bessel functions (first kind) of order zero and one respectively.

γ_n denotes the n th zero of $J_1 (\gamma)$

$X = \dfrac{r}{a}$ is normalized distance from the center of the conductor

$\tau = \dfrac{\mu a^2}{\rho}$ is the diffusion time as defined in section 4-4.

$g = \dfrac{t}{\tau}$ is normalized time

$\alpha = \alpha^1 \tau$

$\beta = \beta^1 \tau$

α^1 and β^1 as used in equation (C-1) are identical to α and β as used in (4-1) and elsewhere in the main text.

The significance of the three terms of (C-2) may be summarized as follows: The term containing $e^{-\alpha y}$ is effective until the pulse has decayed and therefore resembles a steady state effect. The term containing $e^{-\beta x}$ is due to the rise time of the pulse and quickly decays. The infinite summation is a statement of the transient effects. As long as this term is dominant, most of the current is confined to the outside of the conductor. This term has time constant $\dfrac{\tau}{\gamma_1^2}$ where $\gamma_1 = 3.83$.

C-2

If $\alpha^1 < \dfrac{\gamma_1^{\,2}}{\tau}$ then the term containing $e^{-\alpha y}$ is dominant. Conversely if $\alpha^1 > \dfrac{\gamma_1^{\,2}}{\tau}$ the term containing $e^{-\gamma_n^{\,2} y}$ (transient effects) is dominant. In either case, an inverse skin effect develops after sufficient time has passed, and the current density at the center of the conductor will exceed that at the surface. Haines attributes this to the development of a back EMF near the surface of the conductor as the pulse decays.

If $\alpha^1 > \dfrac{\xi_1}{\tau}$ where $\xi_1 = 2.4048$

is the first zero of J_o, then the polarity of current density in the outer portion of the conductor will be reversed; after sufficient elapsed time the current reversal will occur for radius greater than $r = \dfrac{\xi_1 a}{\gamma_1} \approx 0.63a$

A computer program was written to evaluate equation (C-2) and applied to examples using a typical lightning pulse and physical parameters for stainless steel (type 304) and carbon steel (Monitor AA). Results obtained were consistent with the principles stated above and are plotted in Figure 4-15. Parameters useful for interpretation of these examples are given in Table C-1. The computer program is included in this appendix.

TABLE C-1

Parameters used for computation of transient skin effect in stainless steel and carbon steel

	Stainless Steel	Carbon Steel
Peak Current (I_o)	2.1×10^4	2.1×10^4
	1.7×10^4	1.7×10^4
	3.5×10^6	3.5×10^6
a (mm)	4.76	4.76
	1	100
ρ (microohm/cm)	7.2×10^{-7}	2.08×10^{-7}
τ (seconds)	39.5×10^{-6}	13.67×10^{-3}
	3.72×10^{-6}	1074
	1.46×10^{-6}	423
Dominant term:	steady state	transient

FORTRAN names used in computer program:

AP	α'
BP	β'
A	α
B	β
FIO	I_o
FMUR	μ_r
RHO	ρ
RAD	a
TAU	τ
G(K)	γ_n
FIZ (IR, IT)	i_z (x, y)
FIA (IT)	Mean current - driving current divided by cross-section area

```
1.     C       DIFFUSION OF LIGHTNING CURRENT INTO A
2.     C       CYLINDRICAL CONDUCTOR.  THE LIGHTNING IS MODELED
3.     C       AS AN OVERDAMPED EXPONENTIAL PULSE OF THE FORM:
4.     C       I(T) = IC*(EXP(-AP*T)-EXP(-BP*T))
5.     C       THIS MODEL INCORPORATES THE EFFECT OF INVERSE
6.     C       SKIN EFFECT - REF:  M.G. HAINES, 'THE INVERSE
7.     C       SKIN EFFECT, PROC. PHYS. SOC.,V75,PT5,576-85(1959)
8.             DIMENSION G(99),R(6),T(101),FIZ(6,101),FIA(101)
9.            1,XPLT(707),YPLT(707),IPLOT(8)
10.            DIMENSION FI1(6,101),FI2(6,101),FIT(6,101)
11.            PI=3.141592654
12.            READ(105,10) AP,BP,FIO
13.            READ (105,10) FMUR,RHO,RAD
14.            OUTPUT AP,BP,FIO
15.            OUTPUT FMUR,RHO,RAD
16.            READ(105,15) KMX,NR,NT,TMAX
17.            OUTPUT KMX
18.         10 FORMAT(3(10X,E10.7))
19.         15 FORMAT(3(5X,I5),5X,E10.7)
20.            DELT=TMAX/FLOAT(NT-1)
21.            DELR=RAD/FLOAT(NR-1)
22.            FMU=FMUR*(4.*PI*(1.E-7))
23.            TAU=FMU*(RAD**2)/RHO
24.            WRITE (108,17) FMU,RHO,RAD
25.         17 FORMAT('0','PERMEABILITY = ',1PE10.3,'DENSITY = ',
26.           11PE10.3,'RADIUS = ',1PE10.3)
27.     C       CROSS SECTION IN SQ MILLIMETERS
28.            AREA=PI*(RAD**2)*1.E6
29.            A=AP*TAU
30.            B=BP*TAU
31.            OUTPUT A,B
32.            WRITE(108,20) TAU
33.         20 FORMAT('0',10X,'DIFFUSION TIME = ',E10.4)
34.            A1=SQRT(A)
35.            B1=SQRT(B)
36.            CALL BESLJ(A1,1,FJ1A,.0001,IE)
37.            CALL BESLJ(B1,1,FJ1B,.0001,IE)
38.            A2=A1/(FJ1A*2.*AREA)
39.            B2=B1/(FJ1B*2.*AREA)
40.     C       COMPUTE ZERO'S OF J1
41.            DO 30 K=1,KMX
42.            S=FLOAT(K)+.25
43.         30 G(K)=S *PI-3./(8.*S *PI)+9./(384.*((S**3)*(PI**3)))
44.            DO 90 IT=1,NT
45.            T(IT)=DELT*(IT-1)
46.         90 FIA(IT)=FIO*(EXP(-AP*T(IT))-EXP(-BP*T(IT)))/AREA
47.            DO 101 IR=1,NR
48.            R(IR)=DELR*(IR-1)
49.            X=R(IR)/RAD
50.            A1X=X*A1
51.            B1X=X*B1
52.            CALL BESLJ(A1X,0,FJOA,.0001,IE)
```

```
53.          CALL BESLJ(B1X,0,FJOB,.0001,IE)
54.          FIZ(IR,1)=0.
55.          DO 100 IT=2,NT
56.          Y=T(IT)/TAU
57.    C     NOTE:  THE SUMMATION TERM CONVERGES VERY SLOWLY
58.    C     FOR SMALL X AND BECOMES INSIGNIFICANT FOR LARGE X.
59.    C     THE LIMIT KM IS TAPERED TO AVOID UNNECESSARY ITERATIONS.
60.          SUM=C.
61.          KM=(1.+FLOAT(KMX)*EXP(-5.*Y))
62.          DO 99 K=1,KM
63.          GX=X*G(K)
64.          CALL BESLJ(G(K),C,FJOG,.0001,IE)
65.          CALL BESLJ(GX,0,FJOGX, .0001,IE)
66.      99 SUM=SUM+FJOGX*(G(K)**2)*EXP(-Y*(G(K)**2))*
67.        1(1./(A-G(K)**2)-1./(B-G(K)**2))/(AREA*FJOG)
68.          FI1(IR,IT)=A2*FJOA*EXP(-A*Y)*FIO
69.          FI2(IR,IT)=B2*FJOB*EXP(-B*Y)*FIO
70.          FIT(IR,IT)=SUM*FIC
71.      100 FIZ(IR,IT)=(A2*FJOA*EXP(-A*Y)-B2*FJOB*EXP(-B*Y)-SUM)*FIO
72.      101 CONTINUE
73.          WRITE(108,105)
74.      105 FORMAT('1',7X,'TIME',9X,'AVERAGE'10X,'CURRENT DENSITY')
75.          WRITE (108,106) (R(IR),IR=1,NR)
76.      106 FORMAT(21X,'CURRENT',3X,3(7X,'R=',F6.5),/)
77.          DO 110 IT=1,NT
78.          WRITE(108,109) T(IT),FIA(IT),(FIZ(IR,IT),IR=1,NR)
79.      109 FORMAT(8(5X,1PE10.3))
80.          N=NR+1
81.      110 CONTINUE
82.          STOP
83.          END
```

```
 1.          SUBROUTINE BESLJ(X,N,BJ,D,IER)
 2.    C     TO HANDLE X=0 FOR BESL1
 3.          IF (X) 10,11,10
 4.       10 CONTINUE
 5.          CALL BESL1(X,N,BJ,D,IER)
 6.          RETURN
 7.       11 IF (N) 10,12,13
 8.       12 BJ=1.
 9.          RETURN
10.       13 BJ=0.
11.          RETURN
12.          END
```

```fortran
         SUBROUTINE BESL1   (X,N,BJ,D,IER)
1.
2.       BJ=.C                                            11100080
3.       IF(N)10,20,20                                    11100090
4.    10 IER=1                                            11100100
5.       RETURN                                           11100110
6.    20 IF(X)30,30,31                                    11100120
7.    30 IER=2                                            11100130
8.       RETURN                                           11100140
9.    31 IF(X-15.)32,32,34                                11100150
10.   32 NTEST=20.+10.*X-X** 2/3                          11100160
11.      GO TO 36                                         11100170
12.   34 NTEST=90.+X/2.                                   11100180
13.   36 IF(N-NTEST)40,38,38                              11100190
14.   38 IER=4                                            11100200
15.      RETURN                                           11100210
16.   40 IER=0                                            11100220
17.      N1=N+1                                           11100230
18.      BPREV=.0                                         11100240
19.      IF(X-5.)50,60,60                                 11100250
20.   50 MA=X+6.                                          11100260
21.      GO TO 70                                         11100270
22.   60 MA=1.4*X+60./X                                   11100280
23.   70 MB=N+IFIX(X)/4+2                                 11100290
24.      MZERO=MAXO(MA,MB)                                11100300
25.      MMAX=NTEST                                       11100310
26.  100 DO 190 M=MZERO,MMAX,3                            11100320
27.      FM1=1.0E-28                                      11100330
28.      FM=.C                                            11100340
29.      ALPHA=.0                                         11100350
30.      IF(M-(M/2)*2)120,110,120                         11100360
31.  110 JT=-1                                            11100370
32.      GO TO 130                                        11100380
33.  120 JT=1                                             11100390
34.  130 M2=M-2                                           11100400
35.      DO 160 K=1,M2                                    11100410
36.      MK=M-K                                           11100420
37.      BMK=2.*FLOAT(MK)*FM1/X-FM                        11100430
38.      FM=FM1                                           11100440
39.      FM1=BMK                                          11100450
40.      IF(MK-N-1)150,140,150                            11100460
41.  140 BJ=BMK                                           11100470
42.  150 JT=-JT                                           11100480
43.      S=1+JT                                           11100490
44.  160 ALPHA=ALPHA+BMK*S                                11100500
45.      BMK=2.*FM1/X-FM                                  11100510
46.      IF(N)180,170,180                                 11100520
47.  170 BJ=BMK                                           11100530
48.  180 ALPHA=ALPHA+BMK                                  11100540
49.      BJ=BJ/ALPHA                                      11100550
50.      IF(ABS(BJ-BPREV)-ABS(D*BJ))200,200,190          11100560
51.  190 BPREV=BJ                                         11100570
52.      IER=3                                            11100580
53.  200 RETURN                                           11100590
54.      END                                              11100600
```

APPENDIX D

TRANSIENT HEAT FLOW

Consider a long metal cylinder of radius s, initially at some uniform temperature T_i. At some time $\tau = \tau_o$ the temperature is instantaneously raised to a value T_s. The instantaneous temperature at time τ and radius r is given by Jakob, [32].

$$T(\tau,r) = T_s + (T_i - T_s) \sum_{\gamma=1}^{\gamma=\infty} 2 \exp \frac{-\frac{\beta_\gamma^2 \alpha\tau}{s^2} J_o(\beta_\gamma \frac{r}{s})}{\beta_\gamma J_1(\beta_\gamma)} \qquad (D-1)$$

where J_o, J_1, respectively represent Bessel functions of order zero and one β_γ is the γ th zero of $J_o(\beta)$

α is the thermal diffusivity of the material as defined below. Note the resemblance of (D-1) to the transient portion of (C-2). Both are forms of the diffusion equation. (D-1) is the theoretical basis of figure 4-18.

α, the thermal diffusivity of the material is given by:

$$\alpha = \frac{K}{\rho C_p} \qquad (D-2)$$

where K, ρ and C_p are, respectively, the thermal conductivity, density and specific heat of the material. Values of these parameters for the materials of interest are:

	Stainless Steel	Carbon Steel	Units (KMS)
Thermal conductivity (K)	16.29	50.3	watts/(m² K°)
Density (ρ)	8027	7833	kg/m³

D-1

		Stainless Steel	Carbon Steel	Units (KMS)
Specific heat (C_p)		502	460	$J/(kg\,K^O)$
Thermal diffusivity	(α)	4.04×10^{-6}	13.95×10^{-6}	m^2/sec

Now assume that at a depth of penetration x, sufficiently small, the surface of the cylinder can be approximated as a plane. For this case the temperature at a depth x is given by

$$T = T_s + (T_i - T_s)\, F\, \frac{x}{2\sqrt{\alpha\tau}} \tag{D-3}$$

where $F(x/2\sqrt{\alpha\tau})$ is the gaussian error integral of argument $x/2\sqrt{\alpha\tau}$.

We have confined our interest to a value in which the mean temperature is such that $(T - T_s) = 0.9(T_i - T_s)$ in which case

$$F\, \frac{x}{2\sqrt{\alpha\tau}} = \frac{T - T_s}{T_i - T_s} = 0.9 \tag{D-4}$$

For this value of F,

$$\frac{x}{2\sqrt{\alpha\tau}} = 1.2 \tag{D-5}$$

Our depth of penetration "δ_p" is the mean value of x for which equation D-3 obtains.

$$\delta_p = \bar{x} = \frac{1}{\tau} \int_0^\tau 2.4\,\sqrt{\alpha\tau}\; d\tau \tag{D-6}$$

$$\delta_p = 1.6\,\sqrt{\alpha\tau} \tag{D-7}$$

For type 304 stainless steel

$$\delta_p = 3.2\,\sqrt{\tau}\;\; \text{mm} \tag{D-8}$$

and for carbon steel (Monitor AA)

$$\delta_p = 5.97\,\sqrt{\tau}\;\; \text{mm} \tag{D-9}$$

APPENDIX E

BIBLIOGRAPHY

[1]   Moore, C. B., Lightning Around Elevated Structures," Paper
        presented to the 1972 Lightning and Static Electricity
        Conference, Air Force Systems Command (1972).

[2]   Chalmers, J. A. and Mapelson, W. W., "Point Discharge Cur-
        rents from a Captive Ballon," J.A.T.P. 6 149 (1955).

[3]   Davis, R. and Standring, W. G., "Discharge Currents Asso-
        ciated with Kite Balloons," Proc. Roy. Soc. Vol. 191A, pp.
        304-322 (1947).

[4]   Vonnegut, B., Markson, R. and Moore, C. B., "Direct Mea-
        surement of Potential Vertical Differences in the Lower
        Atmosphere," J.G.R., Vol 78, No. 21, pp. 4526-28, (1973).

[5]   Cianos, N. and Pierce, E.T., "A Ground Lightning Environ-
        ment for Engineering Usage," Technical Report 1, prepared
        for McDonnel-Douglas Astronautics Company under Contract
        LS-2817-A3, SRI Project 1834, Stanford Research Institute,
        Menlo Park CA. (1972).

[6]   ibid., p.8

[7]   ibid., p. 13

[8]   ibid., p. 20

[9]   Pierce, E.T."Triggered Lightning and Some Unexpected Light-
        ning Hazards," American Association for the Advancement
        of Science, 138th Annual Meeting, Philadelphia (1971).

[10]   Pierce, E.T. "Triggered Lightning and its Application to
        Rockets and Aircraft," proceedings of 1972 Lightning and
        Static Electricity Conference, Air Force Systems Command
        pp.80-188 (1972).

[11]   Cianos and Pierce, op.cit., p. 21.

[12]   Horvath, T., Contribution to International Conference on
        Lightning, see Golde, R. H., "Lightning Protection,"
        p-42, Arnold, London (1973).

[13]   Pierce, E. T., "Atmospheric Electricity "...some themes,"
        Paper presented to the 54th meeting of the American Mete-
        orological Society in Honolulu, Hawaii (1974).

[14]   Hatakeyma, H., "The Distribution of the Sudden Charge of
         Electric Field On Earth Surface Due to Lightning Discharge,"
         Recent Advances in Atmospheric Electricity, L. G. Smith
         (ed), Pergamon Press, N.Y. pp. 289-298 (1958).

[15]   Hodkinson, J., "A Lightning Discharge To A Captive Balloon
         at Cardington", Meteorological Magazine (Great Britian),
         Vol 91, No. 1081, p. 230 (1962).

[16]   Telephone conversation, Mr. James Payne, Air Force
         Cambridge Research Laboratory, Hanscom AFB Mass., and
         Toxey A. Hall, PAFB, FL. (1973).

[17]   · Uman, Martin A., "Comparison of Lightning and a Long Lab-
         oratory Spark," Proc. IEEE, Vol 59, No 4, pp. 457-66 (1970).

[18]   Uman, Martin A., "Spark Simulation of Natural Lightning"
         Air Force Avionics Laboratory - SAE Committee AE-4 on Elec-
         tromagnetic Compatibility (1972).

[19]   Stahman, J. R., "Investigation Report, Lightning Strike
         To A Tethered Balloon," Lightning and Transient Research
         Institute (1972).

[20]   Hoots, L. C.,Amason, M. P. and Cossell, G. J. "Comparative
         Evaluation of a new Radome Lightning Protective System,"
         Lightning and Static Electricity Conference (1972).

[21]   Correspondence, Keith L. Orser, Manager, Research and
         Development, Columbia Rope Company, Auburn, N. Y. to Toxey
         A. Hall (March 20, 1972).

[22]   Correspondence, Keith L. Orser, Columbia Rope Company, to
         Toxey A. Hall (1974).

[23]   Stahman, J. R., "Lightning Survivability of Tethered Bal-
         loon Cables," Lightning and Transient Research Institute
         (1969).

[24]   Cianos & Pierce, op cit., p. 53-55.

[25]   ibid. p. 25-29.

[26]   Uman, M. A., Lightning, Chapter 4, McGraw - Hill (1969).

[27]   Uman, M. A. and Mclain, D.K., "Lightning Criteria
         Relative to Space Shuttle Current and Electric Field
         Intensity In Florida Lightning," NASA Contractor Report
         CR 2161 (1972).

[28]   Haines, M. G., "The Inverse Skin Effect," Proc. Phys.
         Soc., Vol 75, pp. 5, 576-84 (1959).

[29]   Vance, E. F., "Prediction Of Transient In Buried Shielded
         Cables," interim technical report covering the period
         1 Jan to 1 Mar 1973, Stanford Research Institute,
         Menlo Park CA., p. 28 (1973).

[30]   ibid. p. 29

[31]   Correspondence, Martin A. Uman to Toxey A. Hall (1974).

[32]   Jacob, M., Heat Transfer, Volume I, John Wiley & Sons,
         Inc., p. 269 (1949).

[33]   Cianos and Pierce, op. cit. p. 91.

[34]   Brochure, "Well Measuring Line, Change of Mechanical
         Properties With Elevated Temperatures," U.S. Steel Corp.,
         New Haven, Conn.

[35]   Kawiecki, C.J., Kapp, W.H., Pranke, W.T., Steinhoff, H.H.
         and Thompson, R.E., "Lightning and Surge Protection Devices
         for Survivability of Electrical Systems," 1970 Lightning
         and Static Electricity Conference, AFAL, SAE 9-11 (1970).

[36]   Eggers, P.E., Brown, J.B. Jr., and Ollila, R.G., Lightning
         Protection Measures for Low Altitude Tethered Balloon
         Systems, (Contract No DAAH01-72-C-0982 - ARPA Order 2209)
         Baltelle Columbus Laboratories, P. 46.

[37]   ibid. p. 47.

[38]   Space Shuttle Lightning Protection Criteria Document,
         (JSC-07636), Lyndon B. Johnson Space Center, Table G1.
         (1973).

[39]   Cianos, M., Oetzel, G.N. and Pierce, E.T., "A Technique
         For Accurately Locating Lightning At Close Ranges,"
         Journal of Applied Meteorology, Vol II, No. 7, p. 1120-
         1127 (1972).

[40]   Hall, T.A. "A Proposal For Lightning Detection and Location",
         Telta TR74-043, Range Measurements Laboratory, Air Force
         Eastern Test Range, Patrick AFB, FL.   (Jan 1974)

[41.]   Krider, E.P., Noggle, R.C. and Uman, M.A., "Wideband
Magnetic Direction Finder for Lightning Return Strokes."
To be published in the Journal of Applied Meteorology.

[42]   Herman, B.D., Uman, M.A., Brantley, R.D. and Krider,
E.P., "Testing of a Wideband Direction finder for
Lightning Return Strokes," to be published in the
Journal of Applied Meteorology.

[43]   Notes from conversation between Professor Stig Lundquist,
University of Uppsala and Toxey A. Hall aboard Research
Vessel Thunderbolt, Miami, FL. (Jan 1973).

[44]   Cianos, N. and Pierce, E.T., Methods for Lightning
Warning and Avoidance, Standford Research Institute,
(May 1974).

[45]   Large, M.I., and Pierce, E.T., "The Dependence of
Point Discharge Currents on Wind as Examined by a New
Experimental Approach". Journal of Atmospheric and
Terrestrial Physics, Vol 10, pp 251 to 257, (1957).

[46]   Chalmers, J.A., Atmospheric Electricity, 2nd Ed.,
Pergamon Press, New York, p252, (1967).